ERDC/CHL TR-08-X

Coastal and Hydraulics Laboratory

US Army Corps of Engineers®
Engineer Research and Development Center

DRAFT

Seabrook Fish Larval Transport Study

Jennifer N. Tate, Tahirih C. Lackey, and Tate O. McAlpin

July 2009

DRAFT

Approved for public release; distribution is unlimited.

ERDC/CHL TR-08-X
July 2009

Seabrook Fish Larval Transport Study

Jennifer N. Tate, Tahirih C. Lackey, and Tate O. McAlpin

Coastal and Hydraulics Laboratory
U.S. Army Engineer Research and Development Center
3909 Halls Ferry Road
Vicksburg, MS 39180-6199

Technical report

Approved for public release; distribution is unlimited.

DRAFT

Prepared for U.S. Army Corps of Engineers, New Orleans District, Hurricane Protection Office

Contents

Figures and Tables iv

Preface xii

Executive Summary xiii

Unit Conversion Factors xvii

1 Introduction 1

Background 1

Technical Approach 4

Grid Modifications 4

Boundary Condition Development 5

Validation to Observed Data 5

Base and Plan simulations 5

Fish Larval Behavior Development 6

PTM Source Input 6

Base and Plan PTM Model Runs 7

2 Model Development 8

Model Description 8

Mesh Development 8

Boundary Conditions 10

3 Model Verification 16

Model/Field Comparisons 18

Sensitivity Analysis 44

4 Design Alternatives 47

5 Larval Fish Transport 54

Background 54

Method 56

Particle Velocity 58

Anchoring 59

Limitations 60

Simulation Details and Model Input 61

Source Input 62

Recruitment Regions 68

6 Hydrodynamic Results 69

Velocity Magnitudes 69

Water Surface Analysis 86

Circulation Analysis 105

DRAFT

7 Particle Tracking Results 110
Case 1 110
Case 2 111
Case 3 130

8 Particle Tracking Results - Final Plan 133
Case 1 135
Case 3 135
Case 4 138
Incoming Tide- West 138
Incoming Tide- East 150

9 Conclusions 162

References 164

Acknowledgements 166

Appendix A : Hydrodynamic Sensitivity Simulations 167
Plan 3 wide 167
Velocity Magnitudes 167
Water Surface Analysis 176
Cofferdam Simulations 181
Bridge Pier Sensitivity 188

Appendix B : Description of the Adaptive Hydraulics Model (ADH) 196

Appendix C: Description of the Particle Tracking Model Processes and Algorithms 202
Eulerian Transport Calculations 203
Shear Stress 203
Initiation of Motion 205
Transport Mobility 205
Bedform Calculation 206
Potential Transport Rate 207
Lagrangian Transport Calculations 207
Particle Position Integration 208
Velocity Calculations 208
Particle-bed Interactions 210
Hiding and Exposure Function 210
Frequency of Entrainment 211
Particle Deposition and Re-entrainment 212
Boundary Conditions 213

DRAFT

Figures and Tables

Figures

Figure 1-1. Vicinity map ... 3
Figure 1-2. Project area map ... 4
Figure 2-1. Model domain and bathymetry ... 9
Figure 2-2. Manning's Roughness Values ... 10
Figure 2-3. Location of river inflows ... 11
Figure 2-4. River inflow discharges for 2008 ... 12
Figure 2-5. Gage locations for development of tidal boundary ... 13
Figure 2-6. End points and mid point of tidal boundary ... 13
Figure 2-7. Location of New Orleans International Airport wind gage ... 14
Figure 2-8. Wind speed and direction ... 15
Figure 3-1. Water surface elevation field data locations ... 16
Figure 3-2. Discharge field measurement transects for Seabrook ... 17
Figure 3-3. Discharge field measurement transects for GIWW/MRGO area ... 18
Figure 3-4. Mississippi Sound at Grand Pass water surface elevation ... 19
Figure 3-5. Rigolets water surface elevation ... 20
Figure 3-6. Chef Menteur water surface elevation ... 20
Figure 3-7. Paris Road water surface elevation ... 21
Figure 3-8. IHNC South Lock water surface elevation ... 22
Figure 3-9. Bayou Bienvenue East water surface elevation ... 22
Figure 3-10. Bonnet Carre water surface elevation ... 23
Figure 3-11. West End water surface elevation ... 24
Figure 3-12. Lakefront Airport water surface elevation ... 24
Figure 3-13. Tidal constituent comparison of amplitude at Grand Pass ... 26
Figure 3-14. Tidal constituent comparison of amplitude at Paris Road ... 26
Figure 3-15. Tidal constituent comparison of amplitude at Chef Menteur ... 27
Figure 3-16. Tidal constituent comparison of amplitude at West End ... 27
Figure 3-17. GIWW/MRGO discharge for lines 6 and 8 ... 29
Figure 3-18. GIWW/MRGO discharge for lines 4 and 5 ... 30
Figure 3-19. GIWW/MRGO discharge for lines 1, 2, and 3 ... 31
Figure 3-20. IHNC Seabrook discharge ... 32
Figure 3-21. IHNC Seabrook velocity on October 16, 2008 at 15:33 ... 33
Figure 3-22. IHNC Seabrook velocity on October 17, 2008 at 06:30 ... 34
Figure 3-23. IHNC Seabrook velocity on October 17, 2008 at 09:05 ... 35
Figure 3-24. IHNC Seabrook velocity on October 17, 2008 at 13:29 ... 36

DRAFT

Figure 3-25. GIWW/MRGO velocity on July 31, 2008 at 10:30 37
Figure 3-26. GIWW/MRGO velocity on July 31, 2008 at 14:30 38
Figure 3-27. GIWW/MRGO velocity on July 31, 2008 at 16:00 39
Figure 3-28. GIWW/MRGO velocity on August 13, 2008 at 9:00 40
Figure 3-29. GIWW/MRGO velocity on August 13, 2008 at 13:00 41
Figure 3-30. GIWW/MRGO velocity on August 14, 2008 at 16:00 42
Figure 3-31. GIWW/MRGO velocity on August 14, 2008 at 6:00 43
Figure 3-32. GIWW/MRGO velocity on August 14, 2008 at 9:00 44
Figure 3-33. Sensitivity analysis results 45
Figure 3-34. Flow area calculations 45
Figure 4-1. Base configuration: no closures, no structures 48
Figure 4-2. Plan 1 configuration: close the MRGO at La Loutre 49
Figure 4-3. Plan 2 configuration: includes Plan 1 and the Borgne alignment (56 ft X 8 ft gate on Bayou Bienvenue, and two 150 ft X 16 ft gates on GIWW) 50
Figure 4-4. Plan 3 configuration: includes Plan 1, Plan 2 and a 95 ft X 16 ft structure at Seabrook 51
Figure 4-5. Plan 3 Final configuration: includes Plan 1, Plan 2 and a 95 ft X 20 ft sector gate with two side 50 ft X 16 ft auxiliary gates at Seabrook 52
Figure 4-6. Tide signal for both four week analysis periods 53
Figure 4-7. Wind signal for both four week analysis periods 53
Figure 5-1. Description of the Particle Tracking Modeling input and output 55
Figure 5-2. Case 1 initial positions are designated by the red circle 63
Figure 5-3. Locations of areas in which larvae are initiated for case 1. Yellow colored rectangles represent the locations of initial positions. 64
Figure 5-4. Location of areas in which larvae are initiated for case 3. Orange colored region represents the location of initial positions. 65
Figure B-5-5 Location of area in which larvae are initiated. Yellow colored rectangle represents the location of initial positions. 66
Figure 5-6. Locations of larval fish recruitment regions. Larvae that reach these areas are considered recruited. 68
Figure 6-1. Hydrodynamic analysis locations - Seabrook 70
Figure 6-2. Hydrodynamic analysis locations – Bayou Bienvenue Structure, GIWW Sector Gate, and GIWW Barge Gate 70
Figure 6-3. Velocity average for September (positive) 71
Figure 6-4. Velocity average for September (negative) 72
Figure 6-5. Velocity maximum for September (positive) 72
Figure 6-6. Velocity minimum for September (negative) 73
Figure 6-7. Velocity average for March (positive) 73
Figure 6-8. Velocity average for March (negative) 74
Figure 6-9. Velocity maximum for March (positive) 74
Figure 6-10. Velocity minimum for March (negative) 75
Figure 6-11. Percent exceedance of velocity magnitude analysis locations 77

DRAFT

Figure 6-12. Bayou Bienvenue percent exceedance plot for September 77
Figure 6-13. GIWW Sector Gate percent exceedance plot for September 78
Figure 6-14. GIWW Barge Gate percent exceedance plot for September 78
Figure 6-15. Seabrook percent exceedance plot for September 79
Figure 6-16. Chef Menteur percent exceedance plot for September 79
Figure 6-17. Rigolets percent exceedance plot for September 80
Figure 6-18. Lake Pontchartrain percent exceedance plot for September 80
Figure 6-19. Lake Borgne percent exceedance plot for September 81
Figure 6-20. Bayou Bienvenue percent exceedance plot for March 81
Figure 6-21. GIWW Sector Gate percent exceedance plot for March 82
Figure 6-22. GIWW Barge Gate percent exceedance plot for March 82
Figure 6-23. Seabrook percent exceedance plot for March 83
Figure 6-24. Chef Menteur percent exceedance plot for March 83
Figure 6-25. Rigolets percent exceedance plot for March 84
Figure 6-26. Lake Pontchartrain percent exceedance plot for March 84
Figure 6-27. Lake Borgne percent exceedance plot for March 85
Figure 6-28. Location map for water surface analysis 87
Figure 6-29. Inset for water surface analysis location map 87
Figure 6-30. Water surface elevation north of MRGO closure at La Loutre (September) 88
Figure 6-31. Water surface elevation south of MRGO closure at La Loutre (September) 88
Figure 6-32. Water surface elevation north of MRGO closure at Bayou Bienvenue (September) 89
Figure 6-33. Water surface elevation south of MRGO closure at Bayou Bienvenue (September) 89
Figure 6-34. Water surface elevation west of Bayou Bienvenue structure (September) 90
Figure 6-35. Water surface elevation east of Bayou Bienvenue structure (September) 90
Figure 6-36. Water surface elevation west of GIWW structures (September) 91
Figure 6-37. Water surface elevation east of GIWW structures (September) 91
Figure 6-38. Water surface elevation north of Seabrook structure (September) 92
Figure 6-39. Water surface elevation south of Seabrook structure (September) 92
Figure 6-40. Water surface elevation in GIWW at IHNC (September) 93
Figure 6-41. Water surface elevation in Chef Menteur (September) 93
Figure 6-42. Water surface elevation north in Rigolets (September) 94
Figure 6-43. Water surface elevation at Lake Borgne perimeter (September) 94
Figure 6-44. Water surface elevation at Lake Borgne center (September) 95
Figure 6-45. Water surface elevation at Lake Pontchartrain (September) 95
Figure 6-46. Water surface elevation north of MRGO closure at La Loutre (March) 96
Figure 6-47. Water surface elevation south of MRGO closure at La Loutre (March) 96
Figure 6-48. Water surface elevation north of MRGO closure at Bayou Bienvenue (March) 97
Figure 6-49. Water surface elevation south of MRGO closure at Bayou Bienvenue (March) 97
Figure 6-50. Water surface elevation west of Bayou Bienvenue structure (March) 98

DRAFT

Figure 6-51. Water surface elevation east of Bayou Bienvenue structure (March) 98
Figure 6-52. Water surface elevation west of GIWW structures (March) 99
Figure 6-53. Water surface elevation east of GIWW structures (March) 99
Figure 6-54. Water surface elevation north of Seabrook structure (March) 100
Figure 6-55. Water surface elevation south of MRGO Seabrook structure (March) 100
Figure 6-56. Water surface elevation in GIWW at IHNC (March) 101
Figure 6-57. Water surface elevation in Chef Menteur (March) 101
Figure 6-58. Water surface elevation in Rigolets (March) 102
Figure 6-59. Water surface elevation at Lake Borgne perimeter (March) 102
Figure 6-60. Water surface elevation at Lake Borgne center (March) 103
Figure 6-61. Water surface elevation in Lake Pontchartrin (March) 103
Figure 6-62. Direction of flow for incoming tide in Base case 106
Figure 6-63. Direction of flow for incoming tide for Plan 1, Plan 2, and Plan 3 107
Figure 6-64. GIWW velocity analysis locations 108
Figure 6-65. Velocity signal in the GIWW west of MRGO, velocities west of the Borgne alignment on the GIWW decrease with the closure of the MRGO at La Loutre 108
Figure 6-66. Velocity signal in the GIWW east of MRGO, velocities east of the Borgne alignment on the GIWW increase with the closure of the MRGO at La Loutre 109
Figure 7-1 Location and transport path for larvae initiated for case 2. The red circle represents the approximate location of the initial positions 110
Figure 7-2 September, base condition larvae positions after a) 1 day, b) 1 week, c) 4 weeks. Red particles are initiated on the GIWW and yellow particles are initiated on the MRGO. 113
Figure 7-3 September, plan 1 condition larvae positions after a) 1 day, b) 1 week, c) 4 weeks. Red particles are initiated on the GIWW and yellow particles are initiated on the MRGO. 114
Figure 7-4 September, plan 2 condition larvae positions after a) 1 day, b) 1 week, c) 4 weeks. Red particles are initiated on the GIWW and yellow particles are initiated on the MRGO. 115
Figure 7-5. September, plan 3 condition larvae positions after a) 1 day, b) 1 week, c) 4 weeks. Red particles are initiated on the GIWW and yellow particles are initiated on the MRGO. 116
Figure 7-6 March, base condition larvae positions after a) 1 day, b) 1 week, c) 4 weeks. Red particles are initiated on the GIWW and yellow particles are initiated on the MRGO. 117
Figure 7-7. March, plan 1 condition larvae positions after a) 1 day, b) 1 week, c) 4 weeks. Red particles are initiated on the GIWW and yellow particles are initiated on the MRGO. 118
Figure 7-8. March, plan 2 condition larvae positions after a) 1 day, b) 1 week, c) 4 weeks. Red particles are initiated on the GIWW and yellow particles are initiated on the MRGO. 119
Figure 7-9. March, plan 3 condition larvae positions after a) 1 day, b) 1 week, c) 4 weeks. Red particles are initiated on the GIWW and yellow particles are initiated on the MRGO. 120
Figure 7-10. Time series of the number of larvae recruited with time for base, plan1, plan2, and plan3 configurations using September 2007 hydrodynamics. 4800 particles total. 122
Figure 7-11. Time series of the number of larvae recruited with time for base, plan1, plan2, and plan3 configurations using March 2008 hydrodynamics. 4800 particles total. 122

DRAFT

Figure 7-12 Time series of the number of larvae recruited with time for base, plan1, plan2, and plan3 configurations using March 2008 hydrodynamics for GIWW source only (2195 particles total) 124

Figure 7-13. Time series of the number of larvae recruited with time for base, plan1, plan2, and plan3 configurations using March 2008 hydrodynamics for GIWW source only (2195 particles total) 124

Figure 7-14 Comparison of Larvae Recruitment Time Series for the March 2008 Hydrodynamic, Base configuration. 126

Figure 7-15 Percentage of larvae recruited at Seabrook (blue) and Chef Menteur (red) for base, plan1, plan2, and plan3 configurations using September 2007 hydrodynamics 128

Figure 7-16 Percentage of larvae recruited at Seabrook (blue) and Chef Menteur (red) for base, plan1, plan2, and plan3 configurations using the March 2008 hydrodynamics. 129

Figure 7-17. March, base condition larvae positions after a) 1 day, b) 1 week, c) 4 weeks. Particles initiated in Lake Borgne. 131

Figure 8-1 Circulation Diagram of flow direction for incoming tide for all configurations 134

Figure 8-2. March, base condition larvae positions after a) 1 day, b) 1 week, c) 4 weeks. Particles initiated in Lake Borgne. 136

Figure 8-3 September, base condition larvae positions after a) 1 day, b) 1 week, c) 4 weeks. Particles anchored based on incoming tide to the west and are color coded based on behavior. 139

Figure 8-4 September, final plan condition larvae positions after a) 1 day, b) 1 week, c) 4 weeks. Particles anchored based on incoming tide to the west and color coded based on behavior. 140

Figure 8-5 march, base condition larvae positions after a) 1 day, b) 1 week, c) 4 weeks. Particles anchored based on incoming tide to the west. and color coded based on behavior. 141

Figure 8-6 march, final plan condition larvae positions after a) 1 day, b) 1 week, c) 4 weeks. Particles anchored based on incoming tide to the west. and color coded based on behavior. 142

Figure 8-7 Comparison of Larvae Recruitment Time Series for the September 2007 Hydrodynamic, larval fish preferred path to the west. Particles anchored based on incoming tide to the west (2150 particles released) 143

Figure 8-8 Comparison of Larvae Recruitment Time Series for the March 2008 Hydrodynamic, larval fish preferred path to the west. Particles anchored based on incoming tide to the west (2150 particles released). 144

Figure 8-9 Percentage of larvae recruited at Seabrook (blue) and Chef Menteur (red) for base, plan1, plan2, and plan3 configurations using September 2007 hydrodynamics, larval fish preferred path to the west. (Maximum value possible 25%) Particles anchored based on incoming tide to the west. 146

Figure 8-10 Percentage of larvae recruited at Seabrook (blue) and Chef Menteur (red) for base, plan1, plan2, and plan3 configurations using March 2008 hydrodynamics, larval fish preferred path to the west. (Maximum value possible 25%) Particles anchored based on incoming tide to the west. 148

Figure 8-11 September, base condition larvae positions after a) 1 day, b) 1 week, c) 4 weeks. Particles anchored based on incoming tide to the east and color coded based on behavior. 151

DRAFT

Figure 8-12 September, final plan condition larvae positions after a) 1 day, b) 1 week, c) 4 weeks. Particles anchored based on incoming tide to the east and color coded based on behavior. 152

Figure 8-13 March, base condition larvae positions after a) 1 day, b) 1 week, c) 4 weeks. Particles anchored based on incoming tide to the east and color coded based on behavior. 153

Figure 8-14 March, final plan condition larvae positions after a) 1 day, b) 1 week, c) 4 weeks. Particles anchored based on incoming tide to the east and color coded based on behavior. 154

Figure 8-15 Comparison of Larvae Recruitment Time Series for the September 2007 Hydrodynamic, larval fish preferred path to the east. Particles anchored based on incoming tide to the east. 155

Figure 8-16 Comparison of Larvae Recruitment Time Series for the March 2008 Hydrodynamic, larval fish preferred path to the east. Particles anchored based on incoming tide to the east. 156

Figure 8-17 Percentage of larvae recruited at Seabrook (blue) and Chef Menteur (red) for base, plan1, plan2, and plan3 configurations using September 2007 hydrodynamics, larval fish preferred path to the east(Maximum value possible 25%) Particles anchored based on incoming tide to the east. 158

Figure 8-18 Percentage of larvae recruited at Seabrook (blue) and Chef Menteur (red) for base, plan1, plan2, and plan3 configurations using March 2008 hydrodynamics, larval fish preferred path to the east. (Maximum value possible 25%) Particles anchored based on incoming tide to the east. 160

Figure A-1. Hydrodynamic analysis locations – Seabrook 168

Figure A–2. Hydrodynamic analysis locations – Bayou Bienvenue Structure, GIWW Sector Gate, and GIWW Barge Gate 169

Figure A-3. Velocity average for September (positive) 170

Figure A-4. Velocity average for September (negative) 170

Figure A-5. Velocity maximum for September (positive) 171

Figure A-6. Velocity minimum for September (negative) 171

Figure A-7. Velocity average for March (positive) 172

Figure A-8. Velocity average for March (negative) 172

Figure A-9. Velocity maximum for March (positive) 173

Figure A-10. Velocity minimum for March (negative) 173

Figure A-11. Velocity exceedance at the GIWW sector gate for September 174

Figure A-12. Velocity exceedance at the GIWW sector gate for March 175

Figure A-13. Velocity exceedance at the Seabrook structure for September 175

Figure A-14. Velocity exceedance at the Seabrook structure for March 176

Figure A-15. Water surface analysis arc and location reference in 1000 ft increments 177

Figure A-16. Water surface elevation along arc for Base and all plans for August 27, 2007 178

Figure A-17. Water surface elevation along arc for Base and all plans for March 3, 2008 178

Figure A-18. Water surface elevation through GIWW sector gate (August) 179

Figure A-19. Water surface elevation through GIWW sector gate (March) 179

Figure A-20. Water surface elevation through IHNC and Seabrook structure (August) 180

Figure A-21. Water surface elevation through IHNC and Seabrook structure (March) 180

DRAFT

Figure A-22. Seabrook analysis locations for cofferdam simulation 181
Figure A-23. Velocity average for September with cofferdam (positive) 182
Figure A-24. Velocity average for September with cofferdam (negative) 182
Figure A-25. Velocity maximum for September with cofferdam (positive) 183
Figure A-26. Velocity minimum for September with cofferdam (negative) 183
Figure A-27. Velocity average for March with cofferdam (positive) 184
Figure A-28. Velocity average for March with cofferdam (negative) 184
Figure A-29. Velocity maximum for March with cofferdam (positive) 185
Figure A-30. Velocity minimum for March with cofferdam (negative) 185
Figure A-31. Velocity magnitude and direction at the cofferdam for a high flood flow in March (a single snapshot in time) 186
Figure A-32. Velocity magnitude and direction at the cofferdam for a high ebb flow in March (a single snapshot in time) 187
Figure A-33. Plan 3 geometry configuration (95 X 16 ft Seabrook structure) with bridge piers (includes MRGO cut at La Loutre and the Borgne alignment) 189
Figure A-34. Velocity average for September with bridge piers (positive) 190
Figure A-35. Velocity average for September with bridge piers (negative) 190
Figure A-36. Velocity maximum for September with bridge piers (positive) 191
Figure A-37. Velocity minimum for September with bridge piers (negative) 191
Figure A-38. Velocity average for March with bridge piers (positive) 192
Figure A-39. Velocity average for March with bridge piers (negative) 192
Figure A-40. Velocity maximum for March with bridge piers (positive) 193
Figure A-41. Velocity minimum for March with bridge piers (negative) 193
Figure A-42. Velocity magnitude and direction with bridge piers for a high flood flow in March (a single snapshot in time) 194
Figure A-43. Velocity magnitude and direction with bridge piers for a high ebb flow in March (a single snapshot in time) 195

Tables

Table 3-1. Tidal Constituents 25
Table 3-2. Tidal Constituent Amplitude Comparisons (ft) 28
Table 5-1. List of species and representative behavior 61
Table 5-2. Locations of polygon boundaries for initial particle positions for each case 67
Table 7-1 Percentage of larvae recruited for each construction phase for simulations in which particles are initiated in the MRGO and GIWW (Case 2 conditions). 123
Table 7-2 Percentage of larvae recruited for each construction phase for simulations in which particles are initiated in Lake Borgne. 132
Table 8-1 Recruitment Percentages for Case 3 particles – Incoming Tide-West 137
Table 8-2 Recruitment Percentages for Case 3 particles – Incoming Tide East 137
Table 8-3 Percentage of larvae recruited for each construction phase for simulations in which particles are anchored based on incoming tide to the west (2150 particles released). 144

DRAFT

Table 8-4 Percentage of larvae recruited for each construction phase for simulations in which particles are anchored based on incoming tide to the east (2150 particles released). 156

DRAFT

Preface

The model investigation presented in this report was authorized and funded by the U.S. Army Corps of Engineers Hurricane Protection Office (HPO), New Orleans in effort to support the environmental impacts analysis completed as part of the approved Alternative Arrangement provisions of the Council of Environmental Quality Regulations for Implementing the National Environmental Policy Act (40 CFR 1506.11). This modeling effort will be documented in Individual Environmental Report #11 Tier 2 Pontchartrain for the improved protection of the Inner Harbor Navigation Canal. This fish larval transport study into Lake Pontchartrain through Seabrook, including the Mississippi River Gulf Outlet and the Gulf Intercoastal Waterway was conducted by Ms. Jennifer Tate, Dr. Tahirih Lackey, Mr. Tate McAlpin, and Ms. Cassandra Ross.

This work was conducted at the Coastal and Hydraulics Laboratory (CHL) of the U. S. Army Engineer Research and Development Center (ERDC) during the period of November 2008 to March 2009 under the direction of Thomas W. Richardson, Director of the CHL; Dr. Rose Kress, Chief of the Navigation Division, CHL; Mr. Bruce Ebersole, Chief of the Flood Protection Division, CHL; Mr. Ty V. Wamsley, Chief of the Coastal Processes Branch, CHL; Dr. Robert T. McAdory, Chief of the Estuarine Engineering Branch, CHL.

Dr. James R. Houston was Director of ERDC. COL Gary Johnston was Commander and Executive Director.

DRAFT

Executive Summary

Background

The U.S. Army Engineer Hurricane Protection Office (HPO) requested that the USACE Engineer Research and Development Center (ERDC) at Waterways Experiment Station perform a numerical modeling study for the purpose of analyzing the impacts of proposed hurricane and storm damage risk reduction (HSDRRS) measures to be placed in the Gulf Intracoastal Waterway (GIWW) and the Mississippi River Gulf Outlet (MRGO) on the larval fish transport in the area. This study was requested in addition to separate navigation studies to analyze the impacts the protection measures have on the hydrodynamics and vessel traffic.

The MRGO Canal is a 66-mile-long deepwater channel that extends northwest from deep water in the Gulf of Mexico to New Orleans, LA (Figure 1-1). The MRGO merges with the GIWW and continues 5 miles further to the west where it joins the Inner Harbor Navigation Canal (IHNC). The IHNC proceeds another approximately 3 miles north from its intersection with the GIWW to connect with Lake Pontchartrain at Seabrook. To the East of the connection of the GIWW with the MRGO, the GIWW extends northeast approximately 6 miles to its first connection with Lake Borgne and 20 miles with its connection to the Rigolets.

It is known that larval fish migrate from the Gulf of Mexico into Lake Pontchartrain. A particle tracking simulation can be performed such that the particles are given basic larval fish transport behaviors and released at various locations in the area. The hydrodynamic properties move these particles within the system and the changes to the transport due to the planned changes to the system can be analyzed.

Hydrodynamic Numerical Model

The hydrodynamic code used in this study is Adaptive Hydraulics (ADH). ADH is a finite element code that can simulate three-dimensional groundwater, three-dimensional navier-stokes, and two- and three-dimensional shallow water equations. This study utilizes the 2-dimensional shallow water equations of ADH. The model is simulated on high performance computing machines in order to obtain quick results.

DRAFT

Further details on the ADH model and its equations can be found in Appendix C and several publications are available at https://adh.usace.army.mil.

The model is validated with field data from 2008 of water surface elevation, discharge, and velocity. Current bathymetry data was collected by ERDC-CHL in the IHNC, GIWW, and northern MRGO to approximately channel mile 56. The model boundary conditions include tidal boundary, river inflows, and wind forcings.

Model Scenarios

Four plan simulations are modeled in addition to the base condition. The conditions are given below.

- Base – includes the fully open MRGO, GIWW, and IHNC
- Plan 1 – close the MRGO at La Loutre
- Plan 2 – close the MRGO at La Loutre, include the Borgne alignment (close the MRGO south of Bayou Bienvenue, 56 ft X 8 ft gate on Bayou Bienvenue, two 150 ft X 16 ft gates on GIWW)
- Plan 3 – close the MRGO at La Loutre, include the Borgne alignment, include the Seabrook structure (95 ft X 16 ft gate)
- Plan 3 Final - close the MRGO at La Loutre, include the Borgne alignment, include the 95 ft X 20 ft sector gate at Seabrook with two flanking 50 ft X 16 ft auxiliary gates with southern scour hole filled

The Base and four scenarios are modeled according to the validation conditions requested by HPO and the hydrodynamic results are used to drive the particle tracking simulations.

Particle Tracking Simulations

Four cases were simulated using the Particle Tracking Model (PTM) for each of the model scenarios. Cases were differentiated based on initial positions of representative larval fish particles.

- Case 1 – initiated in MRGO at La Loutre

DRAFT

- Case 2 – initiated in MRGO at Bayou Bienvenue and GIWW at constriction
- Case 3 – initiated in Lake Borgne
- Case 4 – initiated in GIWW at constriction

Results are presented as time dependent particle positions, recruitment time series, and percentage of recruited particles relative to various behaviors.

Conclusions

The results of the hydrodynamic simulations show that by cutting off the MRGO at La Loutre, as in Plan 1, the entire circulation pattern within the GIWW/MRGO system changes. A percent exceedence analysis shows that although there are some extreme velocity magnitudes through the structures, these values are not typical and occur a small fraction of the time, typically under strong storm circumstances. "Strong" is defined here as a short lived event with flows and winds speeds of larger magnitudes than those at other times. At these times transport can be high due to the high speed of the flow. The transport, however, is also dependent of the behavior of the species and not only on the flow speed or direction.

Transport of particles within the system is dominated by the hydrodynamics of the system. The tidal intensity and regularity of the tidal signal are a main factor of transport. Particles released during stronger events, such as those seen in the March 2008 hydrodynamic period, may be recruited at a greater rate than a less intense flow condition such as the September 2007 hydrodynamic period. However that is additionally affected by the larval fish characteristic transport behaviors.

Analysis of simulation results signify that the rate of particle recruitment is affected by the plan configuration for cases 2-4. The base configuration shows the highest recruitment values and plan 3 configuration shows the lowest recruitment values. The final plan configuration shows a decrease of particles reaching recruitment areas in comparison to the base design, plan 1, and plan 2. However recruitment values for the simulations using the final plan geometry increase with respect to plan 3. This is most likely due to the increase of cross sectional area at Seabrook shown in the final plan in comparison to plan 3. Results indicate an approximate 10-15 per-

DRAFT

cent recruitment decrease between plans 1 and the final plan. Case 3 results show that there is no real difference between the transport pathways from Lake Borgne to Chef Menteur with respect to the plans. The base case generally has a slightly higher value of recruited particles; however plans1-3 and the final plan differ within 5 percent.

Characteristic fish behavior affects the recruitment rate of particles. When the transport mechanism of anchoring is added to particle transport behavior, recruitment occurs at a much faster rate than without the mechanism. Generally passive particles had the lowest recruitment values, followed by tidal lateral behavior, bottom movers, and finally tidal vertical movers.

DRAFT

Unit Conversion Factors

Multiply	By	To Obtain
acres	4,046.873	square meters
acre-feet	1,233.5	cubic meters
cubic feet	0.02831685	cubic meters
cubic inches	1.6387064 E-05	cubic meters
cubic yards	0.7645549	cubic meters
degrees (angle)	0.01745329	radians
degrees Fahrenheit	(F-32)/1.8	degrees Celsius
fathoms	1.8288	meters
feet	0.3048	meters
foot-pounds force	1.355818	joules
inches	0.0254	meters
inch-pounds (force)	0.1129848	newton meters
knots	0.5144444	meters per second
microns	1.0 E-06	meters
miles (nautical)	1,852	meters
miles (U.S. statute)	1,609.347	meters
slugs	14.59390	kilograms
square feet	0.09290304	square meters
square yards	0.8361274	square meters
yards	0.9144	meters

DRAFT

1 Introduction

Background

The U. S. Army Corps of Engineers Hurricane Protection Office (HPO) is authorized to provide New Orleans with a risk reduction system for the one percent exceedance flood (HSDRRS). The purpose and need for the proposed action is to provide, in a timely manner, the 100-year level of risk reduction from flood damage to the areas surrounding the IHNC due to flooding from hurricanes and other severe storm events. The term "100-year level of risk reduction" as it is used throughout this document refers to a level of risk reduction that reduces the risk of storm surge and wave-driven flooding that the New Orleans Metropolitan Area has a one percent chance of experiencing in any given year. The elevations of the existing Lake Pontchartrain and Vicinity (LPV) HSDRRS in the project area are below the 100-year design elevation. The proposed action resulted from a defined need to reduce flood risk and storm damage to residences, businesses, and other infrastructure from hurricanes (100-year storm events), and other high water events. The completed HSDRRS would lower the risk of harm to citizens and damage to infrastructure during a storm event. The safety of people in the region is the highest priority of the USACE.

This is being accomplished through the construction of a comprehensive system of levees, gates, and drainage structures. Several planned structures (to be located along the levee system) allow for continued navigation in the Inner Harbor Navigational Canal (IHNC), Bayou Bienvenue, and on the Gulf Intracoastal Waterway (GIWW). The IHNC Seabrook, Bayou Bienvenue, and GIWW gate structures are designed to remain open during normal tidal conditions with the ability to close during surge events, however, navigation results may require a change in the operation procedures.

In accordance with the construction of this levee system, it is important to consider the biological effects that will occur due to these proposed projects. In order to model juvenile and fully grown fish, an equation must be available to define their swimming behavior. At this point, there has not been enough research to fully model the fish that inhabit this area. Therefore, insufficient data is available to perform a proper model study of the behavior of juvenile and fully grown fish, but larval fish behave in a much simpler manner and therefore can be modeled as particles with certain native tendencies. This type of modeling is being performed using the Particle Tracking Model (PTM). PTM (McDonald et al.

DRAFT

2006, Lackey and McDonald 2007, Lackey and Smith 2008) is an Engineering Research and Development Center (ERDC)-developed model designed specifically to track the fate of user defined particles (sediment, chemical, debris, biological particles, etc) released from locations within complex hydrodynamic and wave environments. HPO has requested that ERDC, Coastal and Hydraulics Lab (CHL) perform a model study to determine the effect of the proposed HSDRRS system on the passage of larval fish within the system, specifically at Seabrook. PTM is utilized to transport discrete passive particles which have been modified with characteristic larval fish transport behaviors through the hydrodynamic system. This effect will be approximate due to the limitation of the modeling tool to only transport larval fish with specified characteristics. This work will not address the effects on adult fish or behavior patterns that are not included. Figure 1-1 shows the project vicinity. Figure 1-2 shows a more detailed project area.

DRAFT

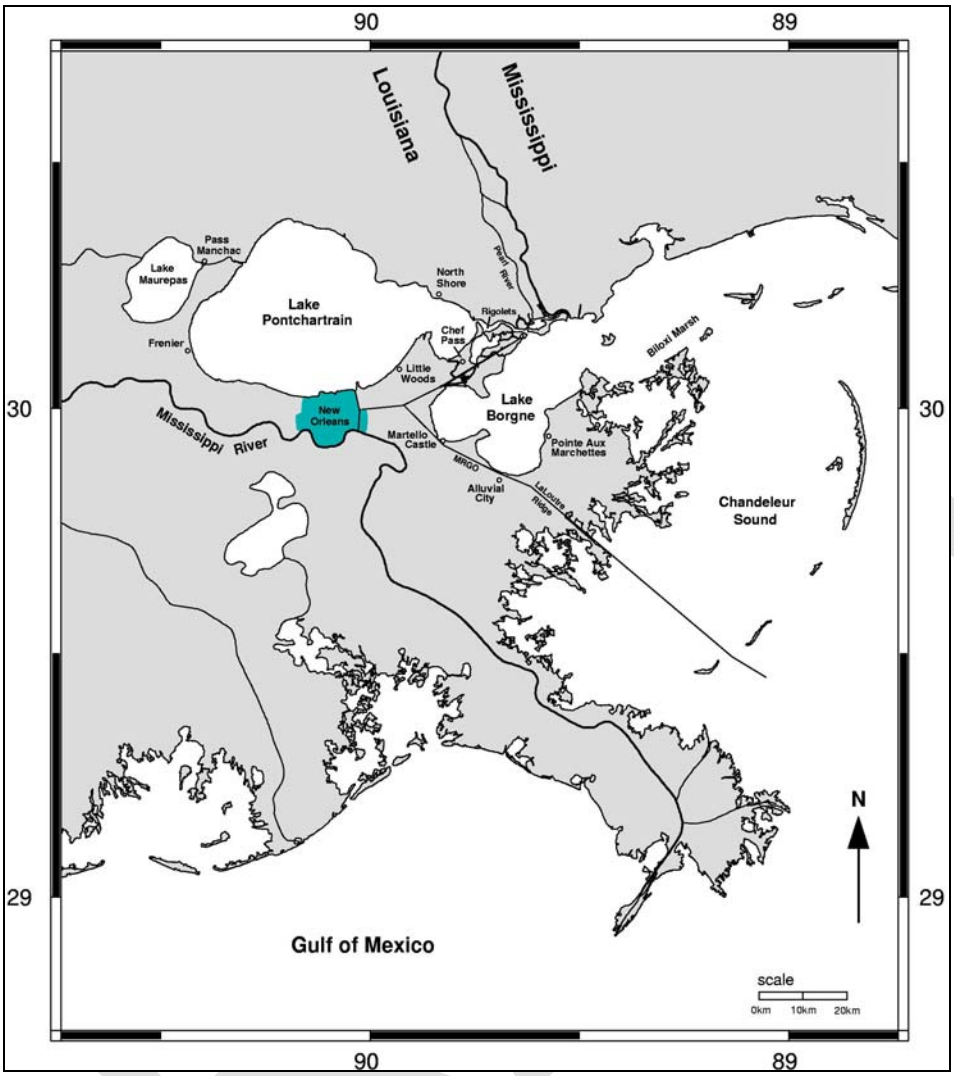

Figure 1-1. Vicinity map

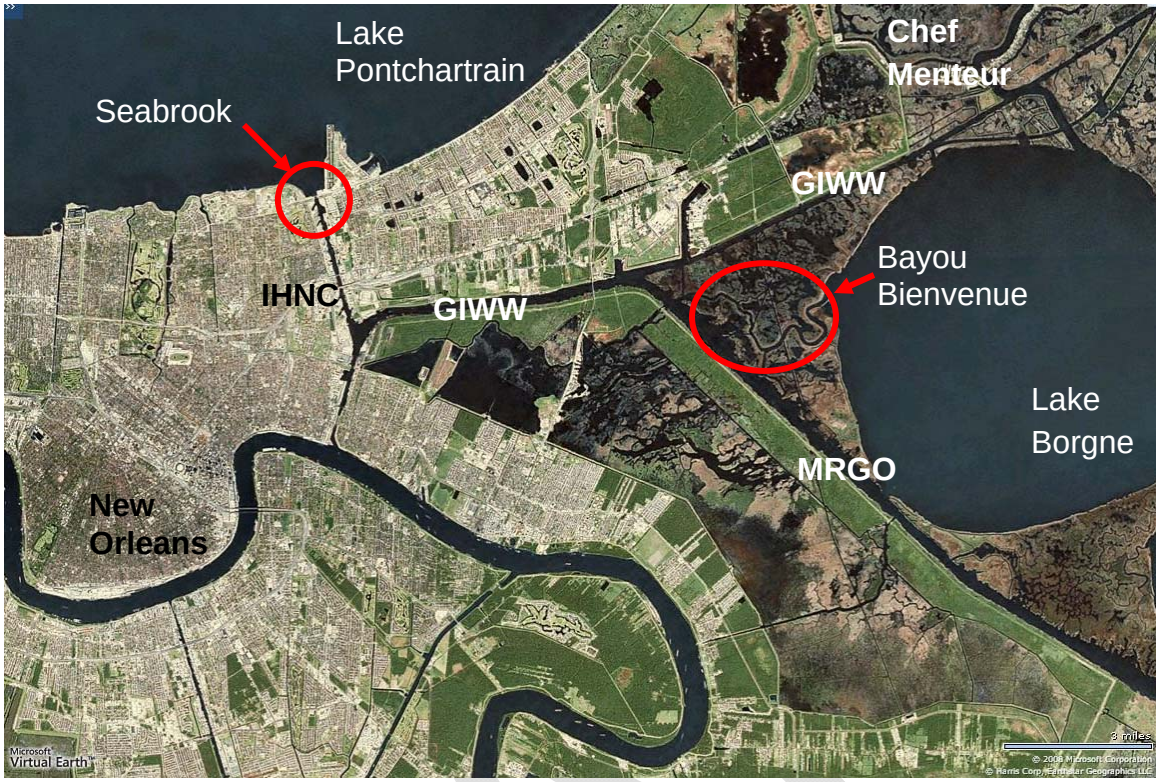

Figure 1-2. Project area map

Technical Approach

The modeling for this study considers hydrodynamic movement using the ADH code in two-dimensions and the fish larval movement using PTM. Velocities are compared with data in hand. As discussed above, this study is designed to determine the approximate effects, only, of planned flood control works on the movement of larvae. Also, since the structures will only be closed a very small percentage of the time, this analysis considers a structure either open or closed for the entire time of a simulation.

The tasks discussed below can be separated into two sections, hydrodynamic modeling and fish larval modeling.

Grid Modifications

A previous ADH model for this area was developed to model navigational effects in the GIWW area under the Lake Borgne Surge Barrier Navigation study directed by HPO (Martin et al. in review). The IHNC area near Seabrook is crudely

represented in the existing model and, using data recently collected, is updated for bank lines and bathymetry. This recently collected data provides improved representation for this fish passage work and also benefits the current navigational study being performed.

Boundary Condition Development

To perform a proper comparison between observed results and model results, the same conditions (time period) will be used for the validation model run. Therefore a boundary condition file is created to model the time period during which the measurements are taken. The boundary condition file consists of the river inflows, wind forcings, and tidal conditions for Jan 1, 2008 to October 21, 2008.

Validation to Observed Data

Although the previous Lake Borgne Surge Barrier model was validated to water surface elevation data, this study made additional comparisons to observed velocity data and water surface data. The validation indicates that the model only requires minor modifications to obtain satisfactory model results. For the purpose of this study, the flow directions are very important. Field discharge measurements are used to ensure that the flow patterns are represented correctly.

Base and Plan simulations

The base (existing conditions) and four additional plan configurations are simulated and the hydrodynamic results are then used in the PTM modeling effort. The scenarios modeled are:

- Base - no structures, no closures
- Plan 1 - Closure on the MRGO at La Loutre
- Plan 2 - Closure on the MRGO at La Loutre with Borgne alignment (56 ft X 8 ft gate on Bayou Bienvenue, and two 150 ft X 16 ft gates on GIWW)
- Plan 3 - Closure on the MRGO at La Loutre with the Borgne alignment and 95 ft X 16 ft gate at Seabrook
- Plan 3 Final - Closure on the MRGO at La Loutre with the Borgne alignment and 95 ft X 20 ft sector gate at Seabrook with two side flanking 50 ft X 16 ft auxiliary gates

Initially, two different two-week periods would be simulated as specified by HPO for PTM analysis. These two periods are the final two weeks of March 2008 and the first two weeks of September 2007. These time periods were selected by the

DRAFT

the interagency team, made up of representatives from National Marine Fisheries Service, U.S. Fish and Wildlife Service, Louisiana Department of Natural Resources, Louisiana Department of Wildlife and Fisheries, and Louisiana Department of Environmental Quality, U.S. Environmental Protection Agency and the USACE, and based on flow and wind conditions best suited for larval fish transport. After initial PTM model testing, the simulation periods were extended to four weeks to include the two weeks prior to those requested by the interagency team. The periods included for these simulations are August 15 – September 15, 2007 and March 1-31, 2008.

Fish Larval Behavior Development

The interagency team provided CHL with the larval fish behavior characteristics portrayed by the local fish population. The interagency team noted eight dominant species with 3 general behavior characteristics. The behaviors listed below are included in the PTM modeling.

1) Tidal Lateral (move to center during incoming tide)
2) Tidal Vertical (move up during incoming tide)
3) Bottom Movers (25 cm from bottom)
4) Passive (as a default)

Since the PTM model will not transport species differently, it would be misleading to divide a behavior type into various species. The statistics of how each species moves within the system would be misrepresented since the model sees no difference in species having the same behavior.

PTM Source Input

The Particle Tracking model is dependent on user defined sources. In this case, those sources represent characteristic larval fish transport behavior. Initial start locations were provided by the interagency team based on typical conditions for the species being modeled and particles were released over a specified period of time. A recruitment location is defined approximately one mile into Lake Pontchartrain from the Seabrook structure. An additional recruitment area is placed at the entrance of Chef Menteur to Lake Pontchartrain to account for particles that reach the lake through this waterway. Once particles reach these areas they are considered recruited and are no longer part of the system.

DRAFT

Base and Plan PTM Model Runs

All five of the previously mentioned scenarios are modeled in PTM and the results provided to the interagency team. The same ADH simulation periods used in the hydrodynamic tasks will be used in this task. For each configuration and flow condition, four behavior types are modeled. Analysis consists of fish recruitment statistics as well as particle path analysis.

DRAFT

2 Model Development

Model Description

Adaptive Hydraulics (ADH) is the modeling tool used for the simulations in this study. ADH is a finite element model that is capable of simulating three-dimensional Navier Stokes equations, two and three-dimensional shallow water equations, and groundwater equations. It can be used in a serial or multiprocessor mode on personal computers, UNIX, Silicon Graphics, and CRAY operating systems. The uniqueness of ADH is its ability to dynamically refine the domain mesh in areas where more resolution is needed at certain times due to changes in the flow conditions. ADH can simulate the transport of conservative constituents, such as dye clouds, as well as sediment transport that is coupled to bed and hydrodynamic changes. The ability of ADH to allow the domain to wet and dry within the marsh areas as the tide changes is suitable for the shallow marsh environment. This tool is being developed at CHL and has been used to model sediment transport in sections of the Mississippi River, tidal conditions in southern California, and vessel traffic in the Houston Ship Channel.

For this study, the two-dimensional shallow water module of ADH will be used for all simulations. This tool solves for depth and depth averaged velocity throughout the model domain. In this case, density effects due to salinity or other factors are being ignored and therefore their effects on the flow are not included in these simulations and results. More details of the two-dimensional shallow water module of ADH and its computational philosophy and equations can be found in Appendix C or at https://adh.usace.army.mil.

Mesh Development

The computational model domain is given in Figure 2-1. This is the same model domain as in previous studies of this area as described in McAnally et al. 1997 and Tate et al. 2002. This mesh has since been modified to include more recent bathymetry and additional marsh storage and flow pathways for the navigation study of the Borgne alignment. The domain extends east of the Chandeleur Islands in the Gulf of Mexico, follows the coastline of Mississippi and Louisiana on the north, follows the MRGO on the south, and includes Lake Pontchartrain and Lake Maurepas. The actual mesh was taken from that used in the navigation study and modified to fit the ADH format of linear, triangular elements. Bathy-

DRAFT

metry data was collected by ERDC-CHL in the IHNC, GIWW, Bayou Bienvenue and northern MRGO in November 2008. This data were incorporated into the mesh. Mesh boundaries were also better defined along the IHNC, GIWW, and Bayou Bienvenue. The vertical datum for this mesh is NAVD 88 (2004.65). The computational model domain for the base condition contained 32,087 elements and 17,796 nodes with elements ranging in area from 1000 ft² to 100 million ft², the largest located in the Gulf of Mexico.

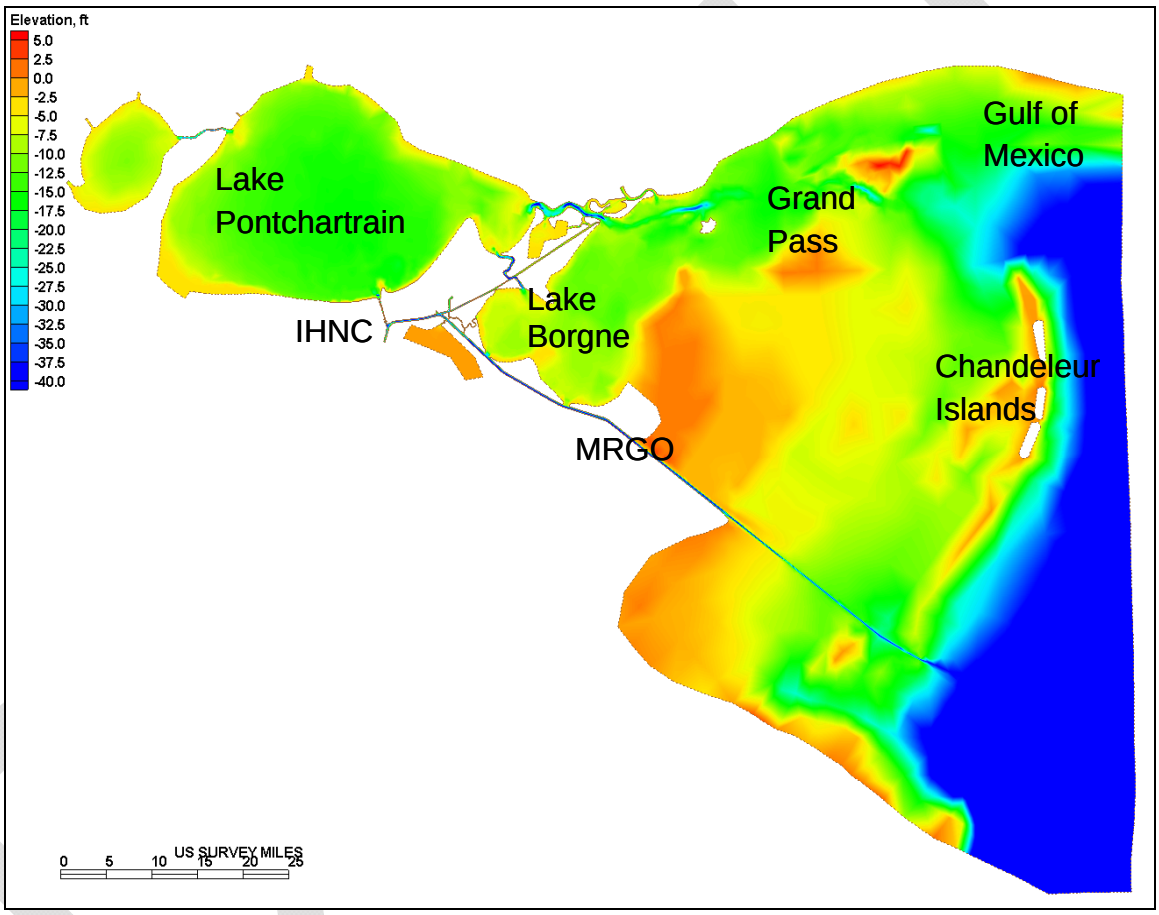

Figure 2-1. Model domain and bathymetry

The friction on the bed is described using a Manning's approach and varies spatially over the domain. Figure 2-2 shows the spatial variation of the roughness parameters. Eight different Manning's roughness parameters are used for this domain and were defined by typical values for these types of locations and adjusted during the validation process in order to determine the best values to represent reality. In the shallow areas the model is more sensitive to these

roughness parameters than in the deeper, channelized regions. ADH uses a roughness algorithm that equates the Manning's roughness value to an estimated roughness height of the bed. By doing this, ADH is able to represent any changes in roughness effects due to the depth of the water with a physical basis, as opposed to other methods that apply an additional algorithm to make these adjustments.

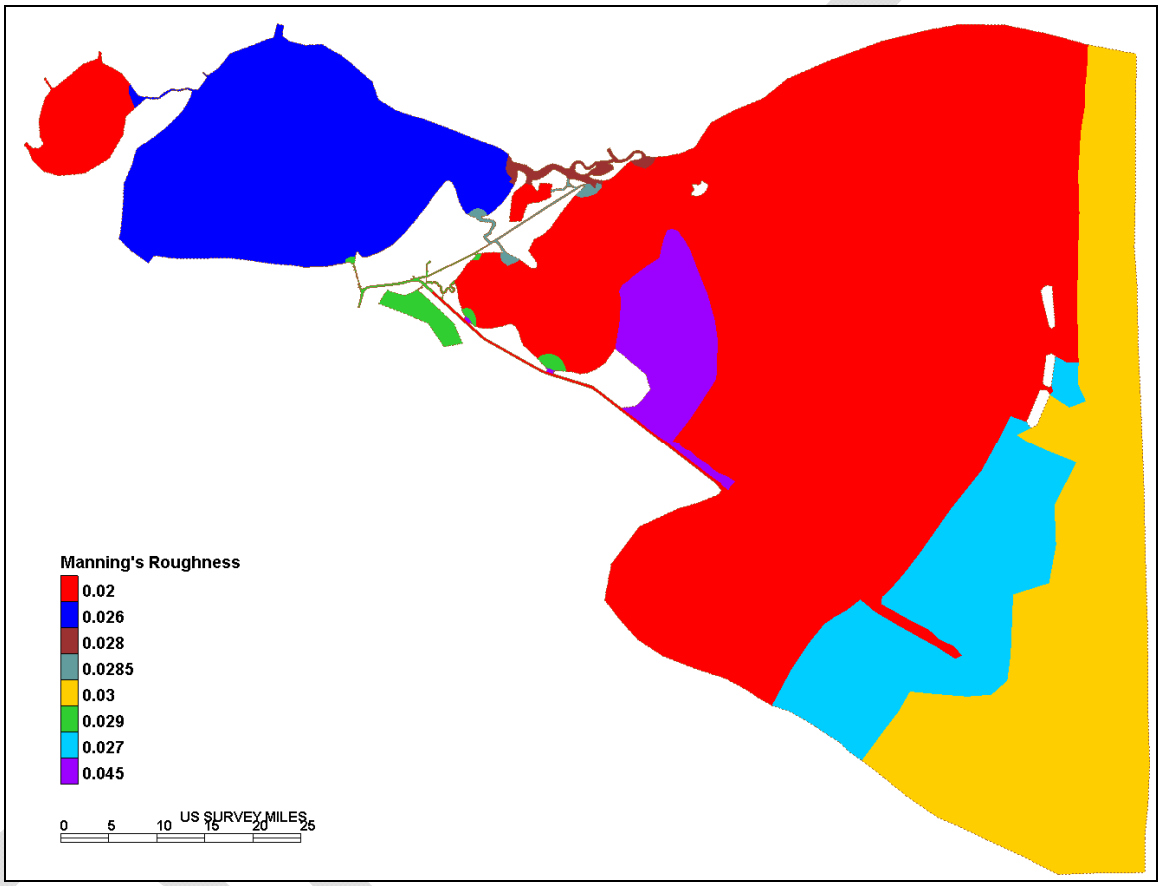

Figure 2-2. Manning's Roughness Values

Boundary Conditions

Boundary conditions for this model include river inflows, tidal water surface elevations, and wind forcings. This information is needed for August 2007 through October 2008 in order to perform the analyses and the model validation. The validation period is January through October 2008. The data used for validation was obtained from several sources.

The river inflows to the model domain are taken from the U.S. Geologic Survey streamflow database. Daily average values are applied to the model at six locations: the Pearl River, the Amite River, the Blind River, the Tchefuncte River, the Tickfaw River, and the Tangipahoa River. The locations of these rivers are shown in Figure 2-3. Flow from the Mississippi River into the Gulf of Mexico is accounted for in the tidal boundary condition since it does not enter directly into the model domain. Ungaged flows are not factored into the model, which includes any flow through the wetland areas along the Mississippi River. The 2008 flows for each of the rivers are shown in Figure 2-4. The Blind River was not included on the plot as it was a constant flow of 216 cfs as determined from previous work due to the lack of data at this location (McAnally et al. 1997). Time 0 corresponds to 12:00 AM on January 1 for all figures, unless otherwise stated.

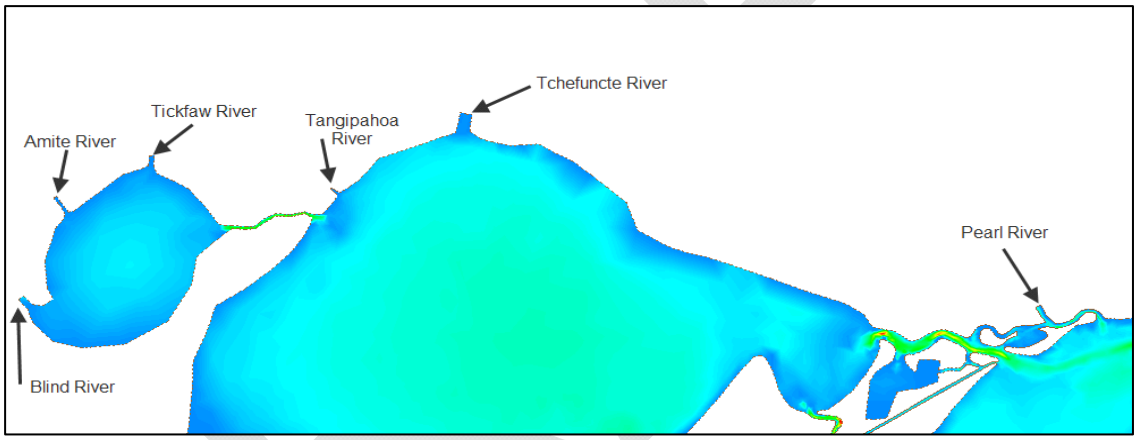

Figure 2-3. Location of river inflows

DRAFT

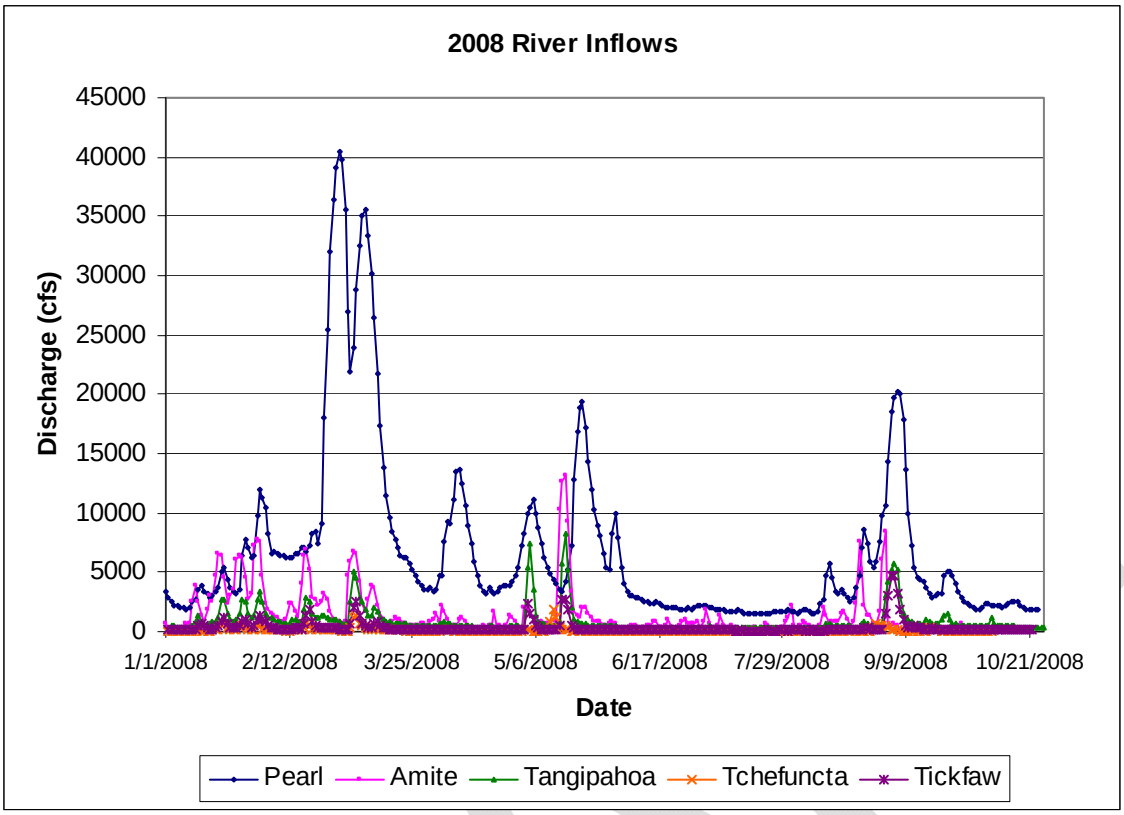

Figure 2-4. River inflow discharges for 2008

The tidal forcings for the hydrodynamic model are generated using 2008 NOAA gage data from Gulfport Harbor (gage #8745557) and Pilots Station East, SW Pass (gage #8760922). Figure 2-5 shows the location of these points as the red dots. This figure was taken from NOAA. The time series for the endpoints of the tidal boundary are shown in Figure 2-5 along with the tide boundary condition at a location at the boundary midpoint. The harmonic constituents and the non-predicted signal (the difference between the predicted value based on tidal constituents and the observed value which includes winds and other factors) for each station are used to generate a tidal forcing or water surface elevation at each node along the tidal boundary over the time of the simulation. The values for each node are determined by performing a linear interpolation of the amplitude and phase for each tidal constituent as well as for the nonpredicted signal. The tide is then reconstituted at each location along the boundary using these interpolated parameters.

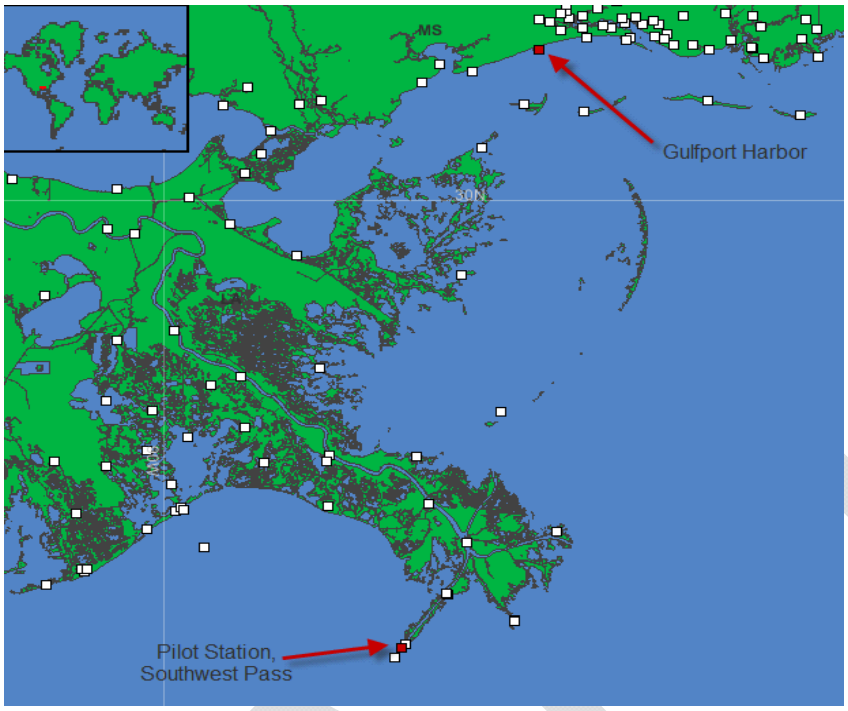

Figure 2-5. Gage locations for development of tidal boundary

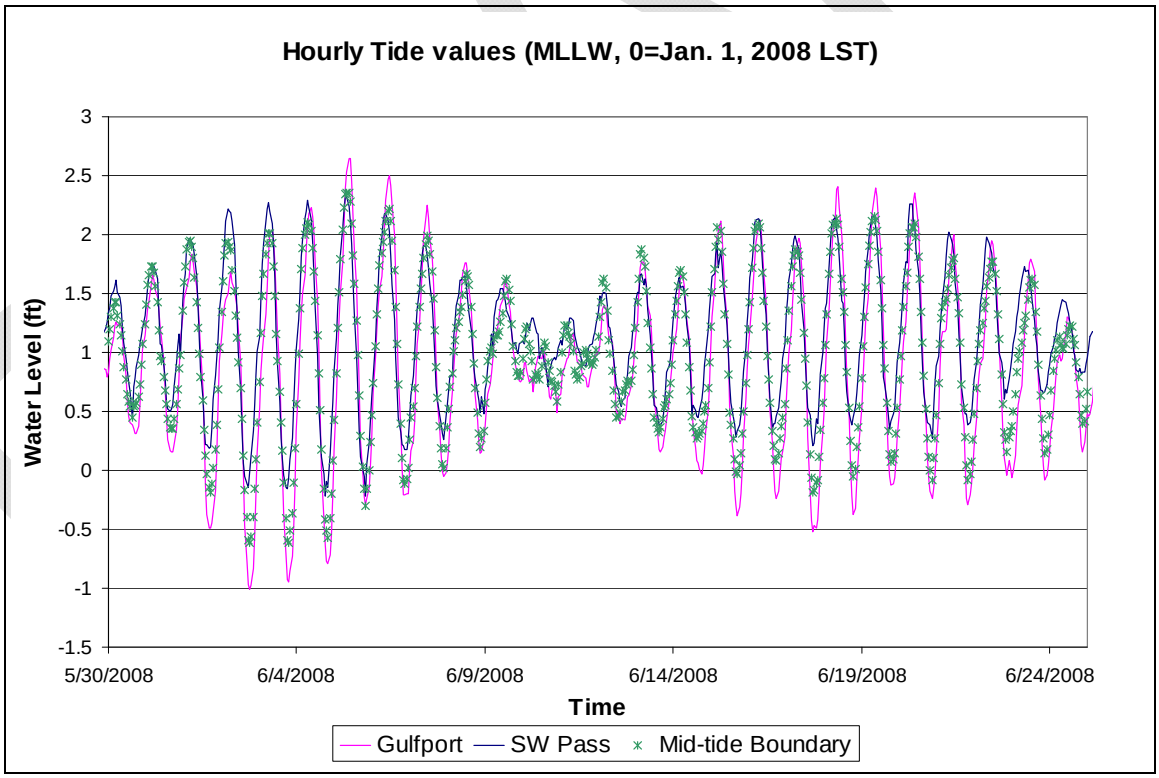

Figure 2-6. End points and mid point of tidal boundary

The wind data used were obtained from the Joint Air Force and Army Weather Information Network and the Air Force Combat Climatology Center in Ashville, NC. These data are hourly surface winds at the New Orleans International Airport (Station 722310 – KMSY). The wind signal is interpolated using a polynomial interpolation for the wind signal components to fill any data gaps. Generally these gaps in the wind data are only on the order of 2 hours; however, there is a 25 hour gap due to machine malfunction during the September analysis period and a 7 hour data gap during the March period. ADH requires that the wind be applied to the model as a shear stress and there are several options for this calculation. The wind speed and direction for this study were converted to wind shear stress using the Wu formulations (Wu 1969). During 2008 the wind speeds rarely exceed 20 mph, although there are several storm events that increase the wind speed, especially during hurricane season. Figure 2-7 shows the location of the wind gage and Figure 2-8 shows the time varying wind speed and direction toward which it is blowing for 2008.

Figure 2-7. Location of New Orleans International Airport wind gage

DRAFT

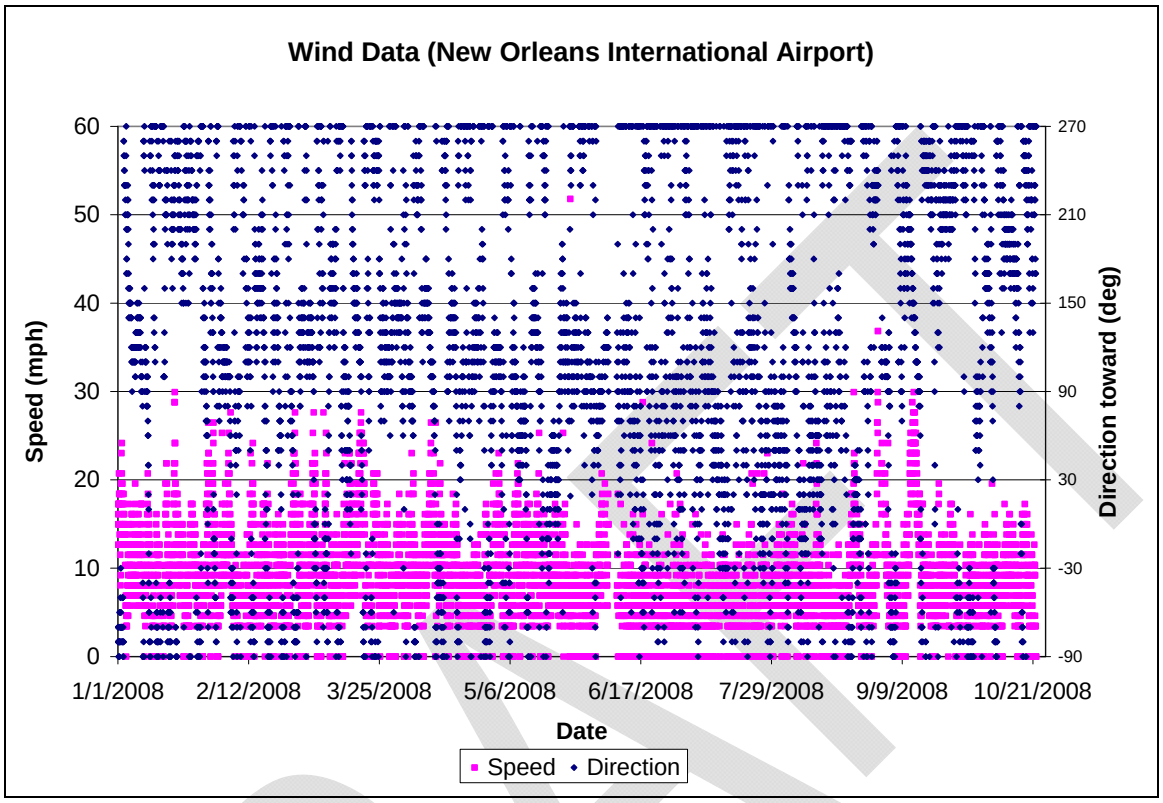

Figure 2-8. Wind speed and direction

DRAFT

3 Model Verification

The ADH model verification is performed using field data from several collection efforts and sources during calendar year 2008. The model results for water surface elevation, velocity, and flow direction are compared to the field at numerous locations, see data points 1 through 9 on Figure 3-1.

Water surface elevations were obtained from www.RiverGages.com which is maintained by the Corps of Engineers. Additional water levels were provided by the U.S Geological Survey (USGS). Figure 3-1 shows the locations of the water surface elevation gages used for model/field comparisons. The gage numbers are given in parenthesis.

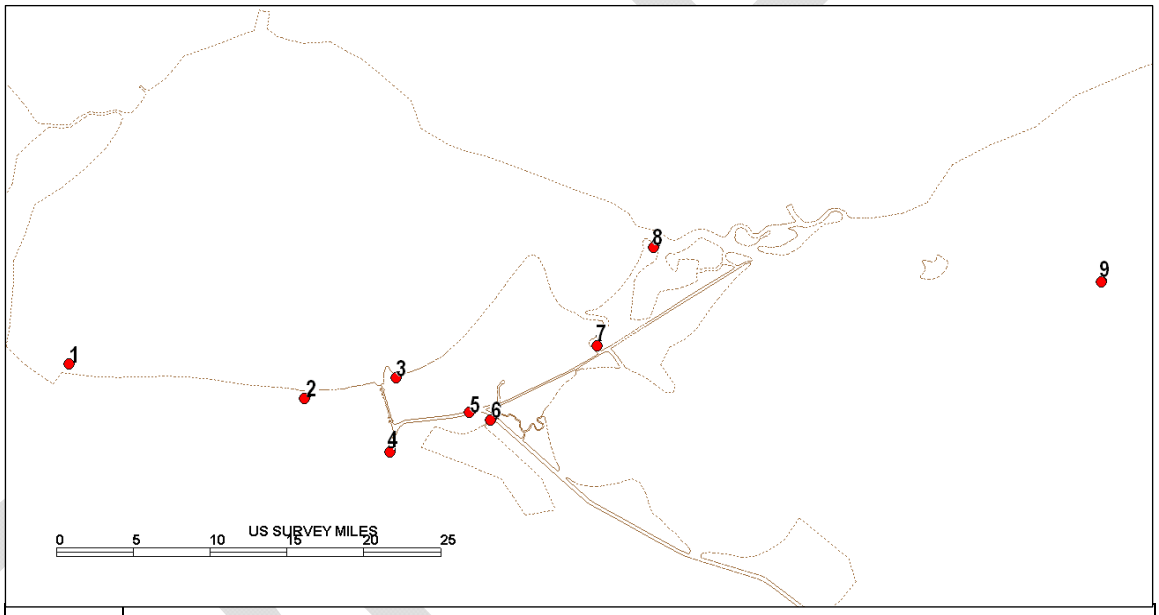

1	Lake Pontchartrain at Bonnet Carre Spillway (85555)
2	Lake Pontchartrain at West End (85625)
3	Lake Pontchartrain at Lakefront Airport (85670)
4	Inner Harbor Navigation Canal at South Lock (USGS) (76160)
5	Gulf Intracoastal Waterway at Paris Road (USGS) (073802338)
6	Bayou Bienvenue Floodgate East (76025)
7	Chef Menteur Pass near Lake Borgne (85750)
8	Rigolets near Lake Pontchartrain (85700)
9	Mississippi Sound at Grand Pass (3007220891501)

Figure 3-1. Water surface elevation field data locations

ADCP discharge and velocity measurements around the intersection of the GIWW and MRGO were collected by ERDC-CHL during 31 July and 13-14 August, 2008. Another collection of ADCP discharges and velocity data was made along the IHNC near Seabrook during 16-17 October 2008. The red lines in Figures 3-2 and 3-3 give the locations of the flow data obtained by ERDC-CHL during these collection efforts. The IHNC collection at Seabrook included 12 passes at each transect over a 25 hour period. The July data collection along the MRGO and GIWW included 4 passes along each transect over a 7 hour period and the August data collection included 9 or 10 passes at each transect over a 25 hour period.

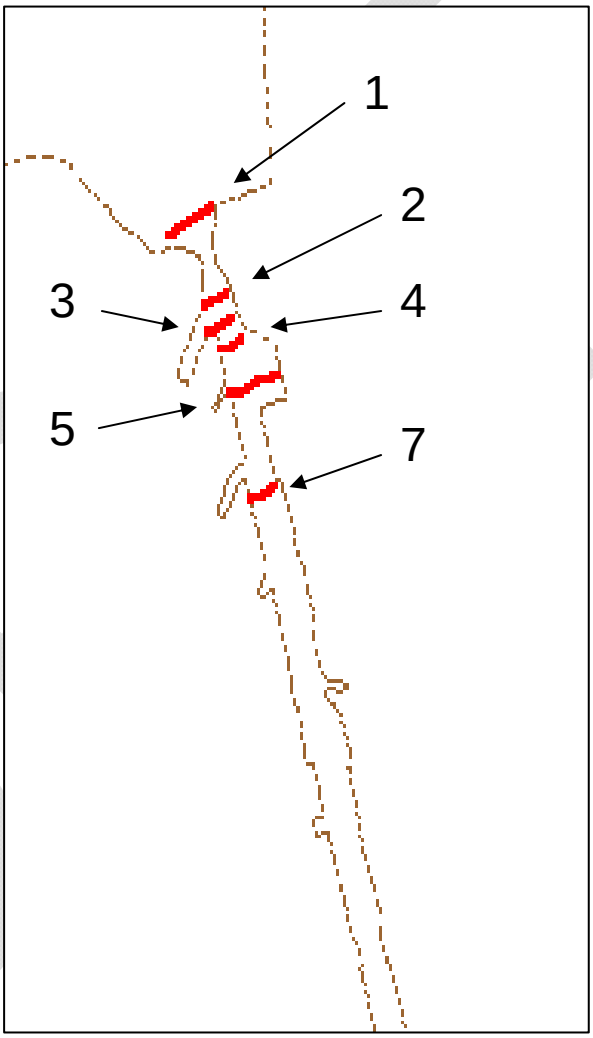

Figure 3-2. Discharge field measurement transects for Seabrook

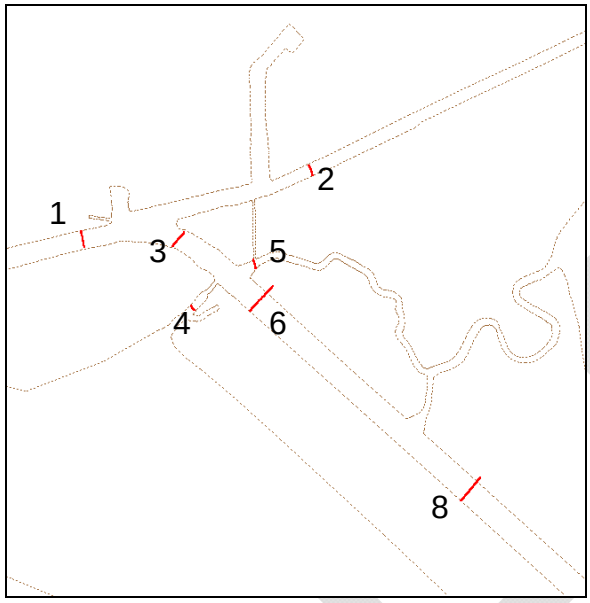

Figure 3-3. Discharge field measurement transects for GIWW/MRGO area

Model/Field Comparisons

Figures 3-4 through 3-12 show the field water surface elevations in blue and the model predicted results in pink. The comparisons shown here are taken for a specific period during the entire year-long simulation (Jan. 23 – Mar. 30, 2008). Although only this subset is shown, the model/field comparisons are made for the entire data set. The vertical scale is set to a constant range from -1 to 3 ft and the only differing horizontal scale is the gage at Grand Pass due to data only being available late in the year (see Figure 3-1).

The model is driven with a tidal elevation along the Gulf boundary and wind shears from data obtained at New Orleans International airport. Although there are river inflows, the tidal boundary is the dominant component. Therefore the comparison at Grand Pass is important for ensuring that the signal is being properly applied to the model. Figure 3-4 shows the comparison of the water level at this location (point 9 in Figure 3-1). On approximately October 9, 2008 there is a shift in the gage datum. Upon inspection, the model continues to reproduce the pattern of the water surface elevation and the signal would have to be shifted at this time to show a realistic comparison.

Progressing further into the system, the gages at Riogolets (Figure 3-5) and at Chef Menteur (Figure 3-6) are analyzed. The model predicts larger water surface

DRAFT

elevation changes at Rigolets than those observed in the field. This gage is actually located in a small waterway that extends from the main channel that is not included in the mesh domain. The field data shown here is that for the channel center. It is not surprising that the data at the actual gage location is different from that obtained from the model due to these differences. The model/field comparison at Chef Menteur, however, is very good, with the model accurately representing the tide range.

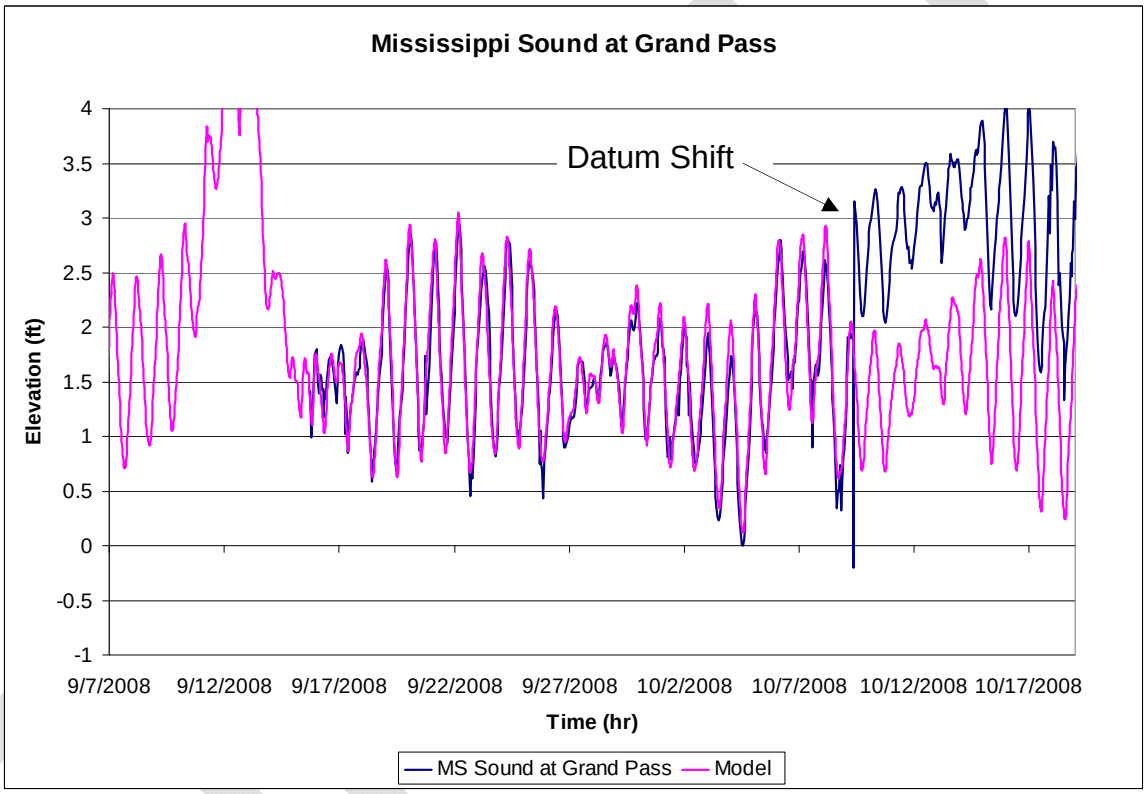

Figure 3-4. Mississippi Sound at Grand Pass water surface elevation

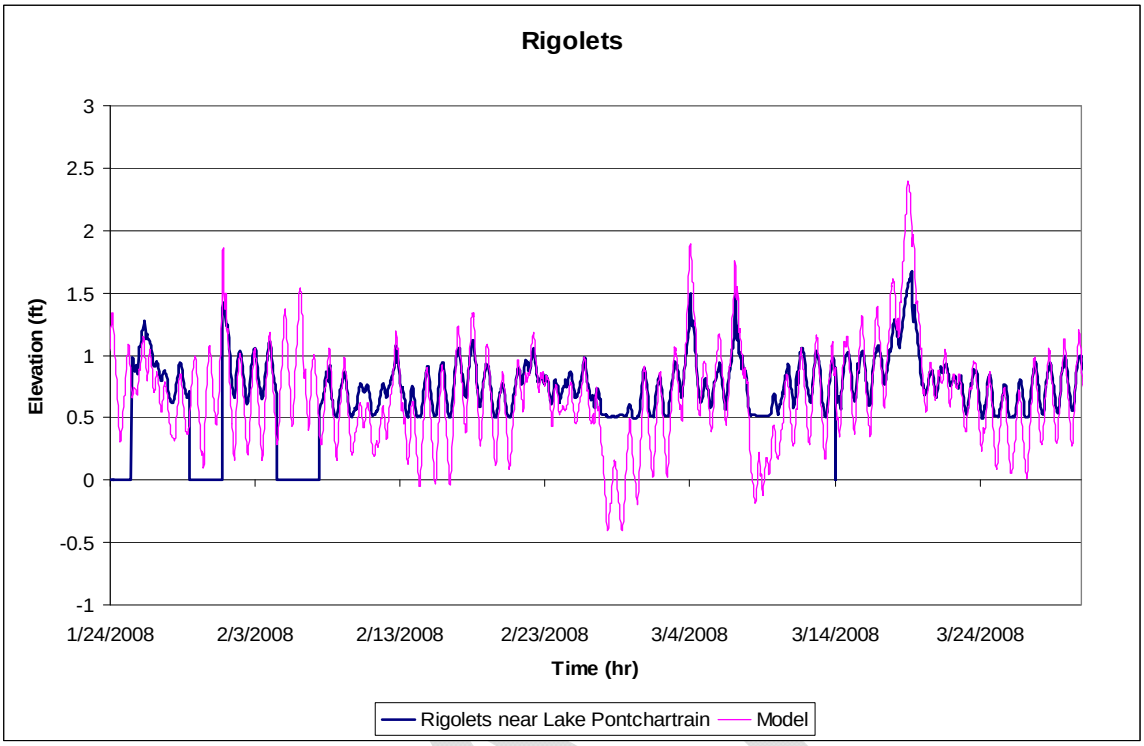

Figure 3-5. Rigolets water surface elevation

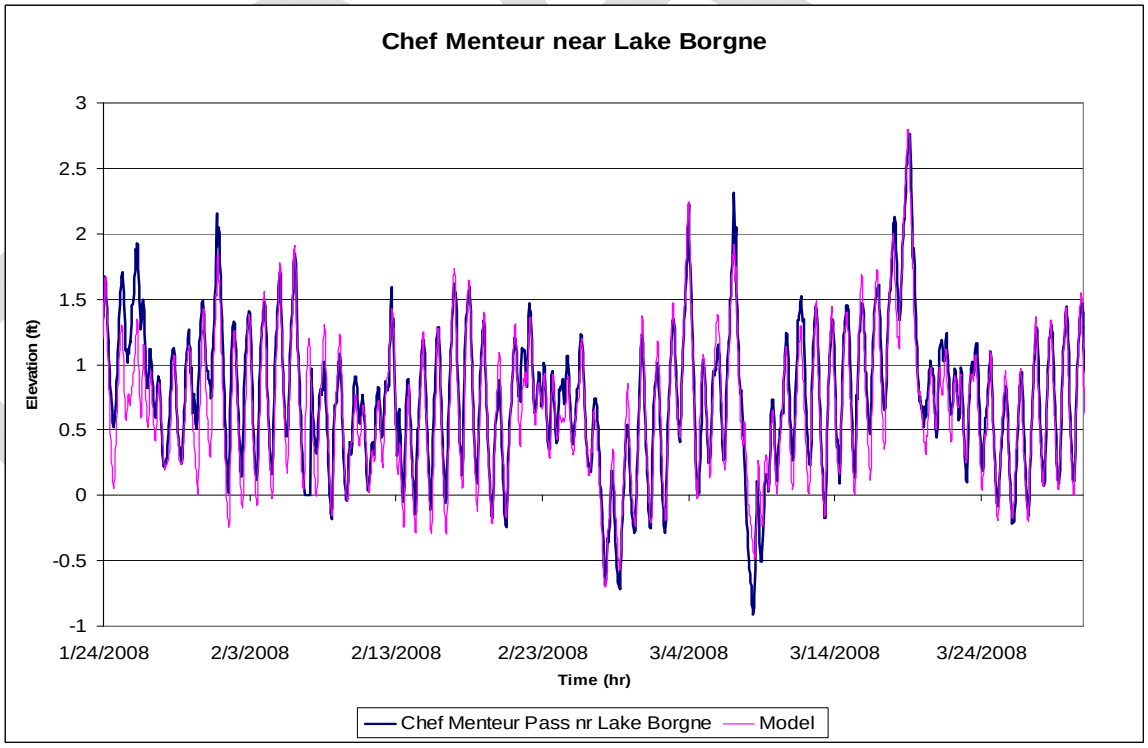

Figure 3-6. Chef Menteur water surface elevation

The gage at Paris Road is located in the GIWW just west of its connection to the MRGO (point 5 on Figure 3-1). This comparison is given in Figure 3-7. Although some of the low range amplitudes are not reproduced, the overall comparison is very good at this location. The low range amplitudes are also missed in the model at the IHNC gage located at the lock on the southern end of the IHNC (point 4 on Figure 3-1) as seen in Figure 3-8. Due to the lock closure and the ADH model not including the details of this structure, reflections and 3-dimensional effects can get produced in the field that are not captured in a 2-dimensional depth averaged model which have an effect on the water levels. The pattern of the water level changes is matched and the higher level amplitudes are better captured in the model.

One gage exists within the model domain at Bayou Bienvenue on the west side of the MRGO (point 6 on Figure 3-1). This comparison is given in Figure 3-9. In the model, this marsh area west of the MRGO (typically known as the Central Wetlands) is described as a storage area and is not detailed due to there being no available bathymetry data for the area. The gage at this location shows that the model is replicating the exchange into this area which is important in the transport of particles as this study is intended.

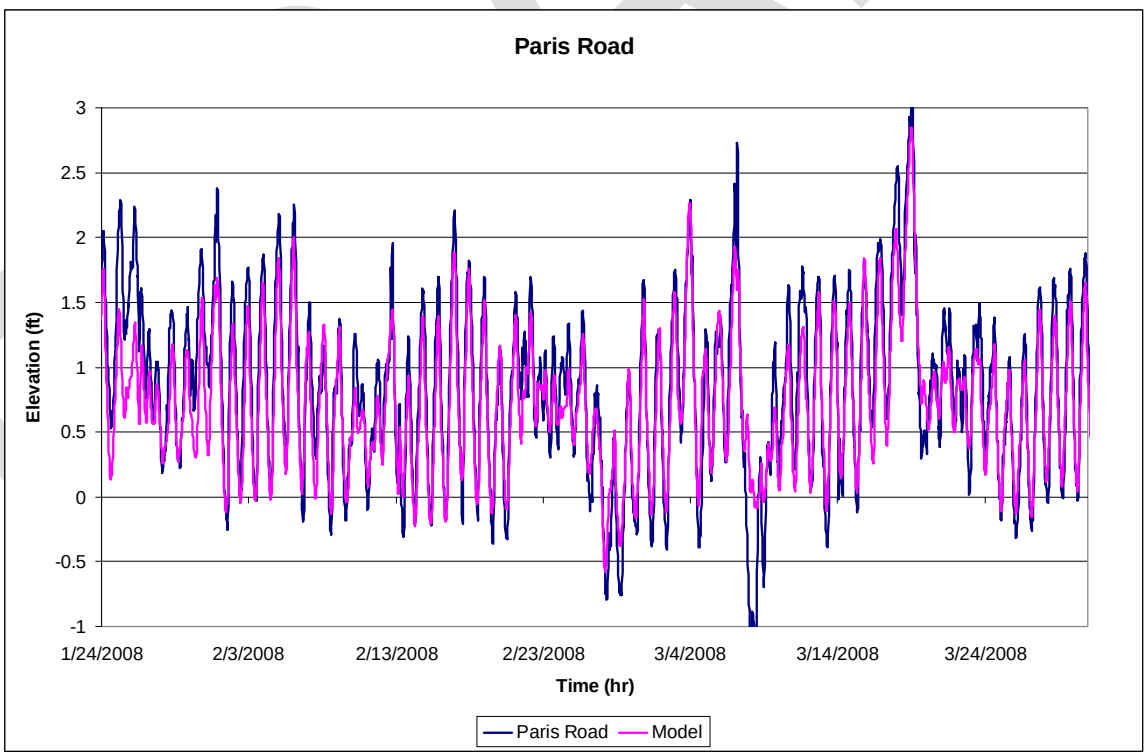

Figure 3-7. Paris Road water surface elevation

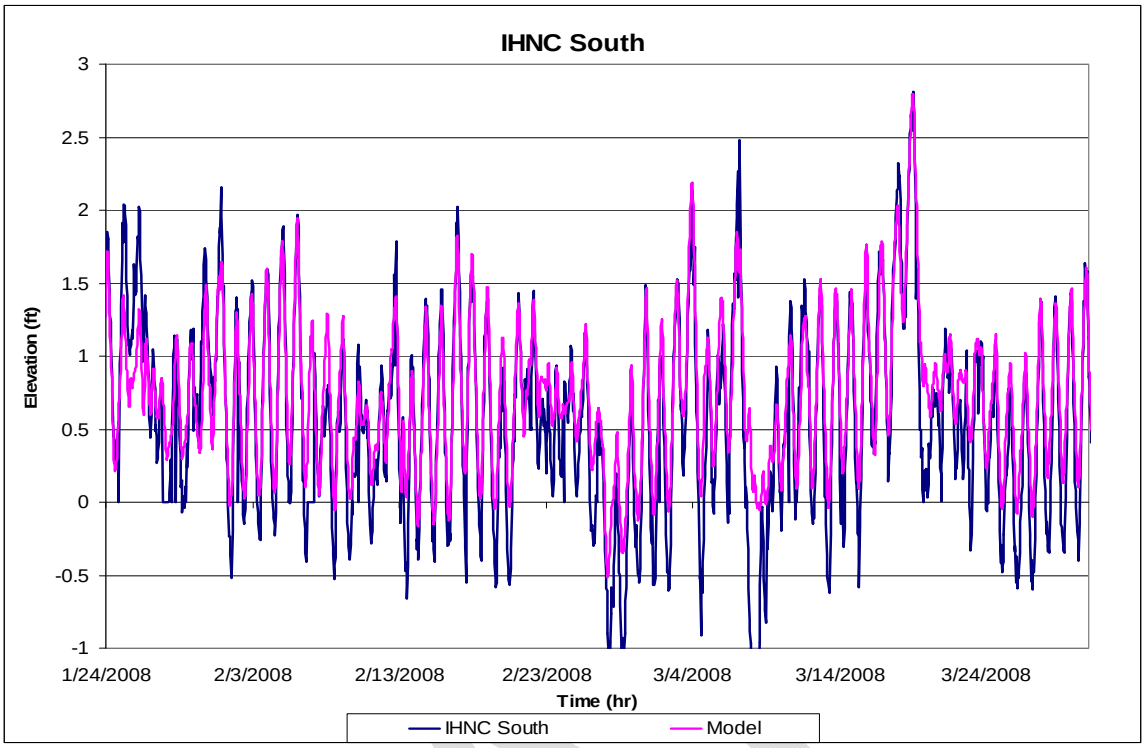

Figure 3-8. IHNC South Lock water surface elevation

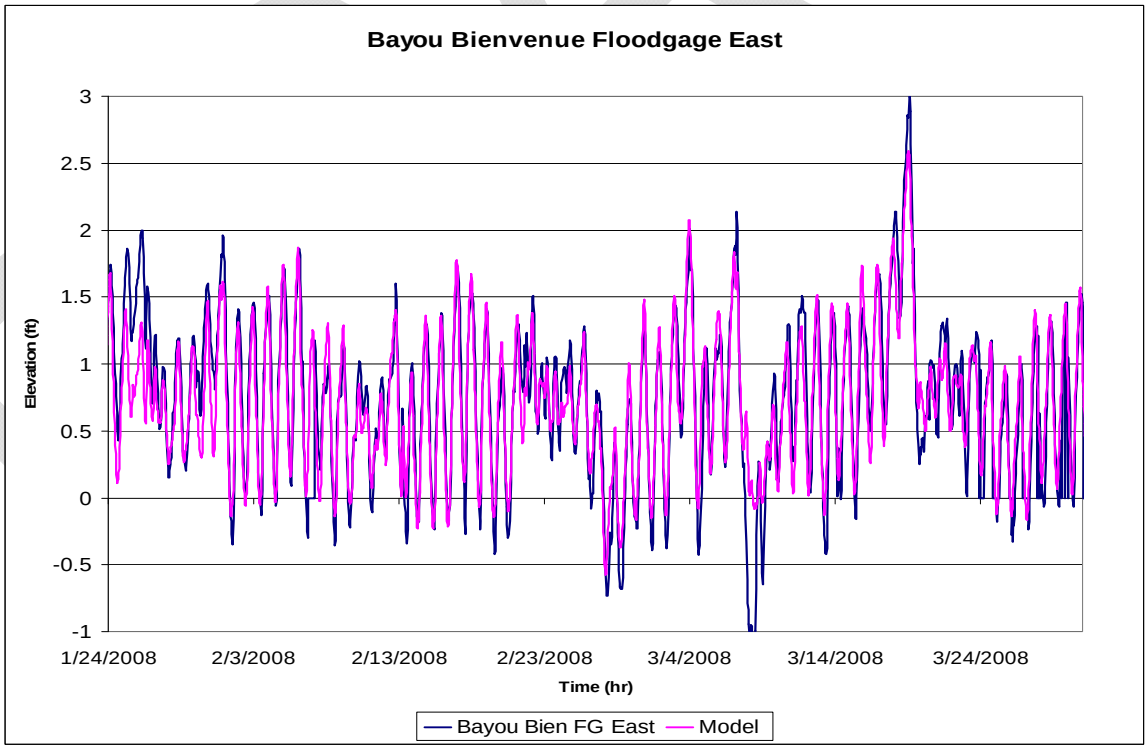

Figure 3-9. Bayou Bienvenue East water surface elevation

The final water surface elevation gages available to compare with model results are located in Lake Pontchartrain (points 1, 2, and 3 on Figure 3-1). Figure 3-10 shows the elevations at the Bonnet Carre Spillway, Figure 3-11 shows those at West End, and Figure 3-12 shows them at Lakefront Airport. The overall amplitude of the water surface elevations is lower in the lake than they are elsewhere. As with the gage at Rigolets, the gages at West End and Lakefront Airport are not located within the model domain. In order to get a comparison, data from the model was taken just within the domain at these locations. Therefore the model/field comparison analysis should consider this difference in the comparison locations. Overall the comparisons at these three gages are good. There are events when the highs or lows are not reproduced fully, but the comparison is acceptable for the intent of this project.

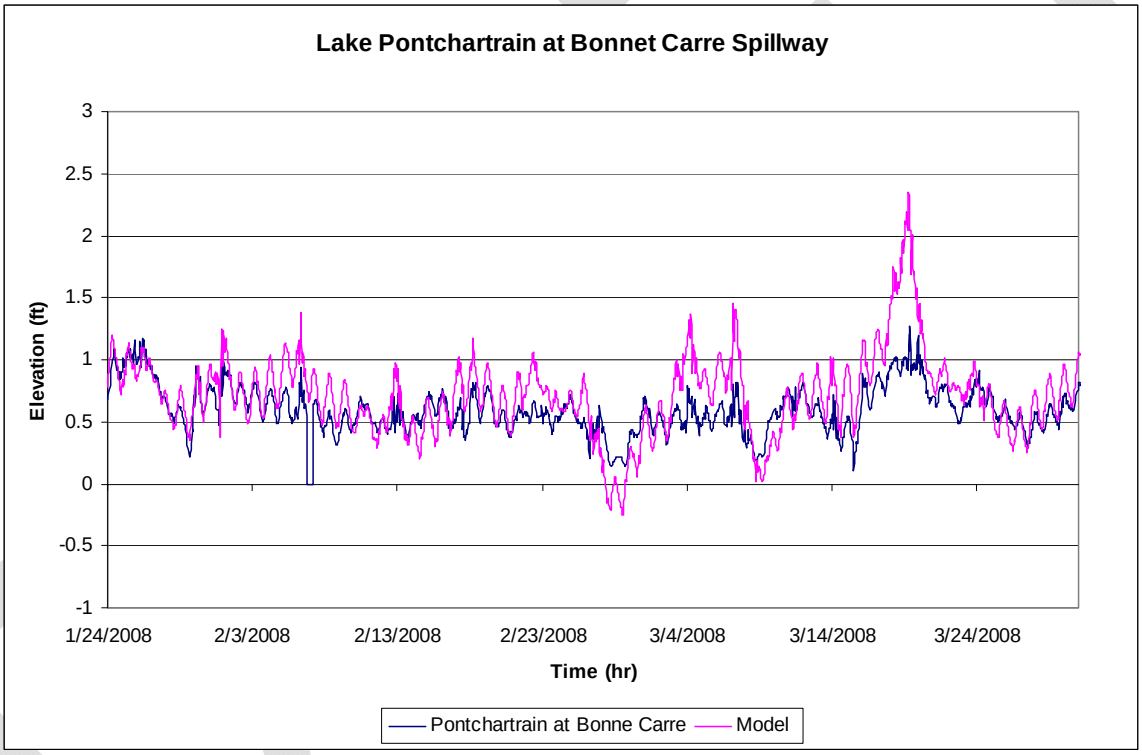

Figure 3-10. Bonnet Carre water surface elevation

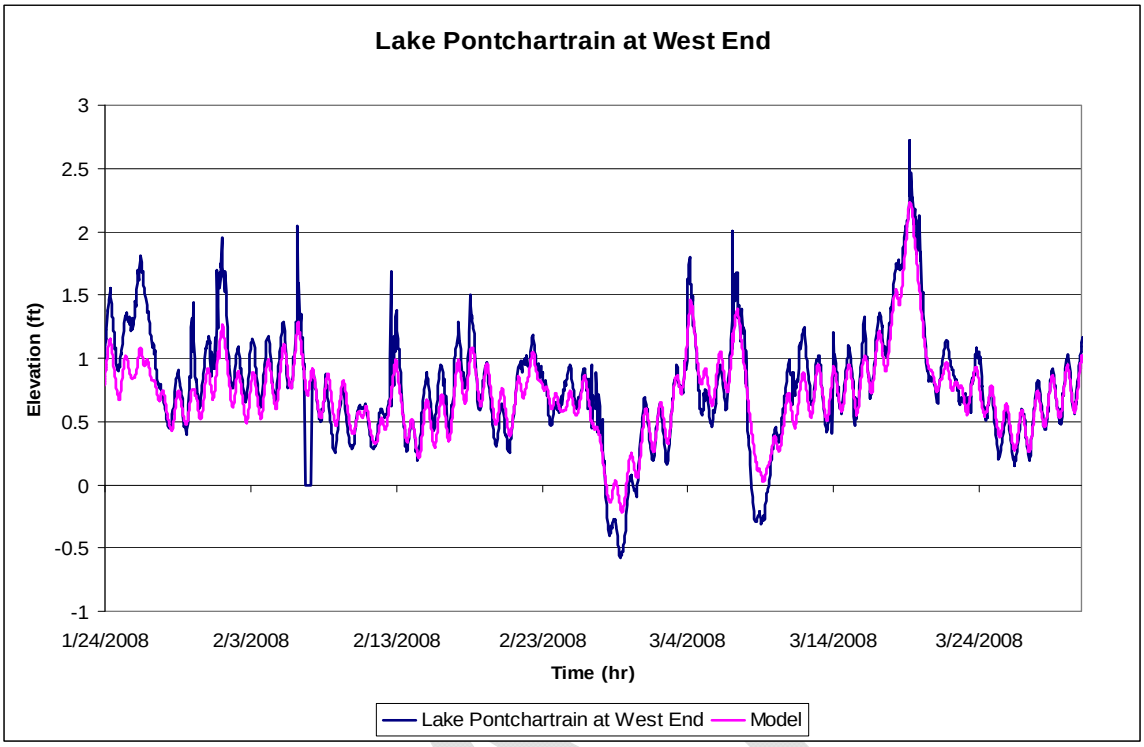

Figure 3-11. West End water surface elevation

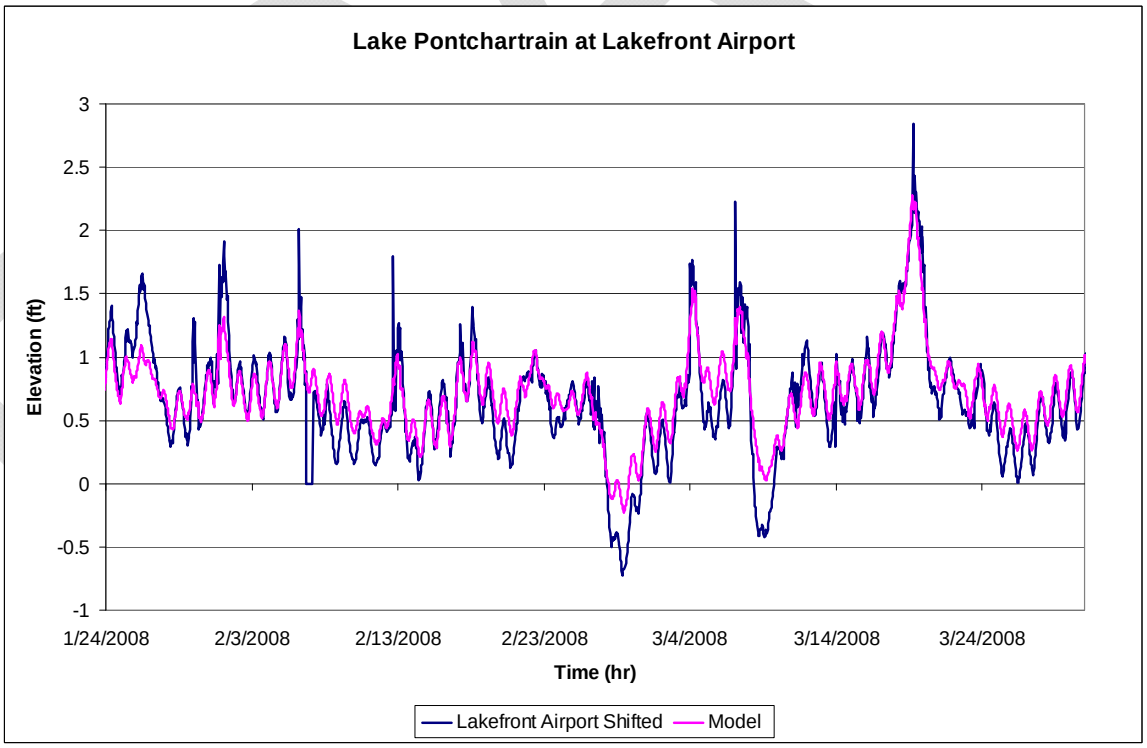

Figure 3-12. Lakefront Airport water surface elevation

A second comparison is made on the water surface elevation computations at selected stations. This comparison is performed on the amplitudes of the major tidal constituents. The constituents chosen for the comparison are those used in ADCIRC modeling simulations – M2, S2, N2, K2, O1, K1, Q1, M4, and M6. These constituents describe different influences on the tide, such as the lunar (M2, N2, O1, K1, Q1) or solar (S2) components or semi-diurnal (M2, S2, N2, K2) or diurnal (O1, K1, Q1) components. Shallow water overtides are include in the M4 and M6 components. A complete description of the tidal constituents can be found at http://co-ops.nos.noaa.gov/harmonic_cons_defs.html. The periods of these signals are given in Table 3-1. The stations where these comparisons are made are Grand Pass, Paris Road, Chef Menteur, and Lake Pontchartrain at West End. See Figure 3-1 for the location of each station. Figures 3-13 through 3-16 show the amplitude comparison for the field and model water surface signals. Table 3-2 gives a summary of amplitude values for the field and model as well as a percent difference between the two. The most significant components are O1 and K1 for all locations. The maximum difference for these constituents is 16.5%. An occasional difference of 15-20% falls within an acceptable range for the project's intent. There are larger differences in constituents that contribute much less to the overall tidal signal. Although some constituents compare better than others , the overall replication is good for the numerical model.

Table 3-1. Tidal Constituents

Constituent	Period (hr)
M2	12.4206
S2	12
N2	12.65835
K2	11.96723
O1	25.81934
K1	23.93447
Q1	26.86836
M4	6.2103
M6	4.1402

DRAFT

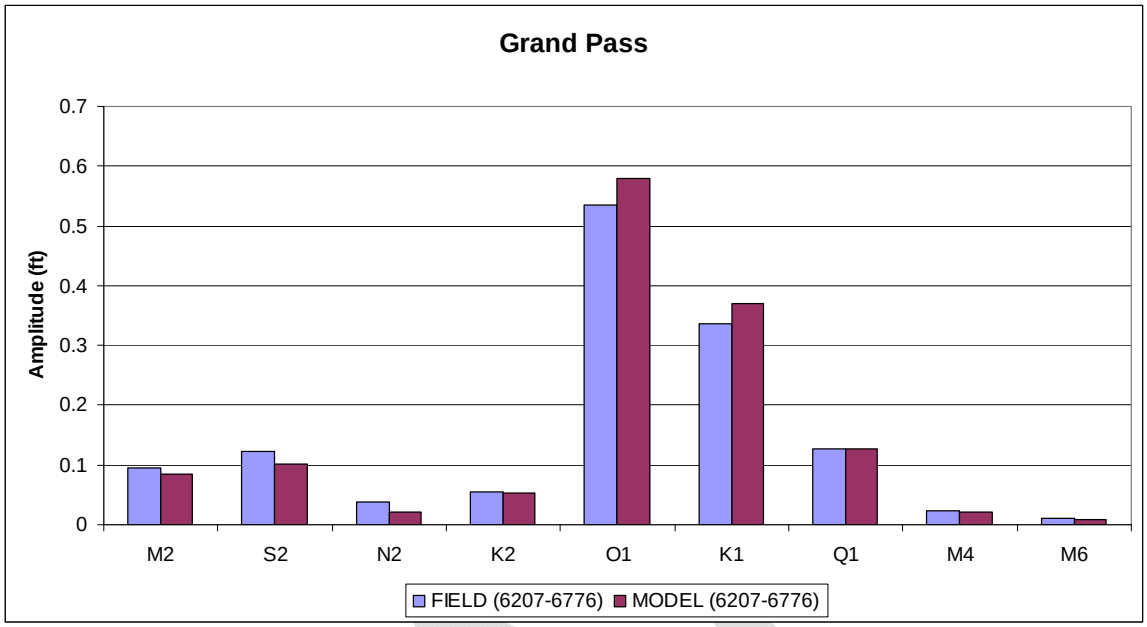

Figure 3-13. Tidal constituent comparison of amplitude at Grand Pass

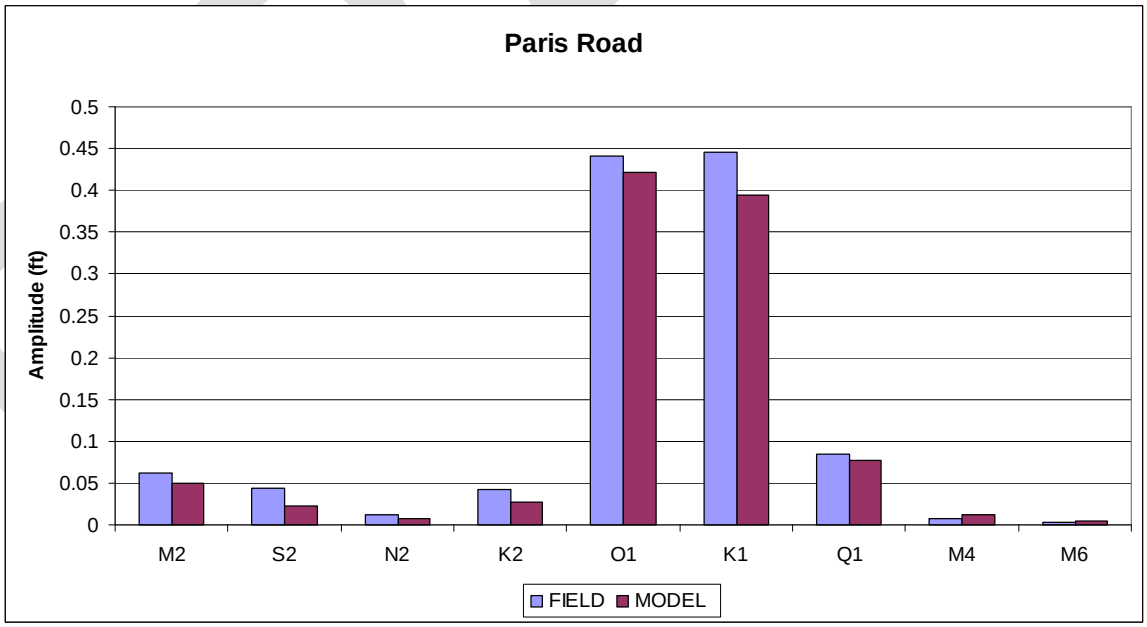

Figure 3-14. Tidal constituent comparison of amplitude at Paris Road

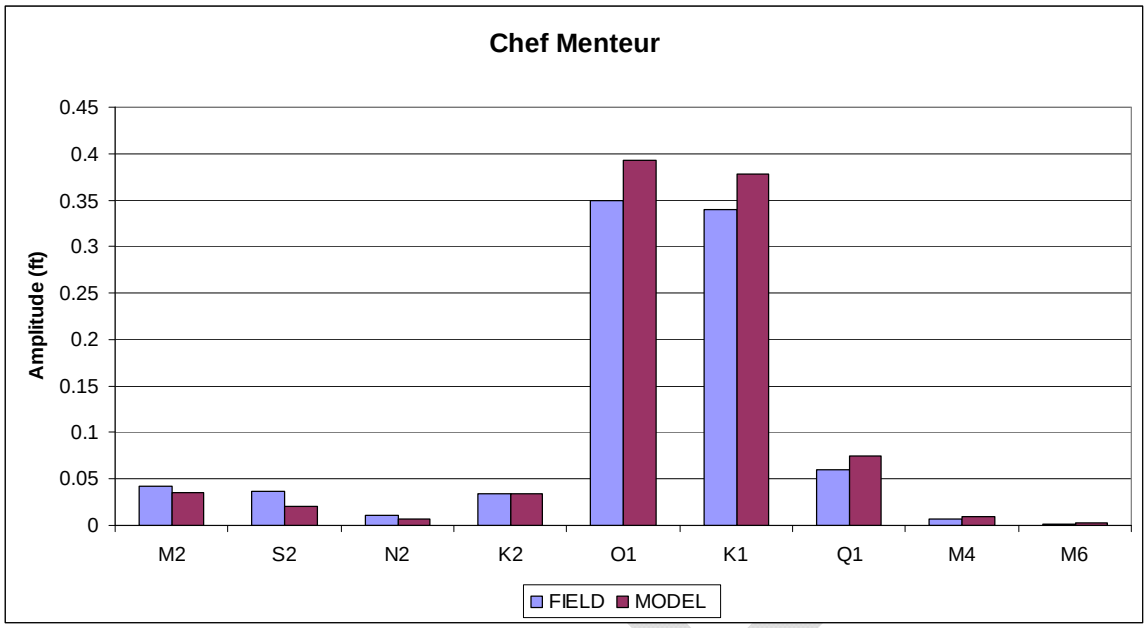

Figure 3-15. Tidal constituent comparison of amplitude at Chef Menteur

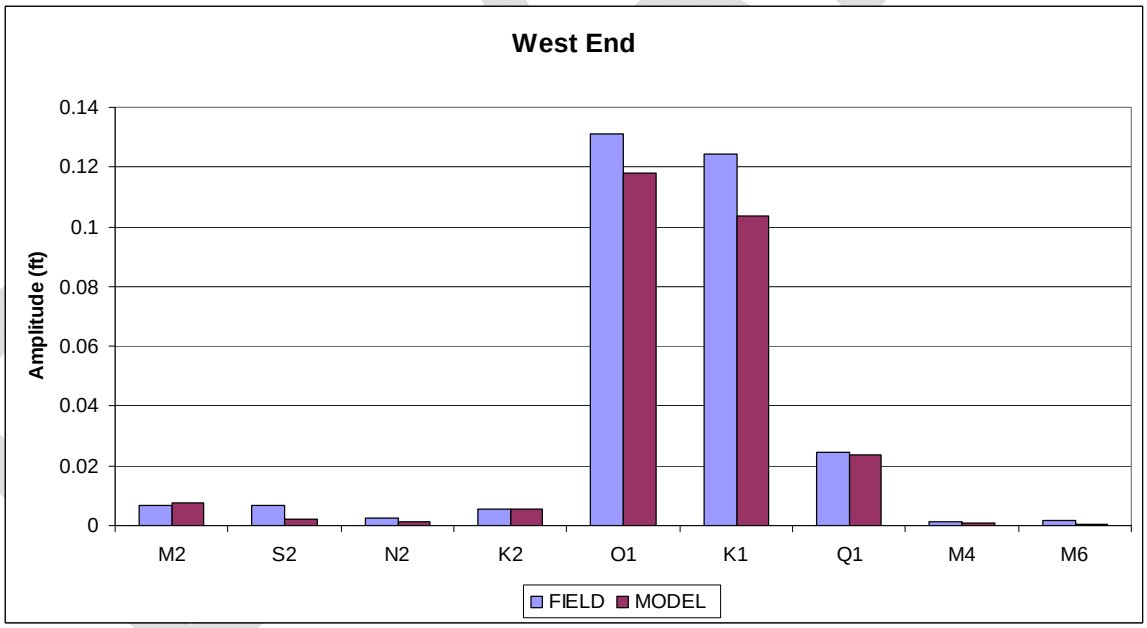

Figure 3-16. Tidal constituent comparison of amplitude at West End

Table 3-2. Tidal Constituent Amplitude Comparisons (ft)

Consti-tuent	Grand Pass			Paris Rd.			Chef Menteur			West End		
	Field	Model	% Diff	Field	Model	% Diff	Field	Model	% Diff	Field	Model	% Diff
M2	0.312	0.274	-12.07	0.205	0.161	-21.17	0.138	0.114	-17.78	0.023	0.025	9.52
S2	0.403	0.333	-17.27	0.145	0.076	-47.55	0.121	0.065	-45.97	0.023	0.007	-67.77
N2	0.127	0.066	-47.86	0.037	0.025	-32.27	0.036	0.022	-39.33	0.009	0.004	-60.15
K2	0.179	0.173	-3.53	0.140	0.091	-35.27	0.111	0.113	1.35	0.018	0.018	3.16
O1	1.757	1.902	8.23	1.445	1.381	-4.43	1.146	1.290	12.55	0.431	0.387	-10.06
K1	1.106	1.217	10.04	1.464	1.295	-11.53	1.116	1.241	11.14	0.407	0.340	-16.49
Q1	0.413	0.416	0.54	0.277	0.255	-7.86	0.198	0.244	23.36	0.081	0.077	-4.40
M4	0.076	0.067	-12.40	0.027	0.041	49.90	0.023	0.033	39.44	0.004	0.002	-47.34
M6	0.036	0.025	-30.06	0.011	0.014	23.52	0.003	0.007	146.42	0.006	0.002	-67.48

The discharge comparisons are made for the transects shown in Figure 3-2. Figures 3-17 through 3-19 give the field value (points) of the total flow passing each transect as well as the model results over time (lines). Flow is positive when moving towards the north or east and negative when moving towards the south or west. The ADH model is reasonably accurate in reproducing the circulation direction and general percentage flow split between the GIWW and MRGO. Field discharge measurements are affected by many things such as instrumentation limits as well as the limitations caused by the physical nature of where the data is being collected. Although recent bathymetry data was collected upstream of the locations on the MRGO, the bathymetry data at these locations is slightly older and the channel boundaries are used as model boundaries. It is likely that the flow at these locations is not as clear-cut as it is depicted in the model due to the marsh conditions in much of this area. The goal of this analysis is to get the trends and direction of the flow as accurate as possible. There is a variation in the comparison over the limited field samples. Figure 3-17 gives the model comparison to the field for transects 6 and 8 which are located along the MRGO. The model shows good agreement to the discharge magnitude and direction at these locations. Figure 3-18 shows the comparison at lines 4 and 5. These transects cross side channels and are low in flow magnitude. Due to Bayou Bienvenue flowing through a very marshy area which is not fully detailed in the model, this area is artificially widened so that the flow passage will include any water filtering in from the surrounding marsh. The model is able to reproduce the flow through these sections as shown in Figure 3-18, although the flow through Bayou Bienve-

DRAFT

nue is not as accurate as desired. Figure 3-19 shows the same comparisons at lines 1 and 2 along the GIWW and at line 3 at the north end of the MRGO. The flow split at this location is such that the flows passing lines 2 and 3 should equal the flow passing line 1. This is reproduced in the model as shown in Figure 3-19. It is in this area that the direction of flow becomes very important. The model is good at maintaining the overall magnitude and direction of the flow.

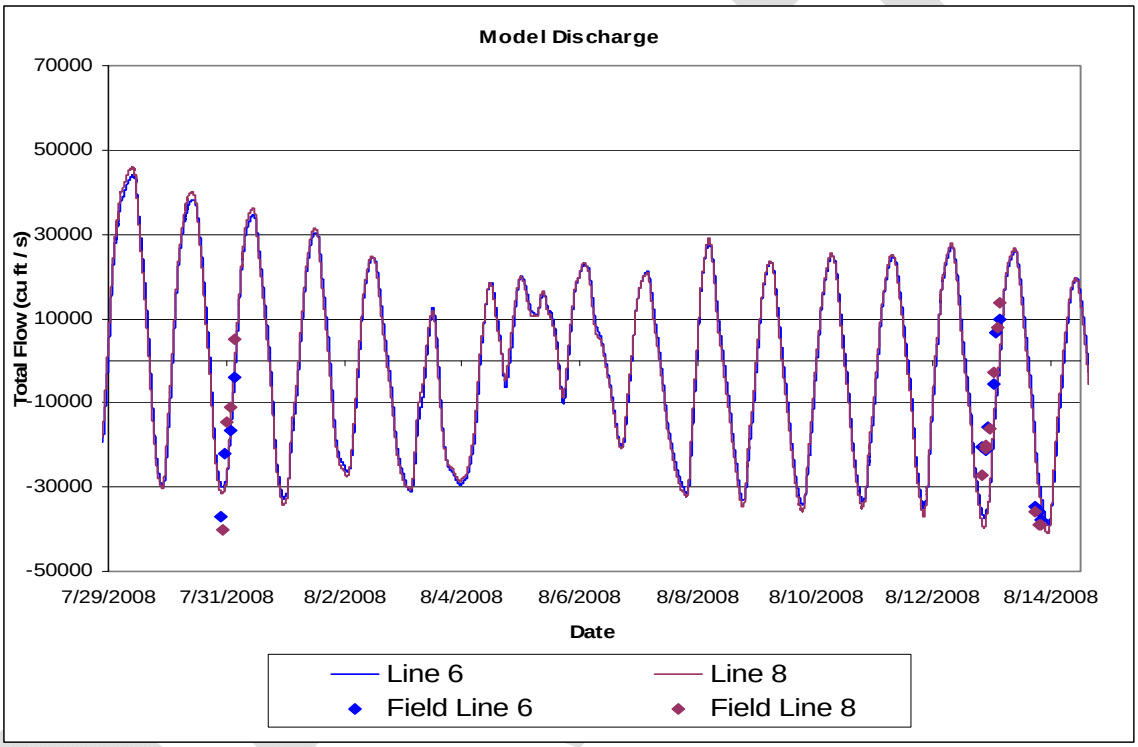

Figure 3-17. GIWW/MRGO discharge for lines 6 and 8

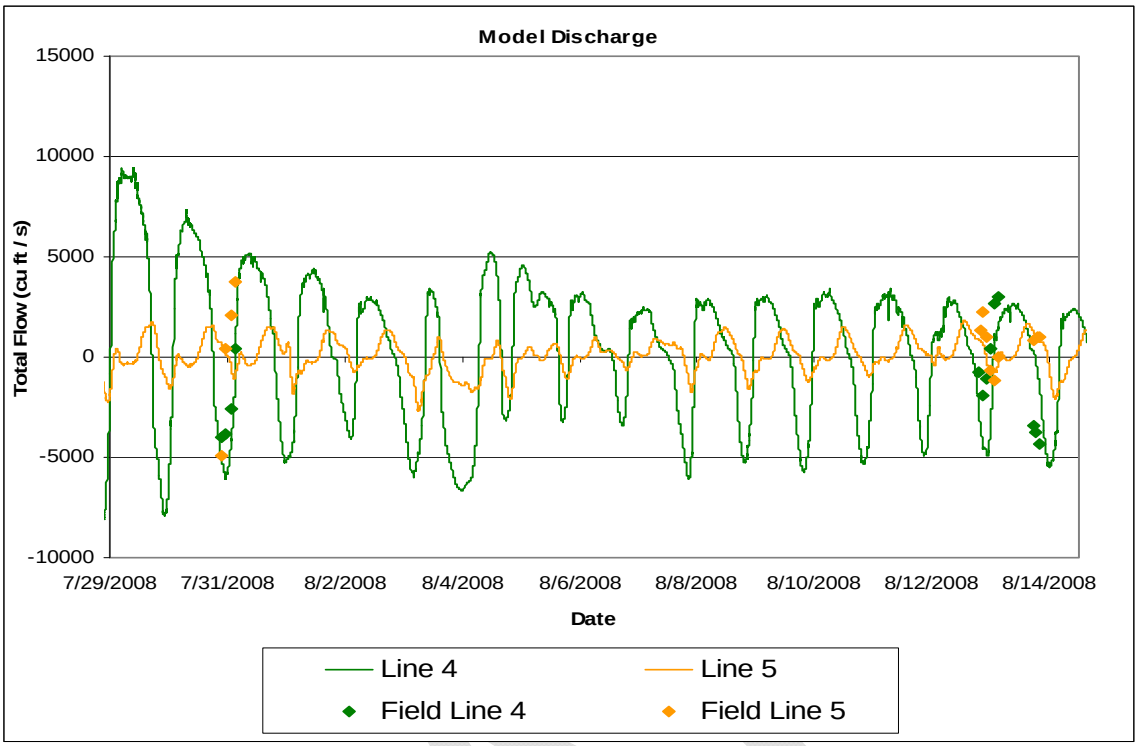

Figure 3-18. GIWW/MRGO discharge for lines 4 and 5

DRAFT

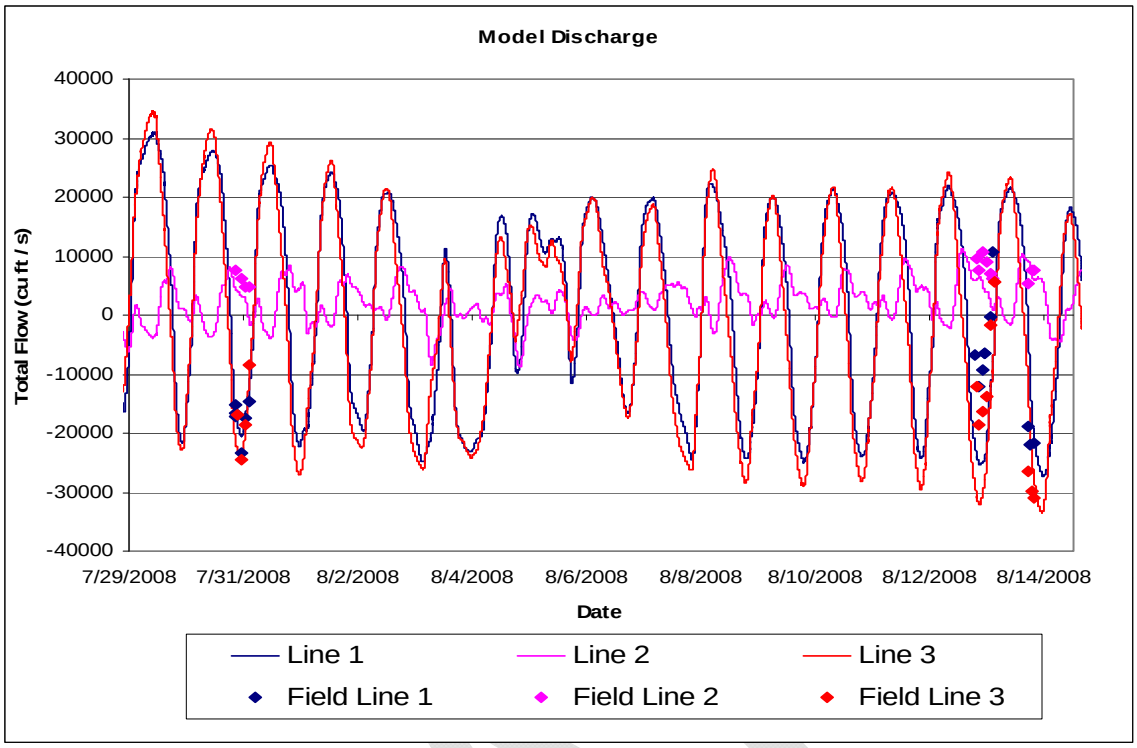

Figure 3-19. GIWW/MRGO discharge for lines 1, 2, and 3

Discharge and velocity comparisons are also performed in the Seabrook area of the IHNC. Figure 3-20 shows the total flow comparison of the model to the field values. Unfortunately no data were collected during the peak flow conditions and data were also only collected during times when the velocity direction was towards the south (positive values in Figure 3-20). Due to instrument limitations, field conditions, and assumptions that are made when obtaining discharge data, model to field comparisons within 20% are typically deemed acceptable, although dependent on the intended use of the model. The model produces flows in this area that are slightly higher than those found in the field but the comparison is within the generally accepted range and is therefore considered good. The velocity comparisons at these transects at various times are shown in Figures 3-21 through 3-24. The black arrows represent the model predicted velocity vectors and the red arrows represent the field data. Both sets of vectors are scaled so that the length of the arrows gives the magnitude of the flow. The direction of the flow and the location of eddies is reproduced well in the model, especially when the magnitude of the flows is large. At higher flow magnitudes, transport occurs more easily and the ultimate intent of this work is to model larval fish transport. Therefore, accuracy of magnitude and direction at higher flows is of great importance.

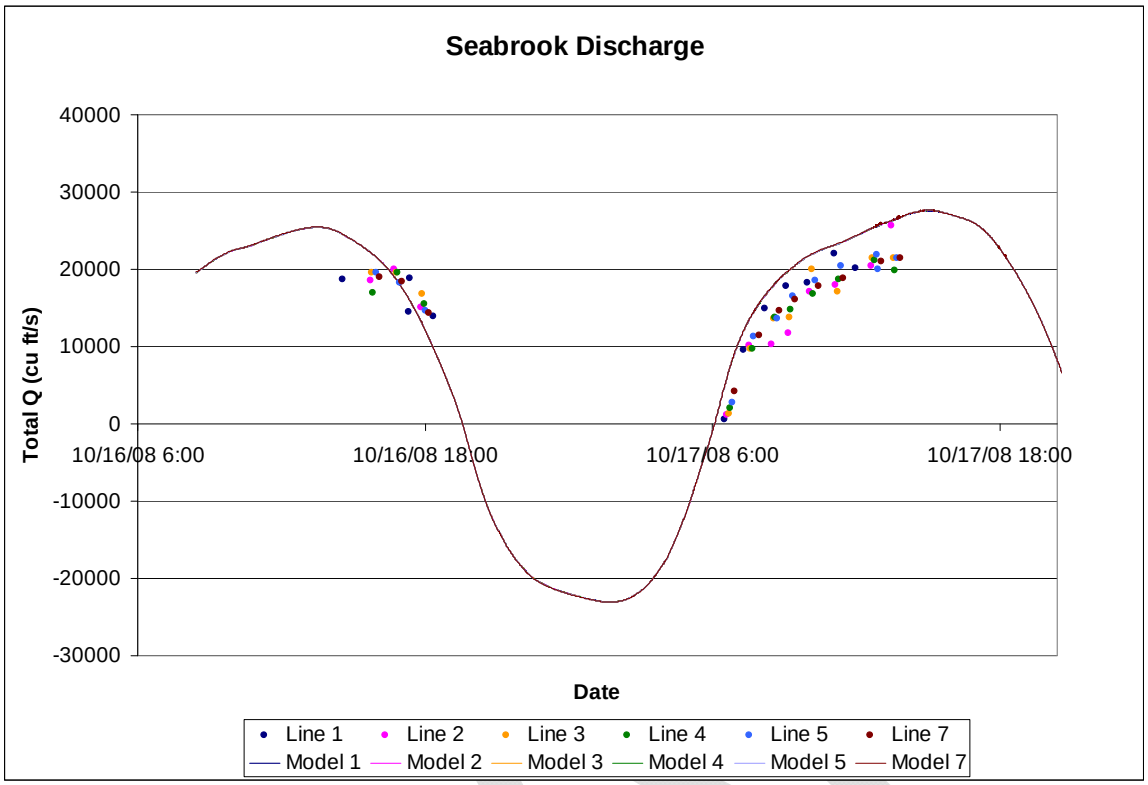

Figure 3-20. IHNC Seabrook discharge

Depth averaged velocity comparison during the time of the discharge comparisons in the GIWW/MRGO area are shown in Figures 3-25 through 3-32. The velocity magnitude is contoured according to the legend on the upper right. The length of the vectors in these figures is defined in the vector legend on the bottom left. The scale shows the length of a vector representing 4.0 ft/s. The general flow patterns are replicated in the model. The timing of the change in direction at locations 4 and 5 does lag the field slightly. However, the discharges are being reproduced within an acceptable range. Due to having no further data to compare to and other locations in the area producing good comparisons to the field, these differences in the model will be accepted.

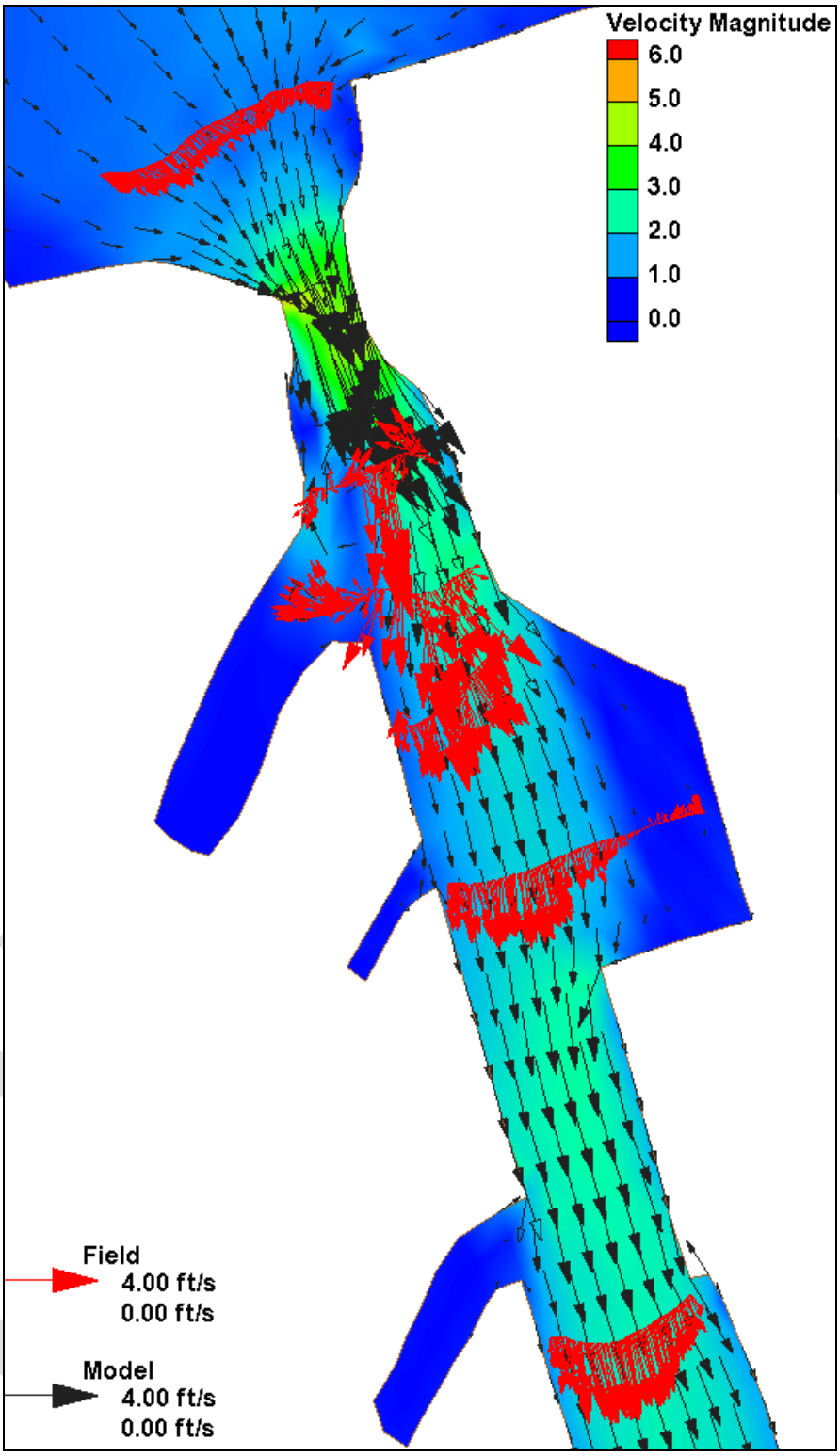

Figure 3-21. IHNC Seabrook velocity on October 16, 2008 at 15:33

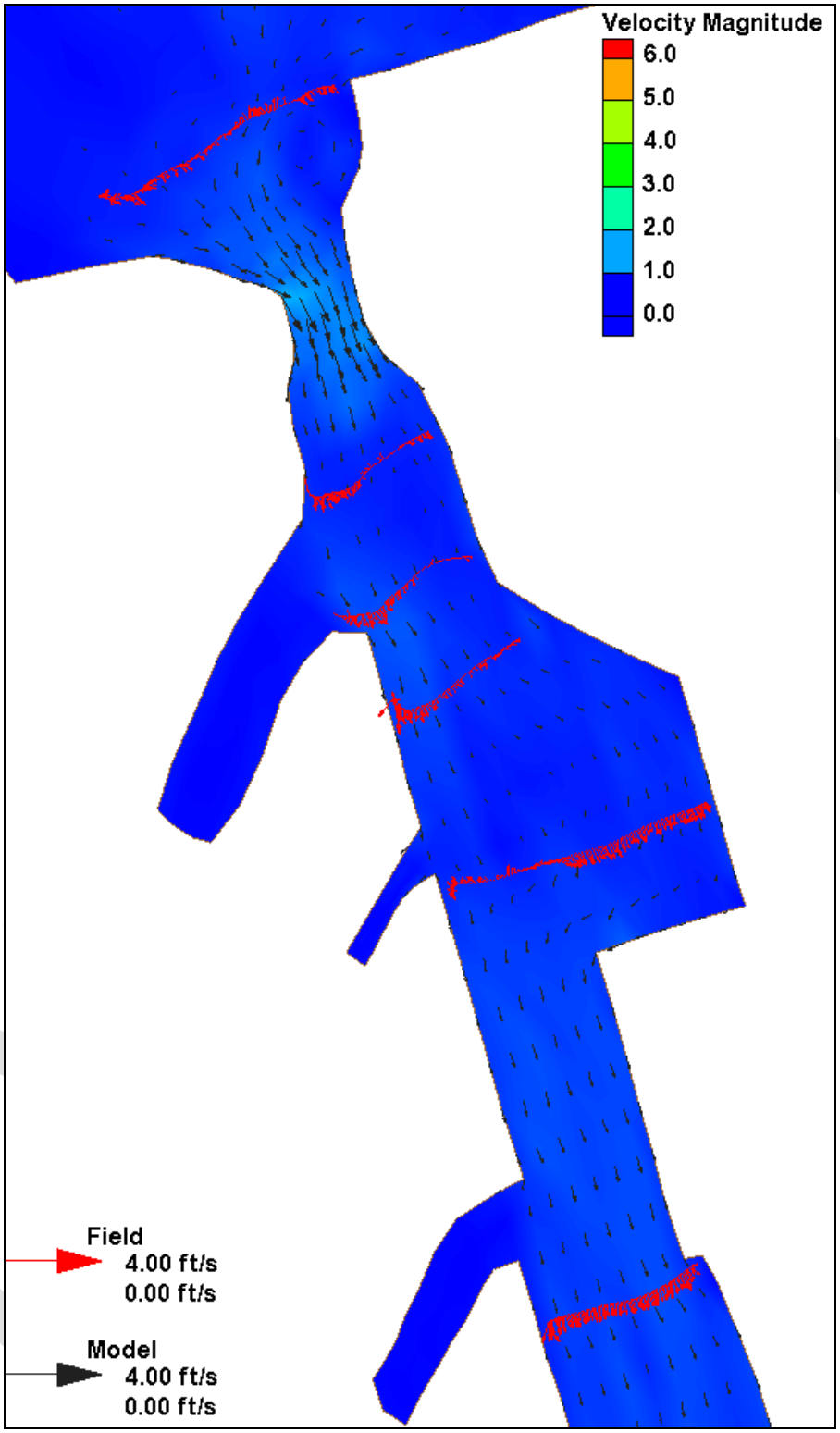

Figure 3-22. IHNC Seabrook velocity on October 17, 2008 at 06:30

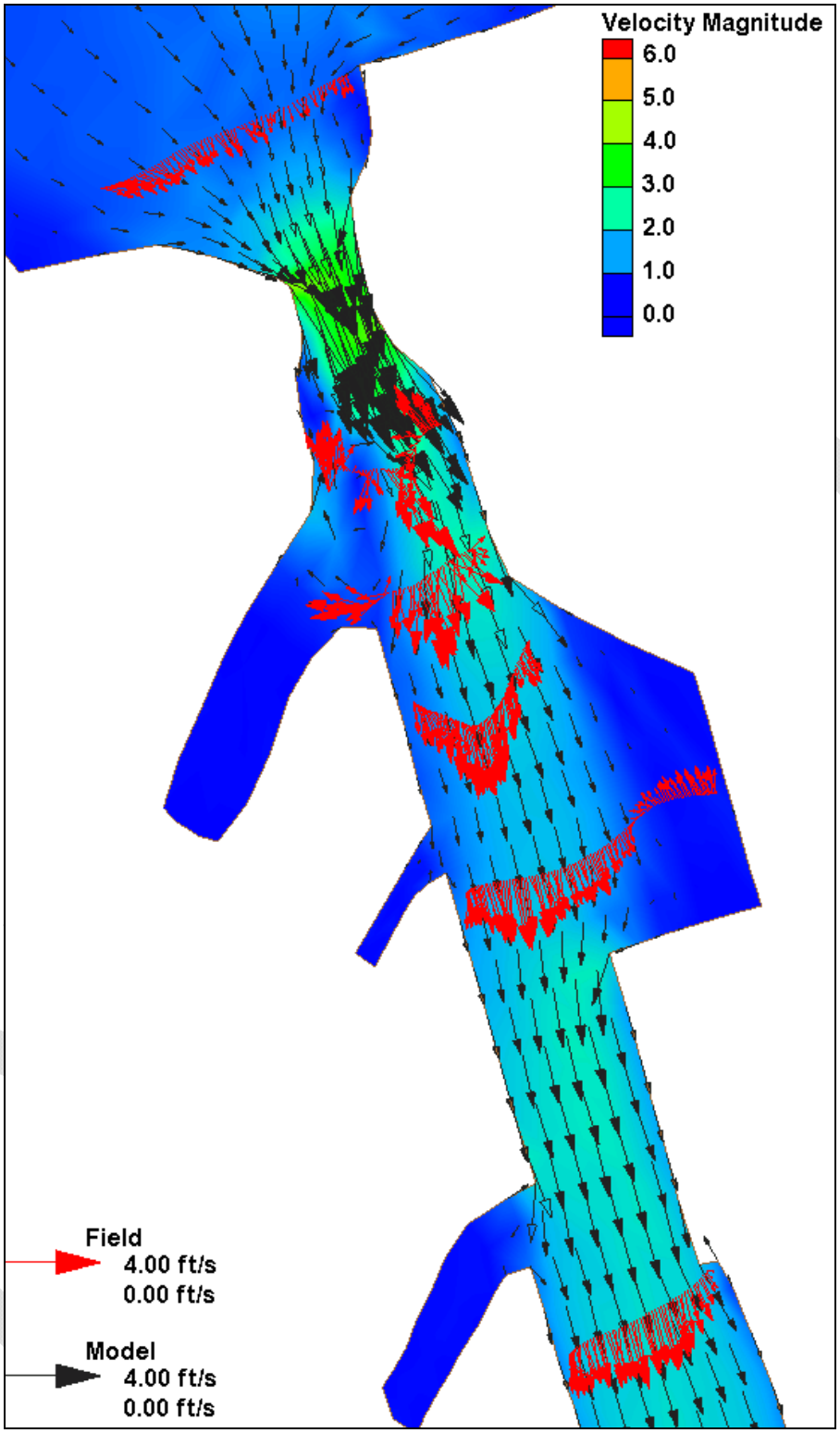

Figure 3-23. IHNC Seabrook velocity on October 17, 2008 at 09:05

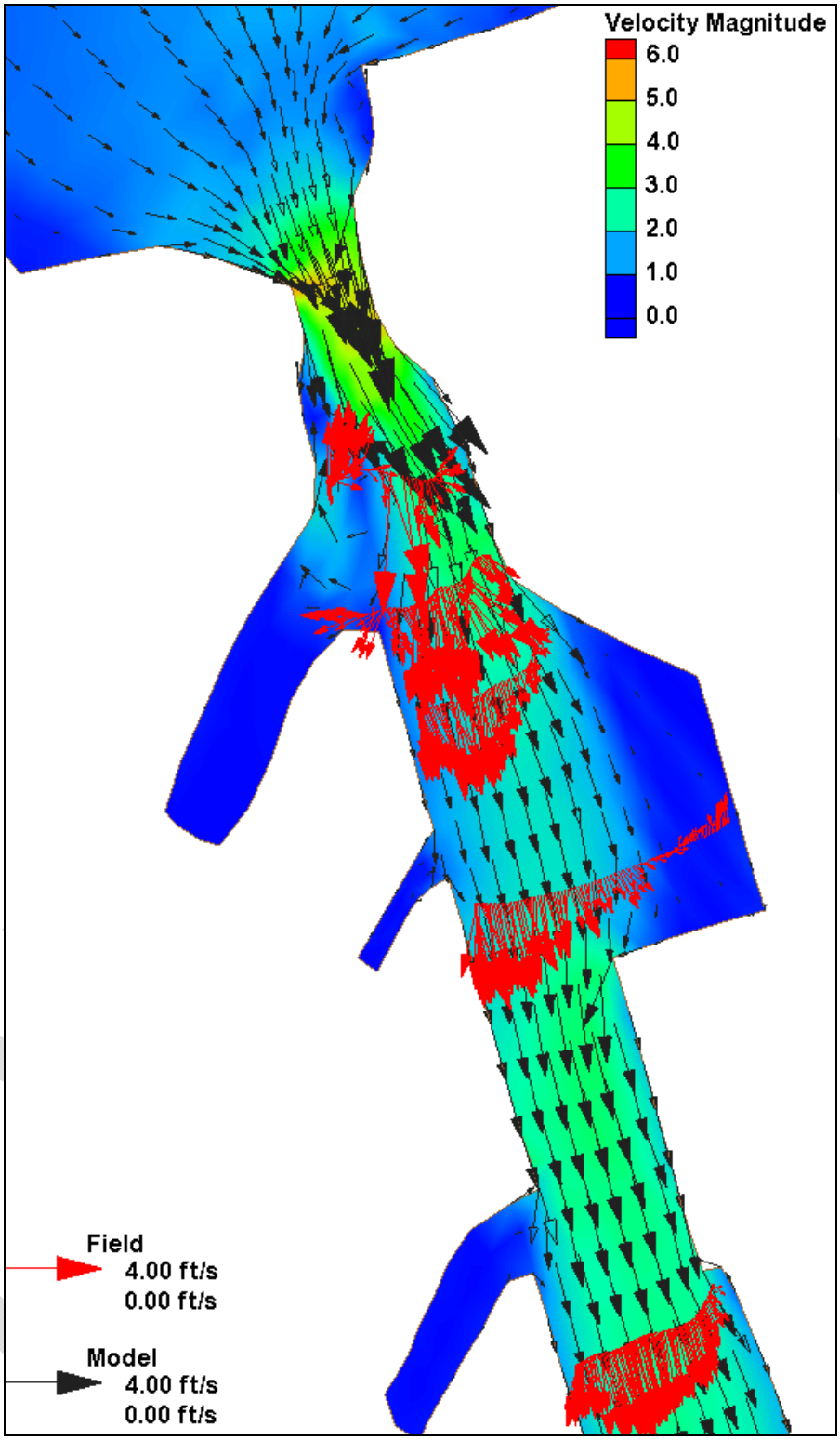

Figure 3-24. IHNC Seabrook velocity on October 17, 2008 at 13:29

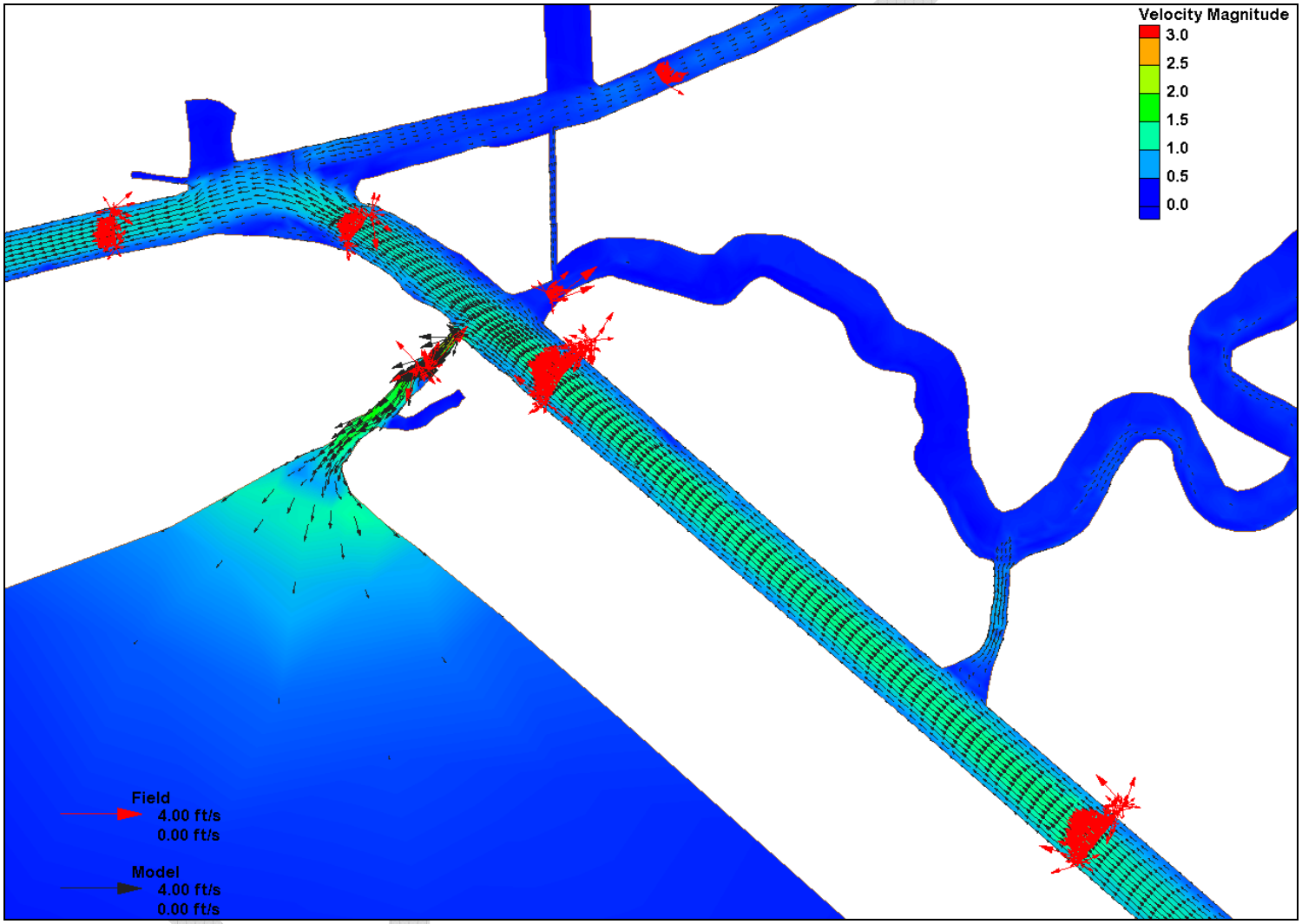

Figure 3-25. GIWW/MRGO velocity on July 31, 2008 at 10:30

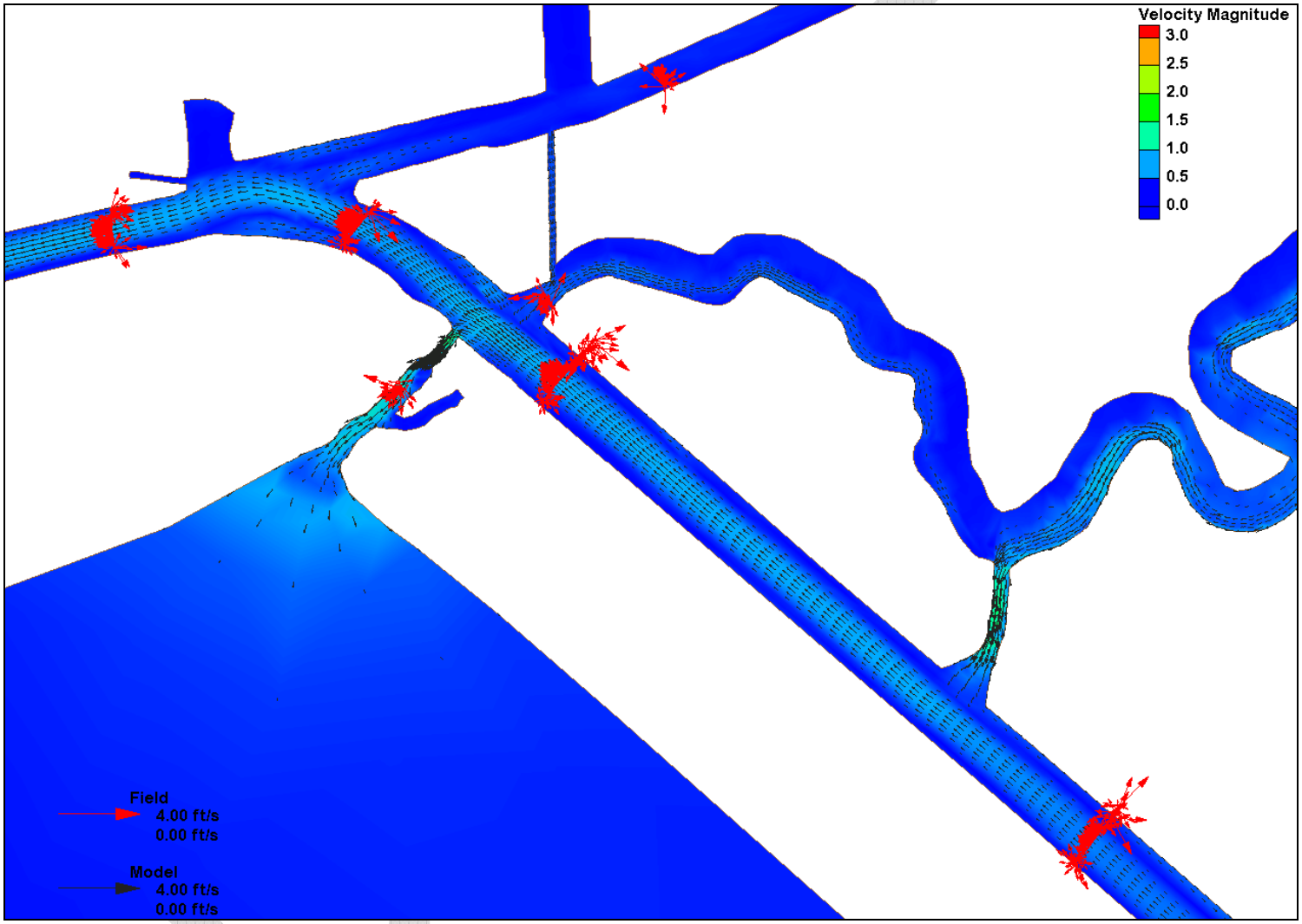

Figure 3-26. GIWW/MRGO velocity on July 31, 2008 at 14:30

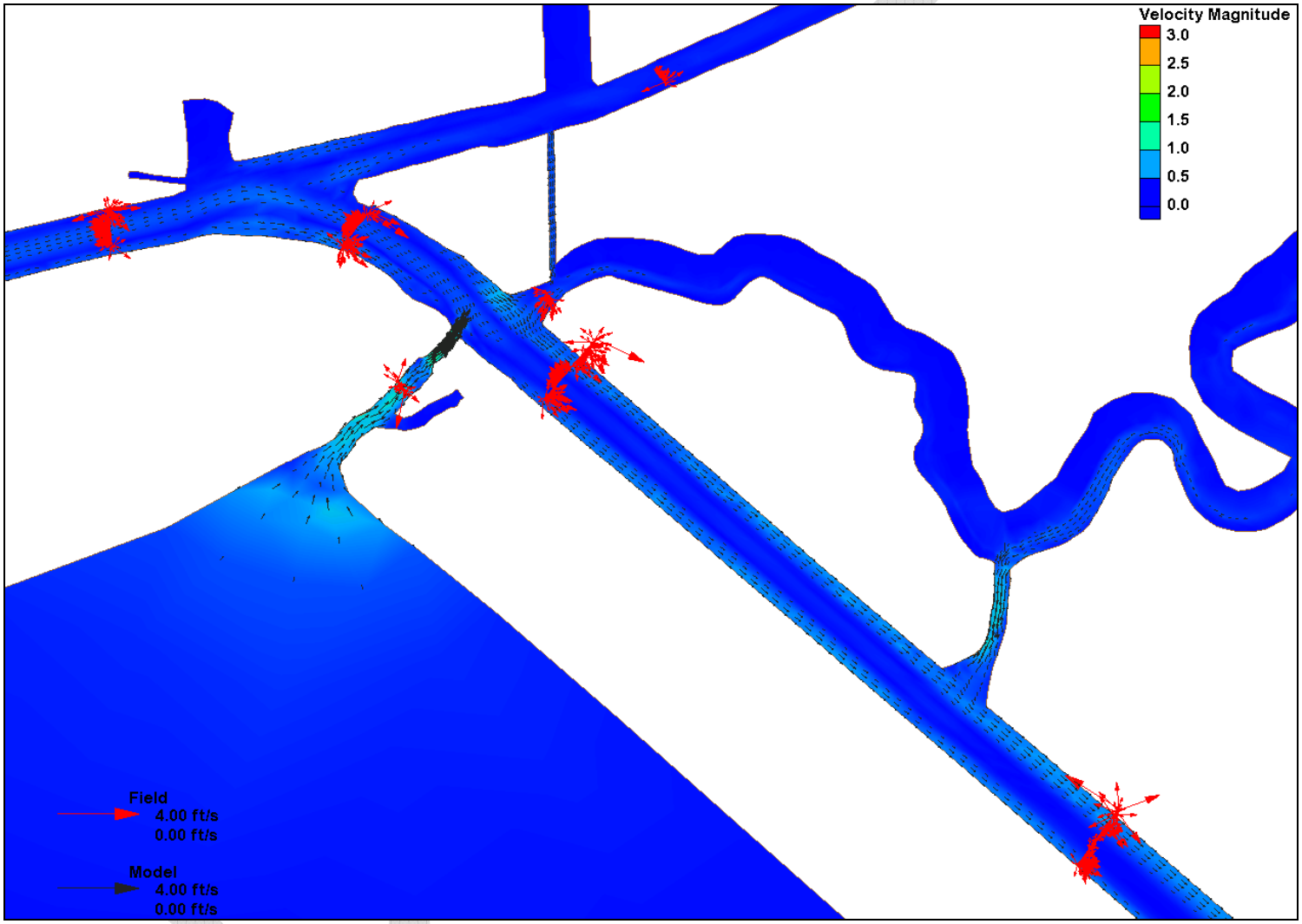

Figure 3-27. GIWW/MRGO velocity on July 31, 2008 at 16:00

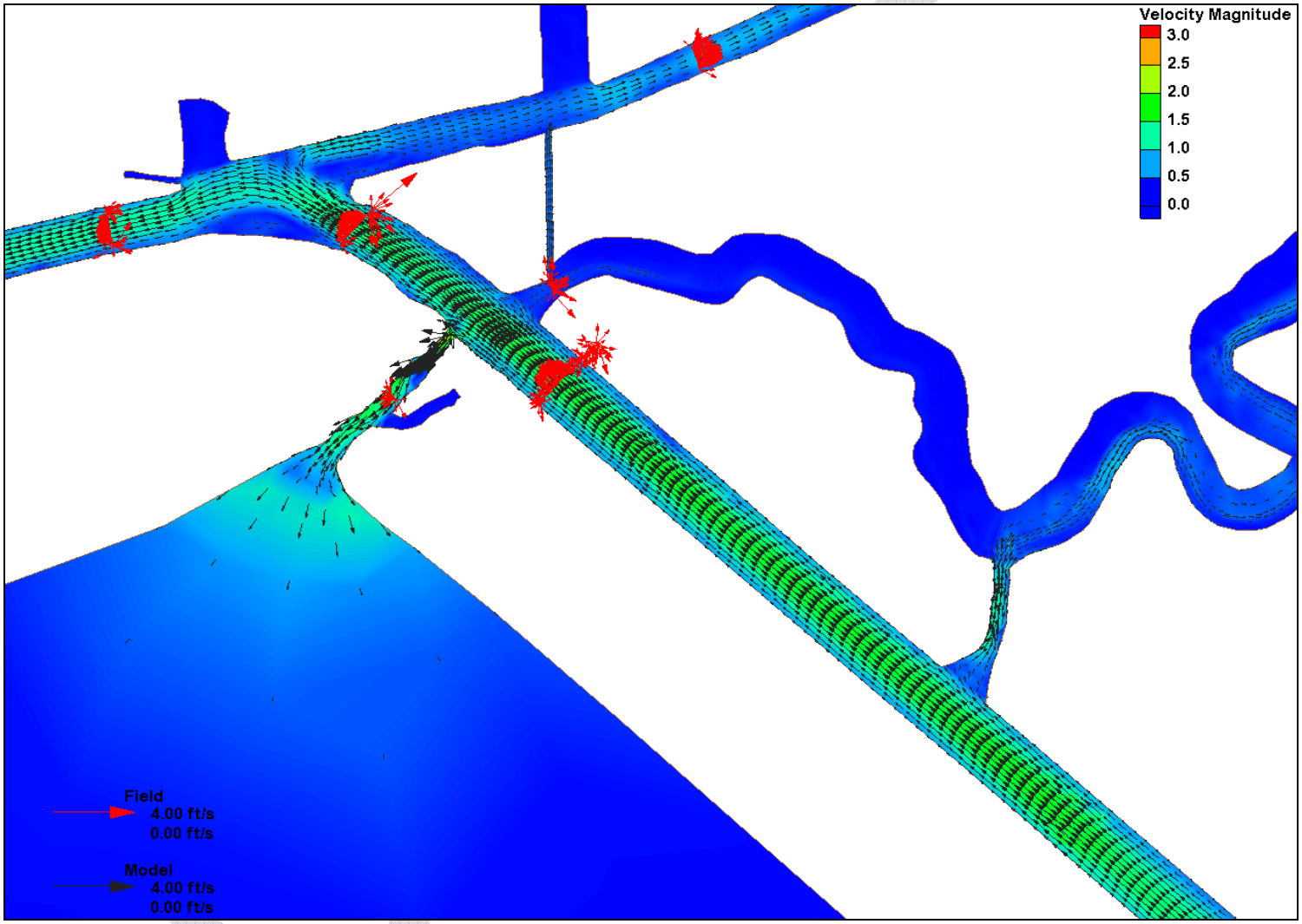

Figure 3-28. GIWW/MRGO velocity on August 13, 2008 at 9:00

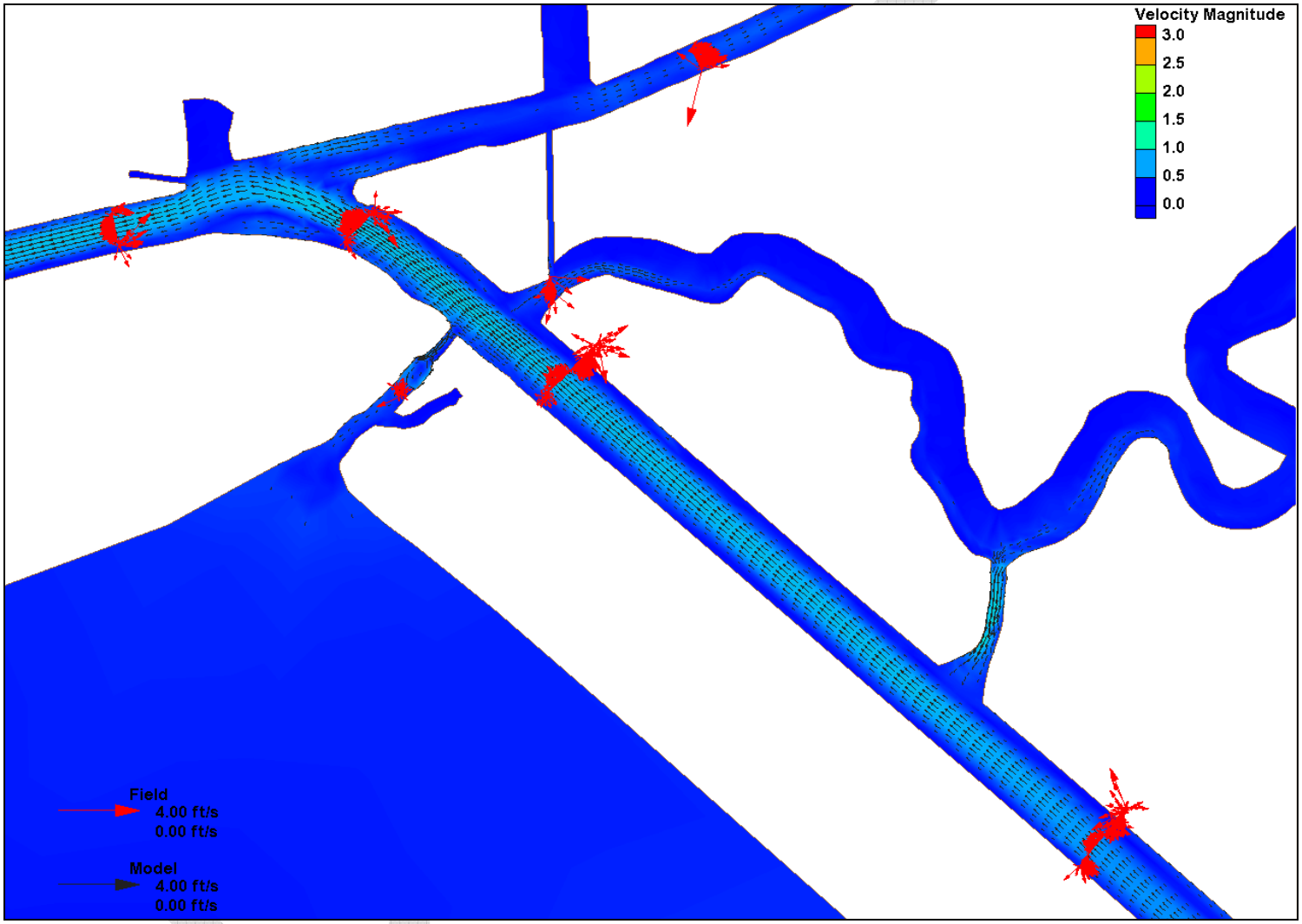

Figure 3-29. GIWW/MRGO velocity on August 13, 2008 at 13:00

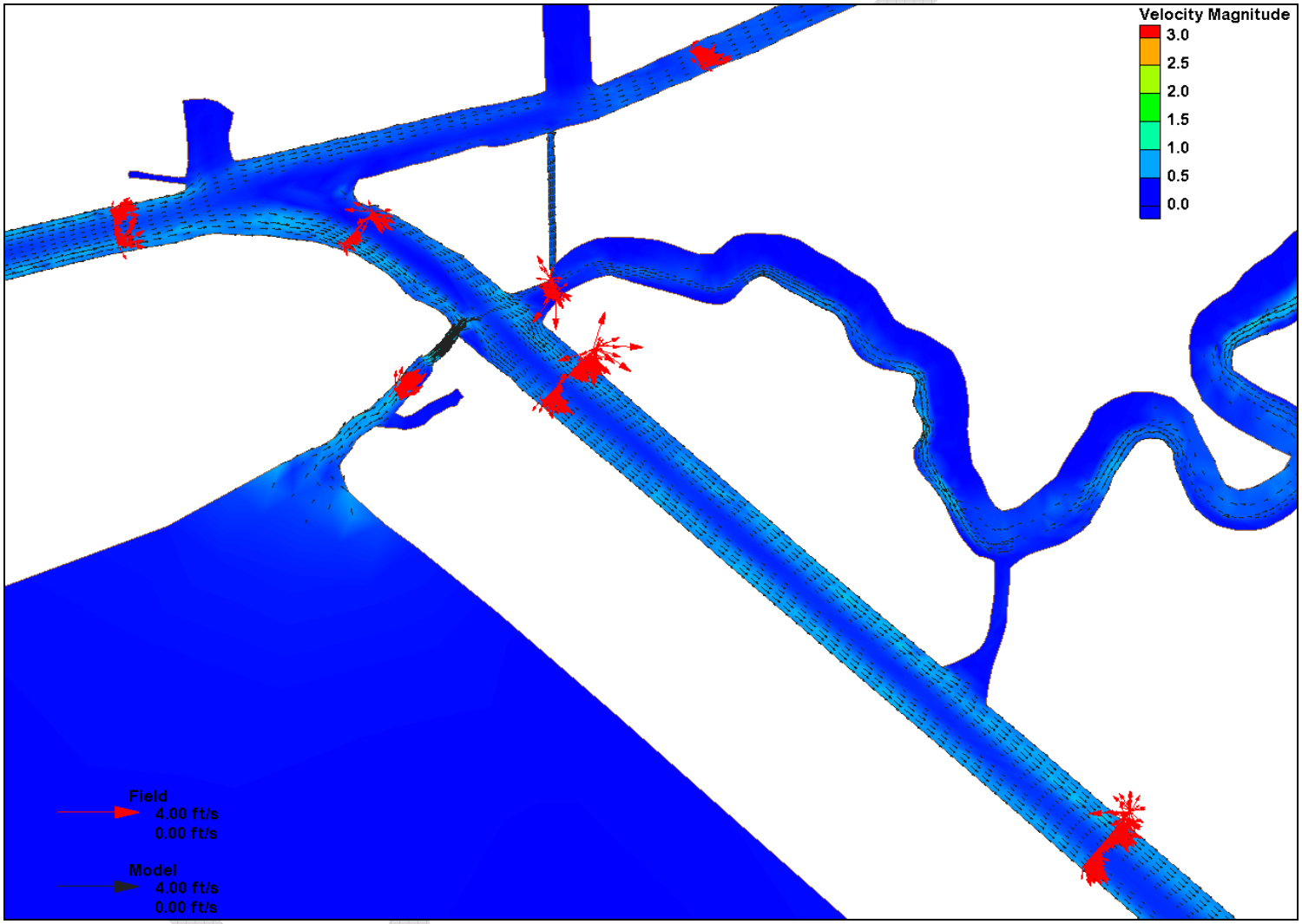

Figure 3-30. GIWW/MRGO velocity on August 14, 2008 at 16:00

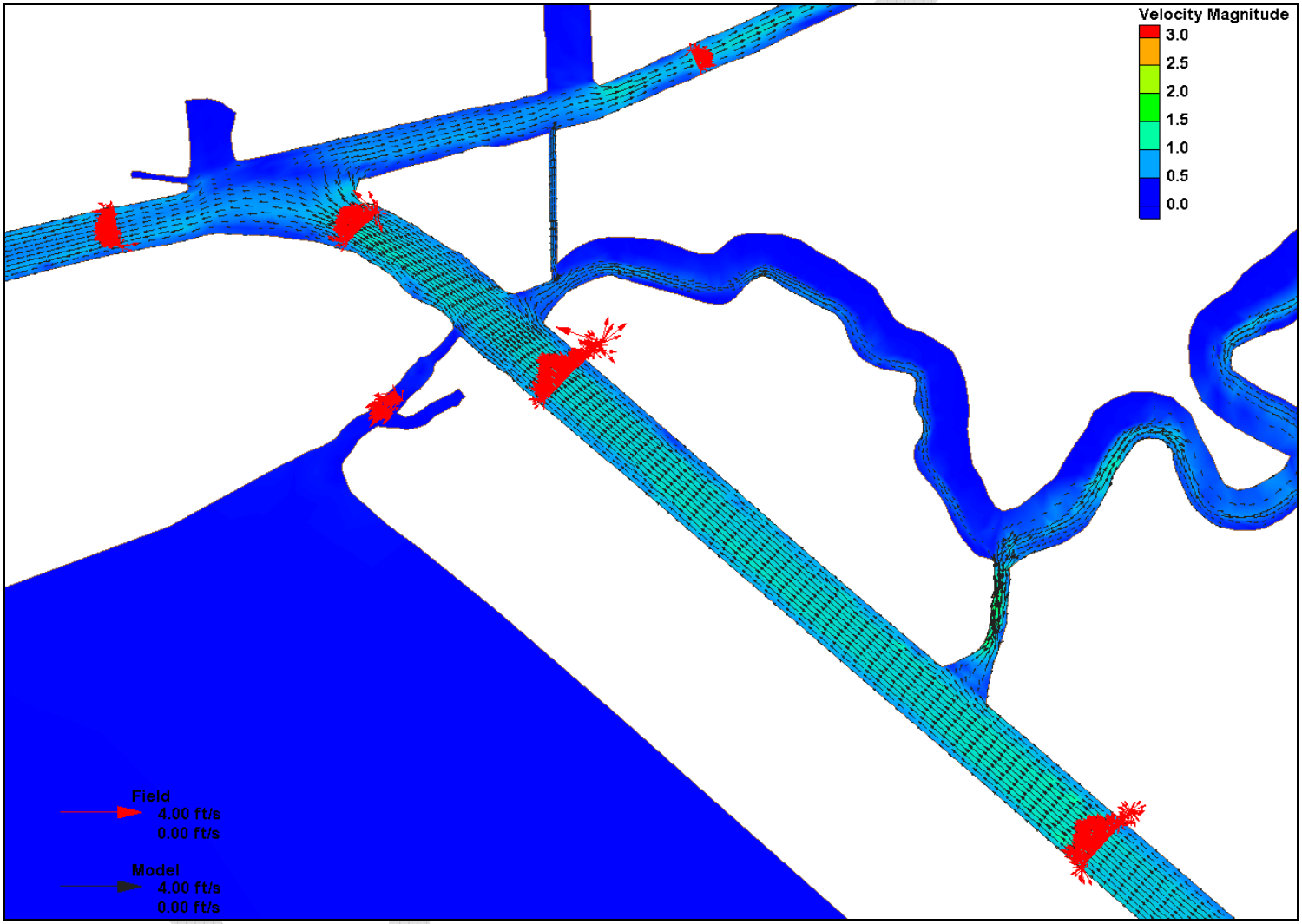

Figure 3-31. GIWW/MRGO velocity on August 14, 2008 at 6:00

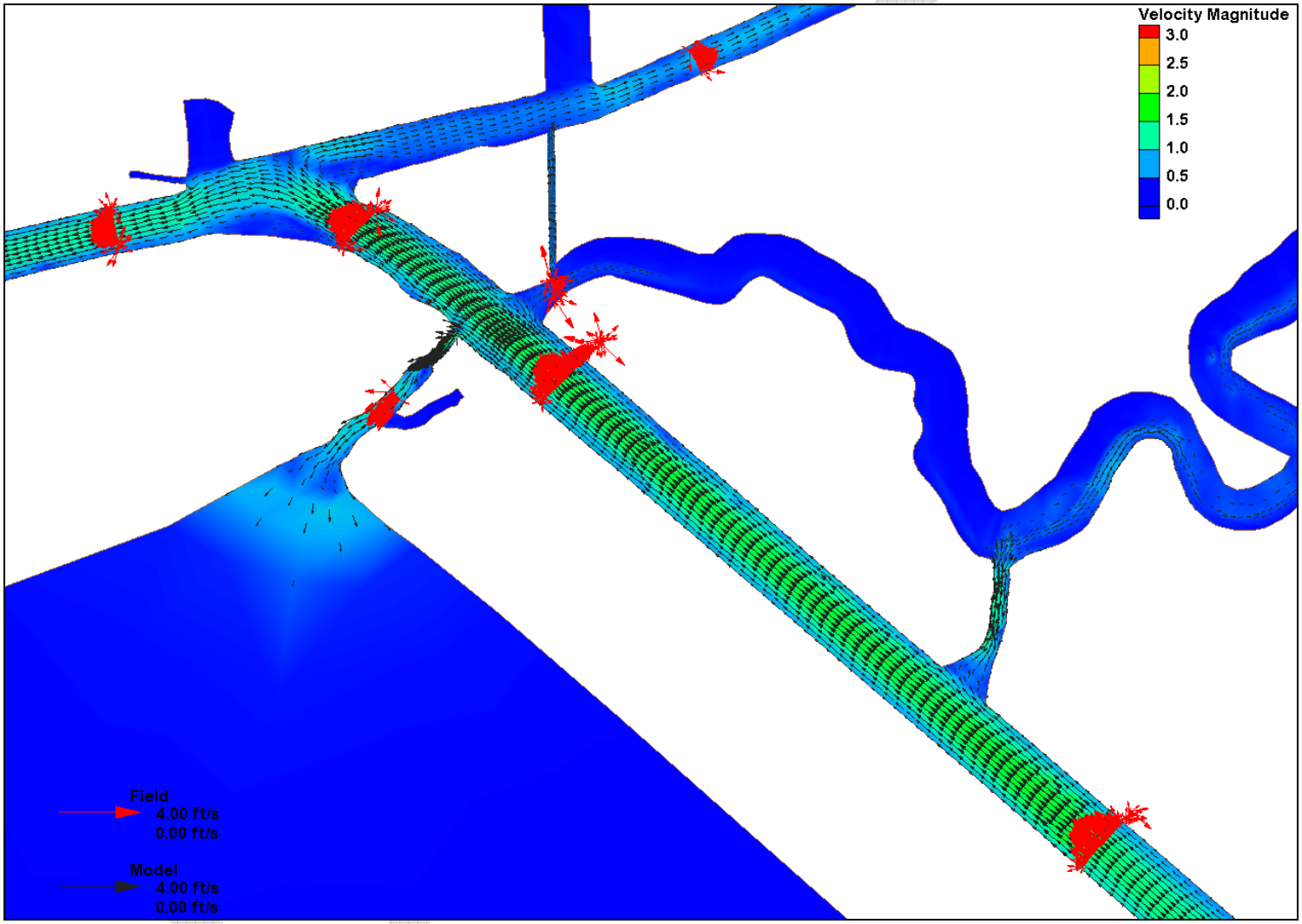

Figure 3-32. GIWW/MRGO velocity on August 14, 2008 at 9:00

It is apparent that some of the flow peaks and exact timings are not captured by the model due to various limitations mentioned in this section, including the use of only one wind station and the simple depiction of the marsh areas. A closer comparison of the model results to the field data could be performed if more time were available for the task as well as additional field data to better define certain locations. However, these differences do not adversely impact the results necessary for the study's intended purpose and the model validation was accepted.

Sensitivity Analysis

A basic sensitivity analysis was performed, focusing in the area of the GIWW. These sensitivity tests include effects of the wind speed as well as mesh boundary depths along the navigable waterways. It is known that wind speeds and directions vary greatly throughout the model domain area. Since a single wind station is used for this simulation, local affects due to varying wind conditions can not be reproduced. A simulation is performed in which the wind speed is increased by 50%. The result of this simulation is given in the blue line in Figure 3-33. A second test is performed in which the mesh boundaries along the GIWW are deepened to -8 ft. See Figure 3-34 for an illustration of this concept. If the model boundary is set at the intersection of the dashed line and the red line, the area in "A" is not accounted for. By deepening the model boundary, the area in "B" gets added to the model to account for that lost from "A". If these depths are not selected carefully, the flow area can be misrepresented in the model. The green line in figure 3-33 shows these results. The pink line is the base model results at line 2 (see Figure 3-3). It is obvious that these changes affect the solution; however this is a model sensitivity test and the differences in the solution do not suggest that changes are needed so the overall effect on the results is determined to be allowable for the intended purposes of this study, which is transport of larval fish.

DRAFT

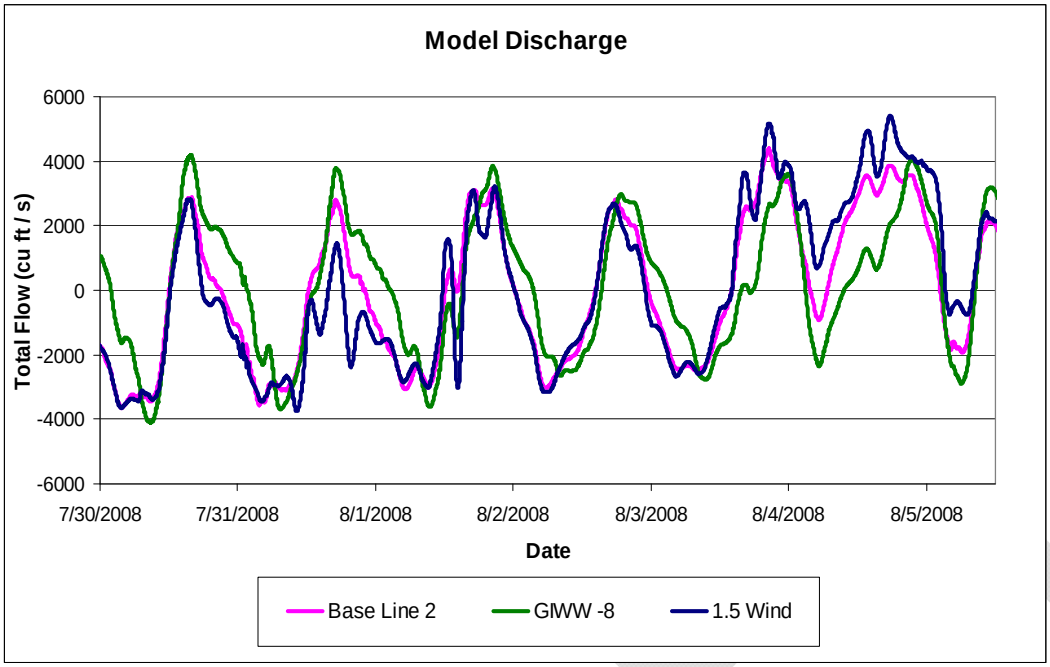

Figure 3-33. Sensitivity analysis results

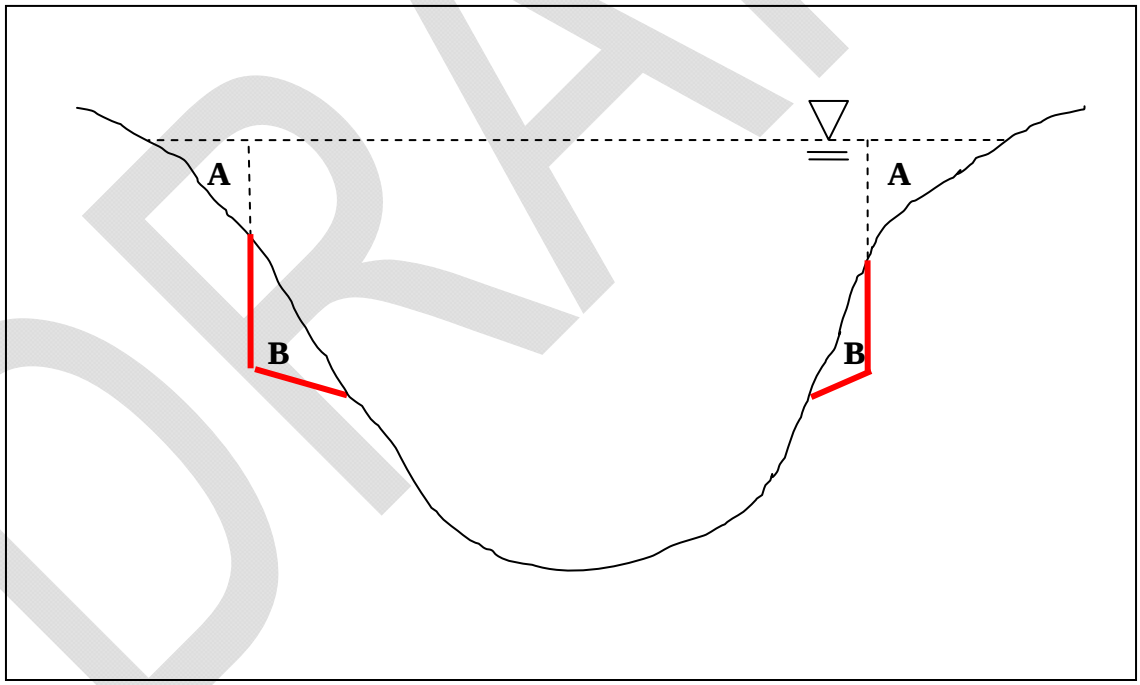

Figure 3-34. Flow area calculations

DRAFT

The validation of the model described above includes comparisons of model output to field data measurements for water surface elevation, discharge, and velocity at various locations within the study area. These comparisons were obtained after much testing of roughness parameters and checking of geometry, bathymetry, and boundary conditions. Given the available information of the system and the historically accepted range of roughness parameters, the parameter set used to generate the comparisons shown represents the best overall agreement to the field data. Now that the geometry and model parameters have been adjusted to give the best representation of the system, plan simulations and base/plan comparisons can be made using the validated model. For this project, hydrodynamic information will be used to drive a particle tracking model to simulate the movement of larval fish into the Lake Pontchartrain area with and without the planned hurricane protection measures.

DRAFT

4 Design Alternatives

The design alternatives are developed with the aim to reduce flooding in the region due to storm passage. The effect that these alternatives have on the larval fish then becomes a question of concern. Three alternatives and the base condition were chosen for testing with the particle tracking model. Much of the design process has focused on the effects of the plans on navigation and not with their effects on larval fish transport. These design alternatives are chosen based on previously planned navigation structures and changes to the system. They are organized into three plans as described below. For all structures, the sill elevation is -16 ft.

- Base - condition includes the fully open MRGO, GIWW, and IHNC (Figure 4-1)
- Plan 1 – close the MRGO at La Loutre (Figure 4-2)
- Plan 2 – close the MRGO at La Loutre, include the Borgne alignment (56 ft X 8 ft gate on Bayou Bienvenue, and two 150 ft X 16 ft gates on GIWW) (Figure 4-3)
- Plan 3 – close the MRGO at La Loutre, include the Borgne alignment, include the 95 ft X 16 ft gate at Seabrook structure with southern scour hole filled (Figure 4-4)
- Plan 3 Final - close the MRGO at La Loutre, include the Borgne alignment, include the 95 ft X 20 ft sector gate at Seabrook with two flanking 50 ft X 16 ft auxiliary gates with southern scour hole filled (Figure 4-5)

The hydrodynamic and particle tracking simulations for the base condition and three plans are run for two different time periods. The analysis period was initially 2 weeks but extended to 4 weeks in order to get better, more representative results. A two week spin-up period is included in the hydrodynamic simulations prior to the analysis period. The two time periods used for this study are August 15 – September 15, 2007 (labeled as September) and March 1 – 31, 2008. A general picture of the tidal signal near the Gulf boundary for these two time periods is shown in Figure 4-6 and the wind speeds at the New Orleans International Airport for these periods

DRAFT

are given in Figure 4-7. It is apparent in these figures that the March winds and tide are indicative of the spring season when conditions are more erratic due to front passages and rain events. The September period shows lower wind speeds and a more typical diurnal tide signal which is expected in the Gulf of Mexico.

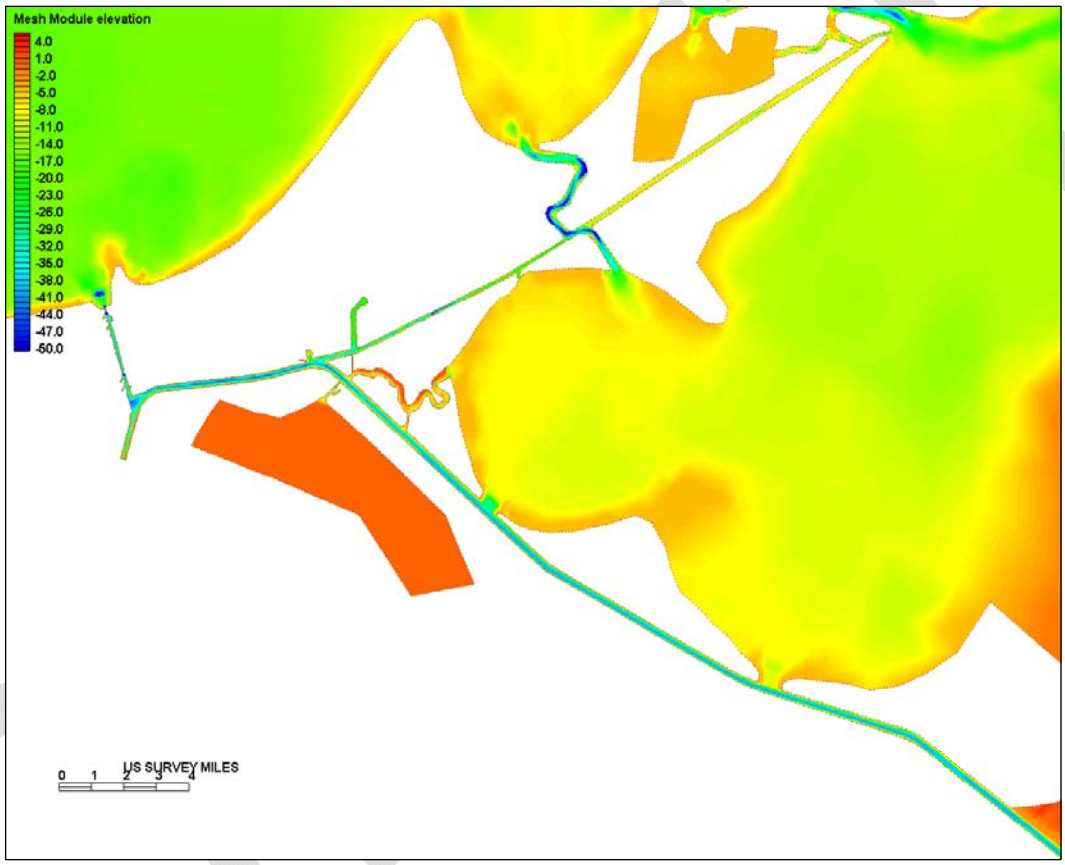

Figure 4-1. Base configuration: no closures, no structures

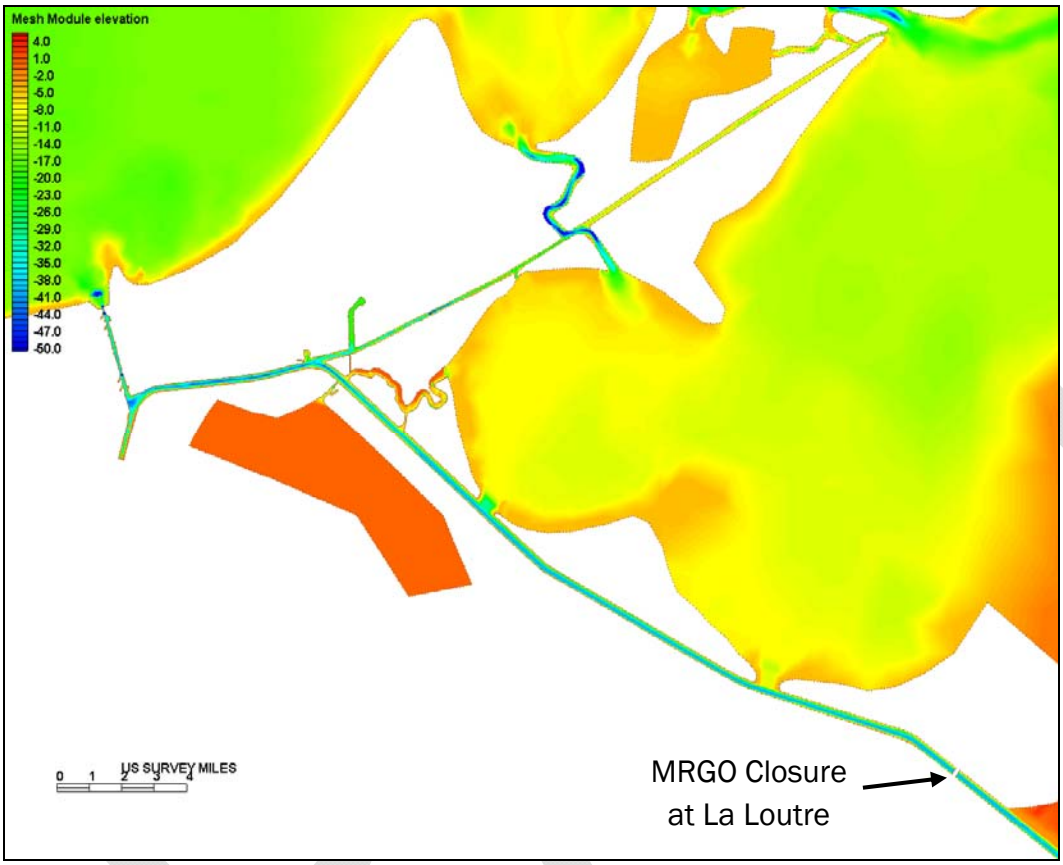

Figure 4-2. Plan 1 configuration: close the MRGO at La Loutre

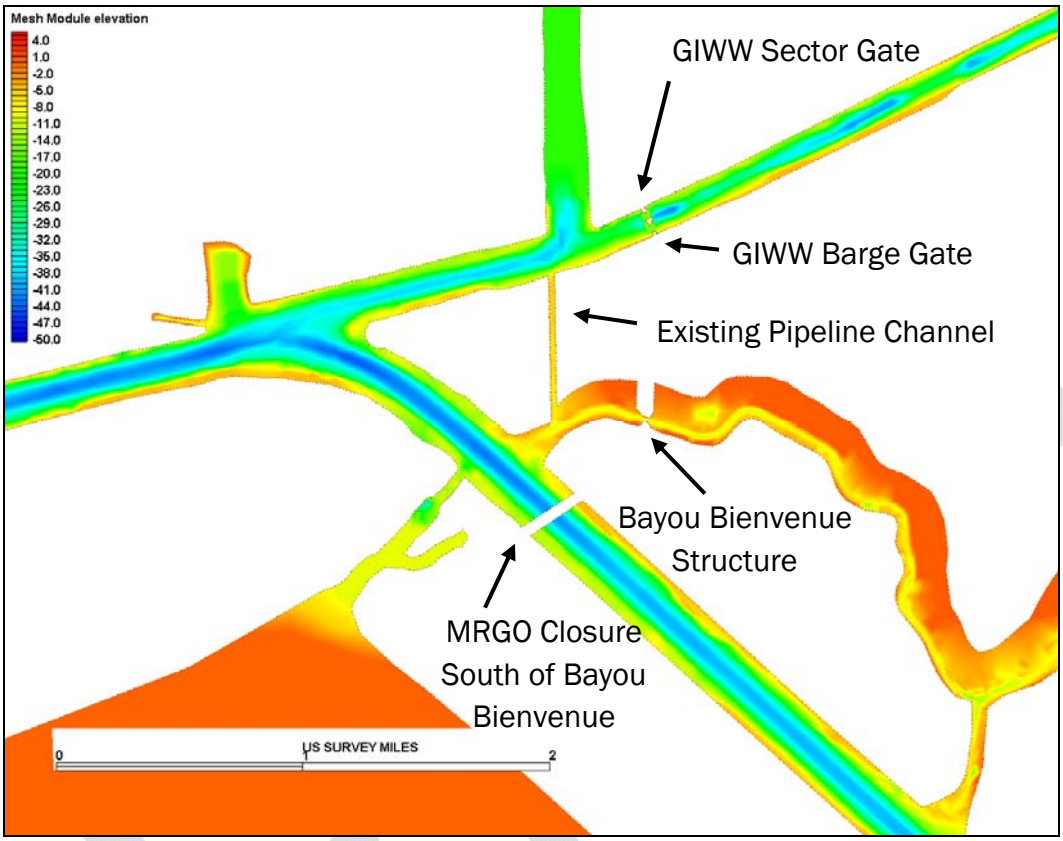

Figure 4-3. Plan 2 configuration: includes Plan 1 and the Borgne alignment (56 ft X 8 ft gate on Bayou Bienvenue, and two 150 ft X 16 ft gates on GIWW)

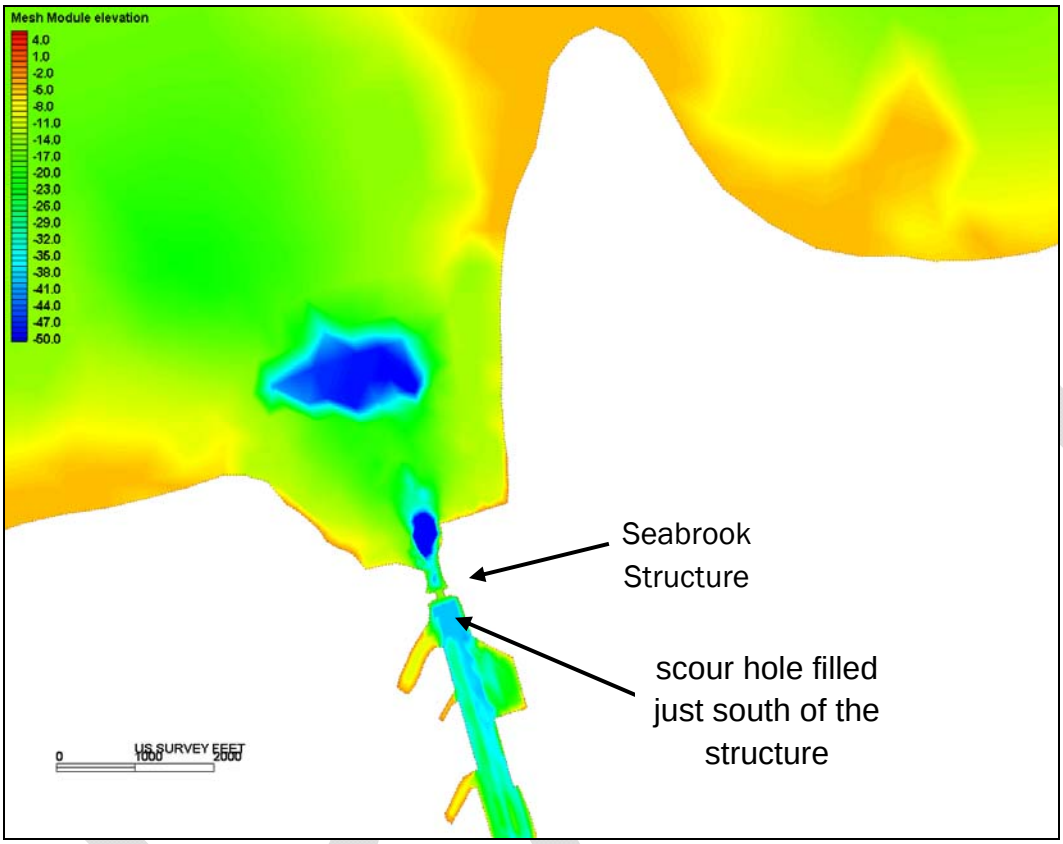

Figure 4-4. Plan 3 configuration: includes Plan 1, Plan 2 and a 95 ft X 16 ft structure at Seabrook

DRAFT

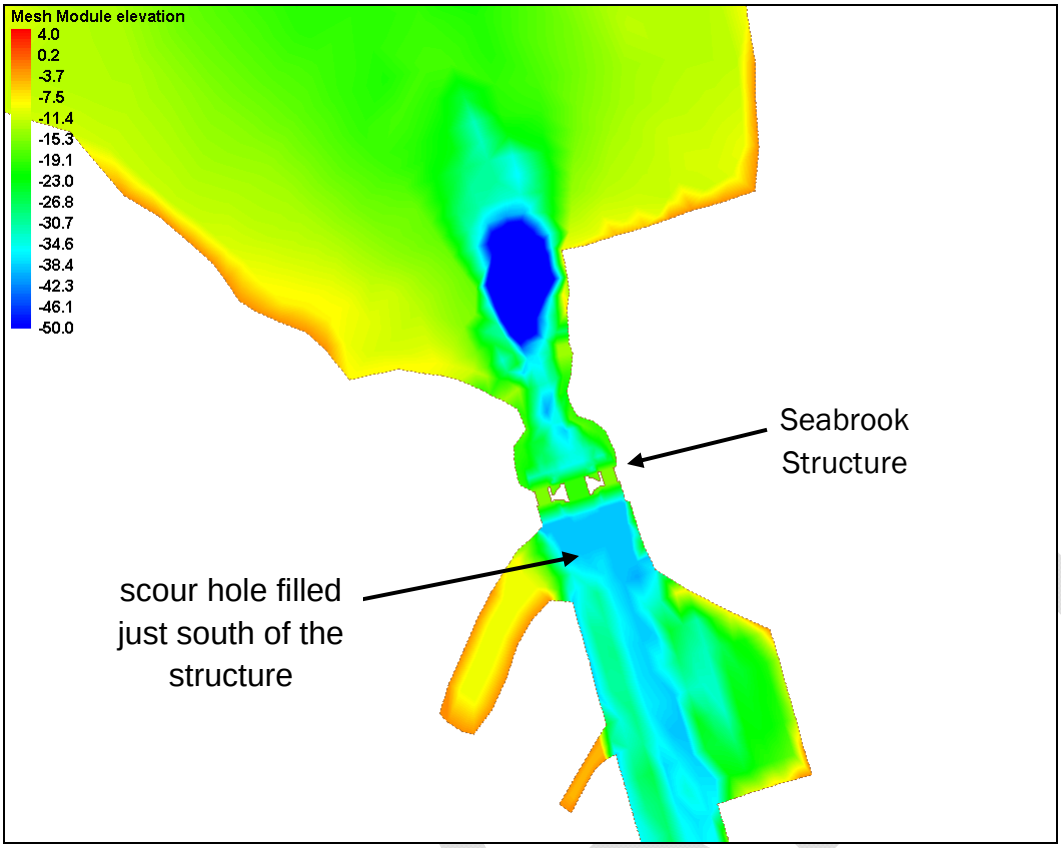

Figure 4-5. Plan 3 Final configuration: includes Plan 1, Plan 2 and a 95 ft X 20 ft sector gate with two side 50 ft X 16 ft auxiliary gates at Seabrook

DRAFT

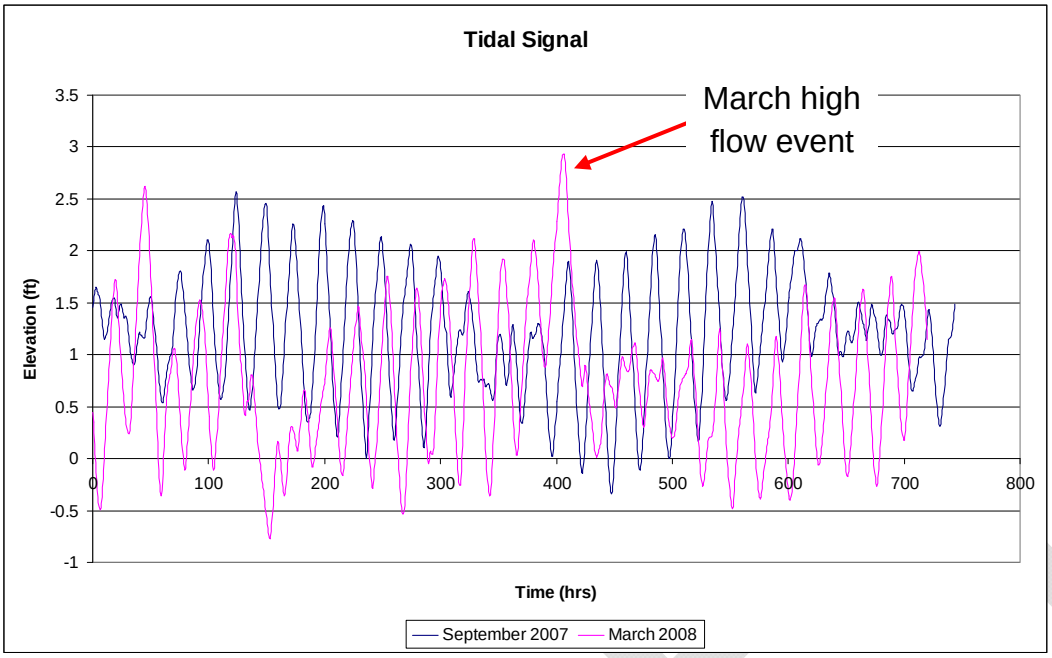

Figure 4-6. Tide signal for both four week analysis periods

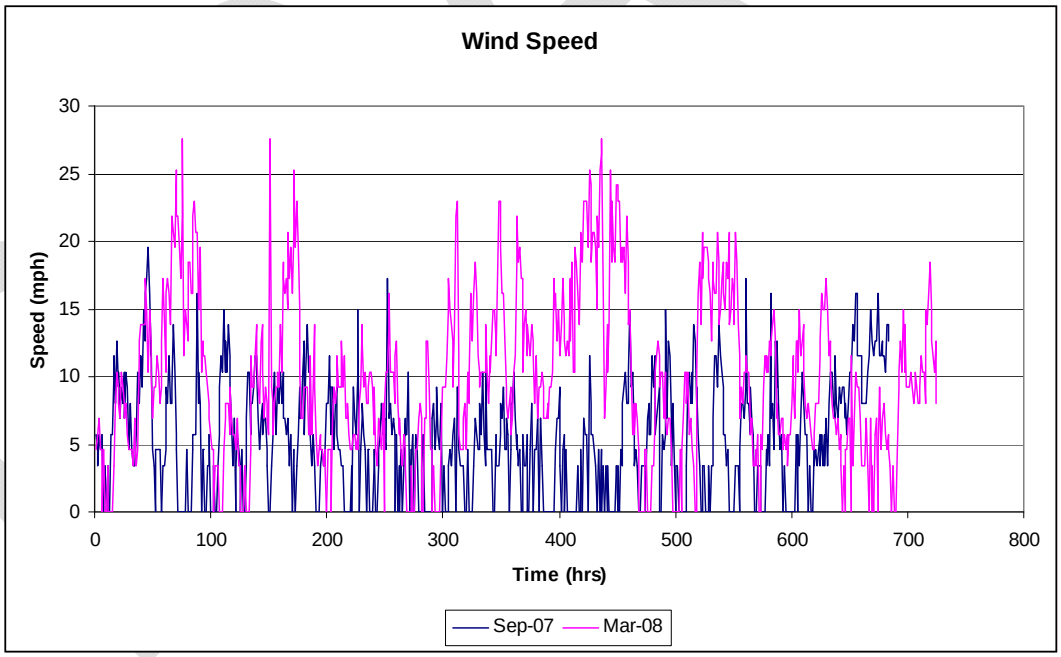

Figure 4-7. Wind signal for both four week analysis periods

5 Larval Fish Transport

Larval fish transport for this project is simulated using the particle tracking model (PTM). This section gives a general background into PTM and discusses the algorithms added to PTM which pertain to larval fish transport. In addition, it gives the simulation details and all model input data. Simulation results based on these algorithms are shown in Chapters 7 and 8.

Background

PTM is an ERDC-developed model designed specifically to track the fate of point-source constituents (sediment, chemicals, debris, biologicals, etc) released from local sources (outfalls, dredges, etc) in complex hydrodynamic and wave environments (McDonald et al 2006, Lackey and McDonald 2007, Lackey and Smith 2008). Each local source is defined independently and may have multiple constituents. Therefore, model results include the fate of each constituent from each local source. PTM simulates transport using pre-calculated periodically saved hydrodynamic (and wave) model output. The hydrodynamic model is not coupled to the transport model and therefore can be run once for multiple PTM simulations. Each particle in PTM represents a specific mass (or number of particulates) of one constituent. Total mass is conserved because particles are conserved, that is all particles that are created, are accounted for through the simulation. Hydrodynamic output does not need to be conservative, so the user can specify hydrodynamic model output for PTM without concern for conservation of water mass. A random walk method is used to represent particle diffusion. PTM simulations can be either 3D or 2D. For this application, the 3D mode is used.

In addition to the hydrodynamic input (i.e. water surface elevation and velocities) that is used as a forcing for particle dynamics, PTM requires mesh and bathymetry information, and sediment characterization of the native or bed sediment. PTM also needs detailed constituent or source information. The user specifies particle characteristics and processes, including settling, critical stresses, and erosion rates. If processes data are not available, these values may be calculated within the model based on verified theoretical relationships. The specific equations for those processes are discussed in Appendix D and are described in further detail by McDonald

DRAFT

et al (2006). Particles can be positively, neutrally, or negatively buoyant. Positively buoyant, for example, would represent floating debris while neutrally buoyant may represent chemicals and negatively buoyant may represent sediment. In the case of larval fish modeling, particles are considered neutrally buoyant with additional characteristic larval fish behavior specified.

Model output includes time dependent parcel positions throughout the domain. Various other attributes such as mass, density, and suspension status are also assigned to each of the output parcels. Elevation in the water column is calculated and stored. PTM setup and execution are done within the ERDC-sponsored Surface Water modeling System (SMS) interface. SMS includes multiple tools for post-processing PTM output to assess distribution of concentration, deposition, and other results at any time during the simulation. These results are processed for each constituent from each source or for combined constituents or sources.

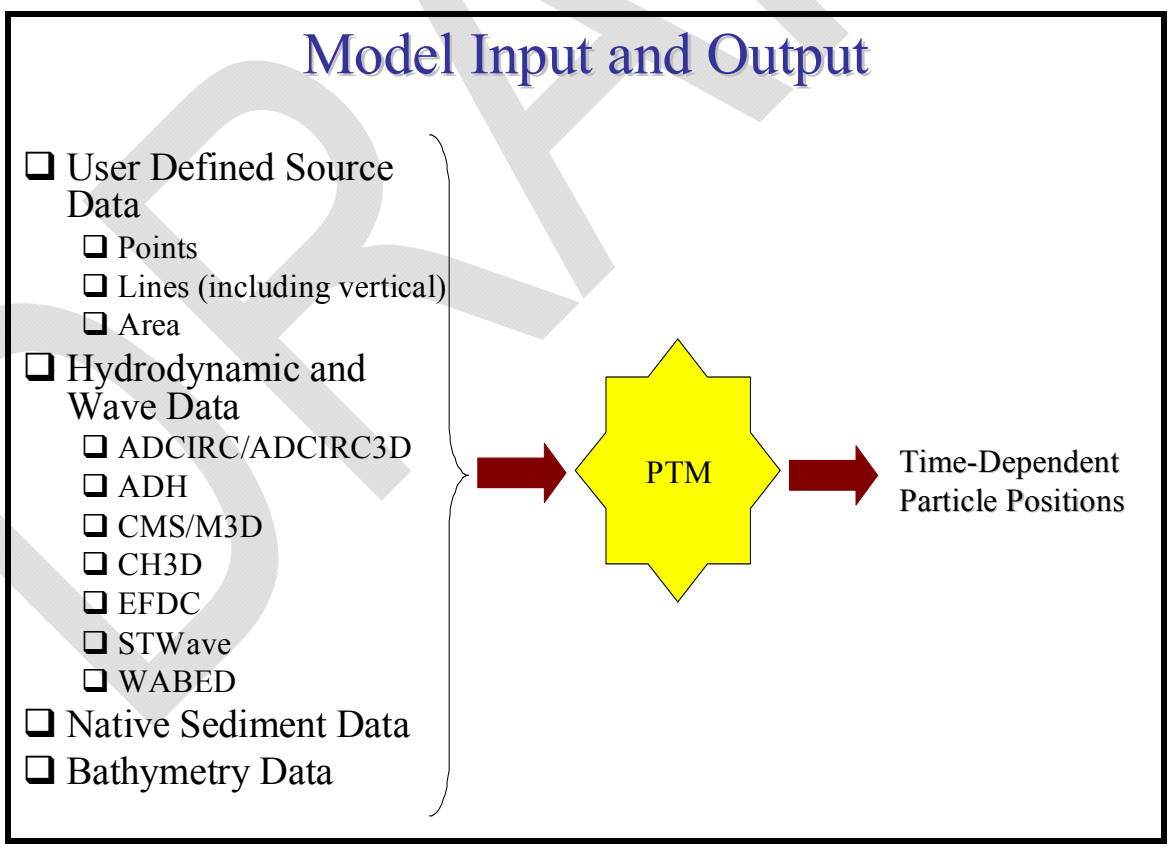

Figure 5-1. Description of the Particle Tracking Modeling input and output

DRAFT

Method

The particle tracking model is a Lagrangian particle tracker. Like most Lagrangian particle trackers, all transport is in the reference frame of the particle, ultimately solving a classic system of equations:

$$\frac{d\vec{\mathbf{x}}}{dt} = \vec{\mathbf{u}} \tag{1}$$

In this system, **x** is the particle position vector **x**=(x,y,z) and **u** is the flow field velocity vector **u**=(u,v,w). Numerically this system of equations can be discretely solved as:

$$\mathbf{x}^{n+1} = \mathbf{x}^{n} + \Delta t \vec{\mathbf{u}}^{n} \tag{2}$$

That is, the new position of a particle at time *n+1* is equal to the old position of a particle at time *n* added to whatever distance it traveled during a time step Δt. This distance is directly dependent on the force of the velocity on that particle at that point. The solution to Equation (1) is applicable primarily to passive particles which are particles that have no real ability to affect their transport or have no additional transport dependencies such as mass or density effects. For most transport performed utilizing PTM, the equation becomes more complex:

$$\mathbf{x}^{n+1} = \mathbf{x}^{n} + \Delta t \mathbf{F}^{n} \tag{1}$$

where **F** is a function of the flow field velocity, diffusion, and multiple other processes. With regard to sediment, this includes settling, burial, etc. However, for PTM larval fish modeling **F** is also a function of the expected behavioral characteristic of the larvae.

$$F(u) = u_{advection} + u_{diffusion} + u_{behavior} \tag{4}$$

For every time step, the model calculates for each particle the velocity due to advection, diffusion, and the larval fish velocity assigned to the particle due to the behavioral characteristic applied to the particle. The velocity due to advection is interpolated from the three surrounding mesh nodes of an element to the particle position within the element. The velocity due to

DRAFT

diffusion is calculated via a random walk diffusion algorithm (McDonald et al 2006).

Currently, PTM models transport for the following behaviors:

1) Tidal Lateral
2) Tidal Vertical
3) Diel Vertical
4) Bottom Movers
5) Top Movers
6) Passive

These behaviors were developed based instructions from the Keith Lake fish passage study interagency team as well as through the Seabrook larval fish transport interagency team.

Tidal Lateral

Tidal lateral behavior describes particles that will move laterally (horizontally) due to changes in the tide. In PTM this means that as the model perceives an incoming tide, particles move towards the maximum velocities. In most channels and rivers, this will be towards the center of the channel. During outgoing tide, particles move towards areas of minimum velocity.

Tidal Vertical

Tidal vertical behavior describes particles that will move vertically due to changes in the tide. In PTM this means that as the model perceives an incoming tide, particles move upwards in the water column. For depth averaged flows, higher velocities will occur at the top of the water column, and due to the logarithmic velocity profile, the velocities will decay to zero at the bed. During outgoing tide, particles move downwards towards the bed and areas of minimum velocity.

DRAFT

Diel Vertical

Diel Vertical behavior describes particles that will move vertically due to the time of day. Currently this behavior is described as particles moving upwards during the daytime and downwards at nighttime. Daytime is currently set as 6am-6pm and nighttime is set as 6pm-6am.

Bottom Movers

Bottom movers are particles which stay in the lower 25cm of the water column. Currently the particles are allowed to move freely by the flow until they move above the 25cm level in the water column. At this point, they are forced lower in the water column.

Top Movers

Top movers are particles which stay in the upper 25cm of the water column. Currently the particles are allowed to move freely by the flow until they move below the 25cm level in the water column. At this point, they are forced higher in the water column

Passive Movers

Passive movers within the water column are moved only via advection and diffusion. These particles do not have any additional applied behavior.

Particle Velocity

For all particles that have applied behaviors, movement occurs based on a maximum velocity C_{max}. C_{max} is defined as 10mm/s. For Chapter 7 simulations, particle movement occurs at a decaying rate. Particles move towards their goal (i.e. the top or bottom of the water column, etc) at a rate of C_{max} when farthest from the goal. Upon reaching the destination, the velocity becomes zero. So for example, tidal vertical movers have a $u_{behavior}$ which is defined by:

$$u_{behavior} = C_{\max}\left(1 - \frac{P_{height}}{Depth}\right) \tag{5}$$

Here P_{height} is the height of the particle above the bed and $Depth$ is the total depth of the water. So as a particle moves upwards in the water column and P_{height} becomes equal to the total depth of the water column, the veloc-

ity contribution from the behavior goes to zero. However if the particle is at the bed, at the lowest percentage of the depth possible, the particle will travel at approximately $C_{max.}$ For Chapter 8 simulations, all particles except tidal lateral movers move at a constant rate C_{max}. Because of their interaction with the channel walls and to accommodate anchoring, tidal lateral particles decay as they reach the side.

Anchoring

Anchoring has been added to three of the particle behavior types for Chapter 8 simulation results: tidal lateral movers, tidal vertical movers, and bottom movers. This behavior allows particles to have a method of preventing themselves from being transported away from recruitment regions during the outgoing tide. As the tide comes in, a particle moves upward in the water column (to the top for tidal vertical movers, between 0.5 and 25cm from the bed for bottom movers). As the tide goes out, particles move towards the bottom. When a particle reaches the bottom it remains stationary until the next incoming tide.

To apply anchoring, an improvement in the implementation of the tidal flag was also needed. Within PTM a flag is required that signals to a particle that the tide is in or out. Originally this signal was determined by focusing on the boundary condition of the flow coming in from the Gulf. By looking at a single position, the incoming tide was determined when the water surface elevation increased and the outgoing tide was determined as the water surface elevation decreased.

Now the determination of the incoming tide is more localized. Multiple positions have been chosen around the system. As a particle enters into the range of these locations, the particle references the signal (tide in or tide out) at that position. The tidal flag is determined by the circulation in an area. The tide is in when the flow is in the direction of the flow for incoming tide and the tide is out when the flow is in opposite direction. For a complex system, such as one in which the tidal direction is difficult to establish, this may cause difficulties in accurately simulating the transport of larval fish. In the case of this study, efforts were made to take into account these difficulties by considering alternate tidal directions.

DRAFT

Limitations

PTM has several limitations. Because the model is not coupled with the hydrodynamics, there is an innate assumption within the model that the particles do not affect the hydrodynamics. Therefore in cases where transported particles affect flow conditions, PTM should not be used or should be used with reservations. For sediment and contaminant transport, PTM does not model each and every individual grain of sand. Instead it models representative parcels. For this type of transport, steps must be taken to determine the number of particles which will sufficiently determine qualitative and quantitative trends.

There are also several limitations to the applied larval fish behaviors. The ultimate goal is to model the behavior of the larvae. However, even if it could be modeled in its entirety, larval behavior is not completely understood. Therefore, PTM is applied with the understanding that it is modeling particles that have the aforementioned characteristics and not actual larvae. That is, these particles do not die or consume or have many of the types of realistic life traits which may or may not affect the transport of living organisms. These particles have simplistic character traits which are suspected to affect transport and recruitment time. Analysis of model results must be addressed accordingly.

Another unknown is the validity of the value $C_{max.}$ The current value of 10mm/s is a best estimate due to knowledge of certain larvae species. A true parameterization of this quantity based on specific species and other conditions may eventually be added to the model.

Because of these limitations, the behavioral aspects of this model are still in development. As further information, algorithms, and behavioral catalysts are determined, larval transport characteristic behaviors will be improved. This means that while the model is useful to larval fish transport studies, these limitations should be taken into account during analysis of results. There should also be an understanding that it might be impossible to model in its entirety the complex behavior of larval fish. Instead, the goal of this modeling effort is to determine the major contributors to transport and focus on those characteristics to determine trends and effects.

DRAFT

Simulation Details and Model Input

The simulations for this study are designed to model pathways and recruitment rates for larval fish that migrate from the Gulf of Mexico into Lake Pontchartrain. Bathymetry and hydrodynamic data input have been described in detail within the previous chapters. Ten conditions, obtained from the ADH hydrodynamic computations, were utilized in the simulations. Two months (March 2008 and September 2007) are modeled to reflect the transport variations that can exist due to changes in the seasonal flows as well as five construction phases.

The simulations have been further categorized into three cases. Each case is distinguished by the initial position of the particles (Table 5-2). The details of these cases will be discussed in the following source input section. Four week simulations were run for each of the eight hydrodynamic conditions and cases. Particles are released for a period of two weeks and then transported throughout the system for the remaining two weeks.

Table 5-1. List of species and representative behavior

Species	Behavior
Blue Crab	Tidal Vertical
Brown Shrimp	Tidal Lateral
White Shrimp	Tidal Lateral
Gulf Menhaden	Tidal Lateral
Bay Anchovy	Tidal Lateral
Atlantic Croaker	Bottom Mover
Red Drum	Tidal Lateral
Spotted Sea Trout	Tidal Vertical

Four behaviors are modeled within the simulations. Three of these behaviors are representative of eight species (Table 5-1) determined to be rele-

DRAFT

vant to the system. In addition, passive particles are also modeled to compare the effect of the behaviors.

Generally native sediment data is important to sediment particle transport simulations. However, because these particles represent larval fish behavior and particle-bed interactions are kept to a minimum, native sediment data is irrelevant to these computations.

Source Input

To simulate fish larval sources, PTM requires the following user specified data:

- Date/Time of source release
- Initial Positions (x,y,z) of source introduced into the water column
- Rate of source introduction
- Characteristic larval fish behavior

The date and time of the particle introduction to the system began at the beginning of each hydrodynamic condition. In this study, three cases are considered based on the initial positions of the particles. In all cases, sources are designed to release particles uniformly for the first two weeks of the four week period. This is at the beginning of the modeled hydrodynamic period (see figure 4-5). In addition, larval fish behaviors are evenly distributed between the particles. Particles are placed vertically in the water column based on their representative behavior. Particles that represent bottom movers are introduced close to the bed. Particles that move laterally or vertically based on the tidal position, as well as passive movers, are initiated at the average depth of the flow. The rate of source introduction into the system is determined based on total number of particles simulated. For example, if 4800 particles are initiated over the two week time period, then approximately 342 particles are introduced into the flow field per day. The number of particles chosen for the simulations is based on numerical efficiency, statistical necessity, and visual information. Particles of all behaviors are introduced into the system concurrently.

DRAFT

Case 1

For case 1, particles are released to the east of the MRGO closure at La Loutre (Figure 5-2). Approximately 500 particles are released in this position during the first two week period of the four week simulation. Larval fish behaviors are evenly distributed between the particles. Figure 5-2 shows the approximate initial position (red circle) of the particles released in Case 1.

Figure 5-2. Case 1 initial positions are designated by the red circle.

Case 2

Due to complexities that will be described in the results section, additional initial conditions were chosen for Case 2 closer to the MRGO Bayou Bienvenue closure and the GIWW constriction (see Figure 5-3). For these simulations 4800 particles are modeled. Particles initiated in the GIWW are placed directly to the northeast of the constriction and particles initiated in the MRGO are placed directly southeast of the 2nd MRGO closure.

DRAFT

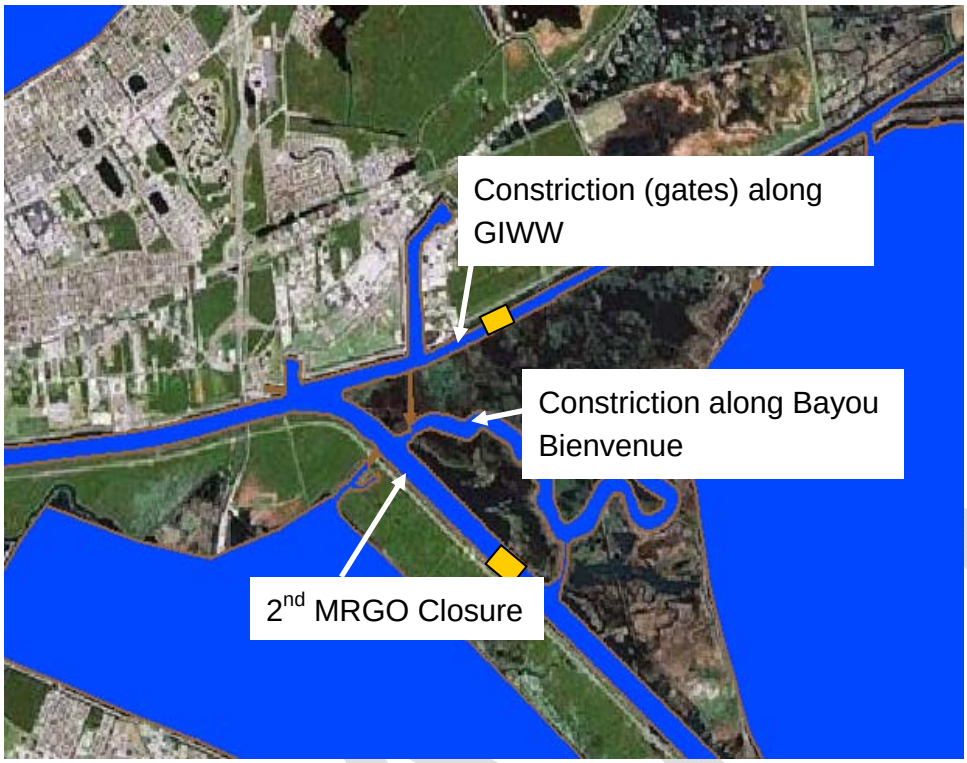

Figure 5-3. Locations of areas in which larvae are initiated for case 1. Yellow colored rectangles represent the locations of initial positions.

Case 3

Case 3 introduces particles within Lake Borgne. These particles are representative of an alternate path (besides the MRGO) through which larval fish are expected to enter the system. Approximately 700 particles are introduced into the system. It should be mentioned that several different positions within Lake Borgne were considered. Initially particles were placed very close to the connection between Lake Borgne and the GIWW. It was determined that ultimately this skewed the results, suggesting that the preferred pathway between Lake Borgne and the Lake Pontchartrain recruitment regions was that connection. Particles were also initiated in the center of Lake Borgne, but statistically relevant recruitment results were difficult to attain utilizing those conditions. That is, not enough particles were able to exit Lake Borgne and subsequently be recruited to determine the effect of the construction phases within the simulation time frame. Finally the conditions seen in Figure 5-4 were developed. Here particles are initiated in a semi circular band along the edges of Lake Borgne representing the paths that particles would take to exit the lake without skewing the results towards any one specific outlet.

Figure 5-4. Location of areas in which larvae are initiated for case 3. Orange colored region represents the location of initial positions.

Case 4

The particle source for this case is similar to that of case 2. However in case 2 there are two source locations. For the case 4 set of simulations, one location (near the 2nd MRGO closure) has been removed (see Figure B-1). In case 4 approximately 2150 particles are released from the GIWW source over a two week period. Particles are then transported for an additional two weeks. The four behaviors are distributed evenly between the particles. In addition, tidal vertical movers and bottom movers have anchoring. Tidal lateral movers and passive movers have no anchoring.

DRAFT

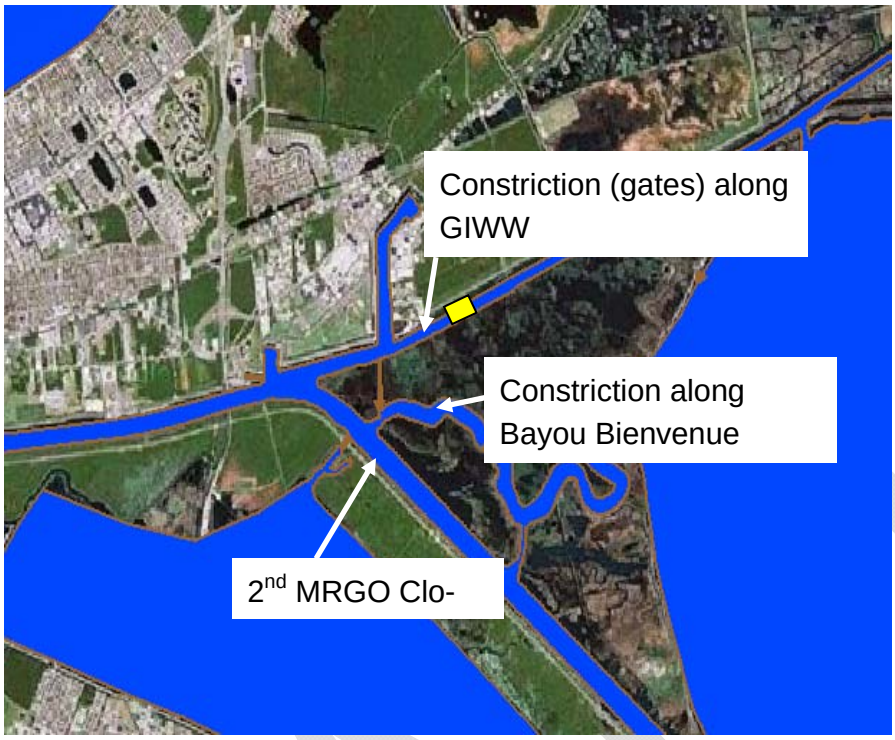

Figure 5-5 Location of area in which larvae are initiated. Yellow colored rectangle represents the location of initial positions.

DRAFT

Table 5-2. Locations of polygon boundaries for initial particle positions for each case

Case	Description of initial starting positions	X coordinate of Polygon in which particles are starting	Ycoordinate of Polygon in which particles are starting
1	Particles initiated in two locations (MRGO @ Bayou Bienevenue and GIWW@ constriction)		
	Location 1	1139268.00	169327.00
		1139315.80	169219.00
		1139458.60	169273.00
		1139405.80	169394.20
	Location 2		
		1137982.00	166224.00
		1138031.00	166125.00
		1138198.70	166269.20
		1138120.00	166362.00
2	Particles initiated in one location (MRGO @ La Loutre)	1170600.00	145890.00
		1170600.00	145690.00
		1170800.00	145600.00
		1170800.00	145780.00
3	Particles initiated in one location (Lake Borgne)	1151870.00	170830.00
		1149610.00	171360.00
		1147090.00	171580.00
		1145130.00	170260.00
		1143820.00	168460.00
		1143370.00	167070.00
		1143480.00	165340.00
		1144270.00	163080.00
		1145510.00	161430.00
		1147200.00	160860.00
		1149570.00	160940.00
		1149570.00	161580.00
		1147730.00	161650.00
		1145890.00	162180.00
		1144680.00	164060.00
		1144040.00	165750.00
		1144460.00	168160.00
		1146490.00	170260.00
		1148290.00	170640.00
		1150550.00	170380.00

DRAFT

Recruitment Regions

A major component of this project is to compare the rate at which larval fish are recruited based on the changes due to the design phase. In this case the term "recruited" refers to particles reaching a position in which they are considered in or near their optimum environmental area where they can then develop into adults. There are two recruitment positions within this system. As shown in Figure 5-5, the first recruitment position is the Seabrook recruitment area (R1). To reach this zone, the particles have to pass through the Seabrook construction area. The second recruitment position is the Chef Menteur recruitment area (R2).

PTM models the recruitment areas using a computational trap. Numerically this is a horizontal arc that is then projected downward through the water column. If particles pass through this arc anywhere within the water column, they are considered recruited. For computational efficiency, once a particle is considered recruited it is removed from the calculations and no longer appear visually in particle position results.

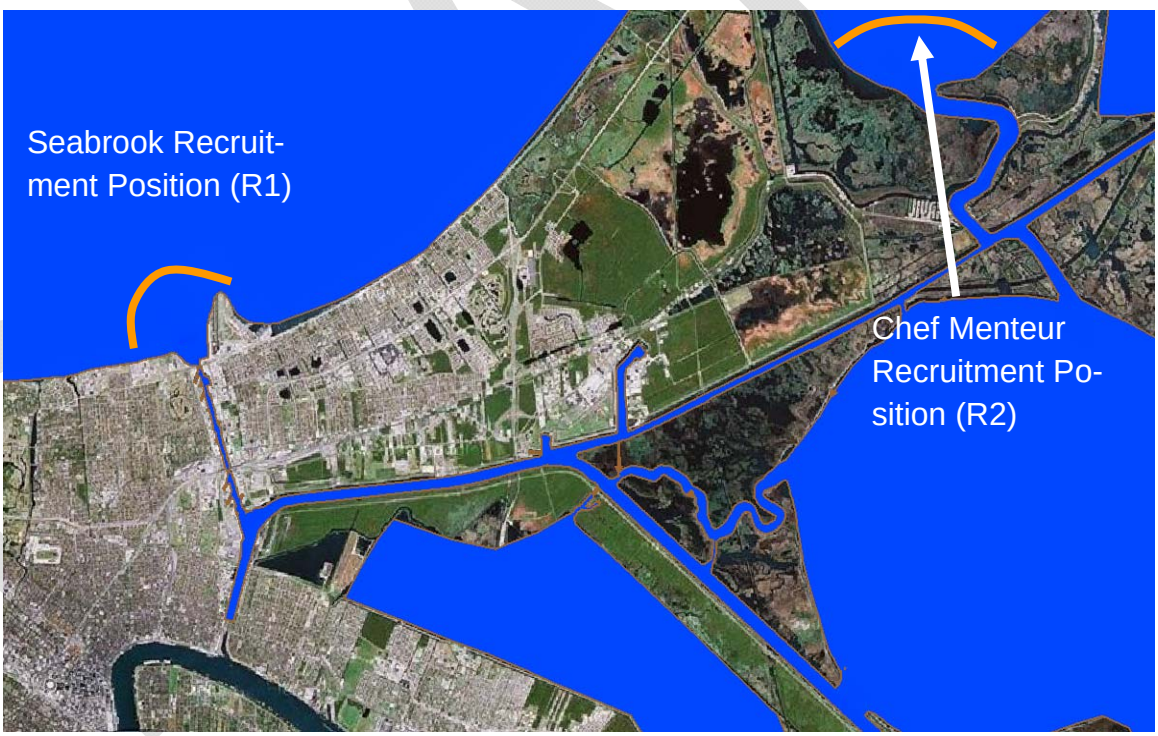

Figure 5-6. Locations of larval fish recruitment regions. Larvae that reach these areas are considered recruited.

6 Hydrodynamic Results

The results of the hydrodynamic simulations are supplied to the particle tracking model in order to drive the transport. An analysis of how the plan conditions affect the velocities and water surface elevations in the area of the structures is given in this section as is a discussion of the circulation changes that result due to the plan conditions.

Velocity Magnitudes

Velocity data were taken in the location of the structures for the Bayou Bienvenue structure, the GIWW sector gate, the GIWW barge gate, and the Seabrook structure. Figures 6-1 and 6-2 show these locations. For the base condition and plans 1 and 2, data are analyzed at a location north of the Seabrook structure location where the velocities are greatest. The analysis for Plan 3 and Plan 3 Final is at the location in each Seabrook structure where the velocity magnitudes are also the greatest. For Plan 3 Final, this location is in the center sector gate. The chosen location of the analysis is the position which yields the velocity maximum for each plan. It is important to keep in mind that velocities will increase given the same flux when the cross-sectional area is reduced simply due to continuity. Although the changes to the system do change the flux passing through the structures, the ratio of the two is not constant and therefore, once a structure is in place at these locations, it is not unlikely that the velocity magnitudes will rise within the structure.

DRAFT

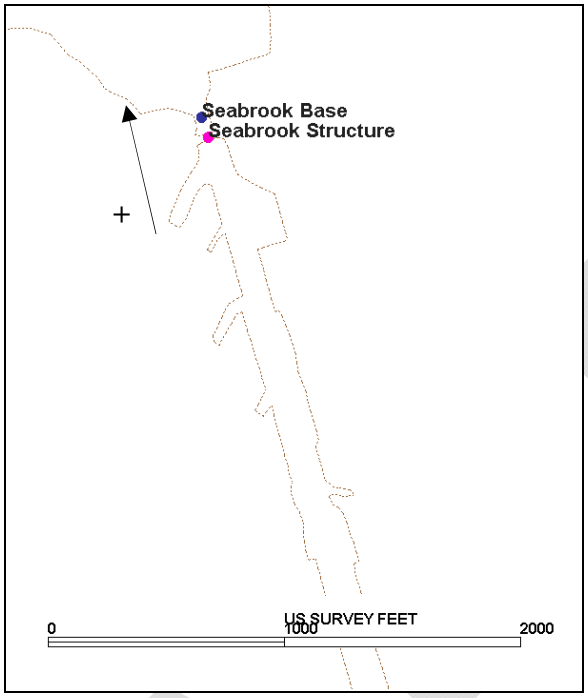

Figure 6-1. Hydrodynamic analysis locations - Seabrook

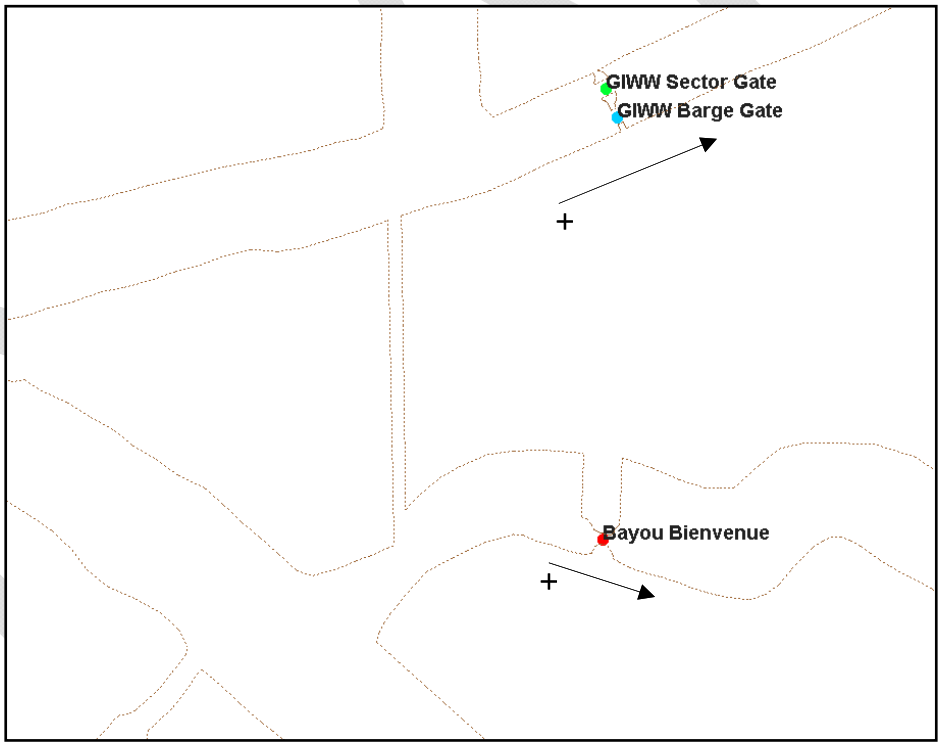

Figure 6-2. Hydrodynamic analysis locations – Bayou Bienvenue Structure, GIWW Sector Gate, and GIWW Barge Gate

The average velocity for flood and ebb are determined at each location and time period for the base and three plans as are the maximum velocities for all conditions. Since there is a circulation within this system through the GIWW, the definition of flood and ebb can be misleading. For this reason a definition of positive and negative or flood and ebb is necessary. Positive values are defined as those directed predominantly toward the north or east and negative values are defined as those directed predominantly toward the south or west. The arrows in Figures 6-1 and 6-2 show the positive direction for each location. The results of this analysis are given in Figures 6-3 through 6-10. A direction arrow is included for each location to help define the flow direction.

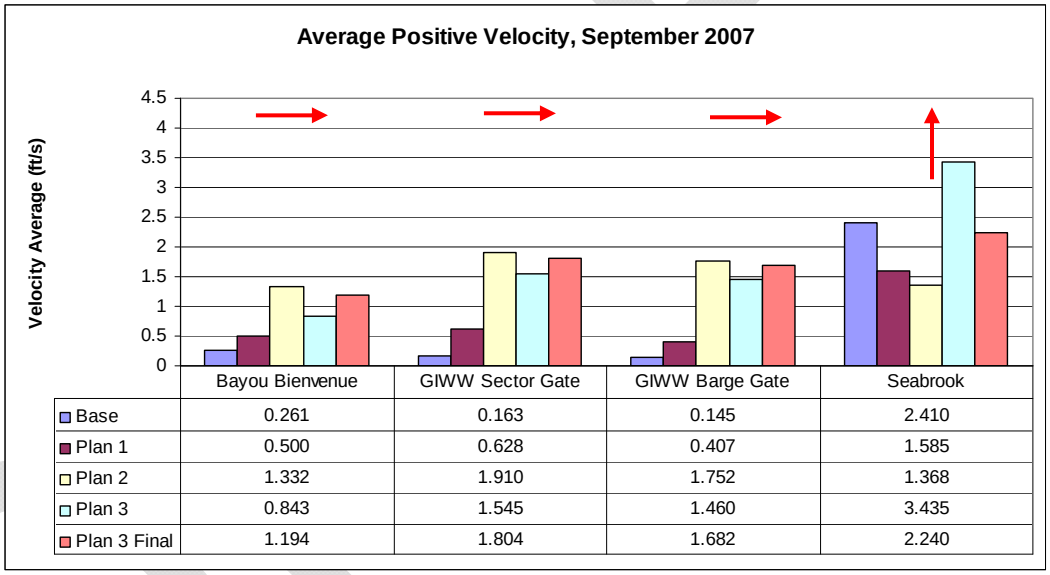

	Bayou Bienvenue	GIWW Sector Gate	GIWW Barge Gate	Seabrook
Base	0.261	0.163	0.145	2.410
Plan 1	0.500	0.628	0.407	1.585
Plan 2	1.332	1.910	1.752	1.368
Plan 3	0.843	1.545	1.460	3.435
Plan 3 Final	1.194	1.804	1.682	2.240

Figure 6-3. Velocity average for September (positive)

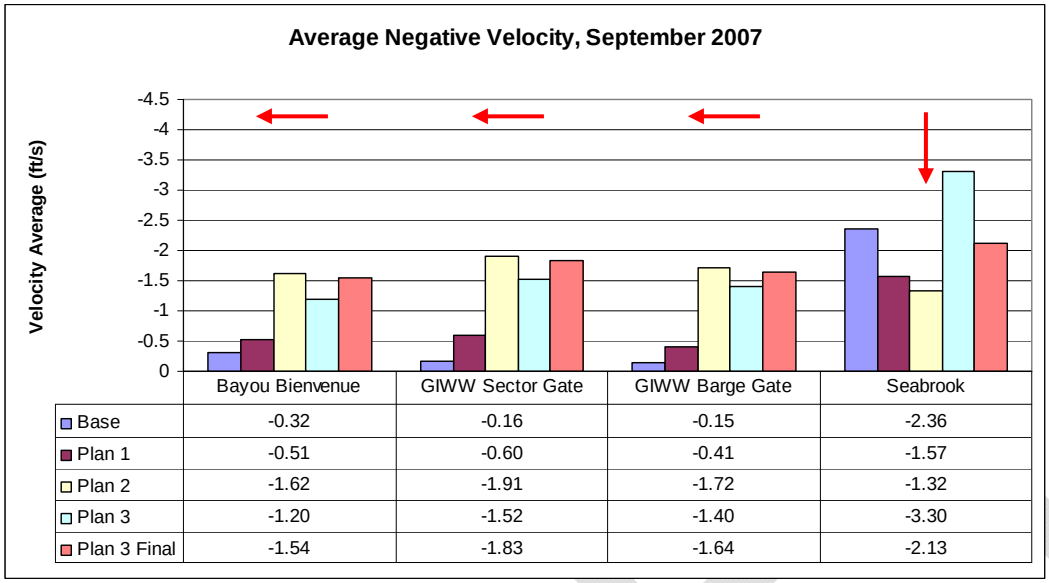

	Bayou Bienvenue	GIWW Sector Gate	GIWW Barge Gate	Seabrook
Base	-0.32	-0.16	-0.15	-2.36
Plan 1	-0.51	-0.60	-0.41	-1.57
Plan 2	-1.62	-1.91	-1.72	-1.32
Plan 3	-1.20	-1.52	-1.40	-3.30
Plan 3 Final	-1.54	-1.83	-1.64	-2.13

Figure 6-4. Velocity average for September (negative)

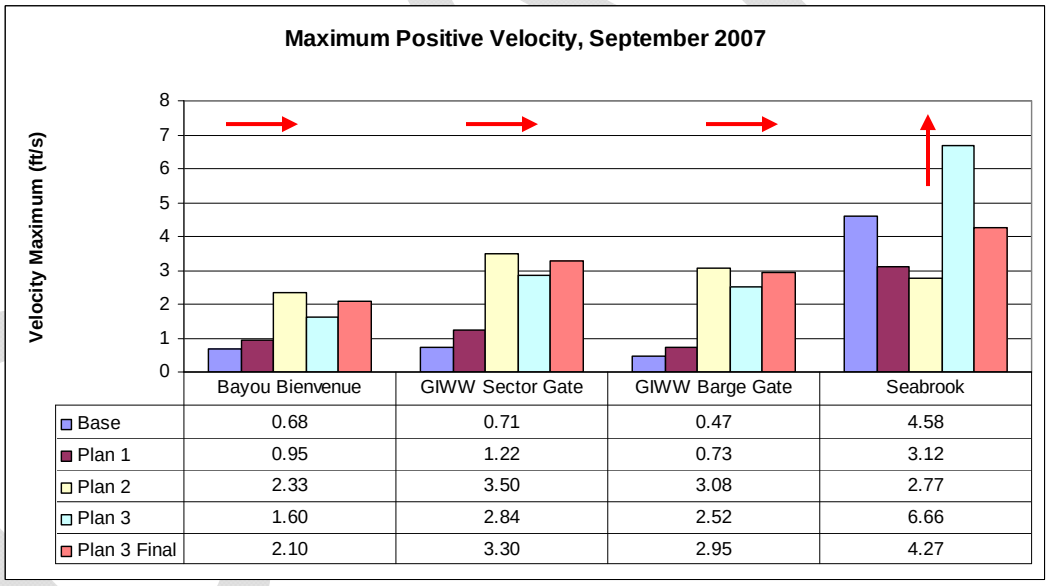

	Bayou Bienvenue	GIWW Sector Gate	GIWW Barge Gate	Seabrook
Base	0.68	0.71	0.47	4.58
Plan 1	0.95	1.22	0.73	3.12
Plan 2	2.33	3.50	3.08	2.77
Plan 3	1.60	2.84	2.52	6.66
Plan 3 Final	2.10	3.30	2.95	4.27

Figure 6-5. Velocity maximum for September (positive)

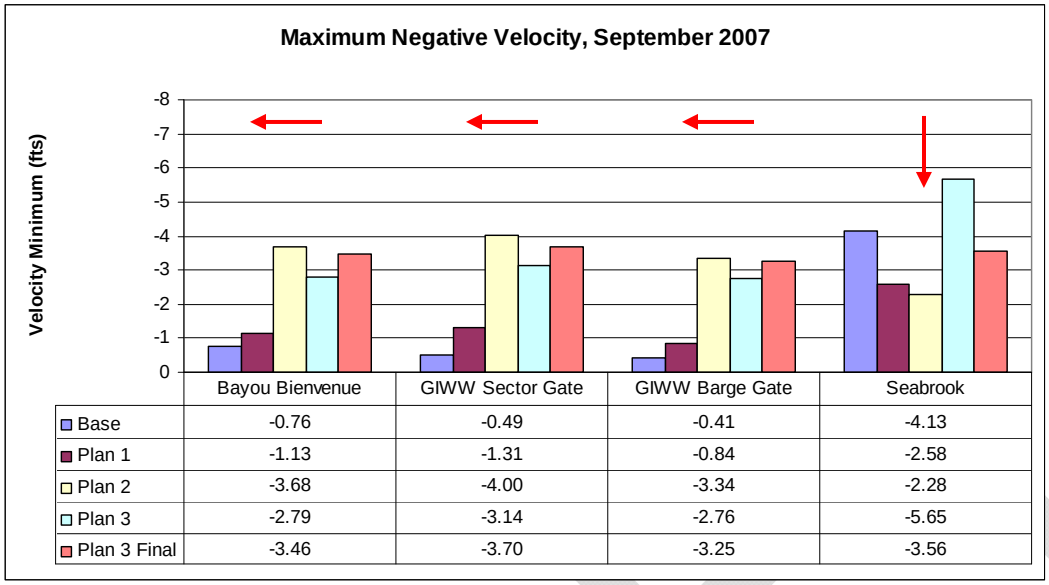

	Bayou Bienvenue	GIWW Sector Gate	GIWW Barge Gate	Seabrook
Base	-0.76	-0.49	-0.41	-4.13
Plan 1	-1.13	-1.31	-0.84	-2.58
Plan 2	-3.68	-4.00	-3.34	-2.28
Plan 3	-2.79	-3.14	-2.76	-5.65
Plan 3 Final	-3.46	-3.70	-3.25	-3.56

Figure 6-6. Velocity minimum for September (negative)

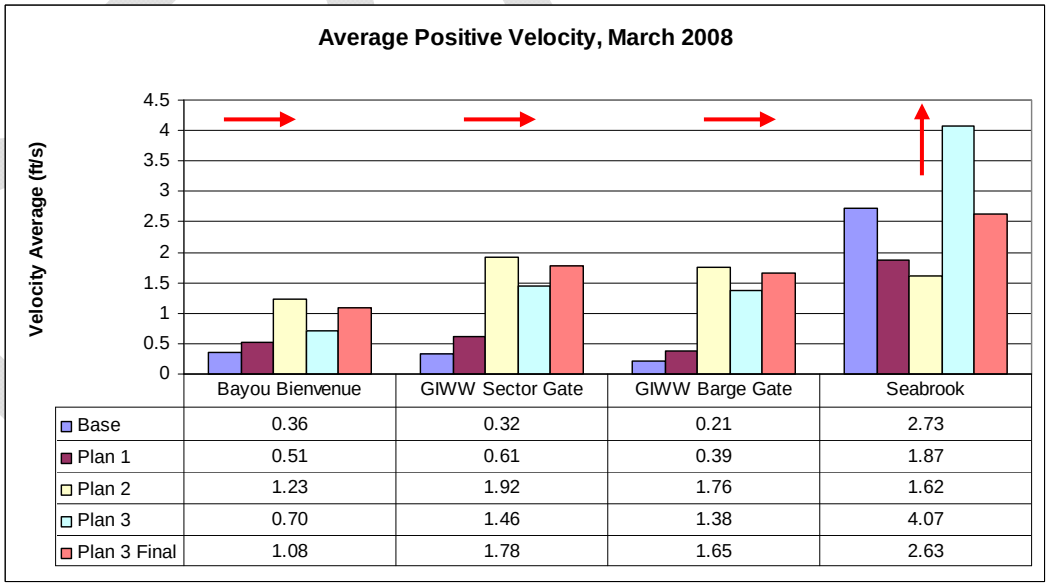

	Bayou Bienvenue	GIWW Sector Gate	GIWW Barge Gate	Seabrook
Base	0.36	0.32	0.21	2.73
Plan 1	0.51	0.61	0.39	1.87
Plan 2	1.23	1.92	1.76	1.62
Plan 3	0.70	1.46	1.38	4.07
Plan 3 Final	1.08	1.78	1.65	2.63

Figure 6-7. Velocity average for March (positive)

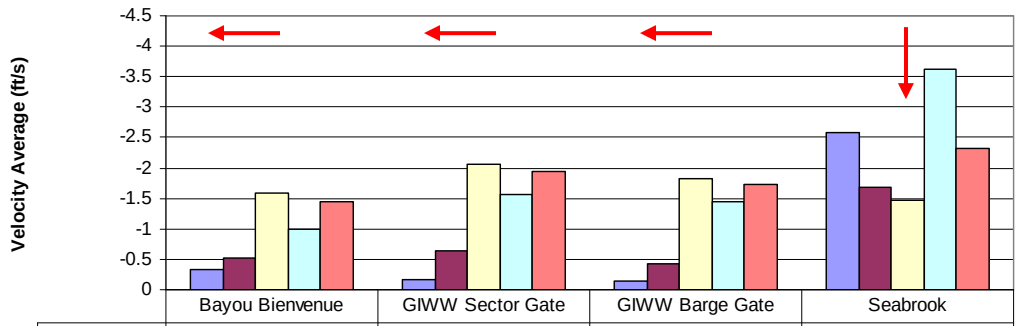

	Bayou Bienvenue	GIWW Sector Gate	GIWW Barge Gate	Seabrook
Base	-0.33	-0.18	-0.14	-2.59
Plan 1	-0.53	-0.65	-0.42	-1.68
Plan 2	-1.58	-2.06	-1.83	-1.46
Plan 3	-1.01	-1.56	-1.45	-3.63
Plan 3 Final	-1.43	-1.93	-1.73	-2.33

Figure 6-8. Velocity average for March (negative)

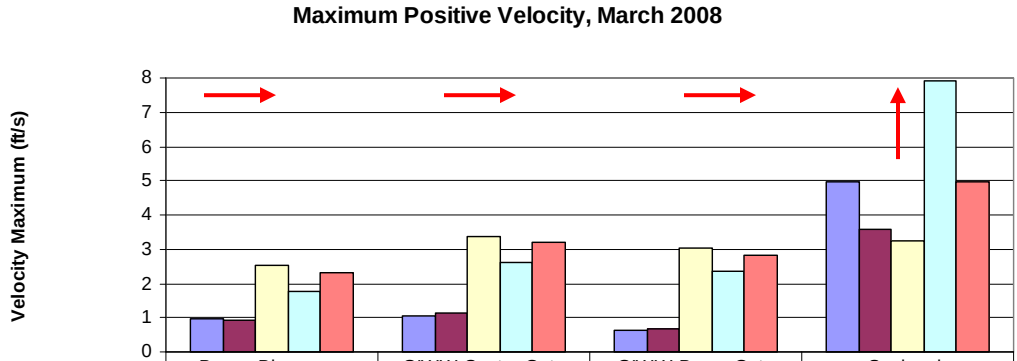

	Bayou Bienvenue	GIWW Sector Gate	GIWW Barge Gate	Seabrook
Base	0.98	1.03	0.64	4.98
Plan 1	0.93	1.16	0.67	3.57
Plan 2	2.52	3.39	3.02	3.23
Plan 3	1.77	2.61	2.34	7.90
Plan 3 Final	2.32	3.20	2.82	4.97

Figure 6-9. Velocity maximum for March (positive)

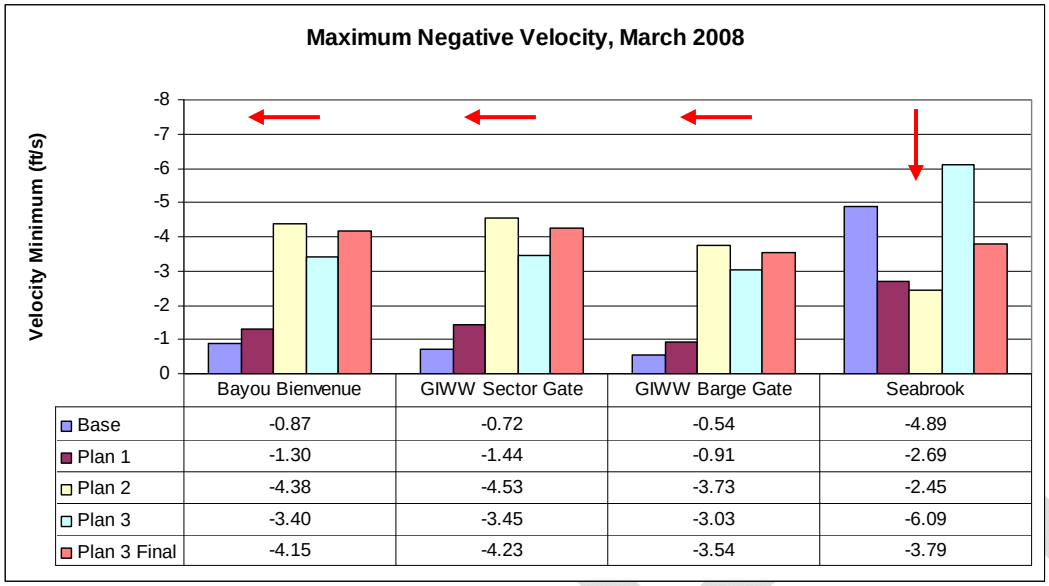

Figure 6-10. Velocity minimum for March (negative)

These figures show that the March conditions for the base case generally produce higher velocity magnitudes than the September conditions, although these differences are not great. Due to the high flow event that occurs around mid-March (see Figure 4-4), the extreme velocity magnitudes will be higher for the March simulations.

In the Plan 1 condition, the velocity increases in the GIWW structure locations as compared to the Base for both September and March. Once the MRGO is initially blocked at La Loutre, the flow in the eastern section of the GIWW in the vicinity of the 150 ft X 16 ft gates is increased. It increases again with the inclusion of the Plan 2 structures, although by a much greater fraction due to the structures being applied at these locations. The velocities at these locations then drop when the Seabrook structure is included with Plan 3. These structures, individually and collectively, restrict the transport of flow in the GIWW and IHNC. Plan 3 Final allows for increased flows through the GIWW structures for the same reason Plan 3 reduces the flows. With Plan 3 Final there is more flow area so the exchange into the system is larger when the three structures are included for flow passage.

At the Bayou Bienvenue structure, the closures of the MRGO at La Loutre and again at the location south of Bayou Bienvenue create an increase in velocity magnitudes through this smaller waterway. As with the GIWW structures, once the structure is in place on Bayou Bienvenue the velocities at this location increase greatly. However, the same effect is seen here as in the GIWW. Once the Seabrook structure is in place for Plan 3, the velocity magnitudes are reduced. Yet Plan 3 Final again allows for more exchange and produces an increase in flow through the Bayou Bienvenue structure.

For March and September the velocities are highest at Seabrook for both the Base and Plan 3 configurations. The drop in velocity magnitude at Seabrook for Plans 2 and 3 is due primarily to the closure of the MRGO at La Loutre and the decreasing flow volume into the system. With each closure (at La Loutre in Plan 1 and south of Bayou Bienvenue in Plan 2) the velocity drops at Seabrook. Once the Plan 3 structure is in place at Seabrook these velocities increase simply due to the constriction created by the gate structure and reduction in cross-sectional area. However, Plan 3 Final generates a reduction in the flows due to the increase in cross-sectional area from Plan 3 such that the flow magnitudes drop at Seabrook to values below those observed for the base condition.

These extreme velocity magnitudes, however, are simply that – a maximum value at some point during the simulation. They do not occur often during the simulation. A percent exceedance (i.e. percent less than) analysis is performed to determine how often during the four week simulation periods the velocity magnitudes are within certain ranges. Figures 6-12 through 6-28 show the percent less than plots for the locations given in Figure 6-11. These locations are the same as those in the previous velocity analysis (see Figures 6-1 and 6-2) as well as additional locations in Lake Borgne, Lake Pontchartrain, Chef Menteur, and the Rigolets. These plots show velocity magnitude on the x-axis and percentage of time on the y-axis. At the maximum velocity magnitude, the percentage is almost 100 since the velocity is less than this over the length of the simulation. All lines cross zero at 0% since the velocity magnitude is always greater than zero. Where each line crosses 50% the velocity is greater half the time and less half the time over the 4 week analysis period.

DRAFT

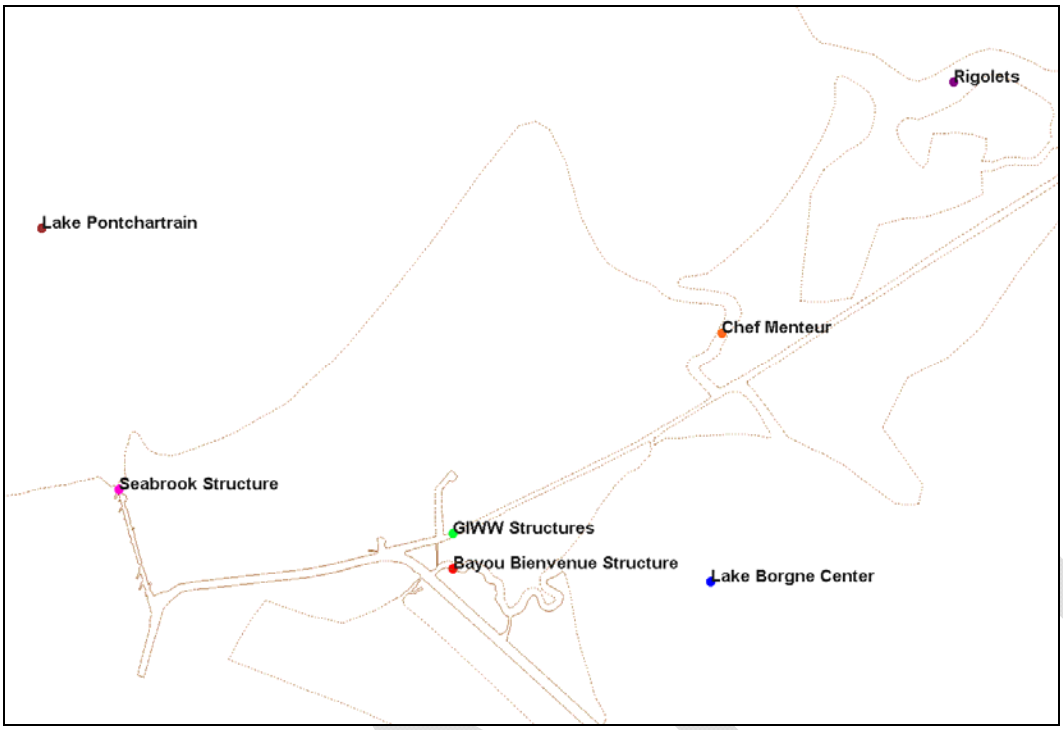

Figure 6-11. Percent exceedance of velocity magnitude analysis locations

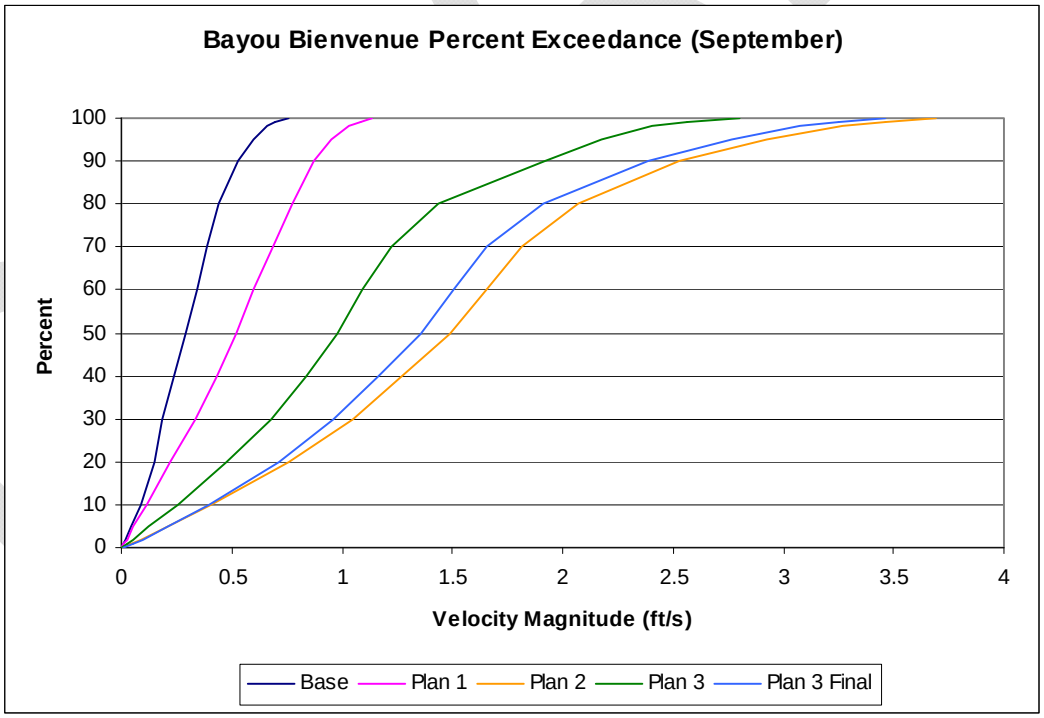

Figure 6-12. Bayou Bienvenue percent exceedance plot for September

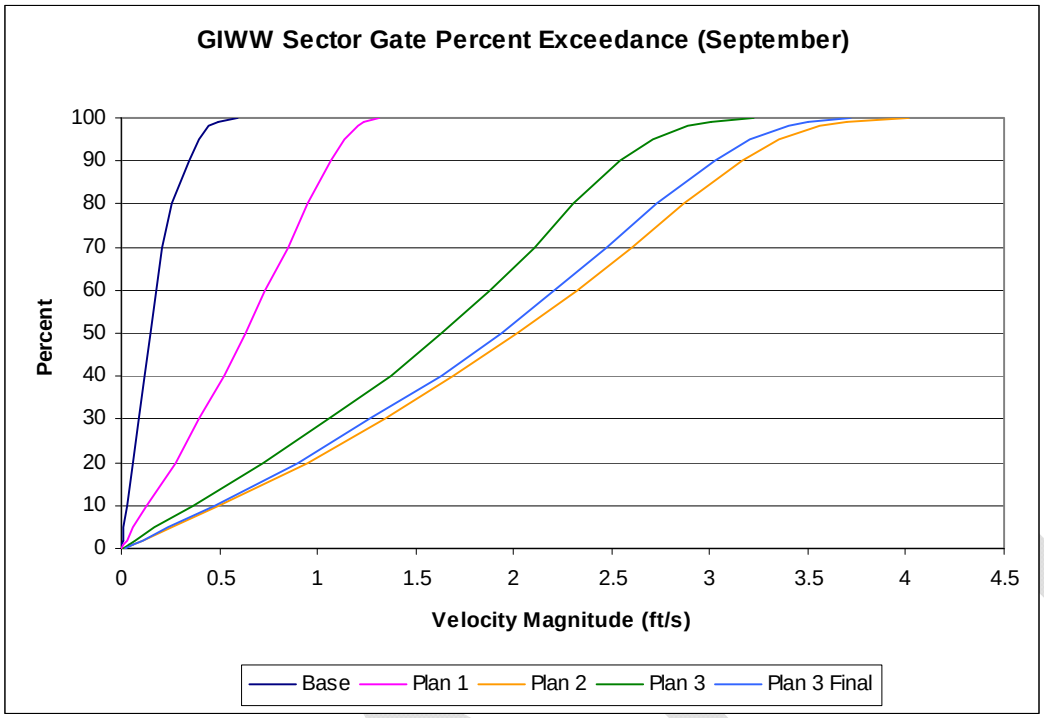

Figure 6-13. GIWW Sector Gate percent exceedance plot for September

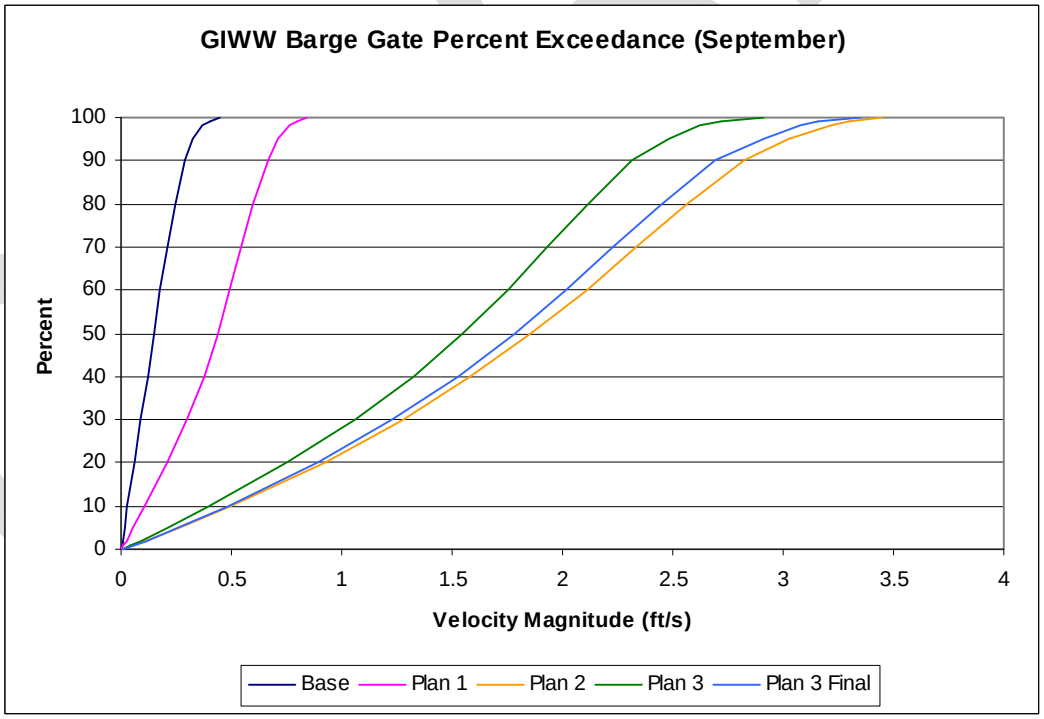

Figure 6-14. GIWW Barge Gate percent exceedance plot for September

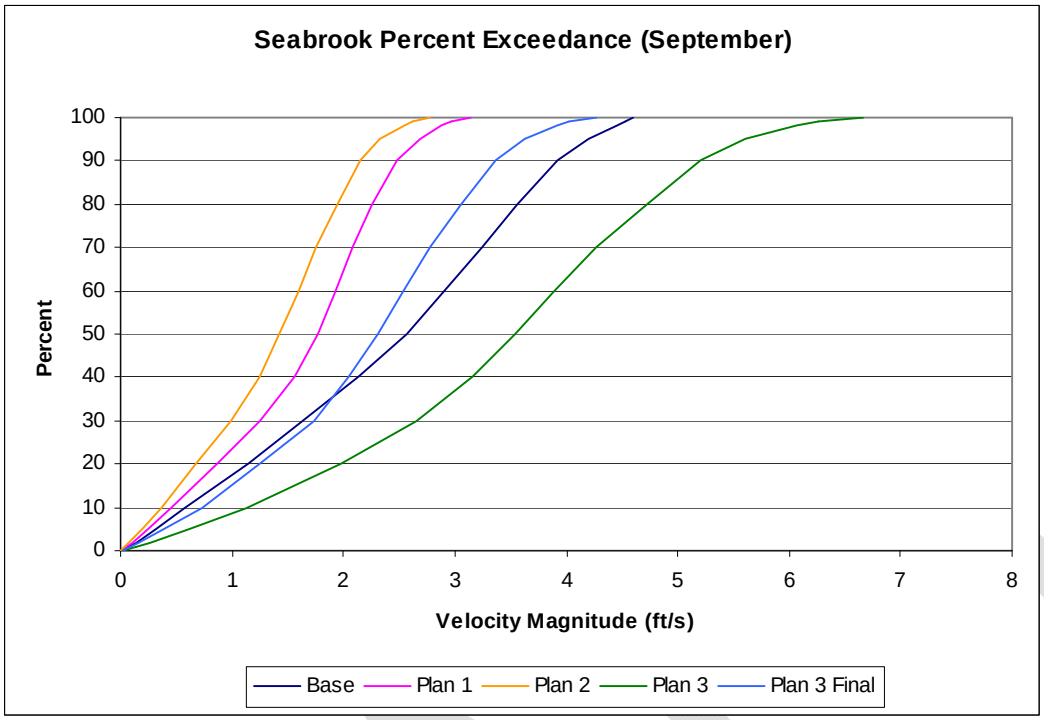

Figure 6-15. Seabrook percent exceedance plot for September

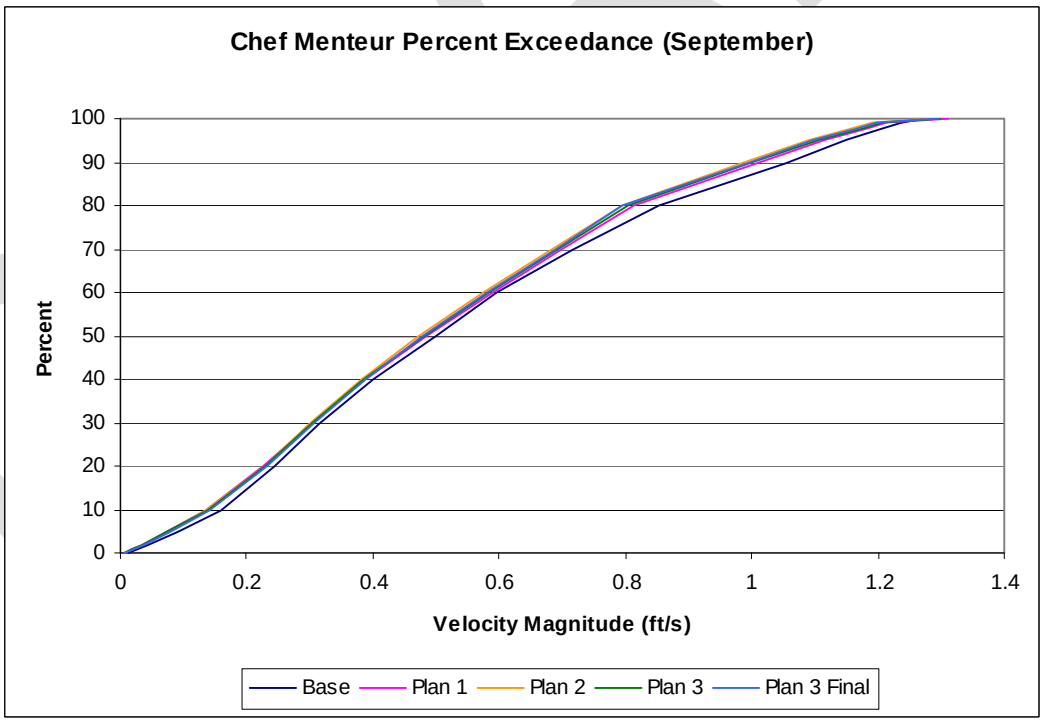

Figure 6-16. Chef Menteur percent exceedance plot for September

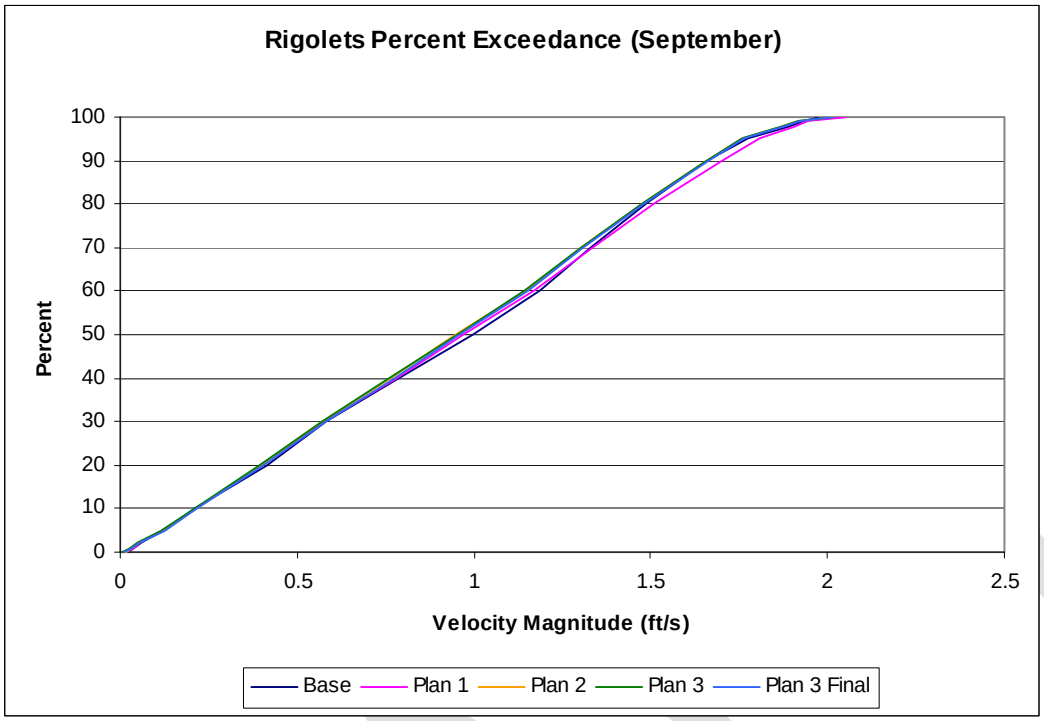

Figure 6-17. Rigolets percent exceedance plot for September

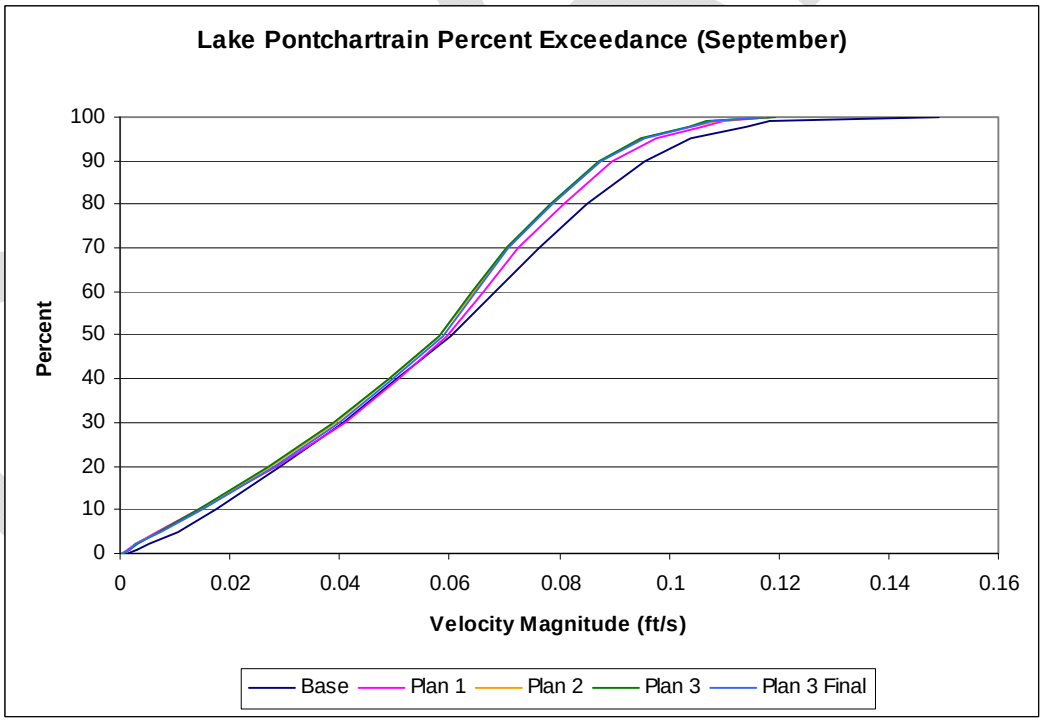

Figure 6-18. Lake Pontchartrain percent exceedance plot for September

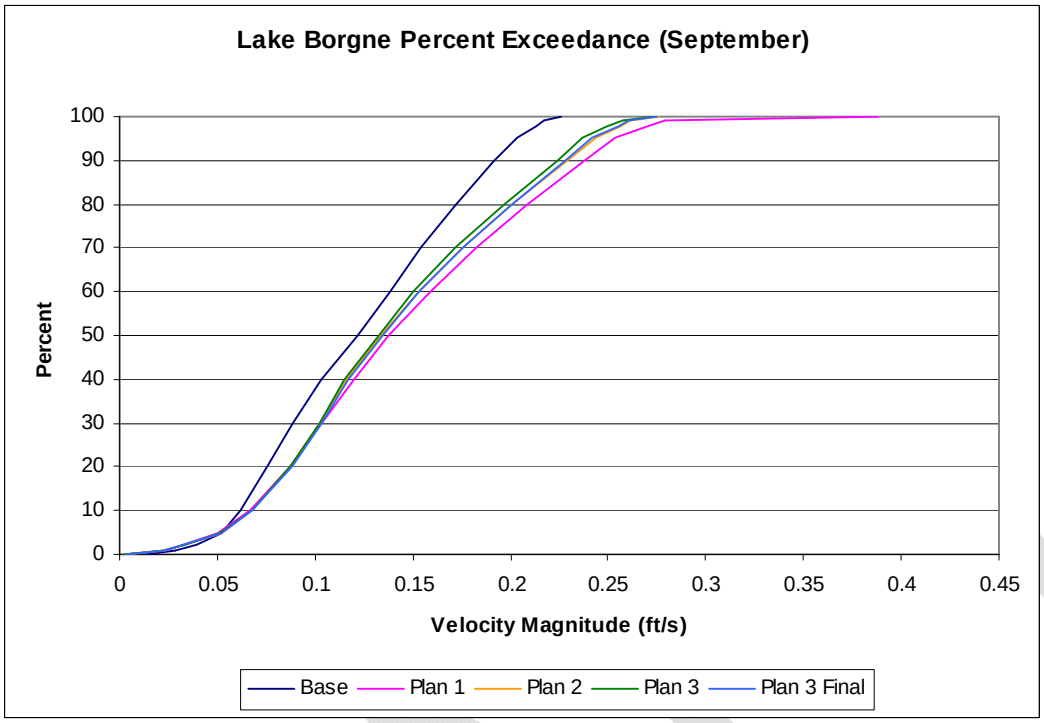

Figure 6-19. Lake Borgne percent exceedance plot for September

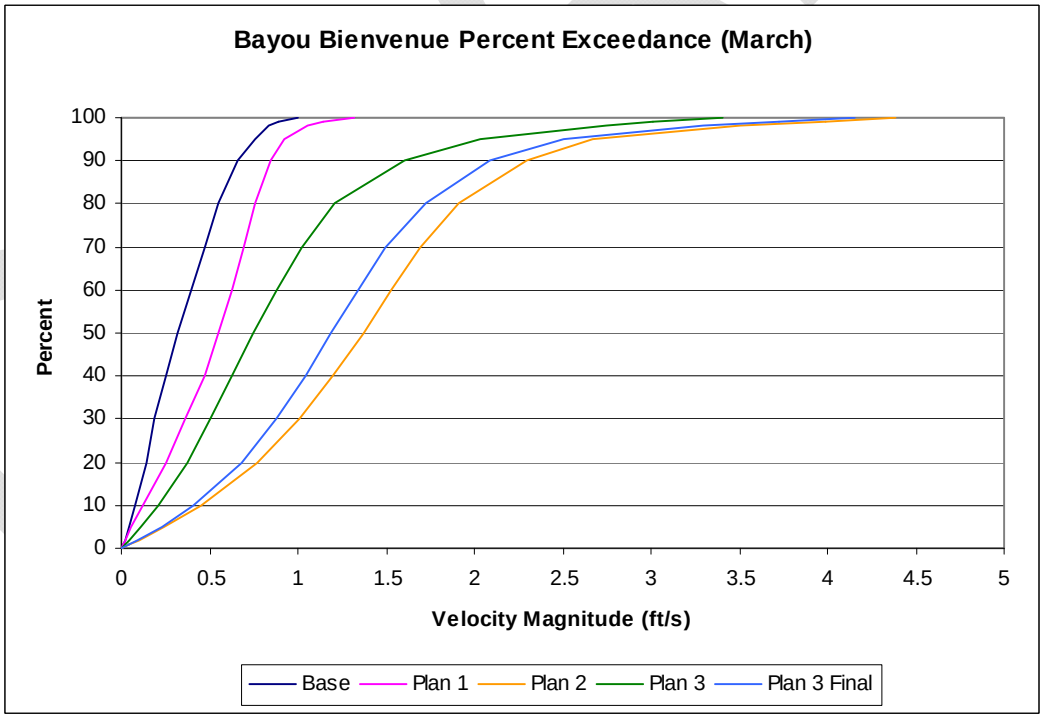

Figure 6-20. Bayou Bienvenue percent exceedance plot for March

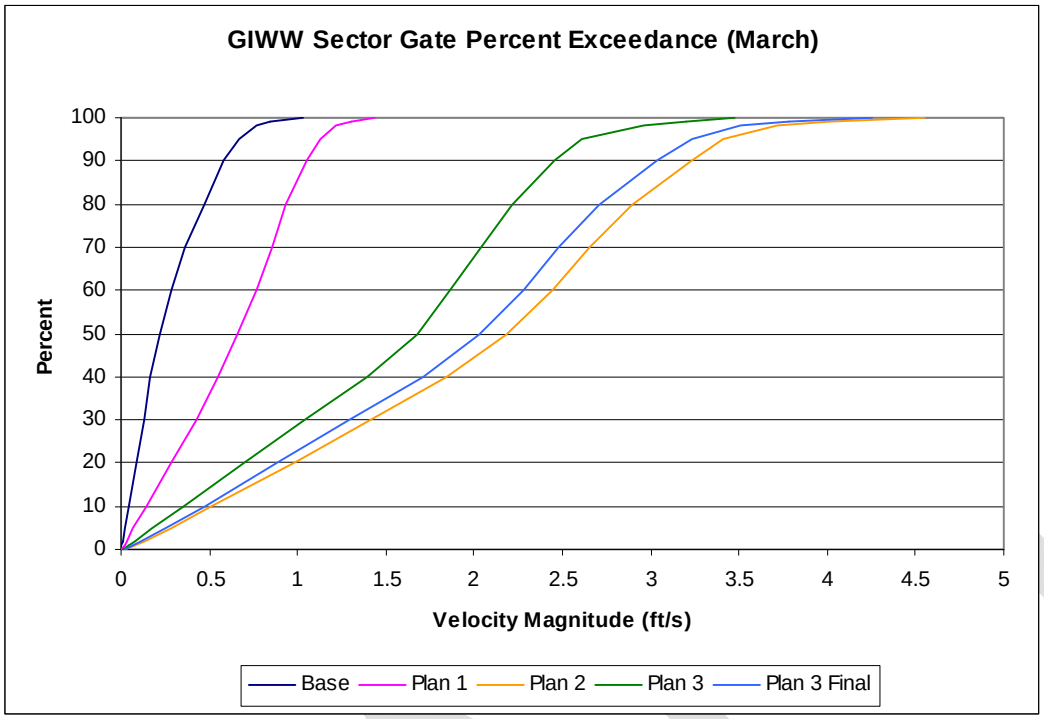

Figure 6-21. GIWW Sector Gate percent exceedance plot for March

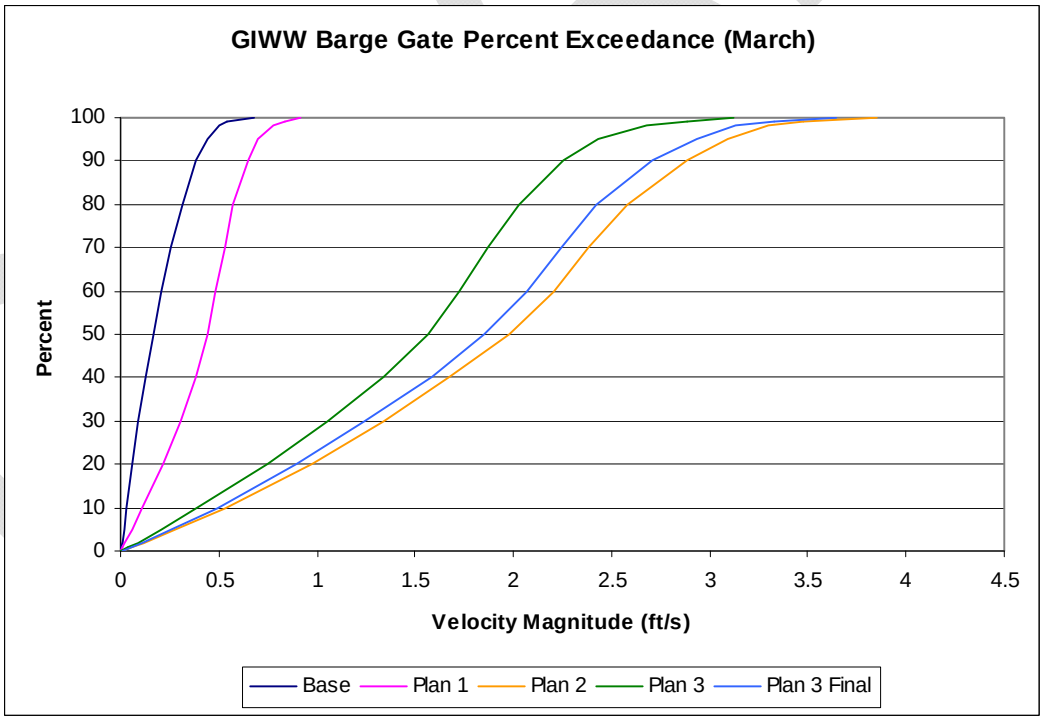

Figure 6-22. GIWW Barge Gate percent exceedance plot for March

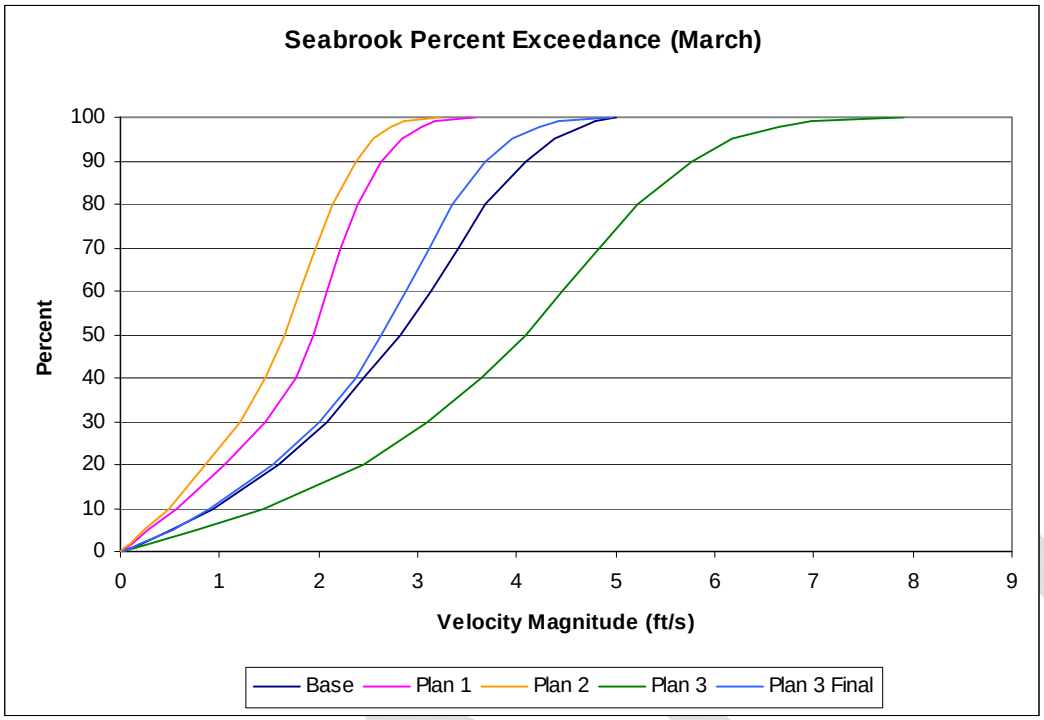

Figure 6-23. Seabrook percent exceedance plot for March

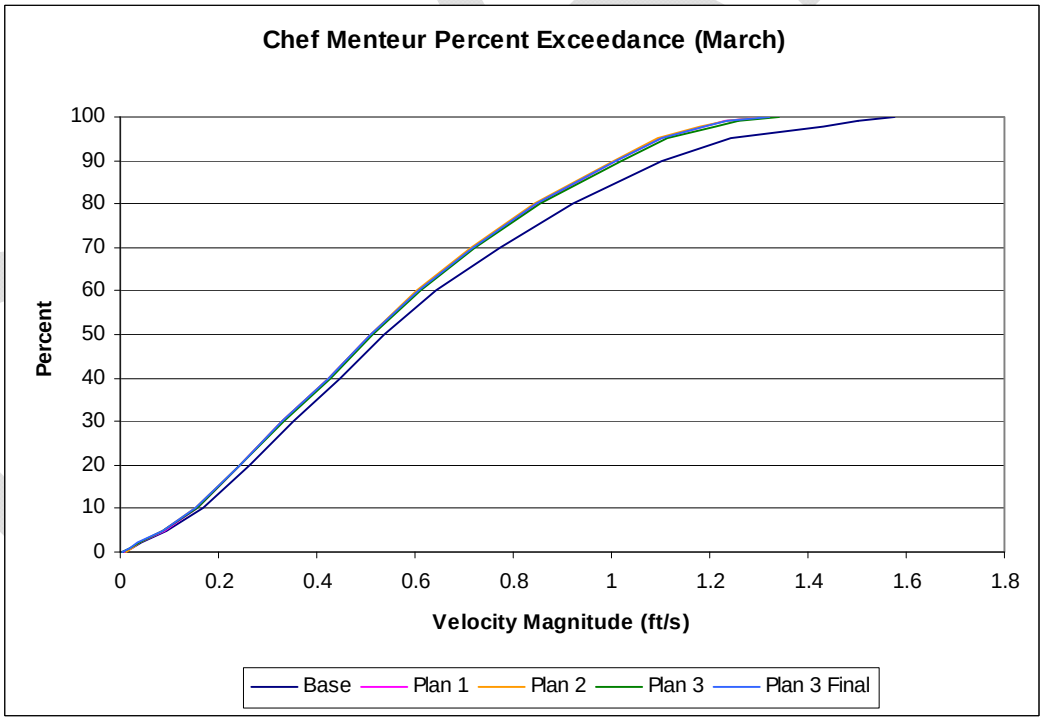

Figure 6-24. Chef Menteur percent exceedance plot for March

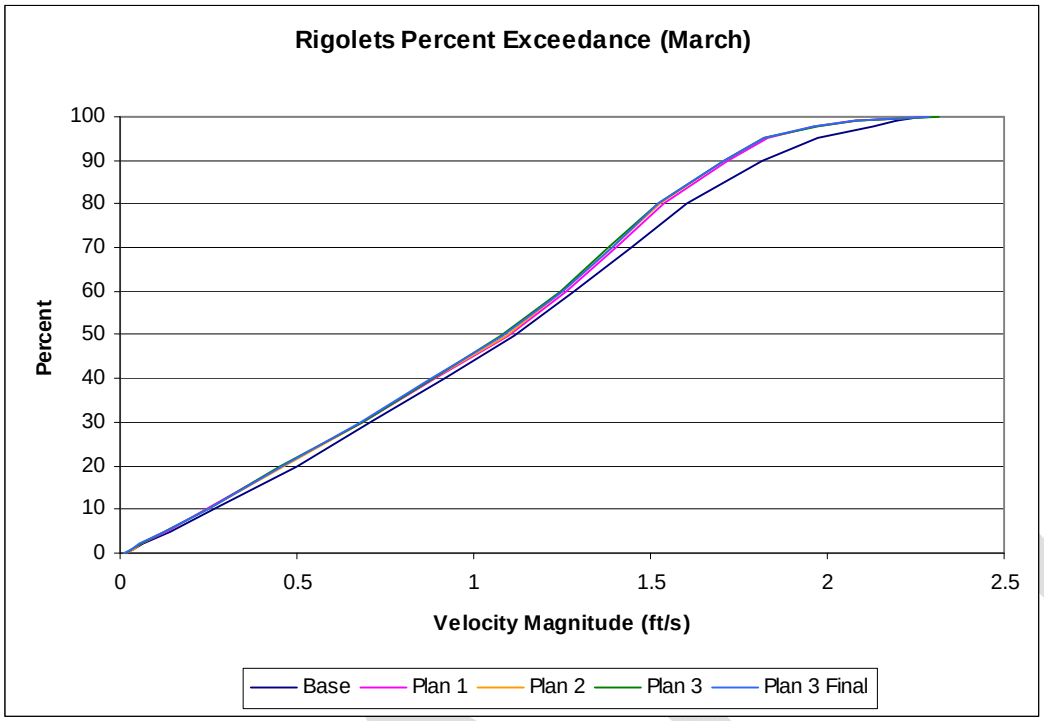

Figure 6-25. Rigolets percent exceedance plot for March

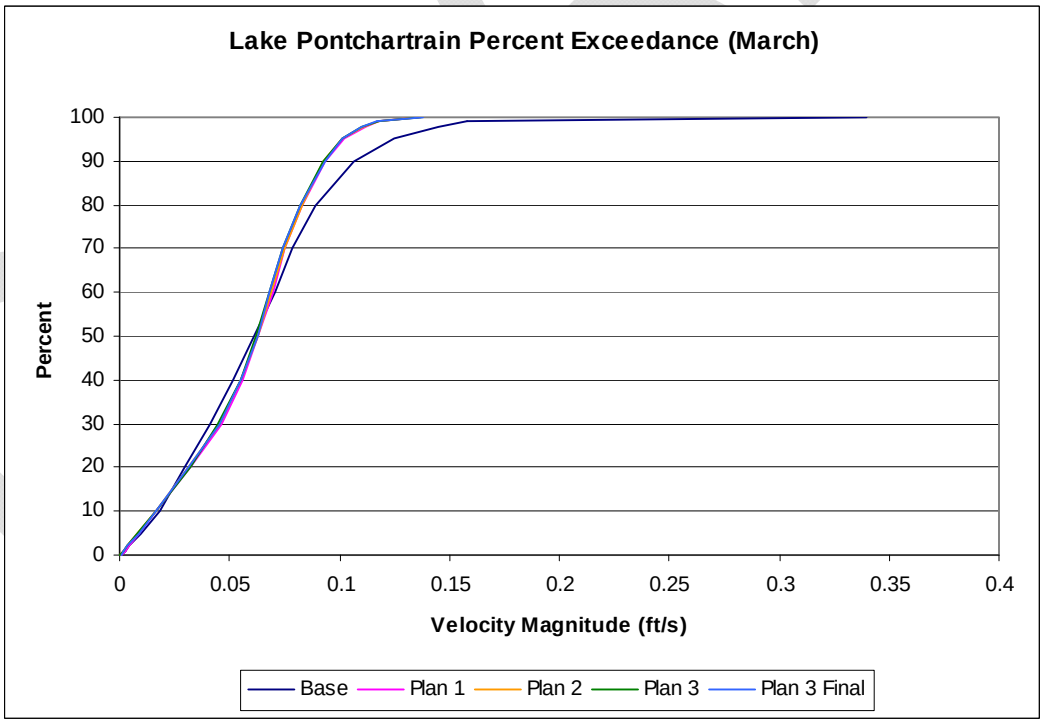

Figure 6-26. Lake Pontchartrain percent exceedance plot for March

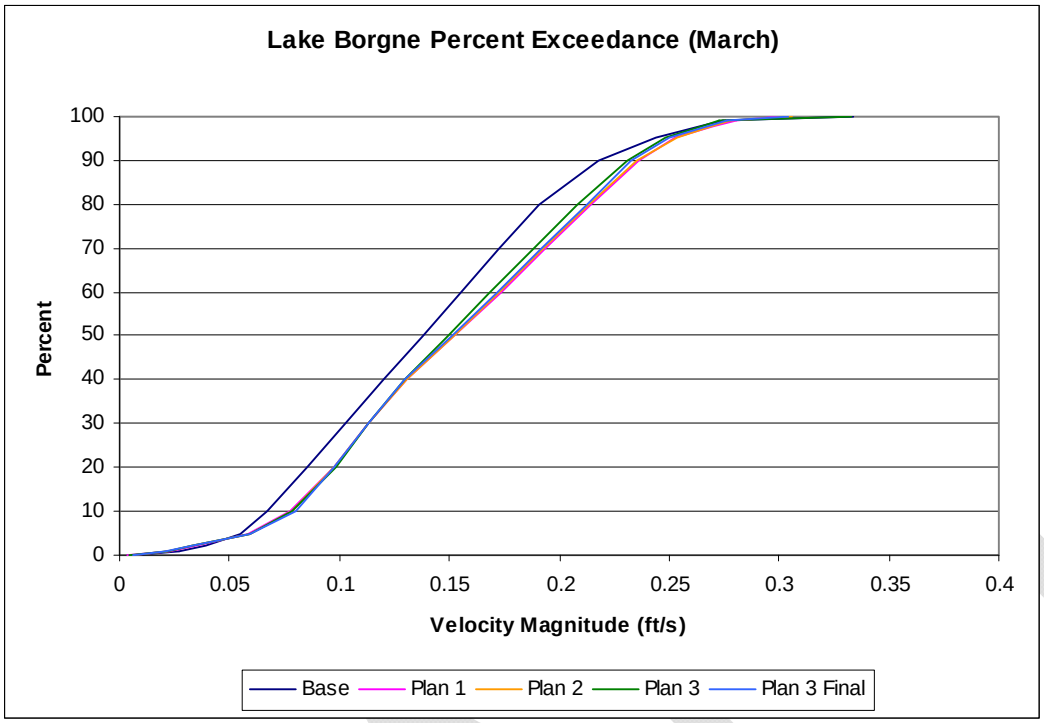

Figure 6-27. Lake Borgne percent exceedance plot for March

Figures 6-12 through 6-27 show that the velocity differences between the base and plan conditions are significant in the location of the structures. Not only are the maximum flood and ebb values larger for the plans but so are the values in general. For the locations in the structures, the velocity patterns are the same as those seen in the previous figures. Plan 1 velocities are higher than the Base in most cases and continue to increase with Plan 2 but then reduce when the Seabrook structure is included. Plan 3 reduces velocities in the structures more than Plan 3 Final since it has a cross-sectional area about half that of Plan 3 Final. The velocities at the Seabrook structure, however, reduce from the Base condition with Plan 1 and Plan 2 due to the reduction in flow from the MRGO and then increase once the structure is in place. In the Seabrook structure, velocities increase with Plan 3 but Plan 3 Final produces a drop in velocity to values comparable with the Base condition. Again, this is due to changes in flow area. These patterns are observed for both the September and March flow conditions.

The percent exceedance plots for Chef Menteur and the Rigolets show that the velocity values, and therefore fluxes, are affected very little when the plan conditions are in place. At Chef Menteur there is a slight reduction in

the velocity magnitudes and the frequency of these magnitudes. This trend is more obvious in March but seen in September as well. At the Rigolets this trend is less noticeable. It appears to occur in March but the September conditions produce little change.

The final two analysis locations are in the center of Lake Borgne and Lake Pontchartrain. These locations are further away from the plan modifications so their analysis can help understand how the flow patterns are changed with each plan alternative. The velocity magnitudes in these two locations are very small. Maximum values are less than 0.4 ft/s for both September and March. In Lake Borgne, the velocities increase once the MRGO is cut off from the Gulf of Mexico with Plan 1. This result is reasonable since the flow that previously traveled the MRGO is now forced into Lake Borgne. In Lake Pontchartrain there is a reduction in velocity magnitude. This result is due to the reduction of total flow into the lake since the MRGO was a large transport mechanism for flow into Lake Pontchartrain. However, the drop in velocity magnitude is very small overall since the Rigolets and Chef Menteur remain open and continue to allow flow into this area.

Water Surface Analysis

A water surface elevation analysis is performed at a total of 16 points within the model domain. The initial locations are set at 250 ft to each side of a proposed structure. Six additional locations are chosen so that an overall response to the system due to the plan alternatives can be observed. Figures 6-28 and 6-29 show the analysis locations. Locations for each side of a structure are shown as a single point. This analysis is performed on both the September and March flow conditions. The water surface elevation for each location and alternative is shown in Figures 6-30 to 6-61. These figures display 12.5 days of the simulation (August 22 – September 3, 2007; March 9 - 21, 2008).

DRAFT

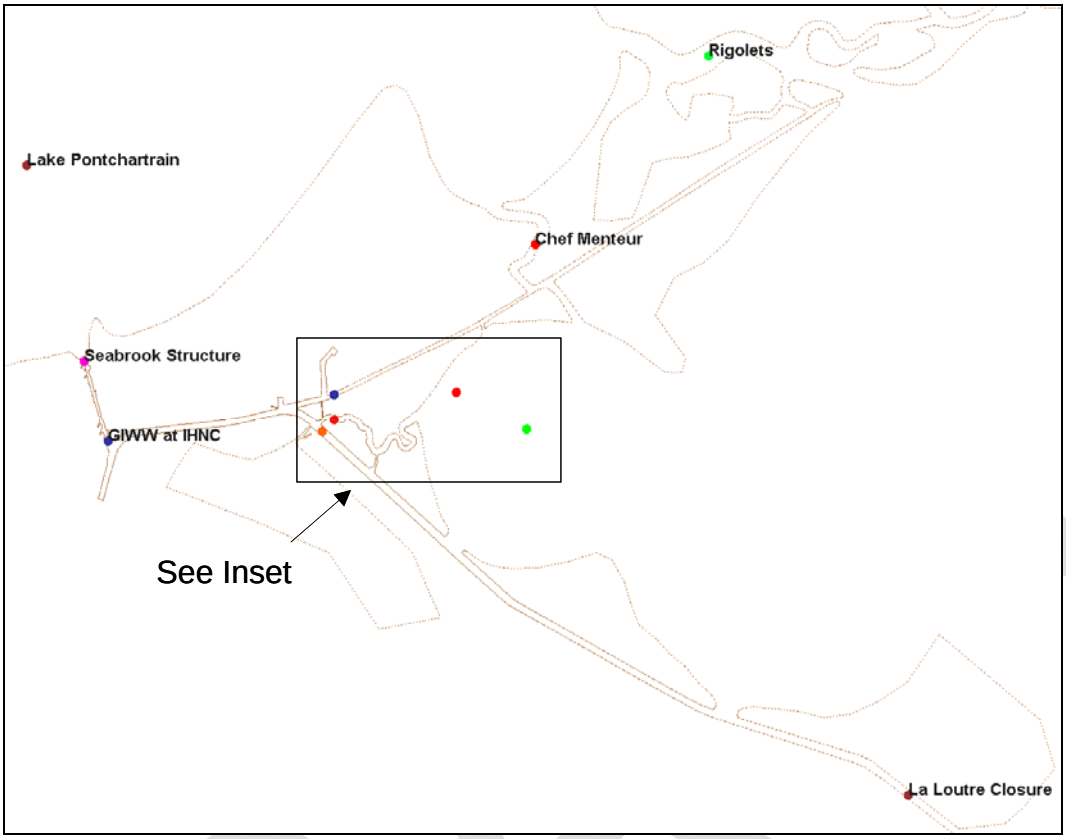

Figure 6-28. Location map for water surface analysis

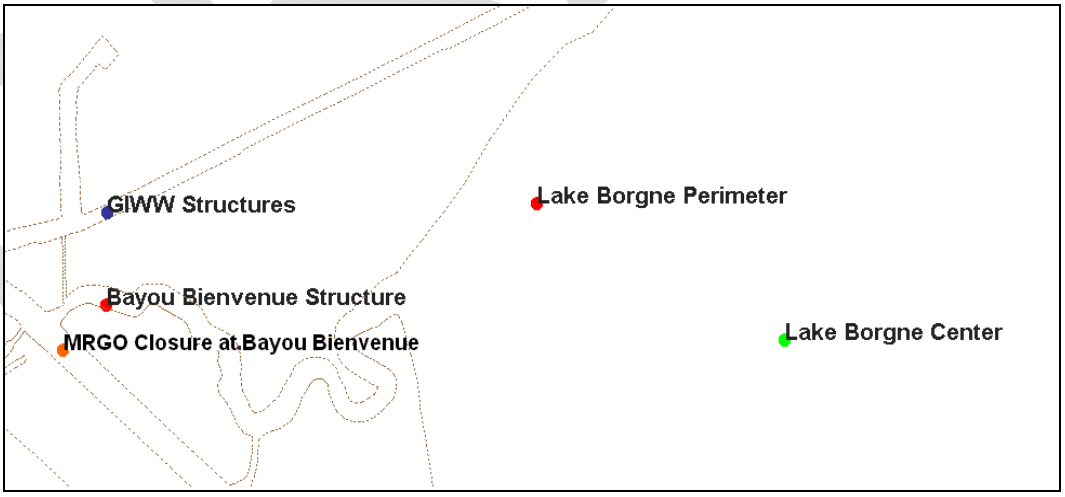

Figure 6-29. Inset for water surface analysis location map

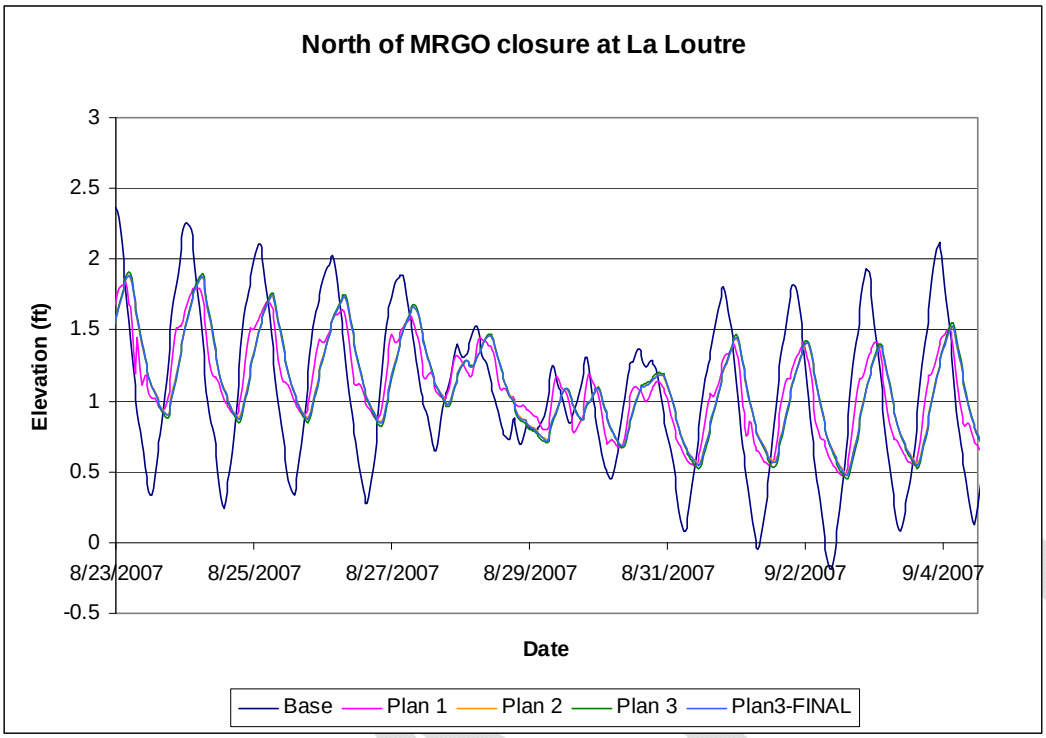

Figure 6-30. Water surface elevation north of MRGO closure at La Loutre (September)

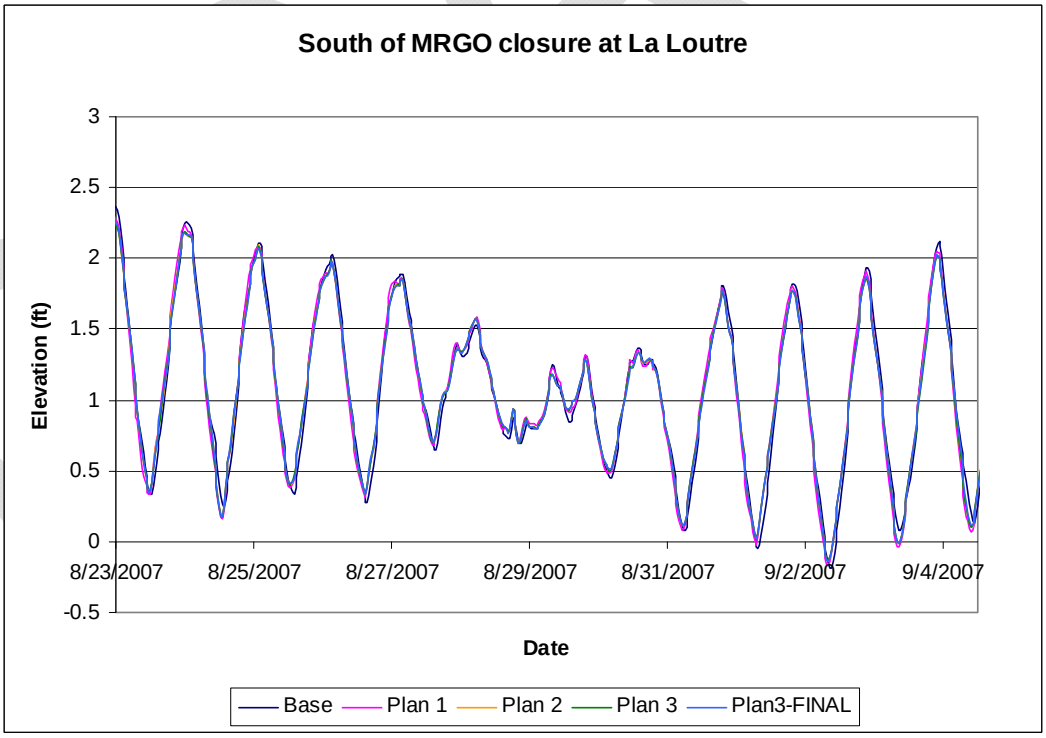

Figure 6-31. Water surface elevation south of MRGO closure at La Loutre (September)

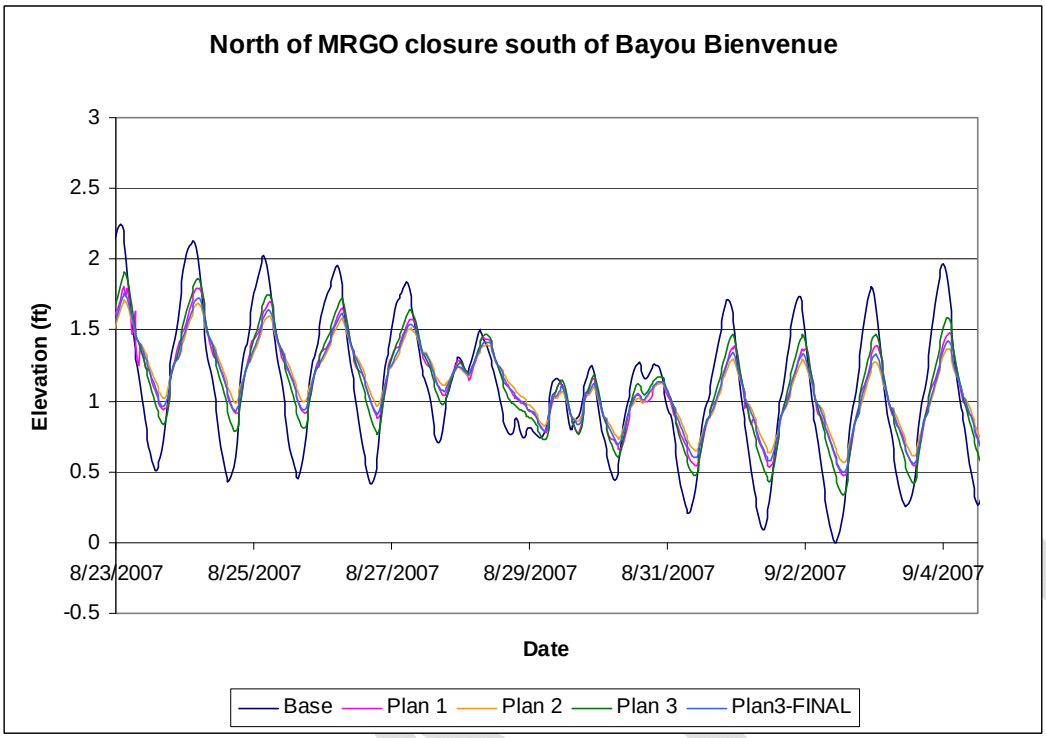

Figure 6-32. Water surface elevation north of MRGO closure at Bayou Bienvenue (September)

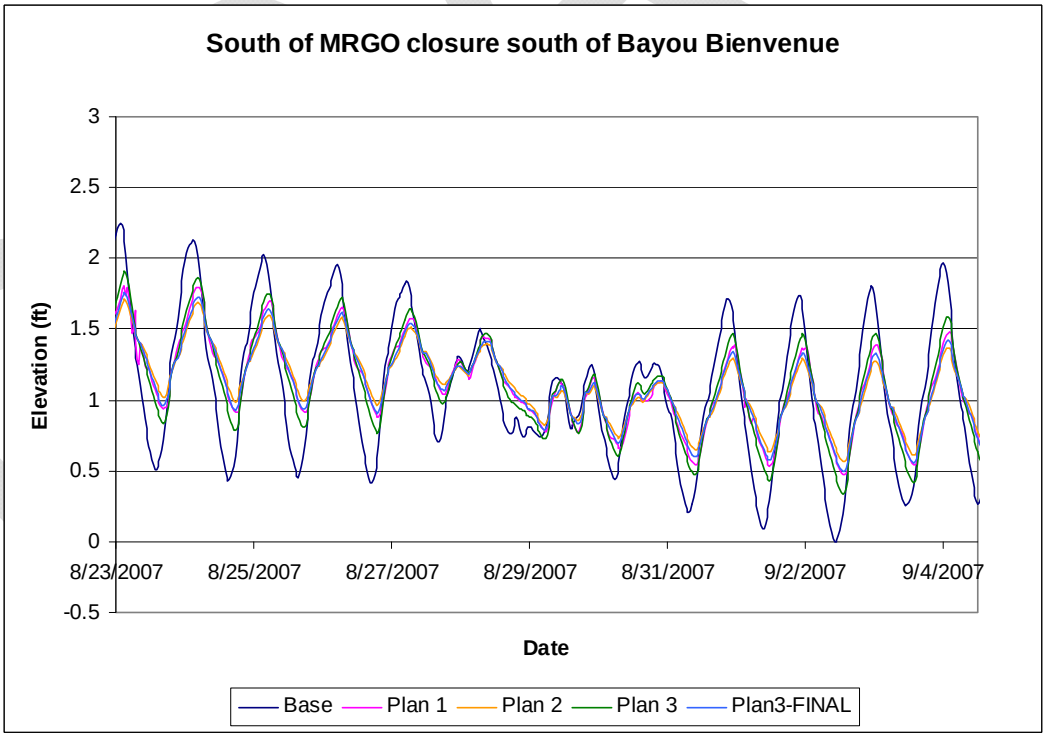

Figure 6-33. Water surface elevation south of MRGO closure at Bayou Bienvenue (September)

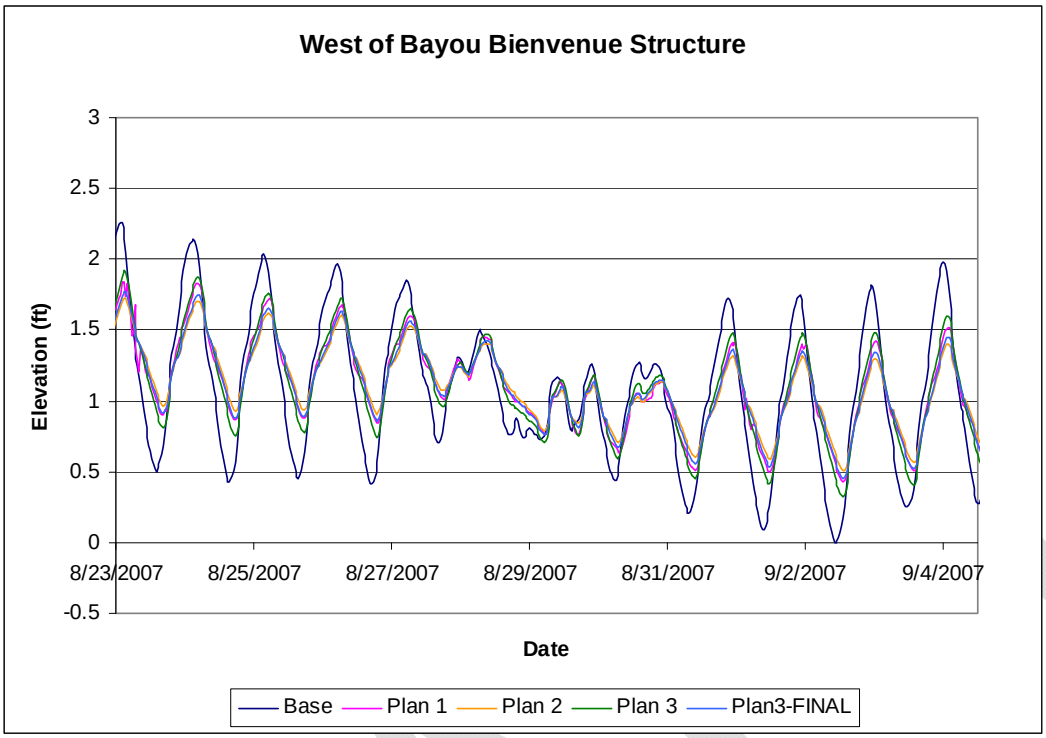

Figure 6-34. Water surface elevation west of Bayou Bienvenue structure (September)

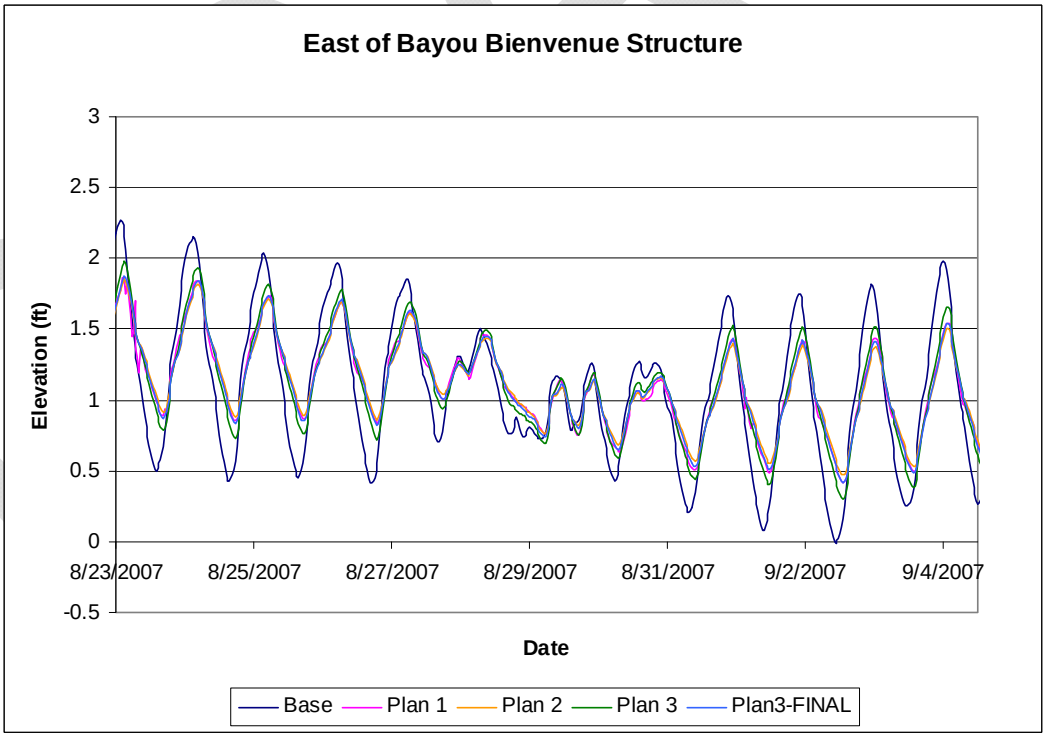

Figure 6-35. Water surface elevation east of Bayou Bienvenue structure (September)

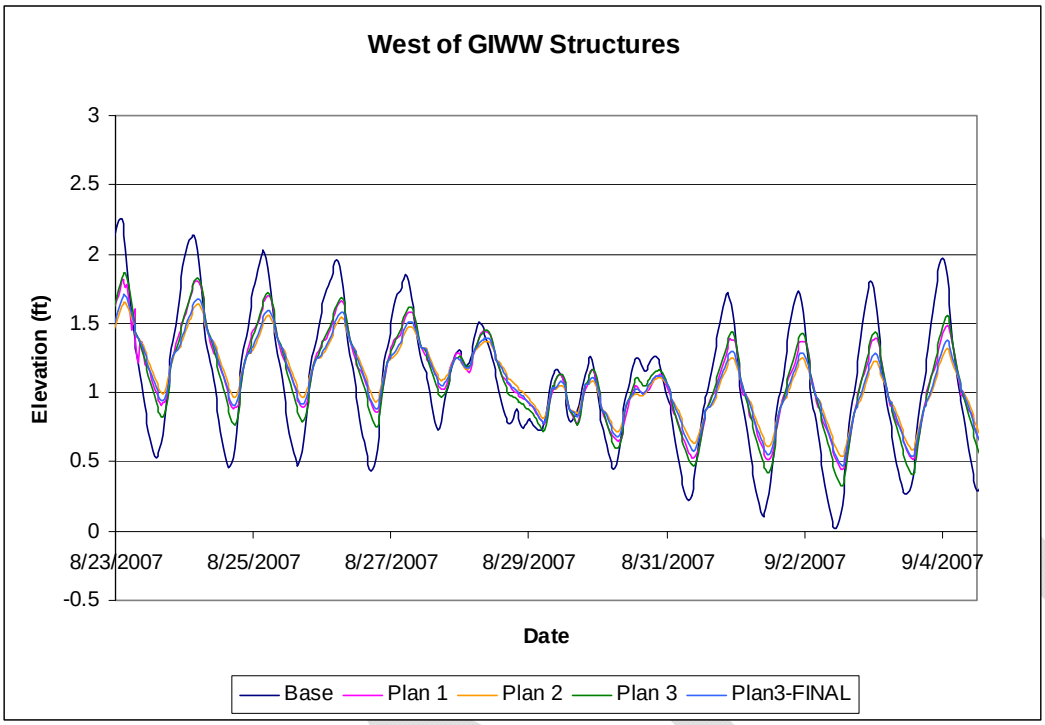

Figure 6-36. Water surface elevation west of GIWW structures (September)

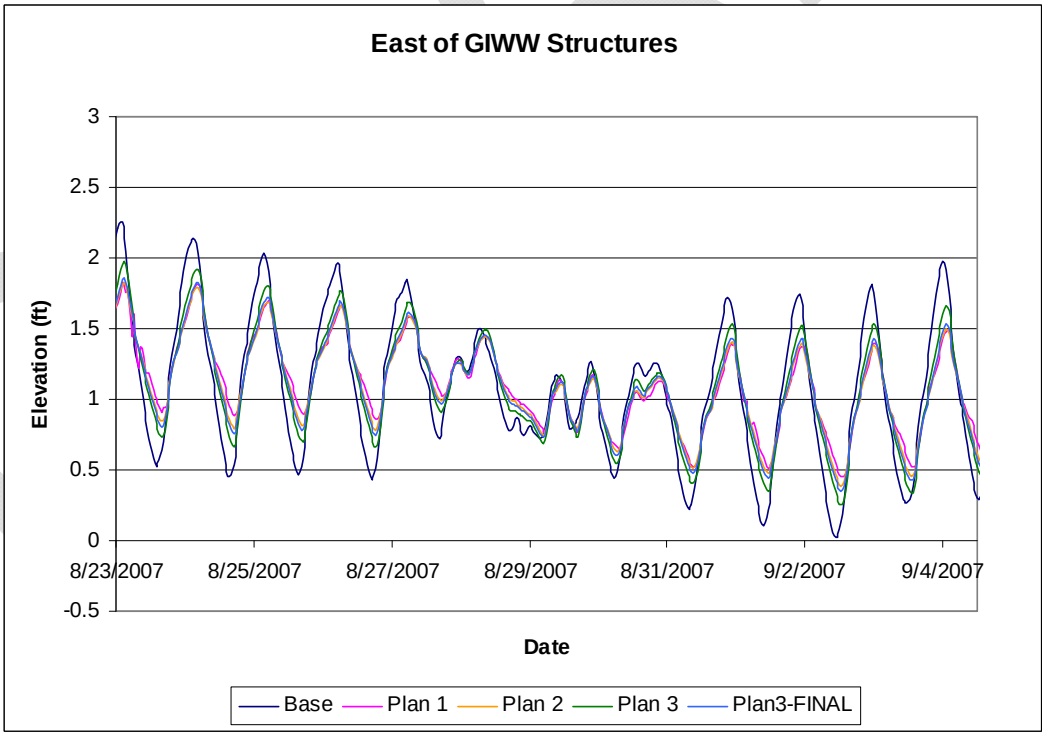

Figure 6-37. Water surface elevation east of GIWW structures (September)

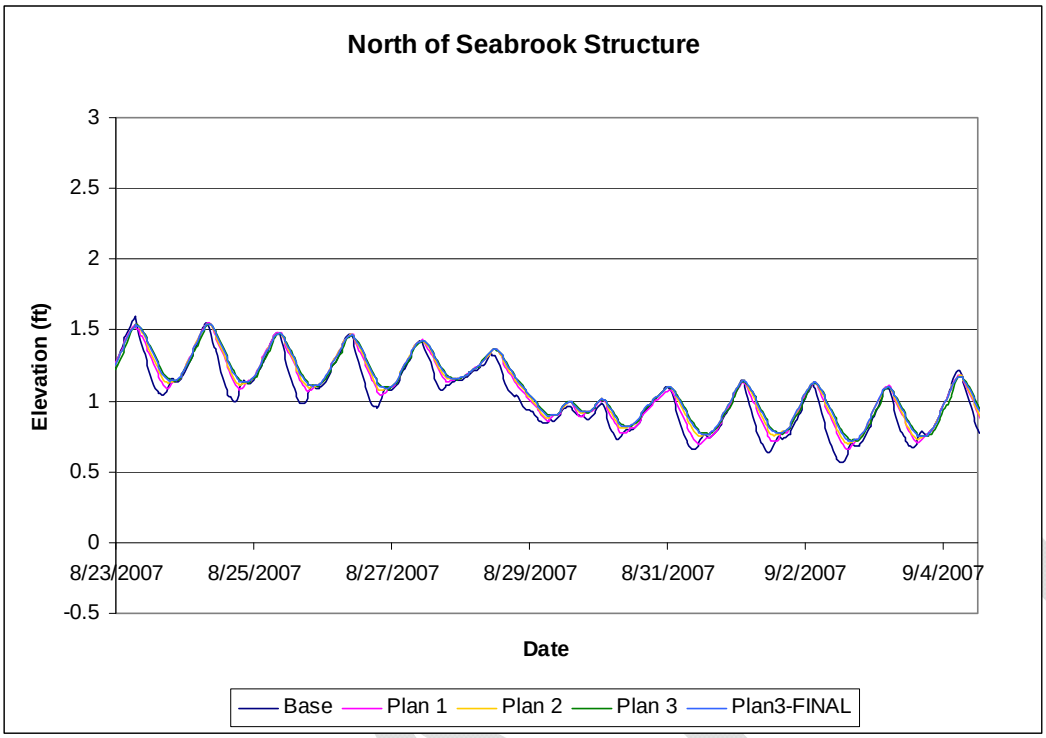

Figure 6-38. Water surface elevation north of Seabrook structure (September)

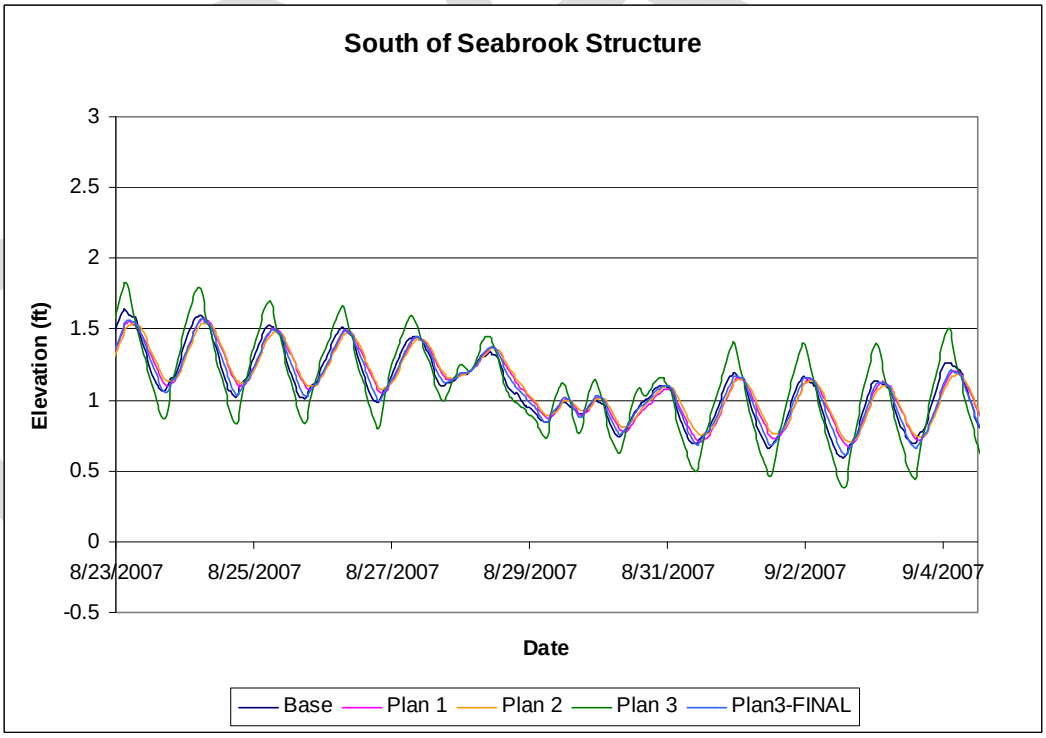

Figure 6-39. Water surface elevation south of Seabrook structure (September)

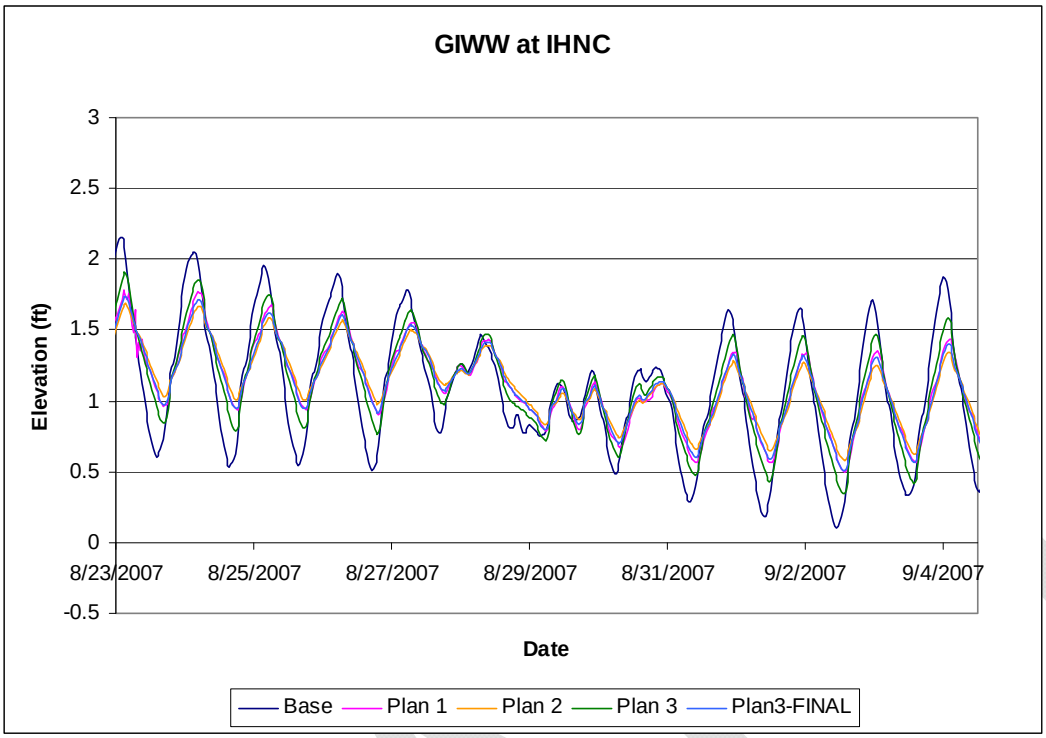

Figure 6-40. Water surface elevation in GIWW at IHNC (September)

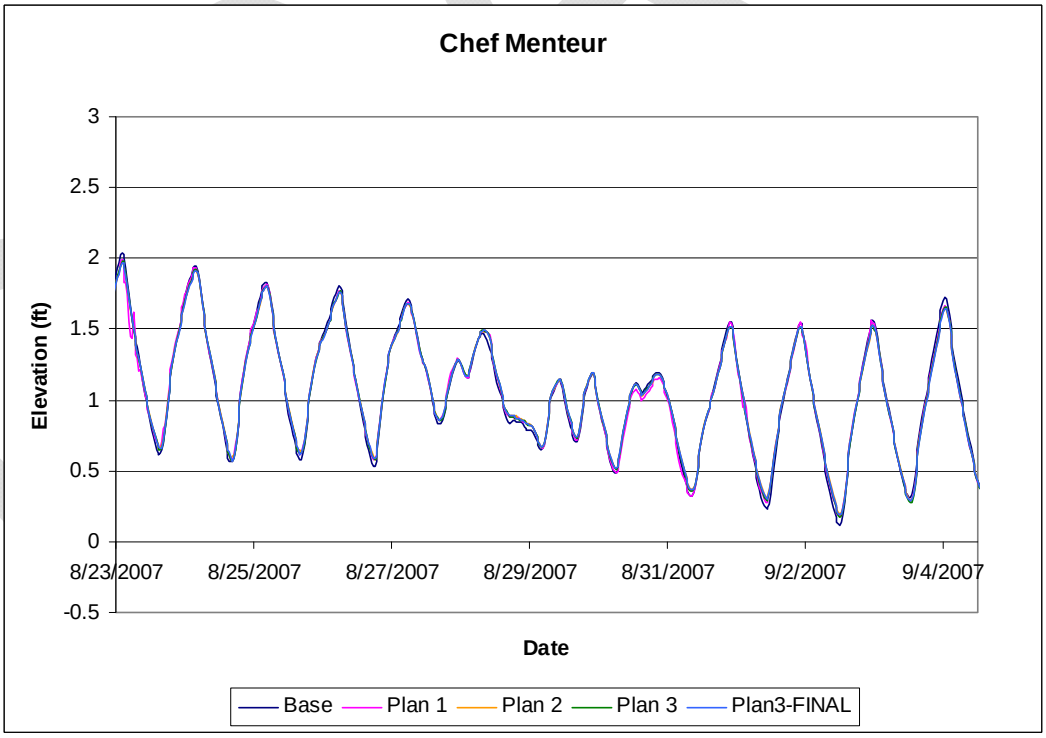

Figure 6-41. Water surface elevation in Chef Menteur (September)

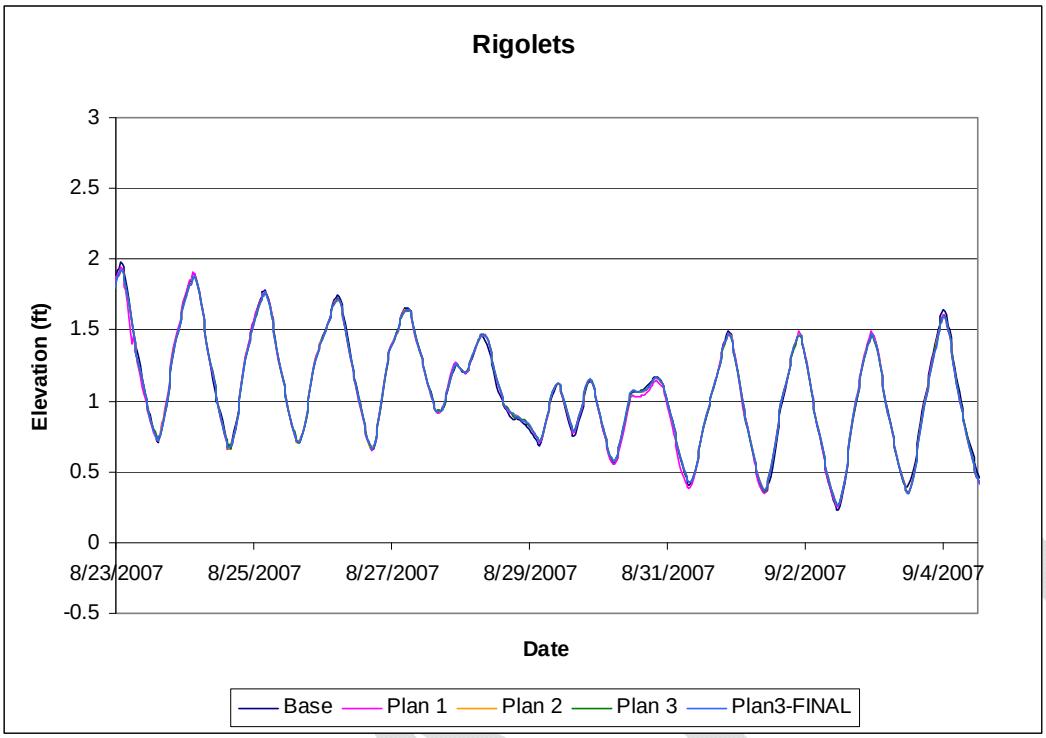

Figure 6-42. Water surface elevation north in Rigolets (September)

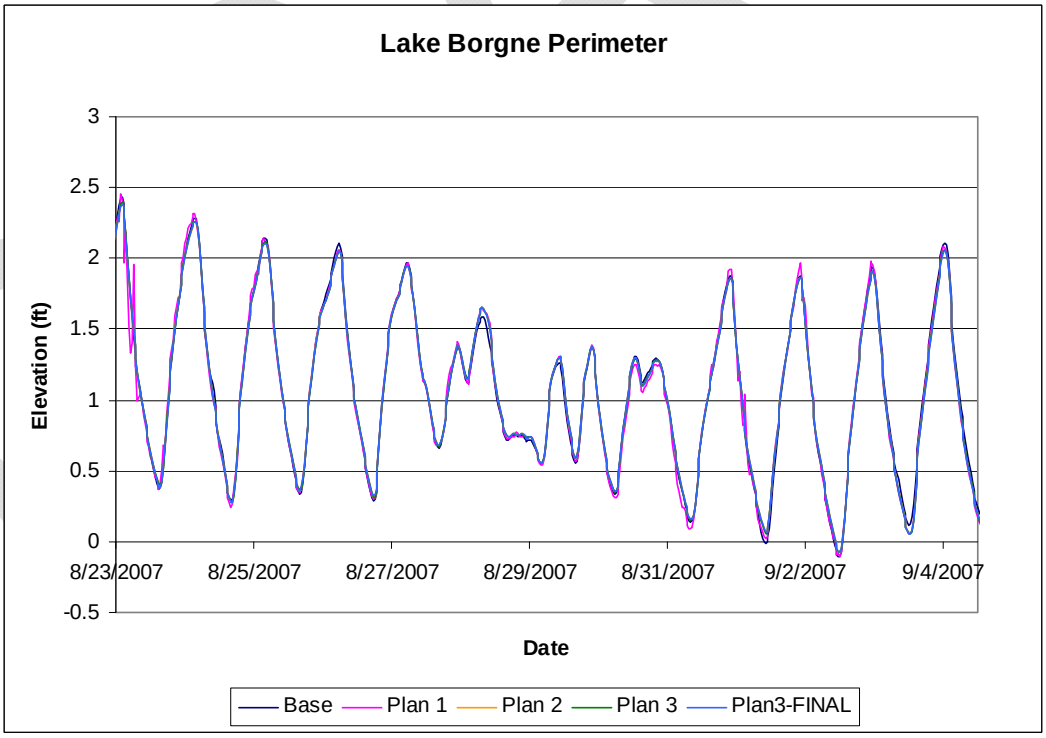

Figure 6-43. Water surface elevation at Lake Borgne perimeter (September)

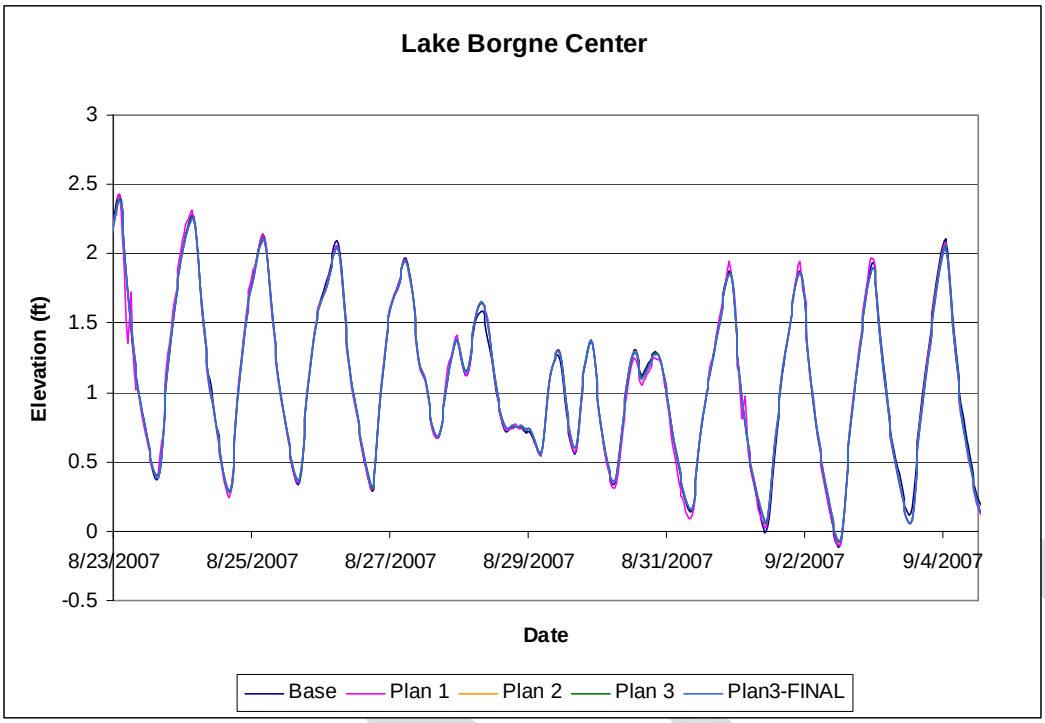

Figure 6-44. Water surface elevation at Lake Borgne center (September)

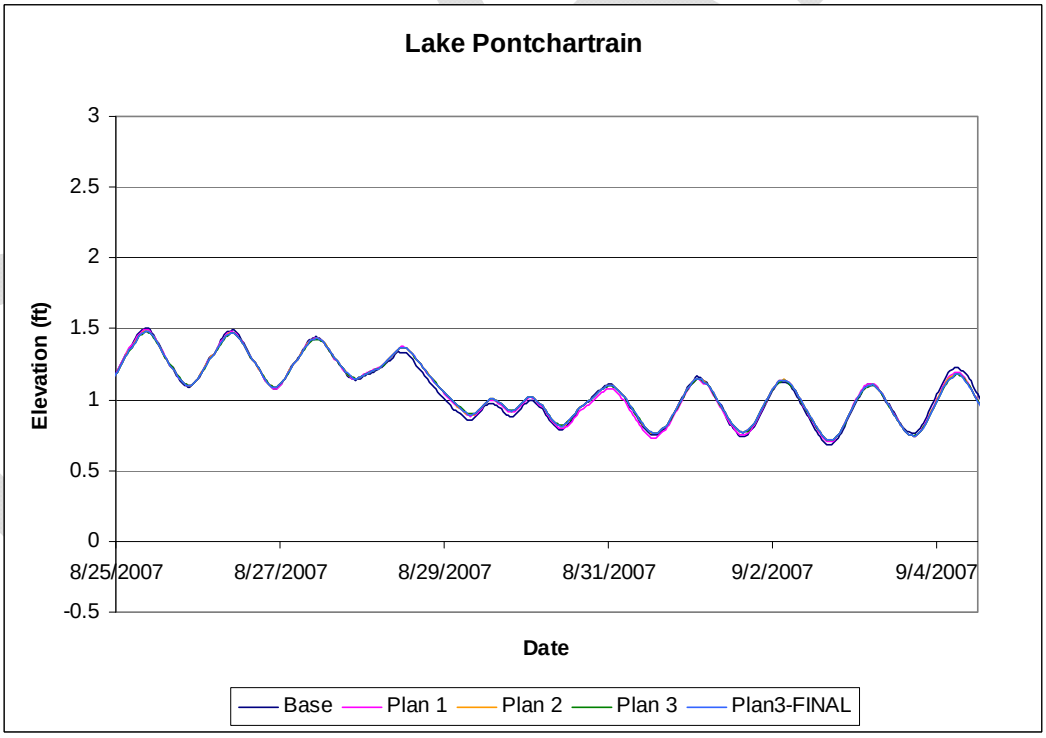

Figure 6-45. Water surface elevation at Lake Pontchartrain (September)

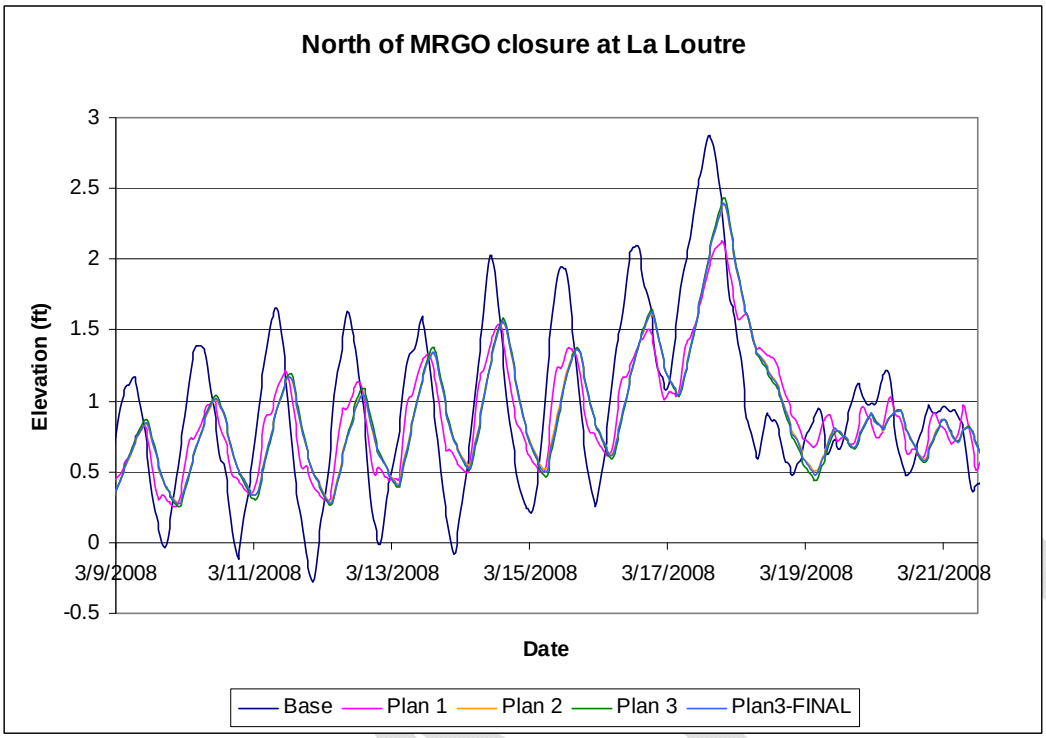

Figure 6-46. Water surface elevation north of MRGO closure at La Loutre (March)

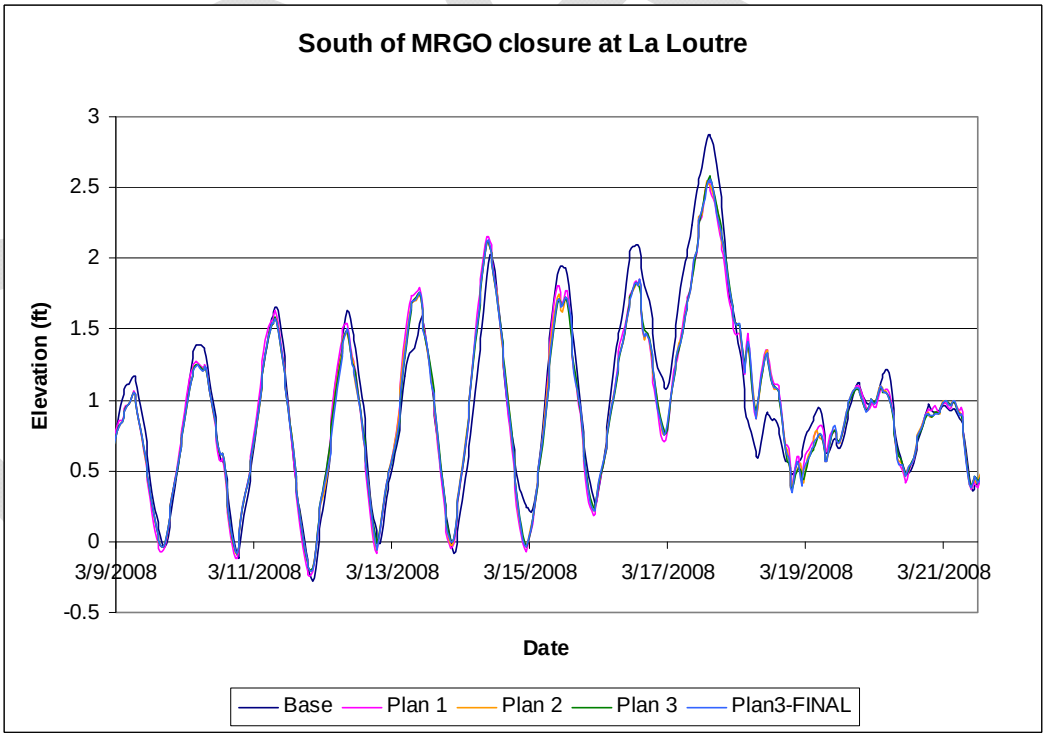

Figure 6-47. Water surface elevation south of MRGO closure at La Loutre (March)

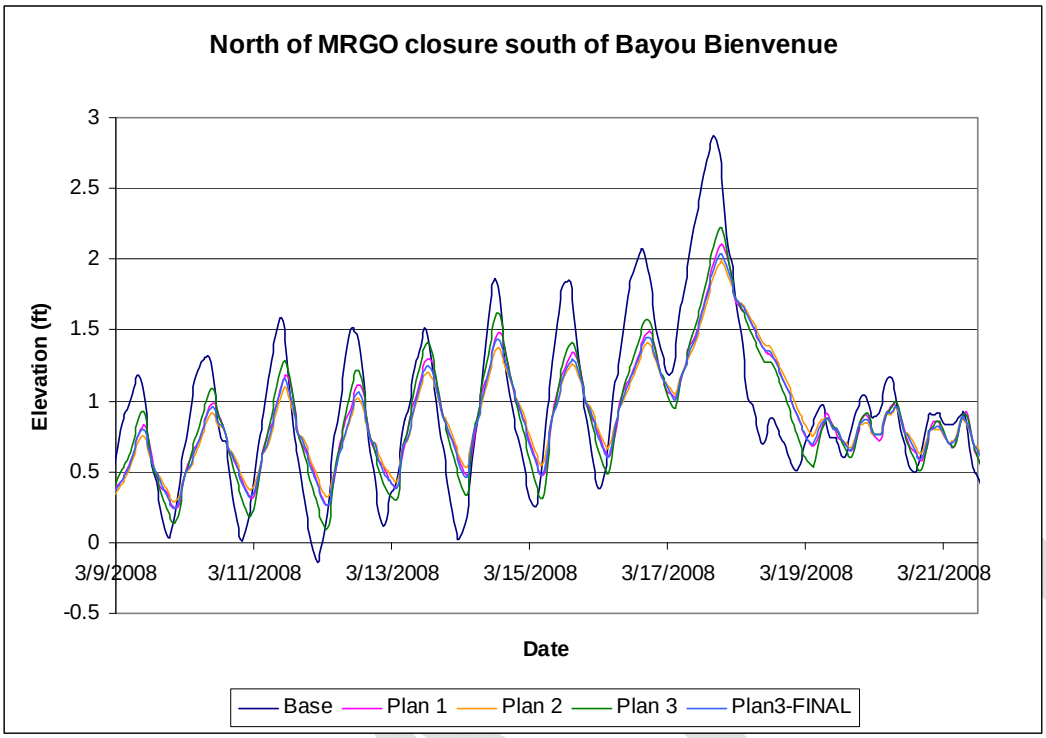

Figure 6-48. Water surface elevation north of MRGO closure at Bayou Bienvenue (March)

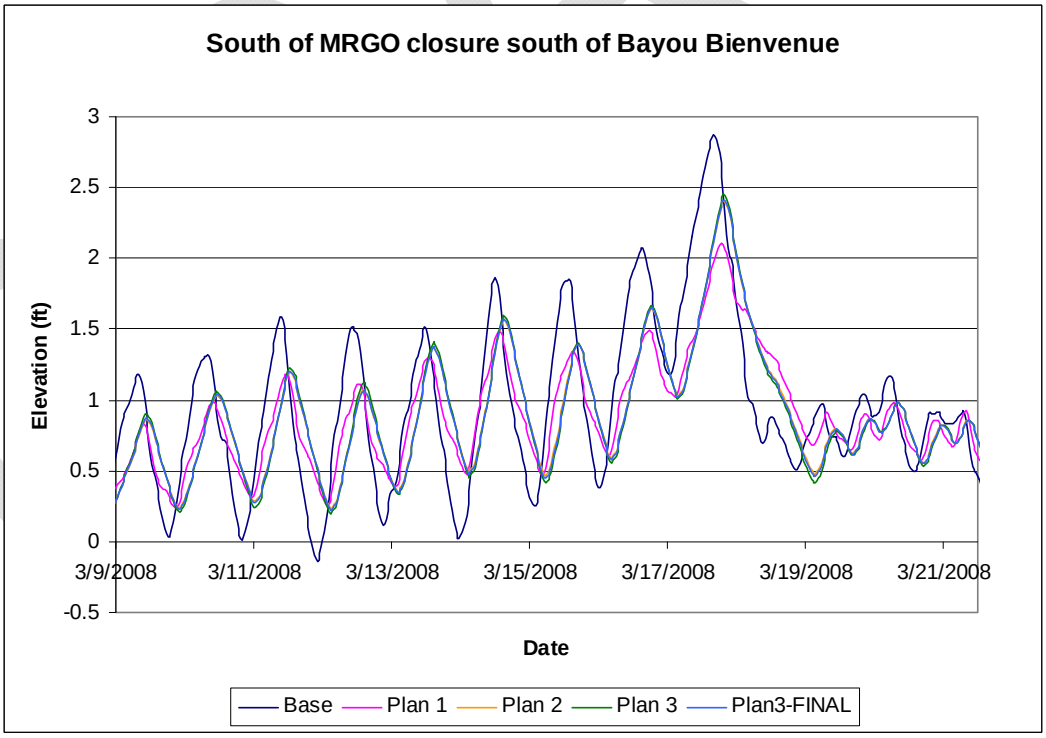

Figure 6-49. Water surface elevation south of MRGO closure at Bayou Bienvenue (March)

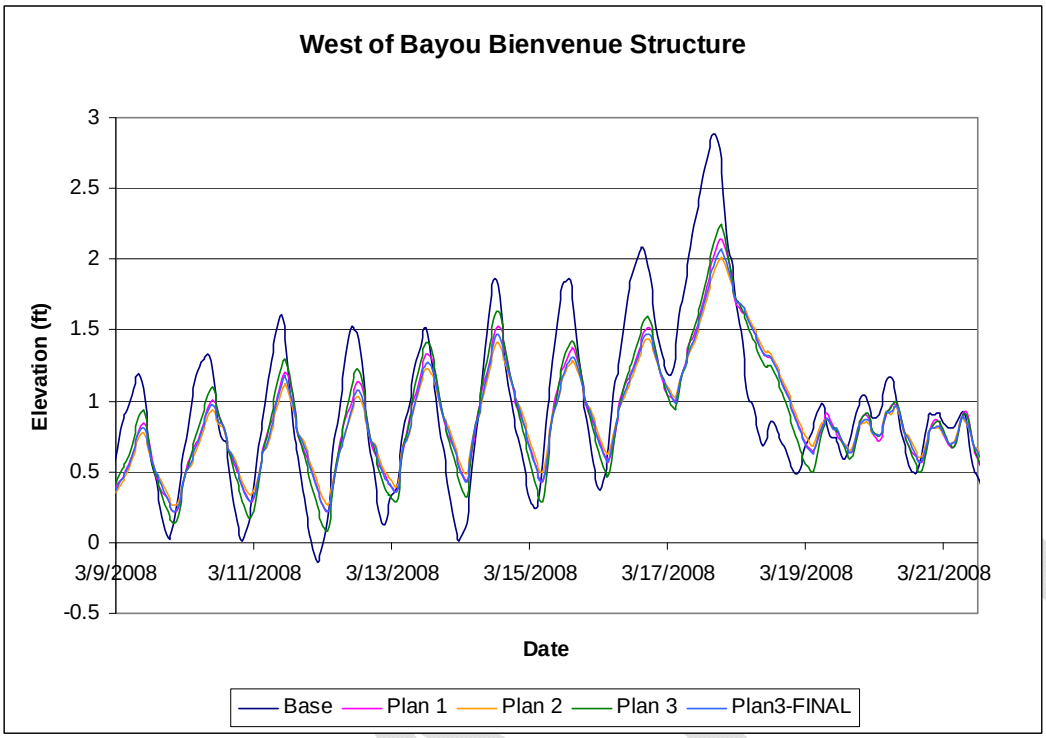

Figure 6-50. Water surface elevation west of Bayou Bienvenue structure (March)

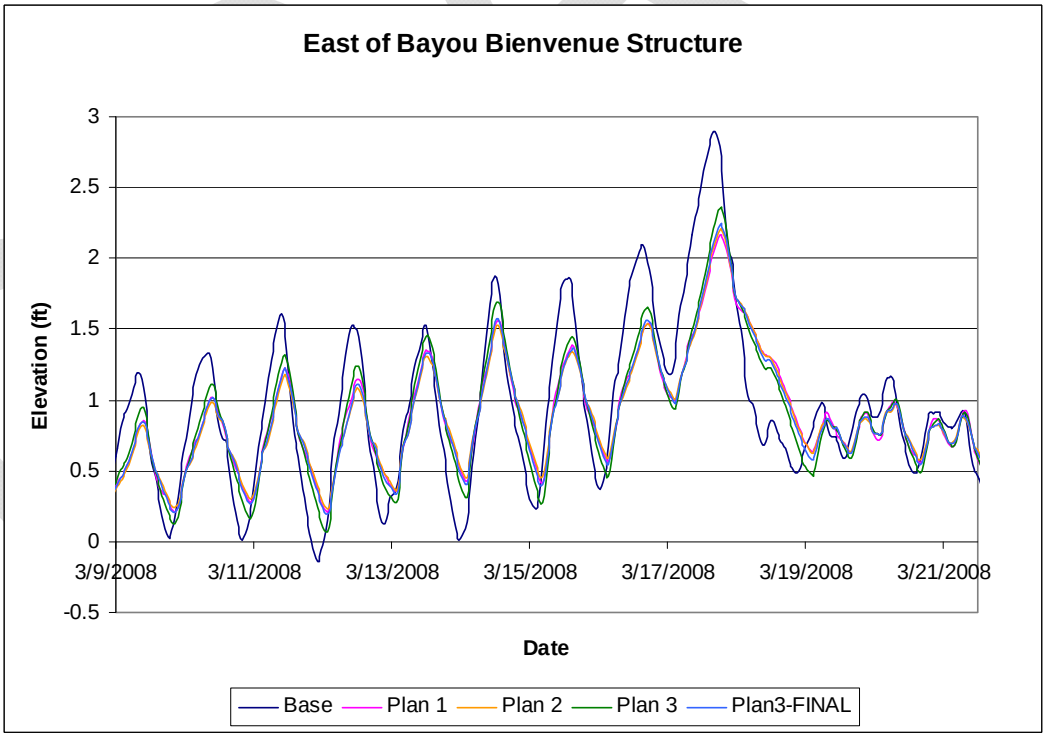

Figure 6-51. Water surface elevation east of Bayou Bienvenue structure (March)

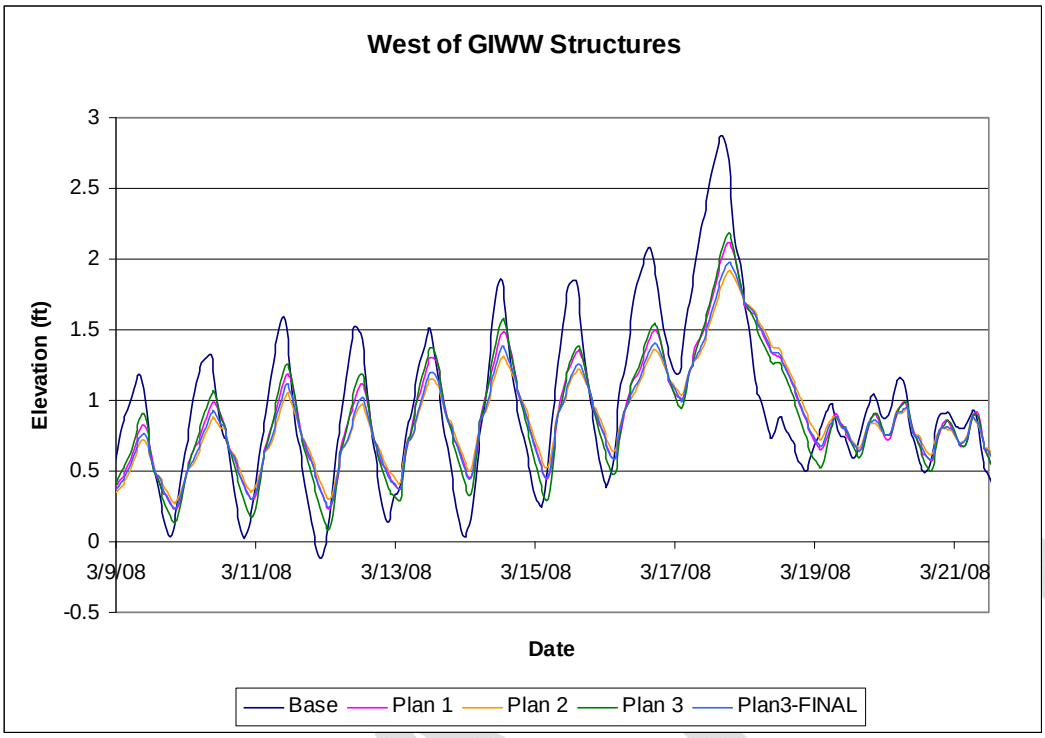

Figure 6-52. Water surface elevation west of GIWW structures (March)

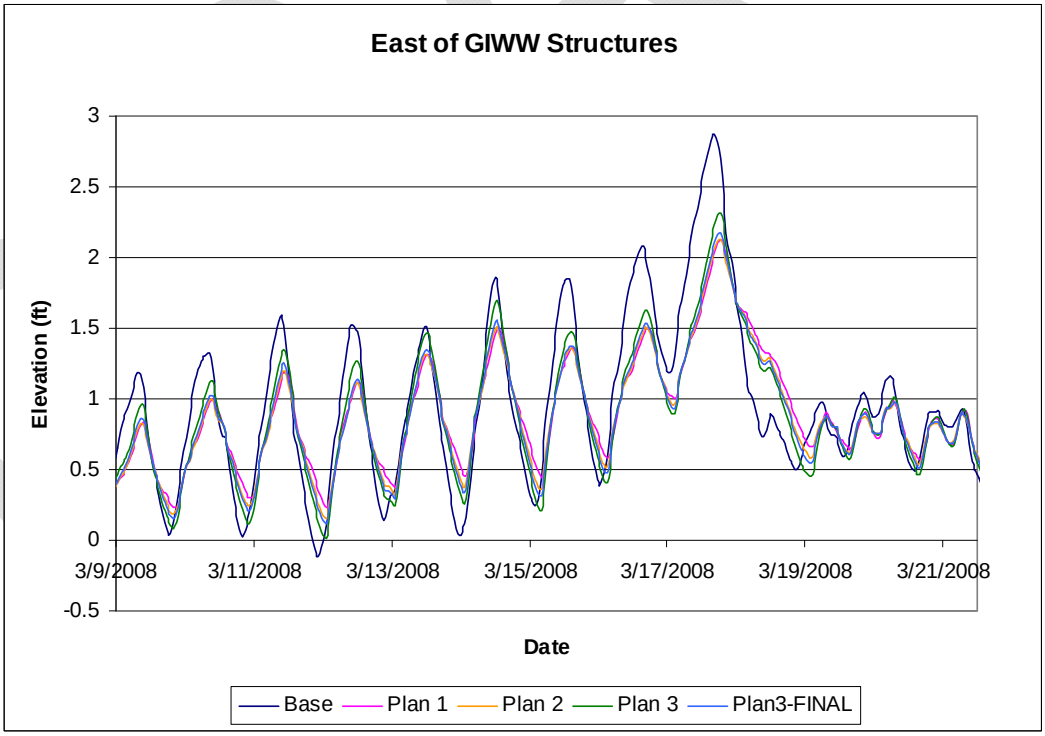

Figure 6-53. Water surface elevation east of GIWW structures (March)

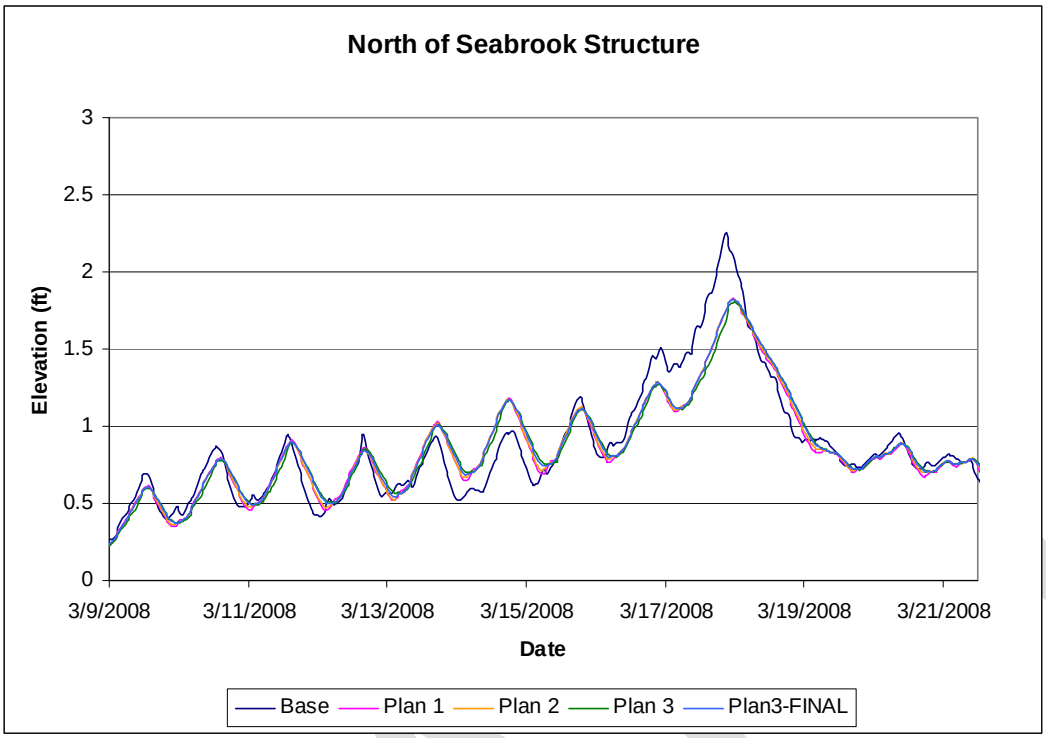

Figure 6-54. Water surface elevation north of Seabrook structure (March)

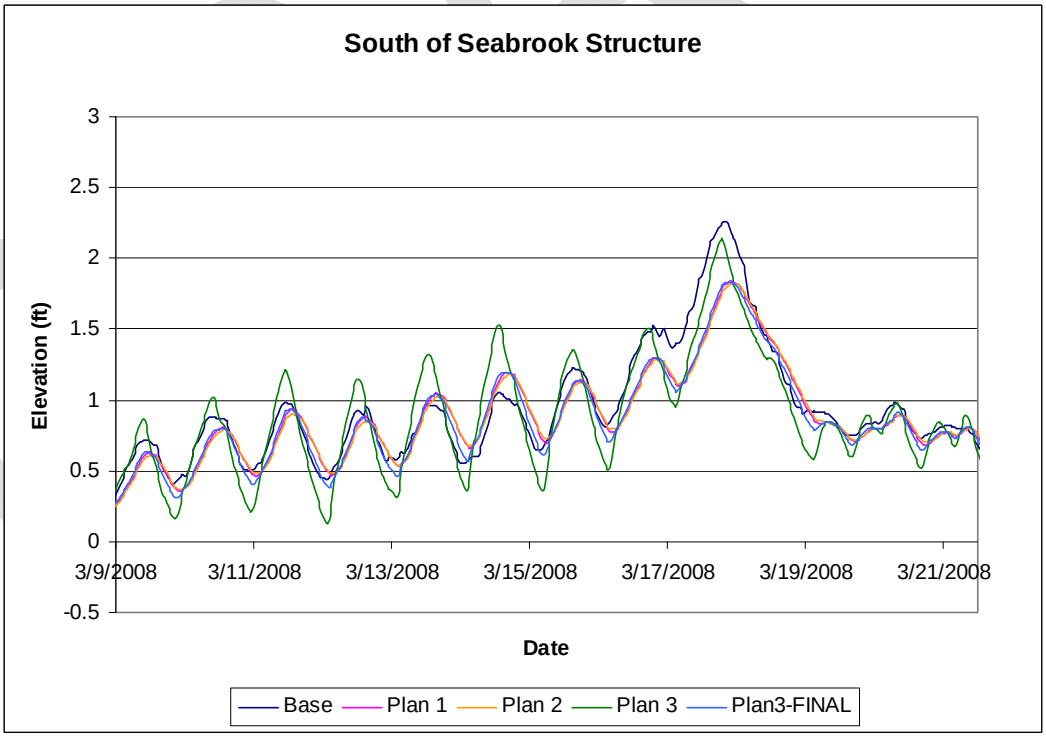

Figure 6-55. Water surface elevation south of MRGO Seabrook structure (March)

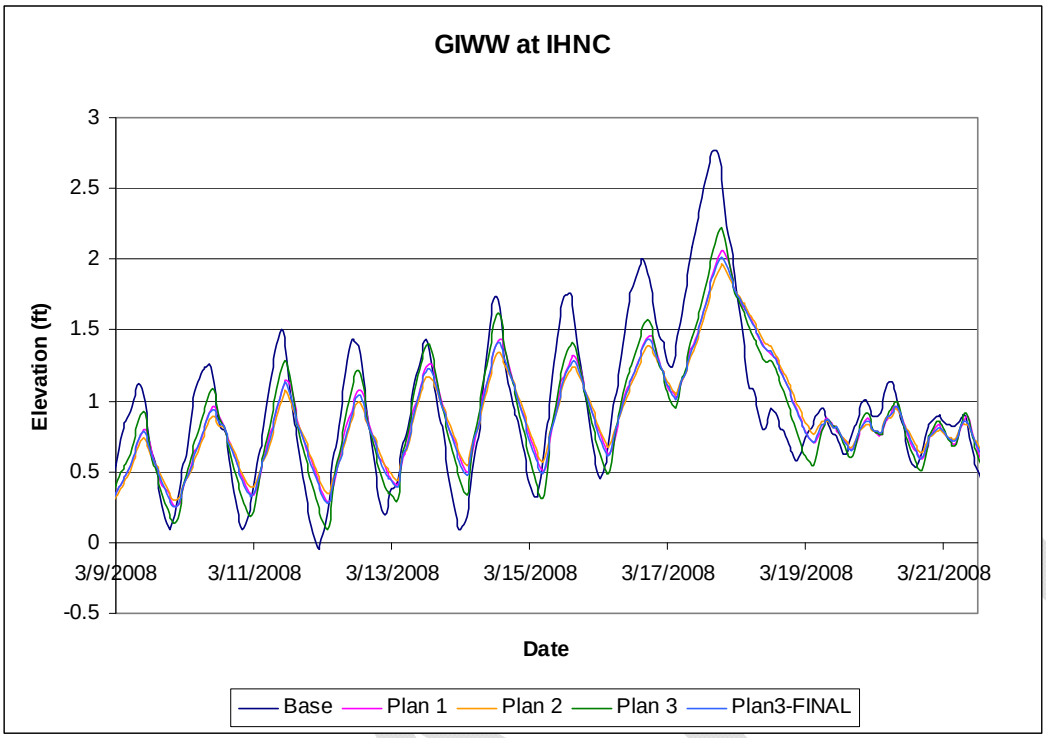

Figure 6-56. Water surface elevation in GIWW at IHNC (March)

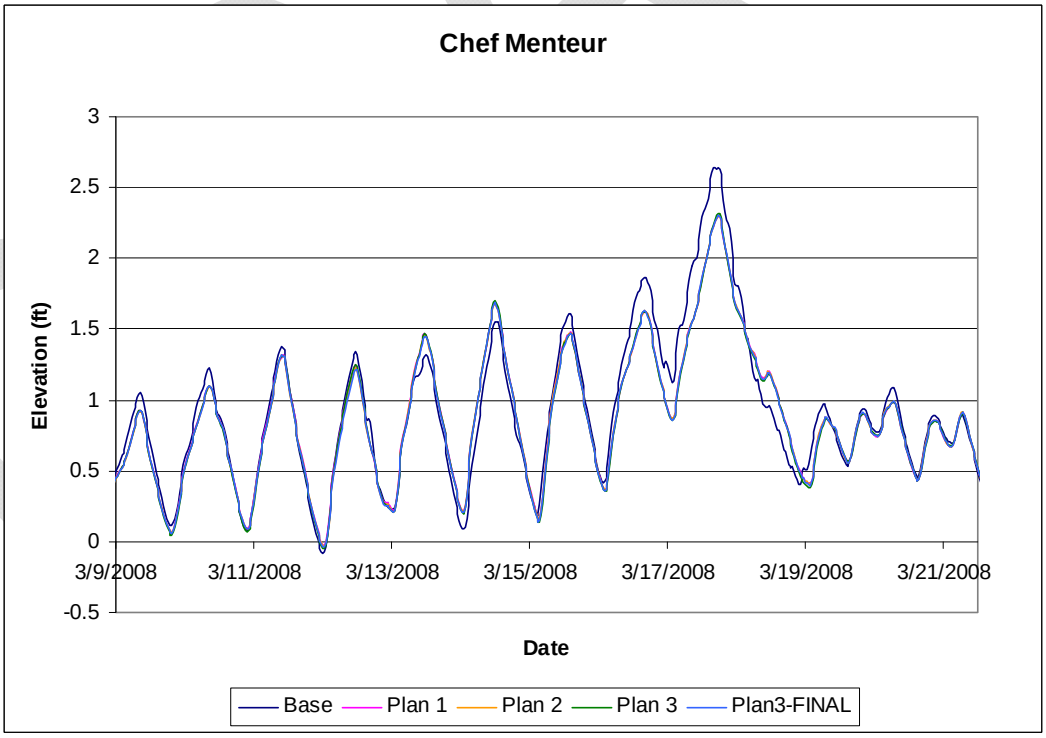

Figure 6-57. Water surface elevation in Chef Menteur (March)

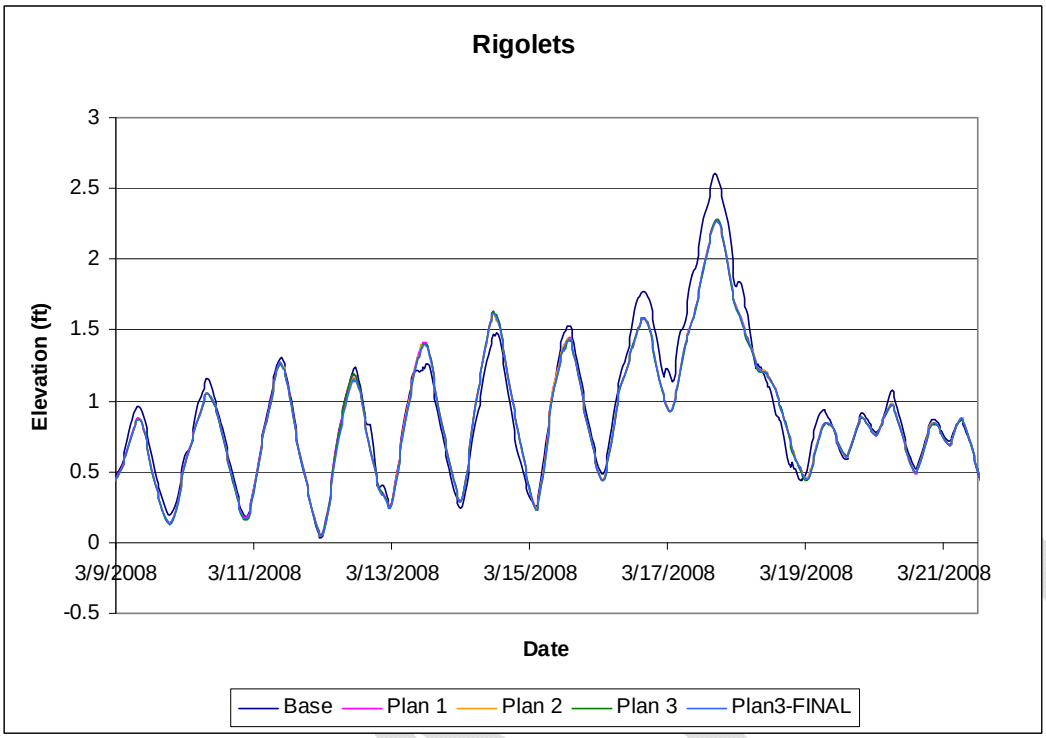

Figure 6-58. Water surface elevation in Rigolets (March)

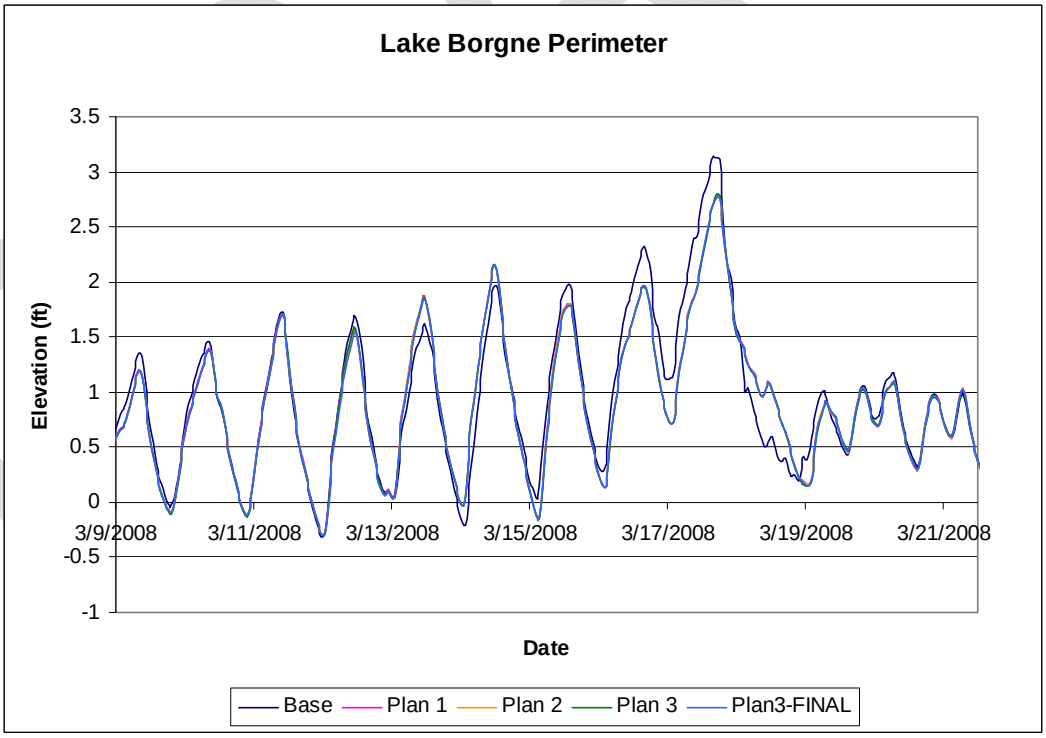

Figure 6-59. Water surface elevation at Lake Borgne perimeter (March)

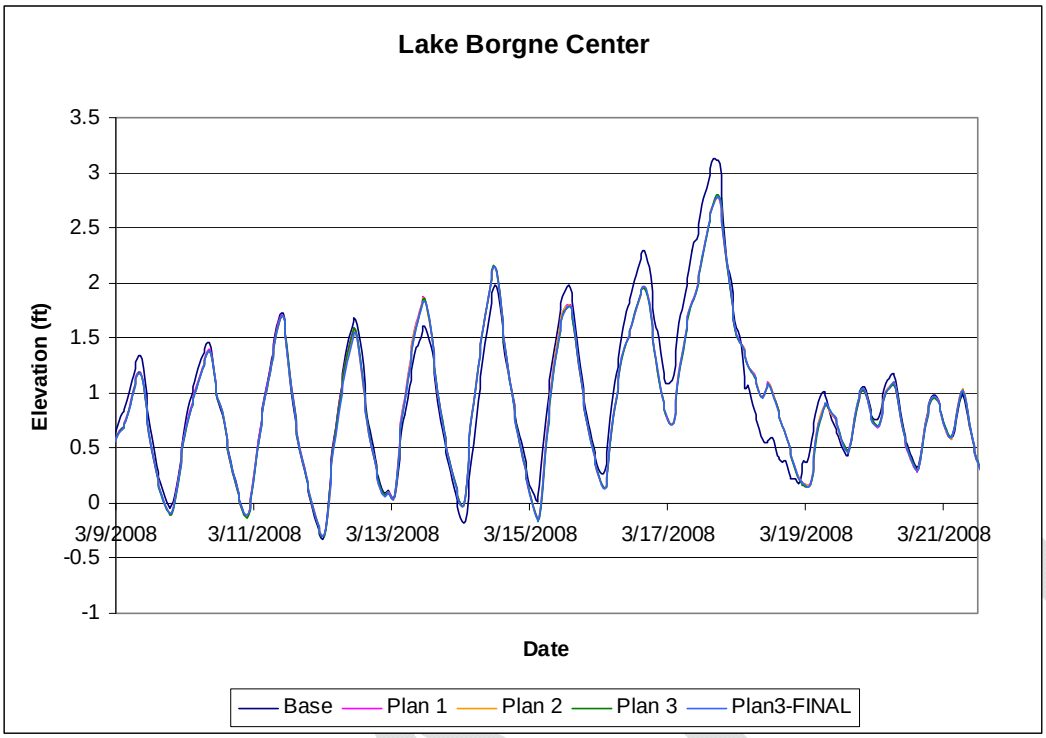

Figure 6-60. Water surface elevation at Lake Borgne center (March)

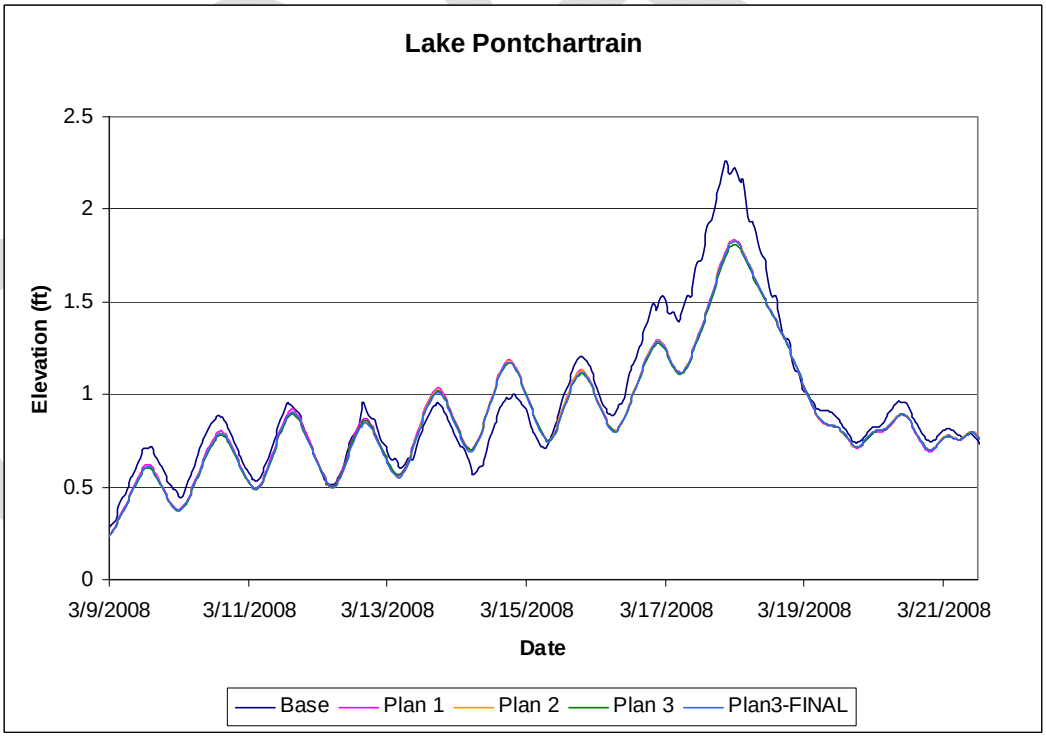

Figure 6-61. Water surface elevation in Lake Pontchartrin (March)

The water surface changes due to the plan conditions are most noticeable at the location where the MRGO is being cut off from the Gulf of Mexico. South of the closure at La Loutre there is very little change for the September condition and slightly more for the March condition when flows are larger and the blockage of the MRGO creates reflections of the wave that affect the amplitude, although the effects here are much less than those at other locations. However, north of this closure there is a large difference in the phasing, approximately a 2.5 hour lag from the Base to Plan 1 results due to the closure at La Loutre and a 4-5 hour lag from the Base to Plan 2/Plan 3/Plan 3 Final results due to the addition of the Borgne alignment. The wave that previously reached this location through the MRGO now travels through Lake Borgne before reaching this point. This greater distance to travel equates to a longer travel time as well as lower range due to the blockage of flow volume. There is also some reflections that occur occasionally at these locations due to the blockage of the MRGO. At the MRGO closure south of Bayou Bienvenue there is also a reduction in elevation range due to these closures as well as a phase shift.

Based on the previous set of figures (Figures 6-30 through 6-61), for almost all of the locations in the area of the plan changes, the greatest change comes with Plan 1, the closure of the MRGO at La Loutre. The differences with each subsequent plan are less extreme. With the second closure and structure implementation of Plan 2, the elevation ranges continue to drop but the phasing generally remains further unchanged. However, once the Seabrook structure is included with Plan 3, the tidal range increases slightly at these locations due to the restriction of flow that it creates within this area of the GIWW and IHNC. Plan 3 Final, though, generates water surfaces ranges, on the order of Plan 1 and Plan 2, since the flow restriction at Seabrook is less in Plan 3 Final than in Plan 3.

The greatest impact of the Seabrook structure is south of its location (Figures 6-39 and 6-55). North of the structure there is little change due to the wider area and open waters of Lake Pontchartrain (Figures 63-38 and 6-54). To the south, however, the space is confined and the effects are felt in the IHNC. Plan 3 and Plan 3 Final include filling the southern scour hole which is at the location of this comparison point. The filling of this scour hole causes changes in the vicinity beyond just the reduction in cross-section due to the structure. This southward influence extends to the location labeled as "GIWW at IHNC." Here, the changes produced with the addition of Plan 3 (as compared to Plan 2) are larger than those produced

DRAFT

with the addition of Plan 2 (as compared to Plan 1) (Figures 6-40 and 6-56). However, at this location, away from the filled hole, the effects are much less than immediately south of the Seabrook structure. For Plan 3 Final, the structure location is further south than for Plan 3 and the impact of the filled scour hole is much less. Plan 3 Final again produces results at this location comparable to those for Plan 1 and Plan 2.

The Chef Menteur location appears unchanged for the September analysis (Figure 6-41) but there is a large effect with Plan 1 that shows up in March (Figure 6-57). It is likely that the higher wind speeds and flows during this time as well as the direction of the wind are ideal for emphasizing effects in this area. This same change is observed at the Rigolets, Lake Borgne, and Lake Pontchartrain (Figures 6-58, 6-59, 6-60, and 6-61). Overall, the effect in March is showing a decline in the range of the water surface elevation during a storm event when compared to the Base condition. Although not included in this research, the exact reason for this decline could be due to the wind direction as well as the direction of the tide at this time. Each of the plan conditions, however, is not generating further changes.

Circulation Analysis

The analysis of the hydrodynamic model results for both time periods uncovers a clear change in circulation once the MRGO is cut off from the Gulf of Mexico. Figure 6-62 shows the direction of flow when the tide is rising for the Base condition. The arrows are not drawn to scale but rather only indicative of flow direction. The flow moves up the MRGO and splits at the GIWW with a portion moving west and up the IHNC and a portion moving east down the GIWW. However, flow also enters the eastern section of the GIWW from Lake Borgne and at times splits to the east and west. Depending on the phase of the wave propagation up the MRGO and that in Lake Borgne, the direction of flow in the central GIWW area (circled in Figure 6-62) can be either to the east or the west for an incoming tide. In other words there is a change in direction as that tidal wave propagates into this area from several locations. Figure 6-63 shows the same information for Plan 1, Plan 2, Plan 3, and Plan 3 Final. Once the MRGO is cut off from the Gulf of Mexico at La Loutre, the tide cannot move up this channel as previously done. Therefore the flow only enters the GIWW at its connections at Lake Borgne. Flow does move through Bayou Bienvenue but the amount of water it transports is much less than the flows

DRAFT

that move up the MRGO or enter through Lake Borgne and it has little effect on the overall circulation pattern through the GIWW. These changes show a clear direction of flow along the GIWW as opposed to a direction that may vary at times.

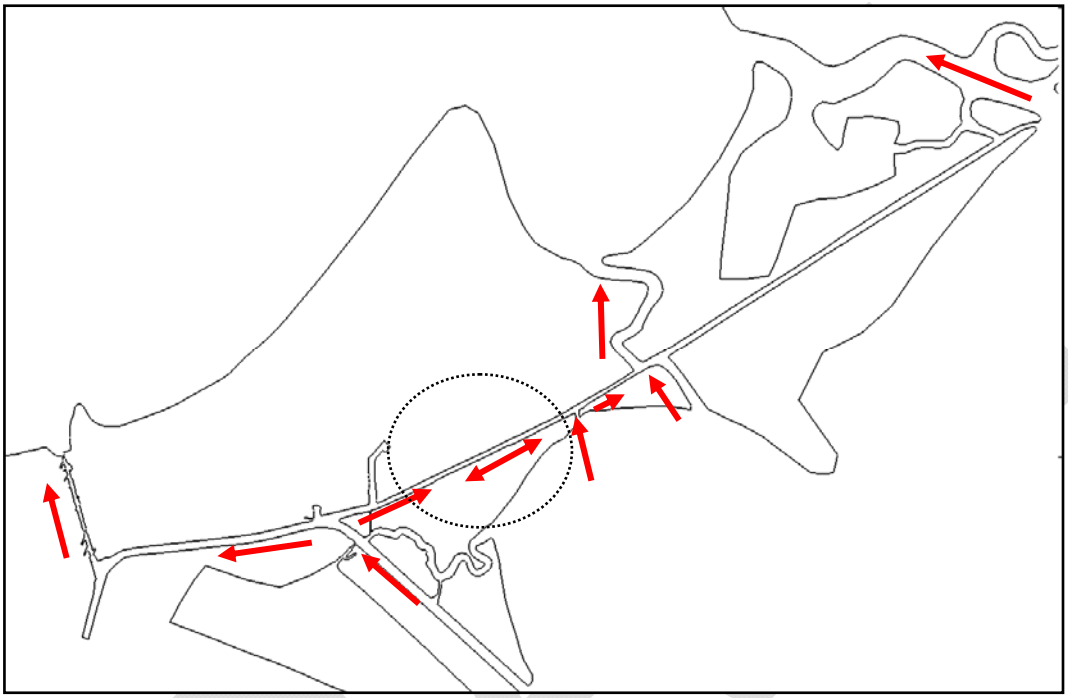

Figure 6-62. Direction of flow for incoming tide in Base case

DRAFT

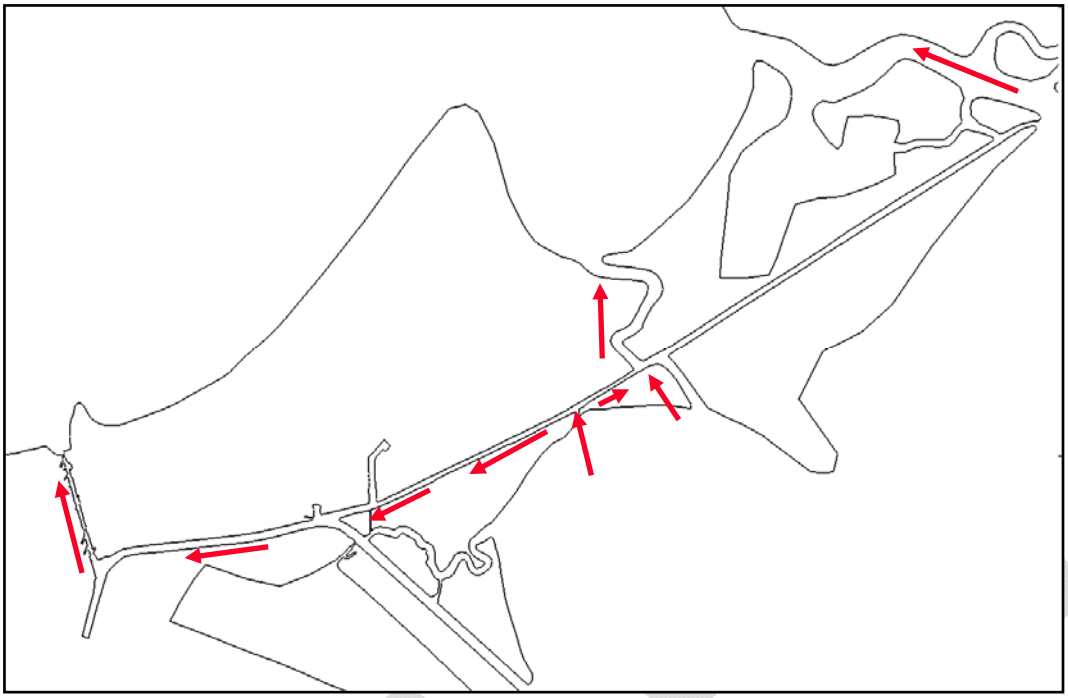

Figure 6-63. Direction of flow for incoming tide for Plan 1, Plan 2, and Plan 3

To further support these circulation changes, the velocity signals are compared at two locations along the GIWW, one on the eastern side of the MRGO and one on the western side. Figure 6-64 gives the location of these analysis points. The velocity values (with directions as defined previously) are given in Figure 6-65 for the point west of the MRGO and Figure 6-66 for the point east of the MRGO. Each line represents the Base or one of the plan conditions. For the western location the velocity drops once the MRGO is cut off at La Loutre (Plan 1) and continues to drop with each subsequent plan. It is important to also note that the flow directions indicate the expected diurnal tide signal and the phasing of the tide remains unchanged in this area. At the eastern location the Base case velocity indicates the changing magnitude and direction during the motion of the tide. Once the MRGO is cut off at La Loutre, however, flow along the GIWW comes in from its connection to Lake Borgne and splits east and west. This creates a smooth signal in the eastern GIWW like that observed in the western GIWW.

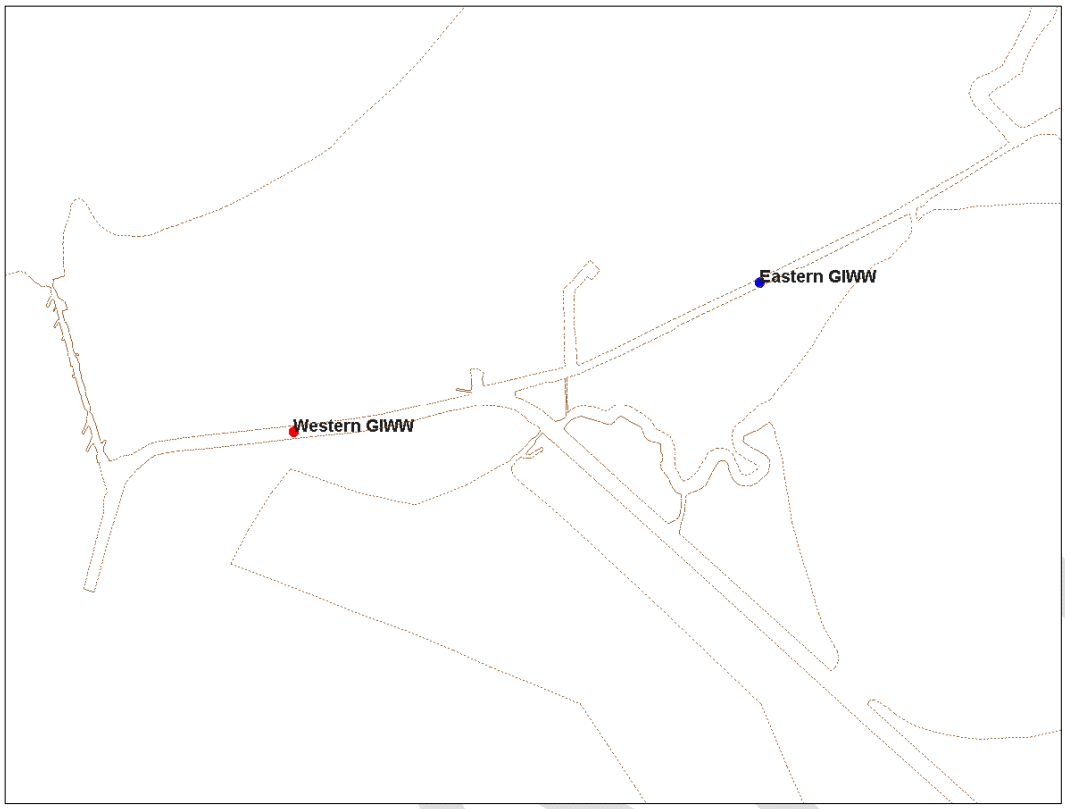

Figure 6-64. GIWW velocity analysis locations

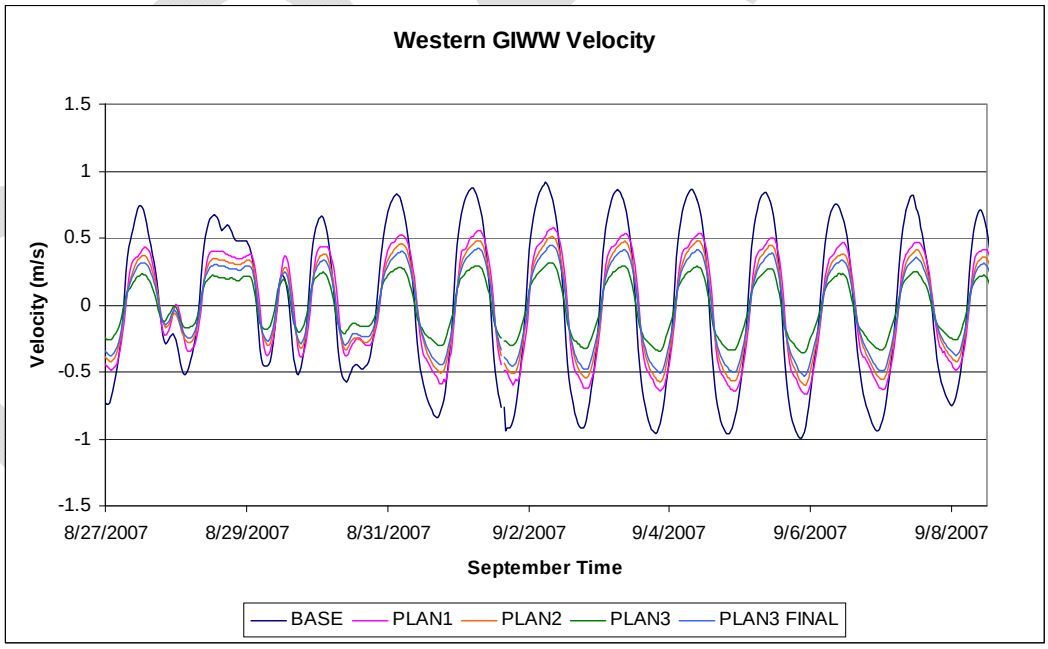

Figure 6-65. Velocity signal in the GIWW west of MRGO, velocities west of the Borgne alignment on the GIWW decrease with the closure of the MRGO at La Loutre

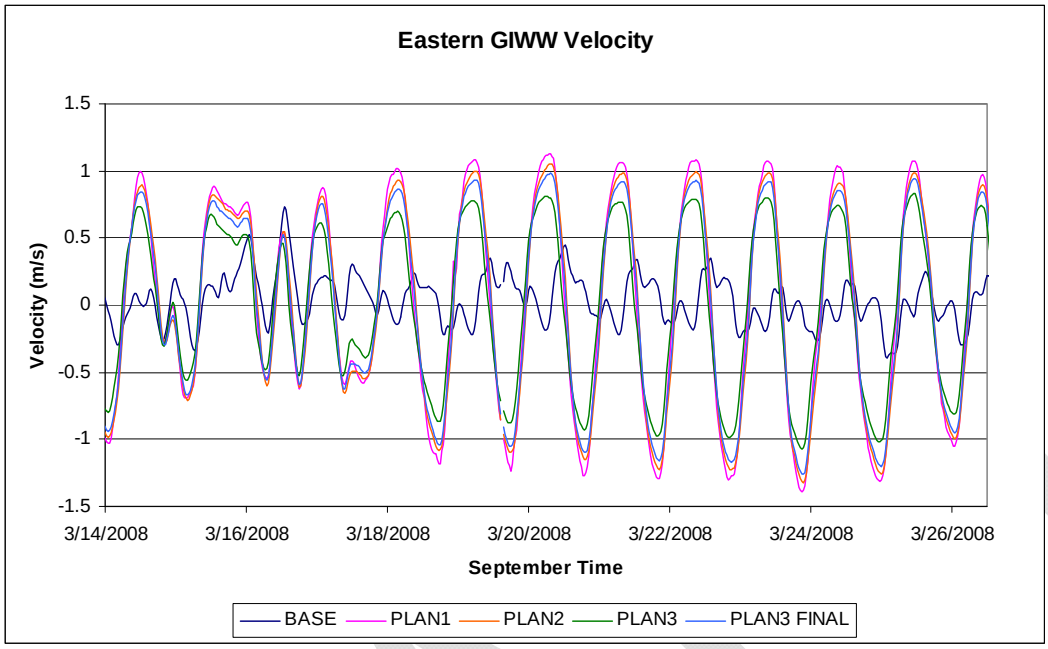

Figure 6-66. Velocity signal in the GIWW east of MRGO, velocities east of the Borgne alignment on the GIWW increase with the closure of the MRGO at La Loutre

The results of the hydrodynamic analysis include velocity magnitude and direction, water surface elevation, and overall circulation changes. Comparisons are made to how the flow in this area changes from the base condition with each plan condition. The initial analysis shows that the implementation of Plan 1, closing the MRGO at La Loutre, creates large changes to all of these parameters. These parameters continue to change with the implementation of Plan2, Plan 3, and Plan 3 Final but the changes due to these configurations is less that the initial changes generated with Plan 1. The changes in the circulation through the GIWW are initiated with the Plan 1 closure as well. The velocity magnitudes in the location of the structures rise greatly when the structures are included due to the reduced cross-sectional area at these locations.

7 Particle Tracking Results

The results of the particle tracking modeling for the larval fish transport are addressed in this chapter for the base case as well as design plans 1-3. The output and analysis of the simulations are separated into Cases 1-3 described in Chapter 5.

Case 1

In this simulation, particles are placed near the MRGO closure at La Loutre. Initial testing of this source revealed several difficulties. For the base case in which there is no construction, particles travel down the path shown in Figure 7-1 which is along the MRGO. However, the transport time for particles to travel down the MRGO to Bayou Bienvenue is approximately 2 weeks for the March 2008 hydrodynamic conditions. The transport time for the September 2007 base condition is longer. To obtain relevant statistics, it is necessary for particles to have time to reach the recruitment areas within the allotted time frame.

Figure 7-1 Location and transport path for larvae initiated for case 2. The red circle represents the approximate location of the initial positions

DRAFT

The plan configurations showed an even greater difficulty. Because all plan configurations include the MRGO closure at La Loutre, the particle pathway becomes obstructed. Alternate pathways around the closure via Lake Borgne are possible; however the recruitment time for that transport pathway is much too long for the allotted simulation time of this project (4 weeks).

Case 2

Case two particles are initiated both at the GIWW constriction and the MRGO 2nd closure (Figure 5-3). Particles are introduced across the width of the channel for two weeks and then transported for the remaining two weeks of the simulation. Approximately 4800 particles are released.

Figures 7-2 thru 7-5 show "snap shots" of particle positions for the September 2007 hydrodynamic conditions. Each frame (a-c) shows a snap shot of where the particles are at a specified time of one day, one week, and four weeks. The particles are color coded based on their initial position. The red particles are initiated in the region of the GIWW to the east of the constriction. The yellow particles are initiated in the MRGO near the eventual second closure position.

In figure 7-2, which shows the results of the base construction phase, after one day particles are transported to the union of the MRGO and GIWW. At this time particles are still being introduced into the flow. This is illustrated by the stream of particles that stretch from the initial points towards the MRGO/GIWW connection. After one week some particles have reached the Seabrook recruitment area (R1). Also mixing of particles between the two different initial source locations has occurred. Particles traveling up the MRGO have turned into Bayou Bienvenue and are moving towards Lake Borgne. Some particles are also taking alternate paths into the wetland region to the southwest of the MRGO. After four weeks, the particles appear to be completely mixed as if initial position has no affect on the final position of the representative particles. It is noticeable that a small number of particles end in Lake Borgne.

Figure 7-3 shows the resulting particle positions utilizing September 2007 hydrodynamics with the plan 1 configuration. At this point, the MRGO closure is in place at La Loutre. The flow along the MRGO is significantly reduced. The effect of this can be seen in Figure 7-3a. The dispersion of the yellow colored particles, initiated in the MRGO to the southeast of the

DRAFT

2nd closure, is smaller after 1 day than the previous base case. However the red particles at this same time step appear to have been transported further. After one week this trend is even more obvious. The yellow particles appear significantly less dispersed than the red particles. Due to the reduced flows in that area, the concentration of particles is appreciably higher. Also the number of particles that are transported into Lake Borgne has increased. This is most likely due to the fact that as the flow along the MRGO has decreased, the GIWW velocity has increased. After the full four week period, it is noticeable that the number of remaining yellow particles is greater than the base case and the distance transported is less.

Plan 2 configuration results are shown in Figure 7-4. Here the 2nd MRGO closure is in place south of Bayou Bienvenue. Particles initiated to the southeast of the closure are initially trapped. The velocity magnitude in this position has decreased drastically. The overall velocity magnitude along the GIWW has decreased, although velocity increases at the GIWW constriction. After 1 week, particles have begun traveling along the GIWW, but the yellow particles (initiated in the MRGO) are still in a very concentrated configuration. Although the number of particles recruited at this point appears to have decreased in comparison with the previous cases, it is also quite visible that the particles that remain are still being transported along the length of the GIWW. Several pathways to Lake Borgne are being utilized/given access due to the velocity decrease. After a four week period, the yellow particles have traveled along alternate pathways (Bayou Bienvenue and Lake Borgne) to reach the MRGO.

Finally, Figure 7-5 shows the September 2007 results for the plan 3 configuration. In this phase, the Seabrook construction is added. The velocity magnitude of the flow along the GIWW has been further reduced. The transport of particles decreases, though generally the flow direction and patterns of behavior are very similar to plan 2 results. The major difference between the particle transport for both of these configurations and the base and plan 1 configuration is that particles near the MRGO closure at Bayou Bienvenue are hindered from moving throughout the system.

Figures 7-6 through 7-9 depict the transport results of the March 2008 hydrodynamic conditions. The March 2008 particle transport is similar to the September case. The base configuration shows particles along both the GIWW and the MRGO. The plan 1 case shows a decrease in transport of particles initiated along the MRGO. The plan 2 and plan 3 configurations

DRAFT

allow for transport along the GIWW, but the MRGO initiated particles follow pathways to Lake Borgne and Bayou Bienvenue. As shown in the hydrodynamic results section, the March 2008 flow has greater intensity in the tidal conditions. Overall transport is much higher than in the September 2007 conditions.

a)

b)

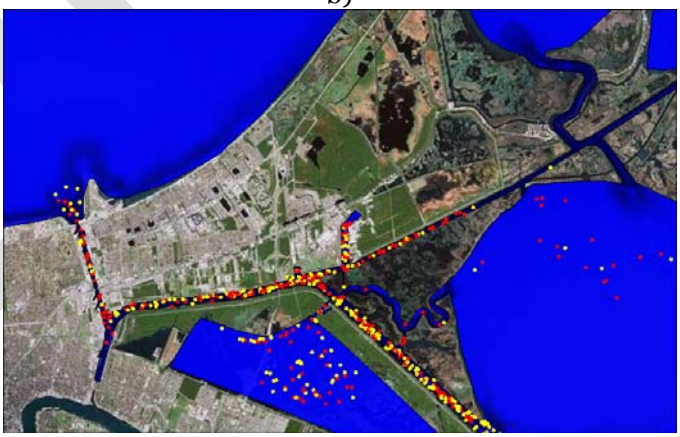

c)

Figure 7-2 September, base condition larvae positions after a) 1 day, b) 1 week, c) 4 weeks. Red particles are initiated on the GIWW and yellow particles are initiated on the MRGO.

DRAFT

a)

b)

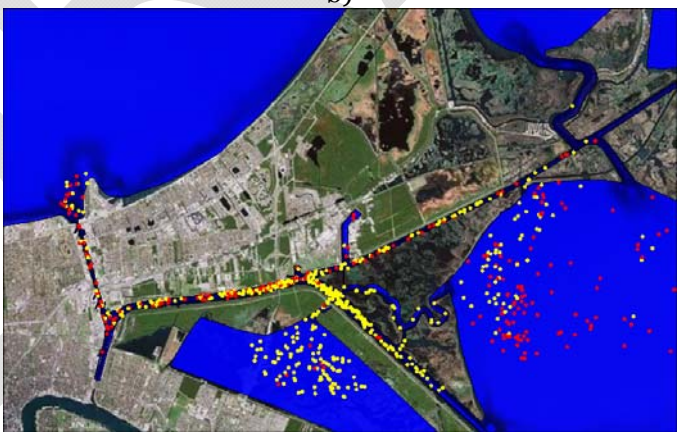

c)

Figure 7-3 September, plan 1 condition larvae positions after a) 1 day, b) 1 week, c) 4 weeks. Red particles are initiated on the GIWW and yellow particles are initiated on the MRGO.

DRAFT

a)

b)

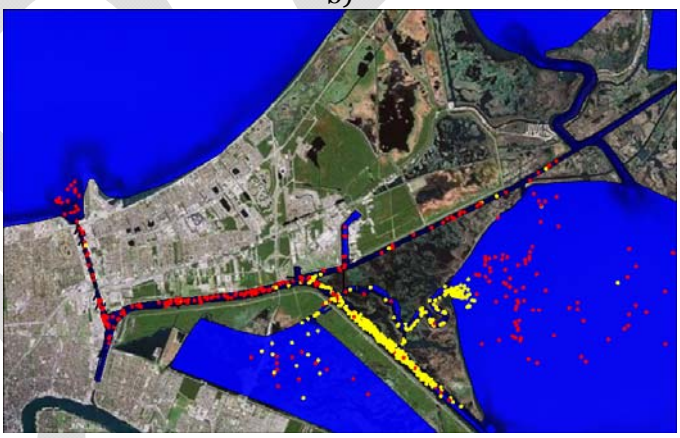

c)

Figure 7-4 September, plan 2 condition larvae positions after a) 1 day, b) 1 week, c) 4 weeks. Red particles are initiated on the GIWW and yellow particles are initiated on the MRGO.

DRAFT

a)

b)

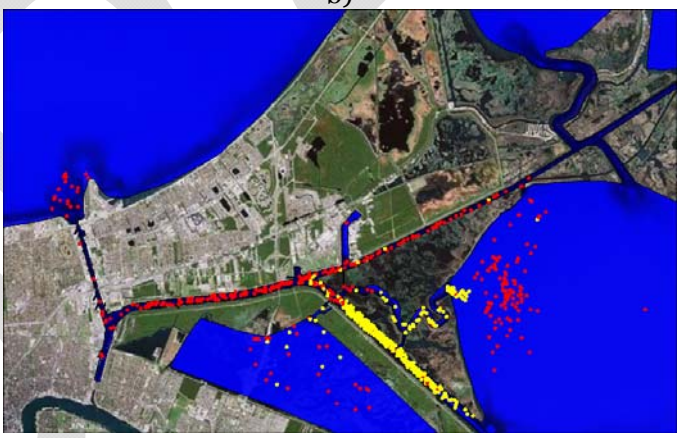

c)

Figure 7-5. September, plan 3 condition larvae positions after a) 1 day, b) 1 week, c) 4 weeks. Red particles are initiated on the GIWW and yellow particles are initiated on the MRGO.

DRAFT

a)

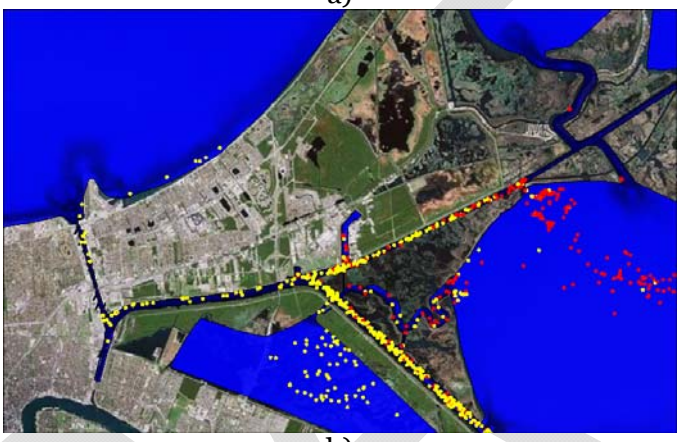

b)

c)

Figure 7-6 March, base condition larvae positions after a) 1 day, b) 1 week, c) 4 weeks. Red particles are initiated on the GIWW and yellow particles are initiated on the MRGO.

DRAFT

a)

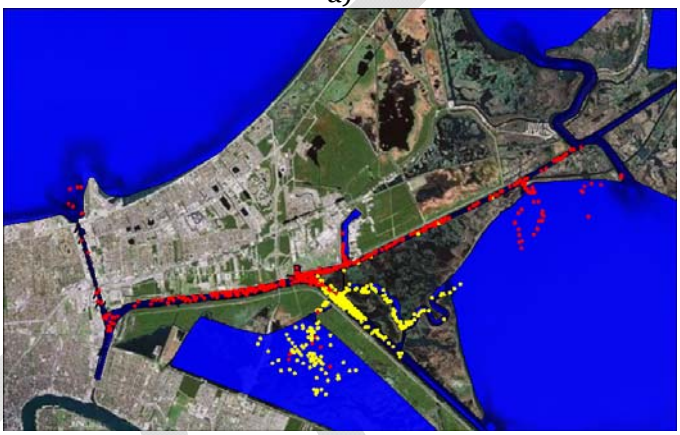

b)

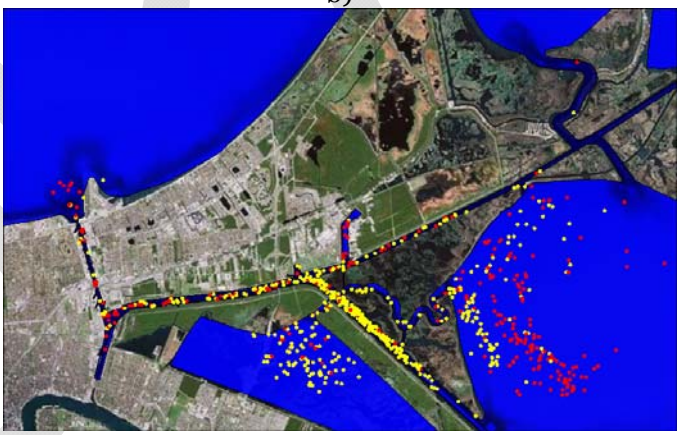

c)

Figure 7-7. March, plan 1 condition larvae positions after a) 1 day, b) 1 week, c) 4 weeks. Red particles are initiated on the GIWW and yellow particles are initiated on the MRGO.

a)

b)

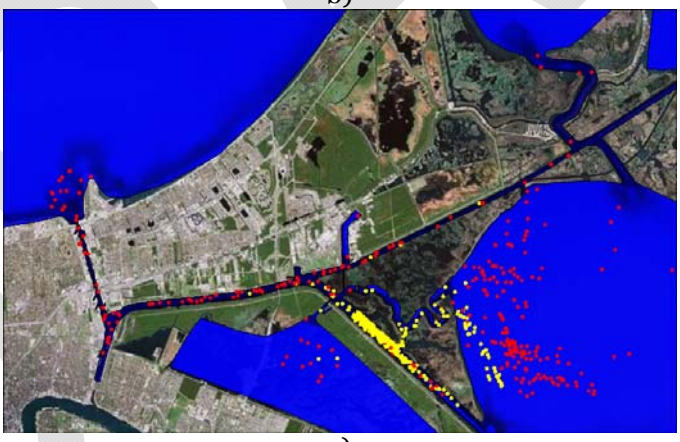

c)

Figure 7-8. March, plan 2 condition larvae positions after a) 1 day, b) 1 week, c) 4 weeks. Red particles are initiated on the GIWW and yellow particles are initiated on the MRGO.

DRAFT

a)

b)

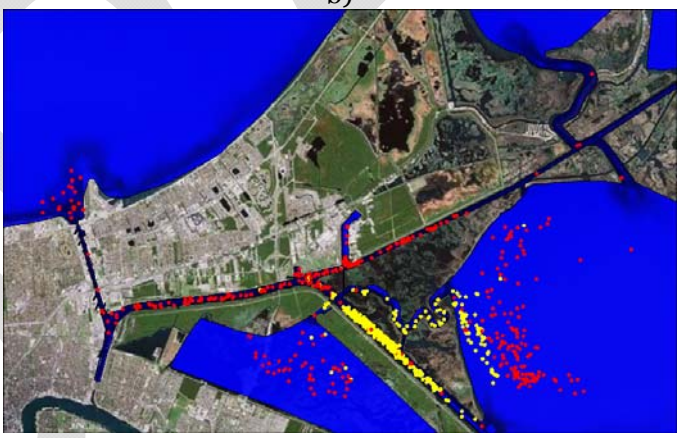

c)

Figure 7-9. March, plan 3 condition larvae positions after a) 1 day, b) 1 week, c) 4 weeks. Red particles are initiated on the GIWW and yellow particles are initiated on the MRGO.

DRAFT

Data analysis of the simulation results for this work is performed using the recruitment information. As particles pass through the recruitment arcs, the number of particles and some of their characteristics such as their starting position and behavior type are collected.

Figure 7-10 shows the time series of the number of larvae that reach both recruitment points with time given in days for the September 2007 hydrodynamic solution. The total simulation time for these model runs is 28 days. The figure shows base, plan1, plan2, and plan3 trends. For the September 2007 flow conditions, the maximum number of larvae recruited is approximately 1400 in the base case. The plan 1 case recruits approximately 800 representative larvae, 500 for the plan 2 case, and approximately 100 particles are recruited in the plan 3 case. This figure also shows the rate at which particles are recruited, represented by the slope of the line. The rise and plateau in the graph are important in understanding the method in which particles are recruited. It is apparent in the graph that for the plan 1-3 cases, the particles appear to be recruited in much the same way, though the number of recruited particles is different. The rise and plateaus appear in the same places for each case; however the overall slope in the lines decreases as the plan number increases. Plans 1-3 all include the MRGO first closure. This reduces the velocity in the MRGO and therefore subsequent transport. In the base case, the time series behaves similarly to the other trends, but abruptly has a significant increase in the slope.

The number of larvae that reach both recruitment areas with time given in days for the March 2008 hydrodynamic solution is shown in Figure 7-11. Generally the plot follows the same trends as the September 2007 results. Similar to those results, there is a marked difference between the base case and the plan cases. The maximum number of recruited particles is approximately 2900 which occurs in the base case. For the plan 1 case, approximately 750 were recruited, 500 for plan 2, and 130 for plan 3. The trends show similarly shaped series, except there is an abrupt increase in the slope of the base case, representing the increased recruitment rate for that configuration.

DRAFT

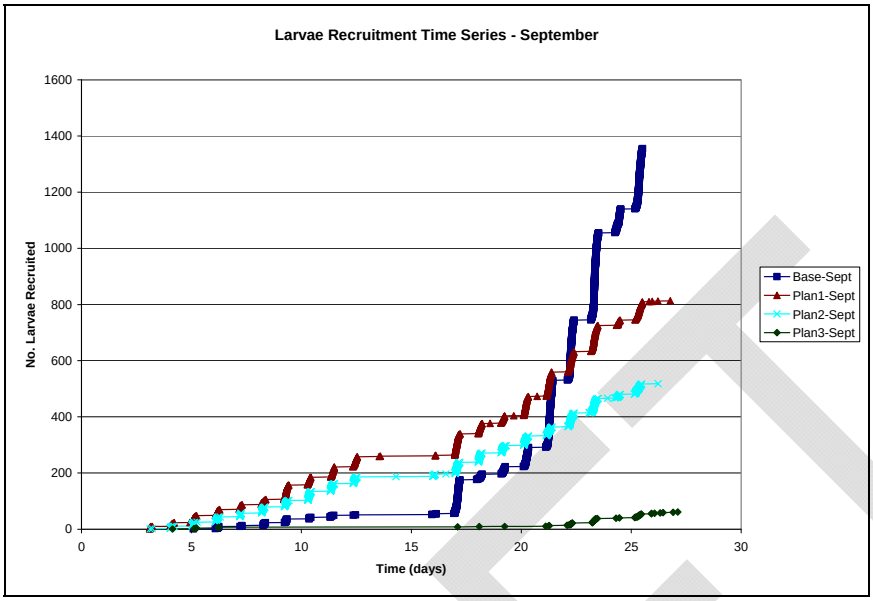

Figure 7-10. Time series of the number of larvae recruited with time for base, plan1, plan2, and plan3 configurations using September 2007 hydrodynamics. 4800 particles total.

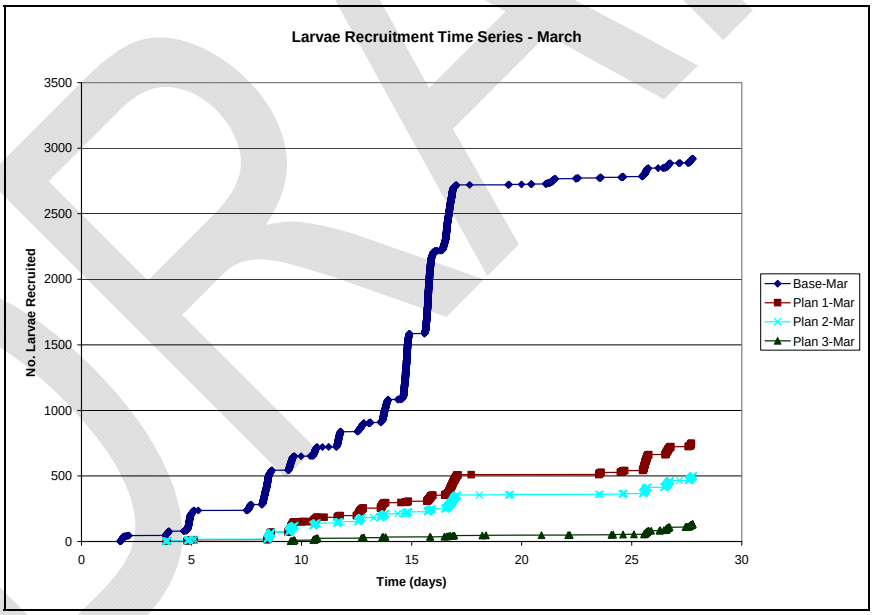

Figure 7-11. Time series of the number of larvae recruited with time for base, plan1, plan2, and plan3 configurations using March 2008 hydrodynamics. 4800 particles total.

DRAFT

A summary of the percentage of particles recruited is shown in table 7-1. Results show that the largest percentages of particles are recruited in the base case. Recruitment values decrease as plan numbers increase. These results reflect the trends shown in Figures 7-10 thru 7-11.

Table 7-1 Percentage of larvae recruited for each construction phase for simulations in which particles are initiated in the MRGO and GIWW (Case 2 conditions).

Construction Phase	Percent Recruited – September 2007	Percent Recruited – March 2008
Base – September 2007	28.2	60.8
Plan 1– September 2007	16.9	15.6
Plan 2 – September 2007	10.8	10.4
Plan 3 – September 2007	1.2	2.7

In an effort to understand the results shown in figures 7-10 and 7-11 a series of tests and sensitivity studies was done on the data. The first consideration was to determine if initiating particles near the MRGO closure might affect the data analysis results. The initial location of the particles released in the MRGO is to the southeast of the 2nd MRGO closure that is included in plans 2 and 3. In the cases of plans 2 and 3, particles placed in the MGRO are not able to easily navigate around the 2nd MRGO closure. There will therefore be greater total recruitment for the base case because of the number of particles released in the MRGO that have a clear pathway to the recruitment areas. It is useful to examine solely the particles which are initiated in the GIWW. Figures 7-12 and 7-13 reveal these results. It can be seen from these figures that differences in the recruitment values between the plan and base configurations decrease. In the March case, the previous graph showed that approximately 60 percent of the particles were recruited in the base case; whereas 15 percent of the particles were recruited in the plan 1 case. When only the GIWW source is considered, the base case shows approximately 28 percent of the particles are recruited and the plan 1 case remains at approximately 15 percent. These results confirm that when the particles which are initiated in the MRGO are not considered, the remaining results are better aligned. It also shows that for

DRAFT

the Plan1-Plan2 configurations, the majority of particles which are recruited come from the GIWW source. This suggests that fish larvae originating in the MRGO may have difficulties determining pathways to the recruitment areas. However, it is unlikely that many larvae will be transported into these areas due to the MRGO closures.

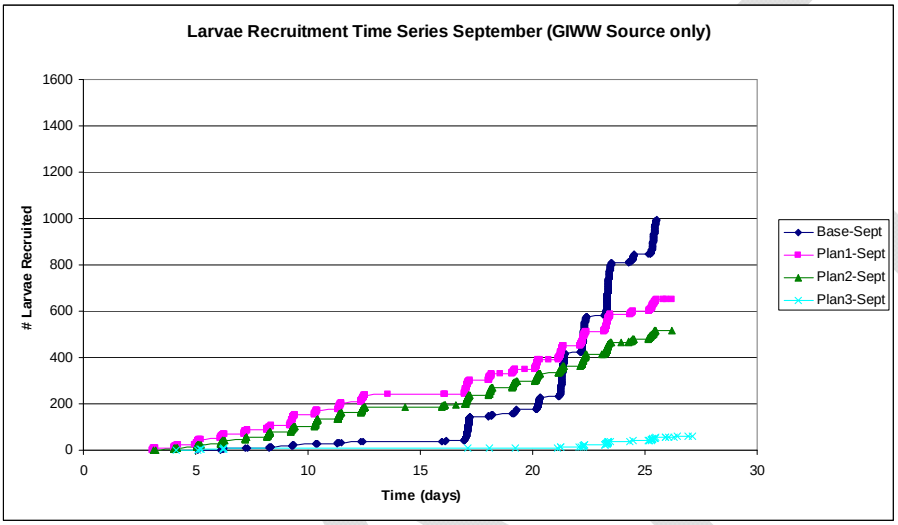

Figure 7-12 Time series of the number of larvae recruited with time for base, plan1, plan2, and plan3 configurations using March 2008 hydrodynamics for GIWW source only (2195 particles total)

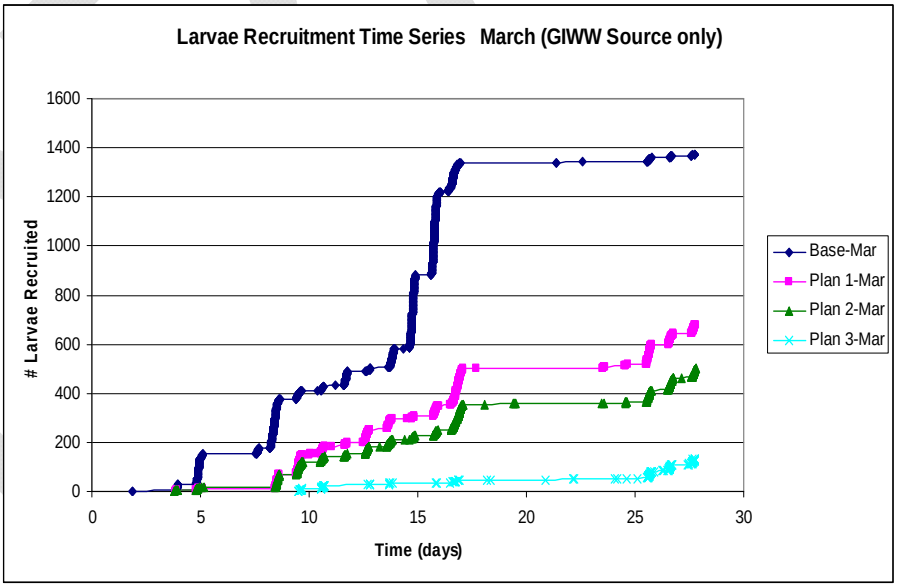

Figure 7-13. Time series of the number of larvae recruited with time for base, plan1, plan2, and plan3 configurations using March 2008 hydrodynamics for GIWW source only (2195 particles total)

Another area of interest is the difference between the March 2008 and September 2007 results. Generally the recruitment values within the March 2008 case are larger. This question is addressed by considering the tidal signal (Figure 4-5). The magnitudes of the tidal signal for the March 2008 case seem to have higher peaks. Particle pathways and the recruitment time series illustrate periods where large numbers of particles are recruited over relatively small periods of time. This is indicative of the flushing of particles out of the system. This causes large jumps in the number of recruited particles.

To determine the effect of the tidal peaks on the larvae recruitment time series, a test was done with 80 particles on the March 2008 hydrodynamic, base configuration (Figure 7-14). The same hydrodynamic results were utilized, except particles were initiated at two different times. One set of particles was initialized at the beginning of the hydrodynamic period. A second set of particles was initiated after an additional week. The "lagged" series follow the same trends as the "original" series, however it can be seen that fewer particles are recruited in the lagged case. This suggests that the timing of particle introduction with regard to the tidal signal is important. If particles are introduced as a large incoming peak in the signal is approached, there is more likelihood that they will be flushed out of the channels and into the recruitment areas.

The peaks of the tidal signals may not be the only reason for the difference between September 2007 and March 2008. Phase differences and flow interaction between the MRGO and GIWW may complicate matters. As seen in the hydrodynamic analysis, there are persistent phase differences between the GIWW and the MRGO. This phase difference may work to the benefit or the detriment of transportation. If the flows move in sync, then particles will be quickly washed in one direction, however if they are moving opposed to each other, then it is also possible that transport may be interrupted.

DRAFT

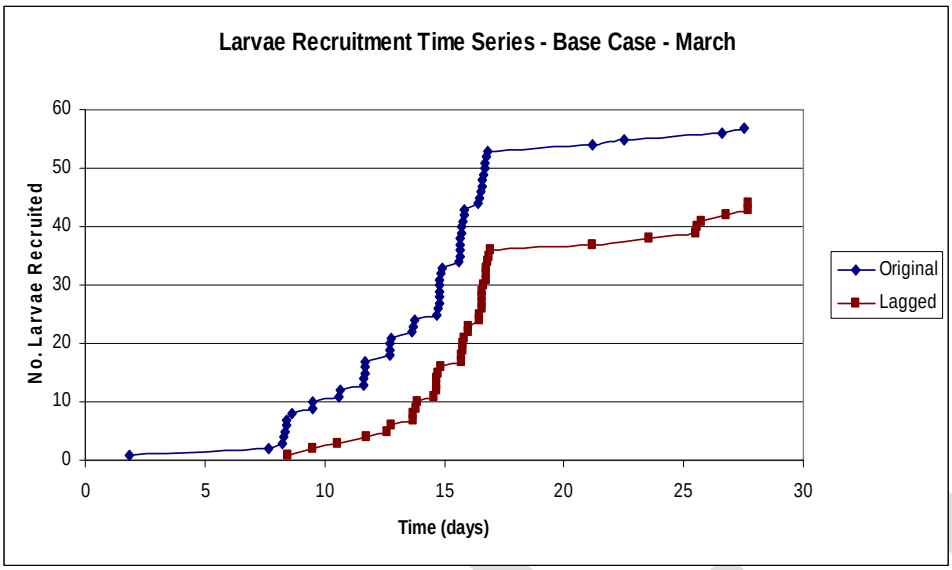

Figure 7-14 Comparison of Larvae Recruitment Time Series for the March 2008 Hydrodynamic, Base configuration.

Finally, the effect of behavior on particle recruitment is studied. The number of larvae (given as a percentage) recruited at both recruitment sites for each type of behavior for the September 2007 period is shown in Figure 7-15. Red zones within the column represent the particles which are recruited at Chef Menteur. Blue zones within the column represent the number of particles which are recruited at the Seabrook recruitment area. The percentage is based on the total number of particles initiated within the simulation (% recruited = number of particles recruited per behavior/total number of particles of that behavior*100). The total number of particles is 4800 and so there are 1200 particles for each behavior.

The largest percentages of recruited particles occur in the base case, as expected from the time series analysis. However, the effects of the behaviors are also apparent. The recruitment for tidal vertical is approximately 42 percent, tidal lateral is 29 percent, passive is 25 percent, and bottom movers is 15 percent. In each plan configuration, it is confirmed that the largest number of particles that are recruited have the tidal vertical behavior and the smallest number of particles recruited have the bottom mover behavior. This trend is reasonable. Bottom movers are affected by only the bottom velocities. Because ADH is a depth averaged flow model, the flow field is assumed to have a logarithmic velocity profile. In such a profile, the velocities at the bottom are a small percentage of the average velocity. Therefore particles will have a tendency to be transported at a

slower rate. It should be reiterated at this time that one of the limitations of the particle tracking model larvae fish movement algorithm is that particles do not currently portray "anchoring" abilities. Results (Chapter 8) suggest that when anchoring is added to the particles, bottom movers have a greater possibility of reaching recruitment zones in an efficient manor.

The trends for the September 2007 case are also seen in the March 2008 data analysis (Figure 7-16). In this case, however, there are greater differences between the base case and the plan cases. The percent of recruited larvae for all behaviors is above 40 percent for the March base case and decreases for the plan configurations. It is also evident that for all configurations in the September and March cases, the preference is for recruitment at Chef Menteur.

DRAFT

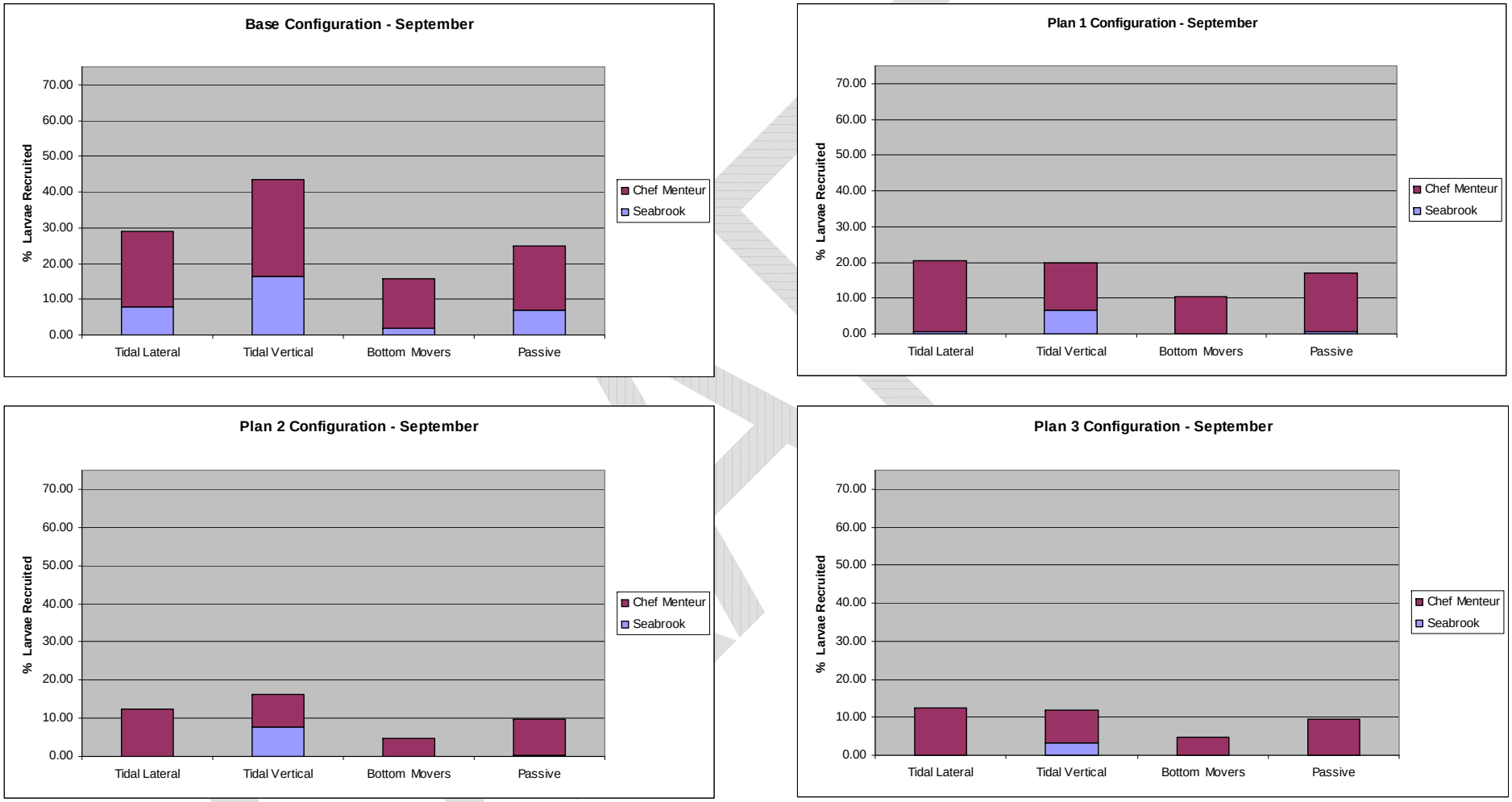

Figure 7-15 Percentage of larvae recruited at Seabrook (blue) and Chef Menteur (red) for base, plan1, plan2, and plan3 configurations using September 2007 hydrodynamics

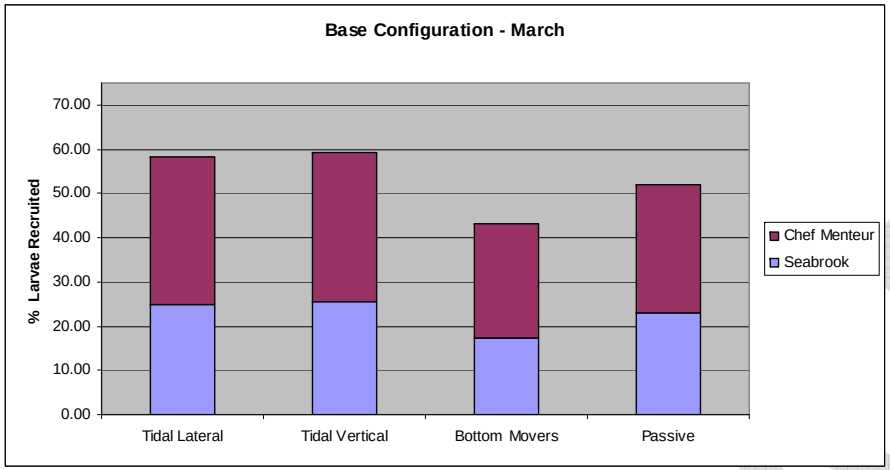

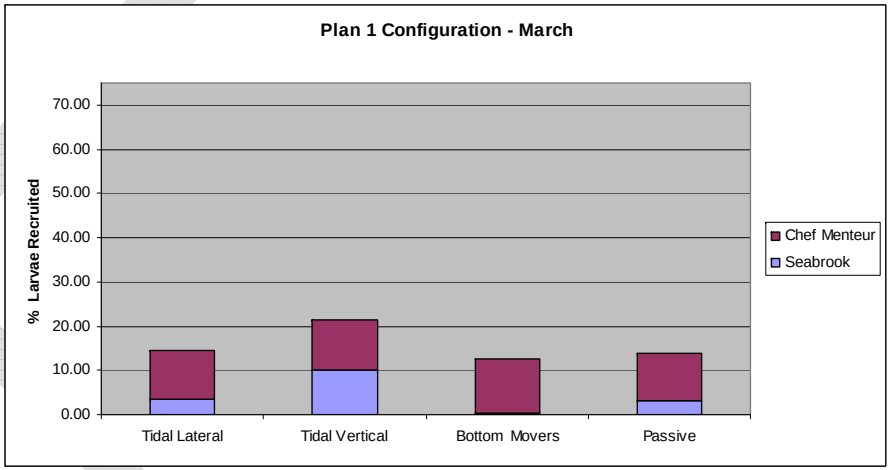

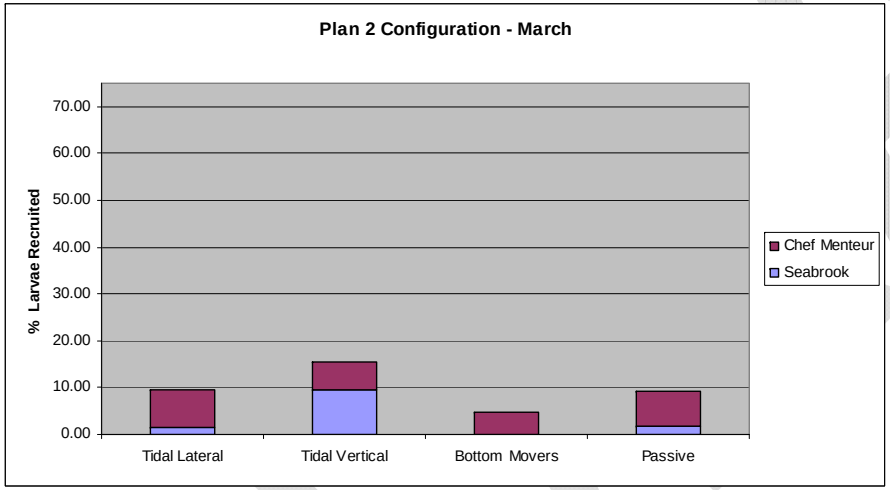

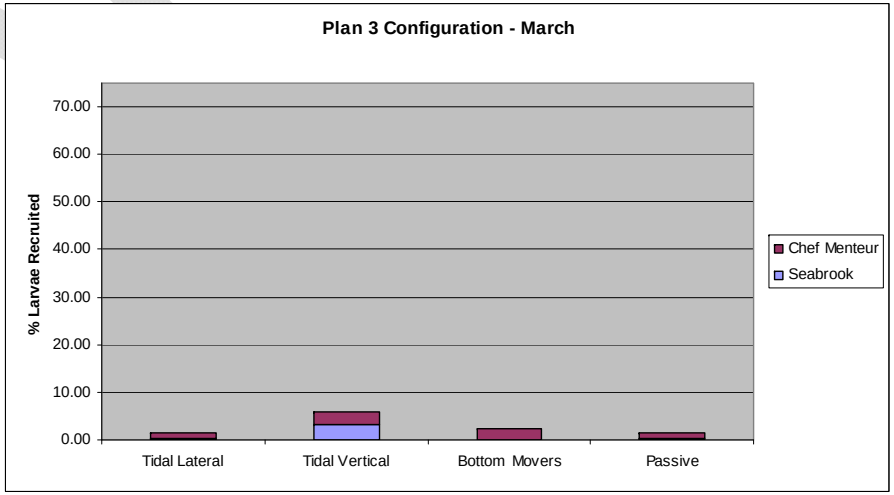

Figure 7-16 Percentage of larvae recruited at Seabrook (blue) and Chef Menteur (red) for base, plan1, plan2, and plan3 configurations using the March 2008 hydrodynamics.

Case 3

The final set of source conditions for particles are those initiated in Lake Borgne. These particles are representative of larvae that are introduced into the system via the eastern edge of Lake Borgne. Computational testing shows that particles must be initiated along the western edge of the lake to develop statistically relevant results (Figure 5-4). However it is reasonable to assume that particles initially introduced into the system through the eastern edge will eventually pass through the western edge of the lake to reach the GIWW and MRGO. Figure 7-17 shows the computed larvae positions for simulations using the March 2008 hydrodynamics and the plan 1 configuration. Each figure (a-c) shows a snap shot of where the particles are one day, one week, and four weeks after the simulation begins.

Almost immediately after the simulation begins, particles are flushed into the Chef Menteur recruitment zone. However, not all particles are transported into the GIWW. A large percentage (see Figure 7-17 c) remains within the lake or gets transported towards the east, into the Gulf. Table 7-2 shows the percentage of particles initiated in Lake Borgne, which are subsequently recruited at the recruitment regions. Only the March 2008 hydrodynamic period is utilized for this case. September 2007 hydrodynamic solutions do not show a significant amount of recruited particles. Almost 100 percent of the particles are recruited at the Chef Menteur recruitment area for all configurations. The analysis shows that for particles initiated in Lake Borgne, there appears to be no real difference between the plan configurations with regard to the percentage of larvae recruited. The base case is slightly higher than plans 1-3, but this may be due to the general influx of flow via the MRGO. That is, in the base case particles that exit Lake Borgne via the south west passage of Bayou Bienvenue into the MRGO may have a greater opportunity for recruitment due to the lack of closures in the MRGO.

DRAFT

a)

b)

c)

Figure 7-17. March, base condition larvae positions after a) 1 day, b) 1 week, c) 4 weeks. Particles initiated in Lake Borgne.

DRAFT

Table 7-2 Percentage of larvae recruited for each construction phase for simulations in which particles are initiated in Lake Borgne.

Construction Phase	Percent Recruited
Base	21.7
Plan 1	16.4
Plan 2	14.7
Plan 3	16.8

DRAFT

8 Particle Tracking Results – Anchoring Effects and Final Plan

In this chapter, simulation results from the final design plan are shown and compared to the base case and plans 1-3. In addition, as stated in Chapter 5, a transport characteristic of some larval fish species is the ability to "anchor" in order to more efficiently reach recruitment areas. This prevents particles from being forced away from recruitment regions due to the hydrodynamics of the tidal system. The addition of this mechanism more accurately represents the behaviors of larval fish during transport. This chapter shows results of simulations which include this characteristic behavior.

The description section of chapter 5 explains that the tidal flag for the rise, fall, and anchoring of particles is determined by the circulation. In an ideal case this would mean that there was always a clear concept of the tidal direction. However, determining the tidal direction can be complicated. Figure 8-1 shows the direction of the flow for the incoming tide for all plan configurations. Based on the configuration, the circulation directions change. In the base case there is a portion of the flow (circled section within GIWW) in which there is no clear direction of flow for the incoming tide.

If the direction of the tide is ambiguous such as in the case in which particles are being released in the GIWW, then it is unclear how a preferred path is chosen by larval fish. Therefore, two sets of simulations are performed. In the first case, the preferred direction is to the west. In the second case the preferred direction is to the east. An implicit assumption is that once a larval fish has chosen its preferred direction it operates within a set of rules which requires that it maintain that direction as the incoming tide direction and behave accordingly. If it is eventually determined how this direction is chosen when the circulation is ambiguous, then the current results can be scaled. It should also be mentioned that based on Figure 8-1b, it appears that westward is the flow direction for the incoming tide in the circled section for plans 1-3 and the final plan.

DRAFT

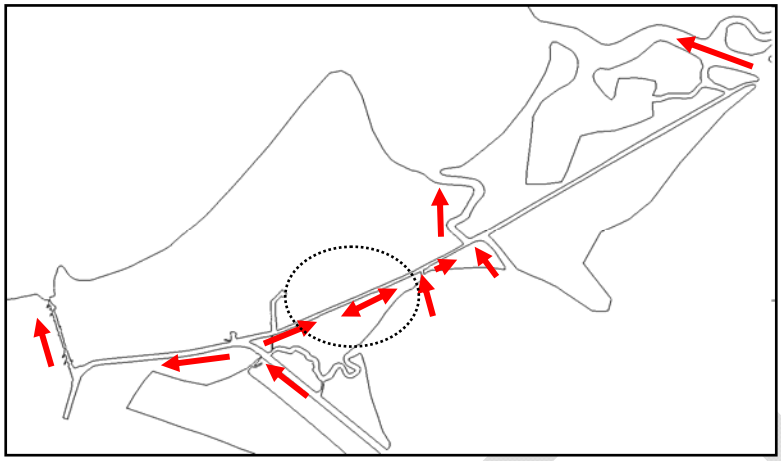

a) Direction of flow for incoming tide in Base case

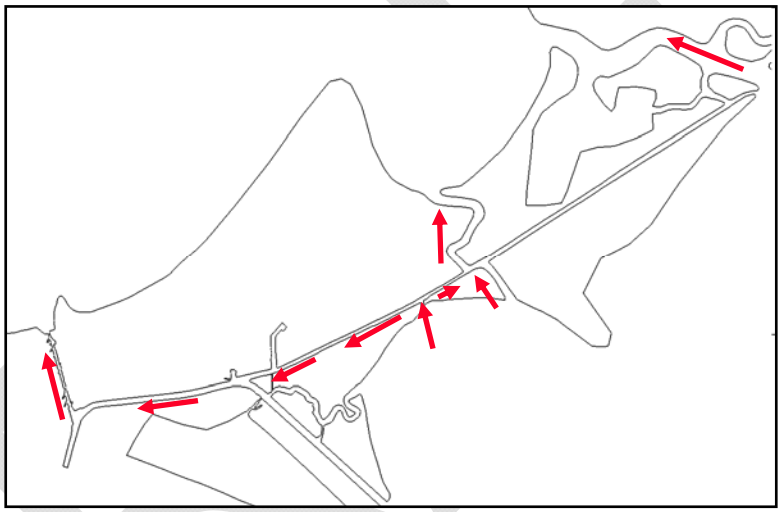

b). Direction of flow for incoming tide for Plan 1, Plan 2, and Plan 3

Figure 8-1 Circulation Diagram of flow direction for incoming tide for all configurations

Case 2 results (Chapter 7) show that particles released near the second closure in the MRGO have limited transport for the plan 2 and plan 3 configurations. The velocity to the southeast of the MRGO closure is very small. When anchoring is added to the other characteristic behavior, the particles take advantage of the higher velocities to reach recruitment regions. However in this case the limited velocities mean that larval fish transport is still extremely slow and the effect is similar to the previous results seen in Figures 7-4, 7-5, 7-8, and 7-9. Subsequent statistics and data analysis which include those particles may skew results slightly. Therefore

in this Chapter, Case 2 initial position of particles is replaced with Case 4 in which particles are initiated only within the GIWW.

Case 1

Results obtained from Case 1 in which particles are initiated near the first MRGO closure are very similar to those results shown in Chapter 7. Particles do not reach the recruitment areas for plans 1-3 or the final plan. For the base case, particles do move along the MRGO faster due to the anchoring. However, very few particles reach the recruitment areas within the given 4 week simulation time period.

Case 3

In this section, particles are initiated within Lake Borgne as shown in Figure 5-4. Two types of simulations are run. In one case particles are anchored with the incoming tide assumed to be towards the west and the second case assumes the incoming tide is towards the east.

Similar to the results shown in Chapter 7, initially particles are transported into the Chef Menteur recruitment zone. However, many particles remain in Lake Borgne. Figures 8-2 a-c show snapshots of particle positions during the March 2008 hydrodynamic period after 1 day, 1 week, and 4 weeks for the final plan configuration. Anchoring is to the west. While in Lake Borgne, anchoring of particles does not affect transport because there is no real tidal direction. Once particles exit into the GIWW or the MRGO, particles are transported quickly towards recruitment zones. Tables 8-1 and 8-2 show the percentage of particles recruited within September 2007 and March 2008 hydrodynamic period for particles anchored to the west and east respectively. As expected, fewer particles are recruited in the September 2007 simulations than in the March 2008 simulations because of the smaller, less intense velocities during that period. Generally it can be seen that the base case contains slightly higher recruitment rate. This is most likely due to the transport of flow within the MRGO. However, Plans 1-3 and the Final Plan remain statistically very similar.

DRAFT

a)

b)

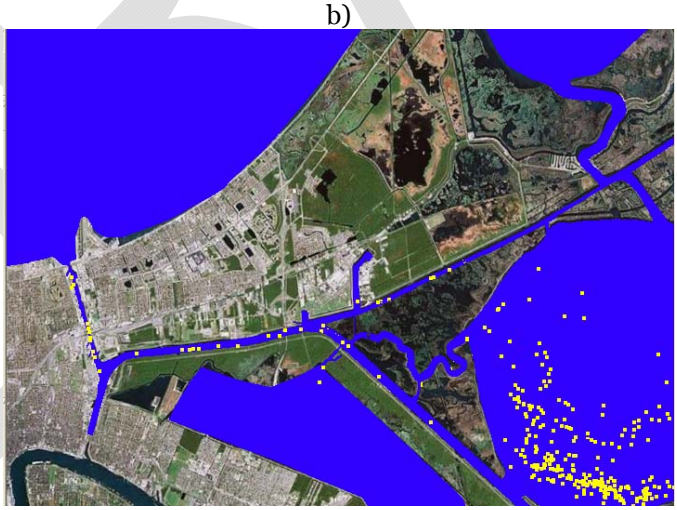

c)

Figure 8-2. March, base condition larvae positions after a) 1 day, b) 1 week, c) 4 weeks. Particles initiated in Lake Borgne.

DRAFT

Table 8-1 Recruitment Percentages for Case 3 particles – Incoming Tide-West

Construction Phase	Percent Recruited – September 2007	Percent Recruited – March 2008
Base	10.22%	26.61%
Plan 1	6.99%	17.34%
Plan 2	6.18%	16.53%
Plan 3	6.32%	17.88%
Final Plan	6.72%	16.94%

Table 8-2 Recruitment Percentages for Case 3 particles – Incoming Tide East

Construction Phase	Percent Recruited – September 2007	Percent Recruited – March 2008
Base	15.59%	24.87%
Plan 1	10.75%	24.46%
Plan 2	9.95%	19.76%
Plan 3	7.53%	17.61%
Final Plan	9.27%	18.41%

DRAFT

Case 4

Incoming Tide- West

Simulation results for particles which specify the incoming tide as westward within the circled region of Figure 8-1 are shown in Figures 8-3 thru 8-6. These figures display snapshots in time after 1 day, 1 week, and 4 weeks. Particles are color coded based on behavior. Cyan particles are tidal lateral, green particles are tidal vertical, yellow particles are bottom movers, and pink particles are passive. For the September 2007 base case, initially particles cluster near the start position in the GIWW. After one week, the particles are dispersed primarily in a westward direction. Some particles have been transported into the MRGO. After four weeks a significant percentage of particles have been recruited, though some particles have made it into Lake Borgne, the MRGO, and the stored water region to the southwest of the MRGO representing the Central Wetlands Area. Similar results are seen in September 2007, final case. However, due to the decrease in flow velocity fewer particles have managed to reach the recruitment region and more particles have made it into Lake Borgne. Based on the color coding, it can be seen that the tidal vertical and bottom mover particles are recruiting at a faster rate than the tidal lateral particles or the passive movers. This is most likely because of the anchoring transport mechanism. In the case of the tidal vertical and bottom mover particles, anchoring is applied almost immediately. The tidal lateral particles have anchoring applied after a delay as particles make it to the channel sides. The passive movers have no anchoring at all.

For the March 2008, base case (Figure 8-5) particles move throughout the system quickly. After one week, particles range along the GIWW from the Seabrook recruitment area to Lake Borgne. The particles seen within Lake Borgne have primarily passive and tidal lateral characteristic behaviors. Within four weeks almost all the particles have been recruited except for those that end in Lake Borgne. These particles may remain there for any length of time before exiting.

DRAFT

a)

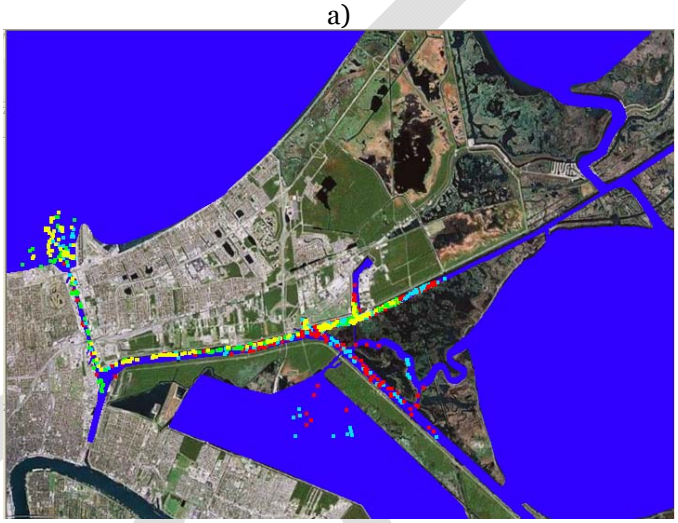

b)

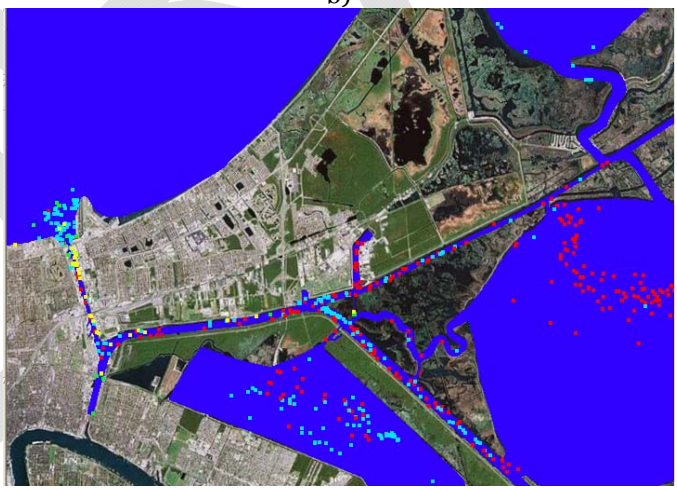

c)

Figure 8-3 September, base condition larvae positions after a) 1 day, b) 1 week, c) 4 weeks. Particles anchored based on incoming tide to the west and are color coded based on behavior.

a)

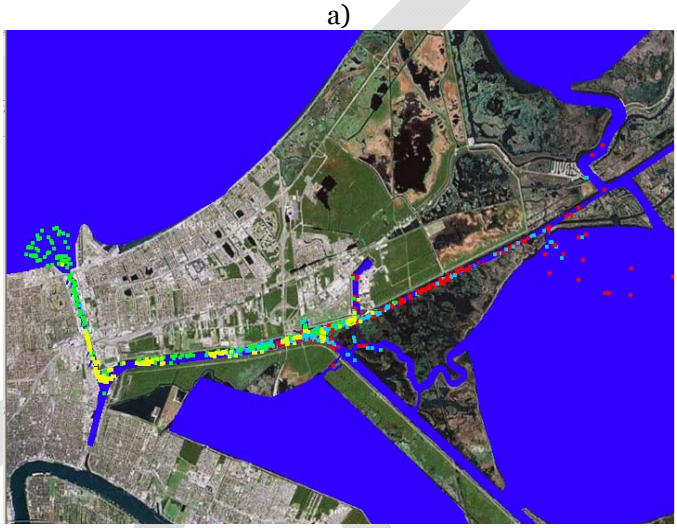

b)

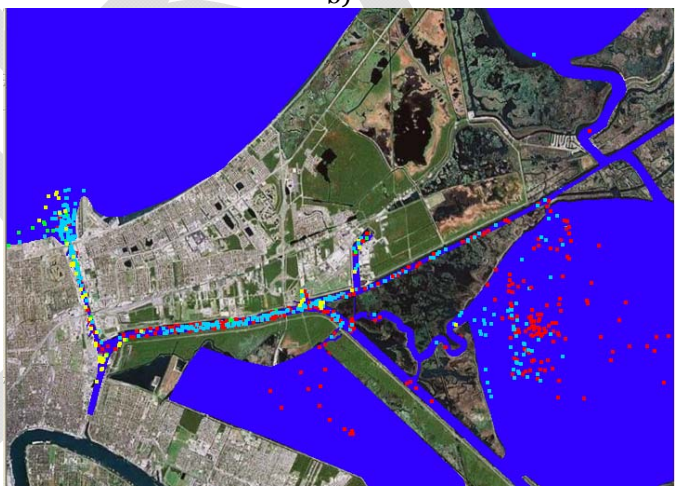

c)

Figure 8-4 September, final plan condition larvae positions after a) 1 day, b) 1 week, c) 4 weeks. Particles anchored based on incoming tide to the west and color coded based on behavior.

DRAFT

a)

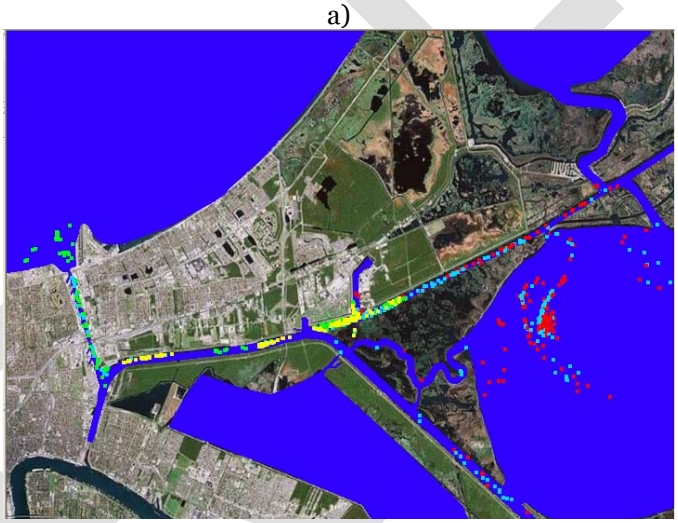

b)

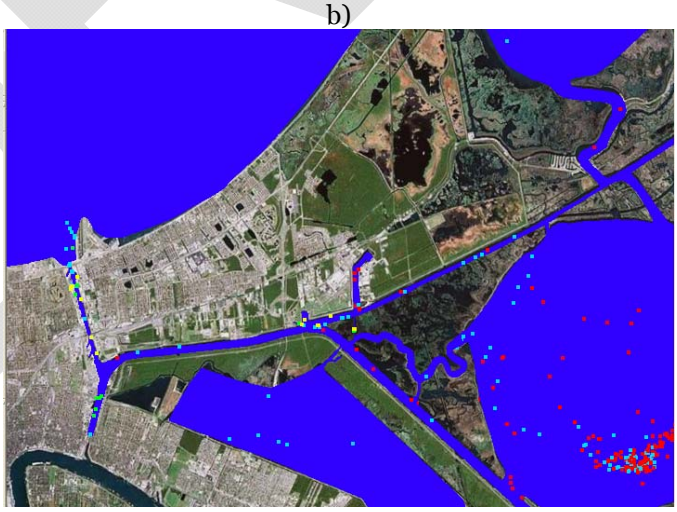

c)

Figure 8-5 march, base condition larvae positions after a) 1 day, b) 1 week, c) 4 weeks. Particles anchored based on incoming tide to the west. and color coded based on behavior.

a)

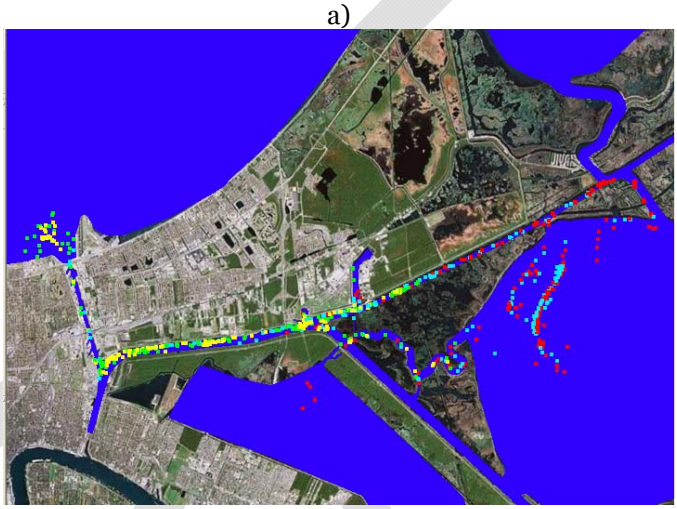

b)

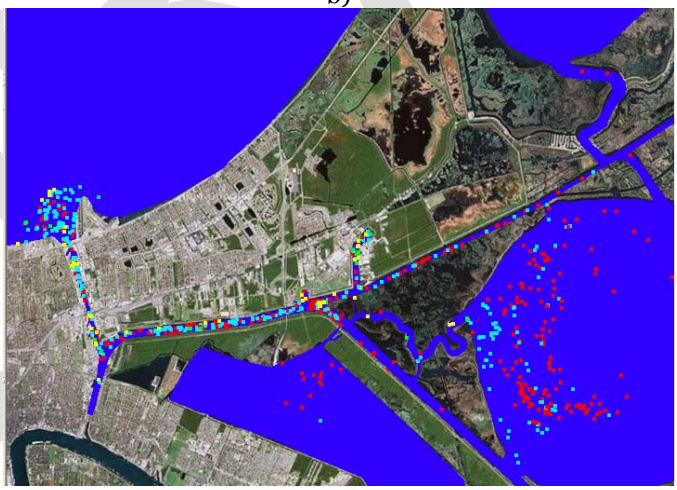

c)

Figure 8-6 march, final plan condition larvae positions after a) 1 day, b) 1 week, c) 4 weeks. Particles anchored based on incoming tide to the west. and color coded based on behavior.

Time series of larval recruitment are shown in Figure 8-7 and 8-8 for September 2007 and March 2008 hydrodynamics respectively. Both simulations result in a similar trend. The base configuration shows the largest recruitment values. There is a decrease in recruitment with respect to increasing plan number for plans 1-3. This is similar to what was seen in the unanchored particle results shown in Chapter 7. However there is a great difference in the total number of particles recruited between the previous results and those shown in Figures 8-7 and 8-8. For the plan 3, September 2007 hydrodynamic condition more than seven times the number of particles is recruited with the one GIWW source (approximately 550) than the combination of both the GIWW and MRGO sources for the unanchored case (approximately 75). The final plan shows an increase of recruitment in comparison to plan 3. In the final plan, two additional gates are added to Seabrook area construction, almost doubling the amount of flow allowed through that area. The results shown in the recruitment percentages of the final plan reflect the increased cross sectional area.

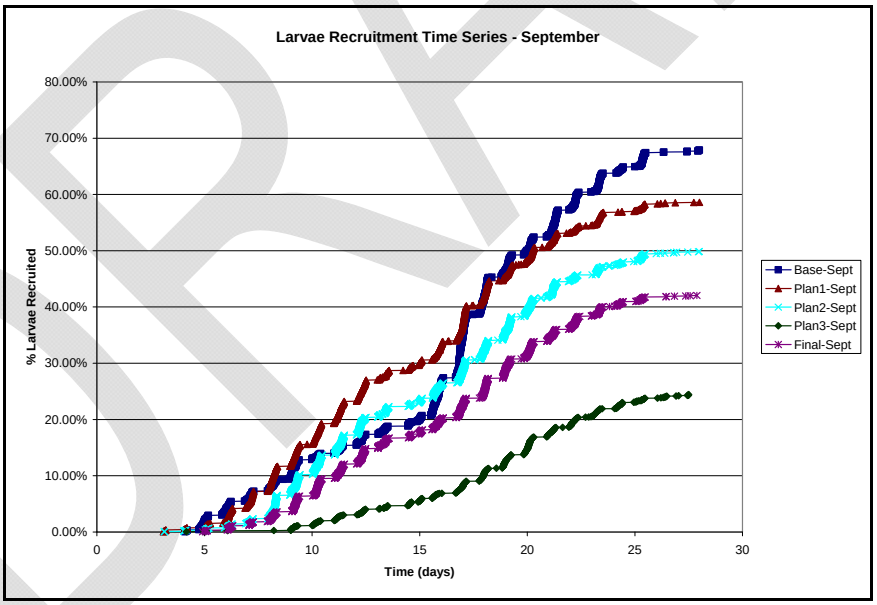

Figure 8-7 Comparison of Larvae Recruitment Time Series for the September 2007 Hydrodynamic, larval fish preferred path to the west. Particles anchored based on incoming tide to the west (2150 particles released)

DRAFT

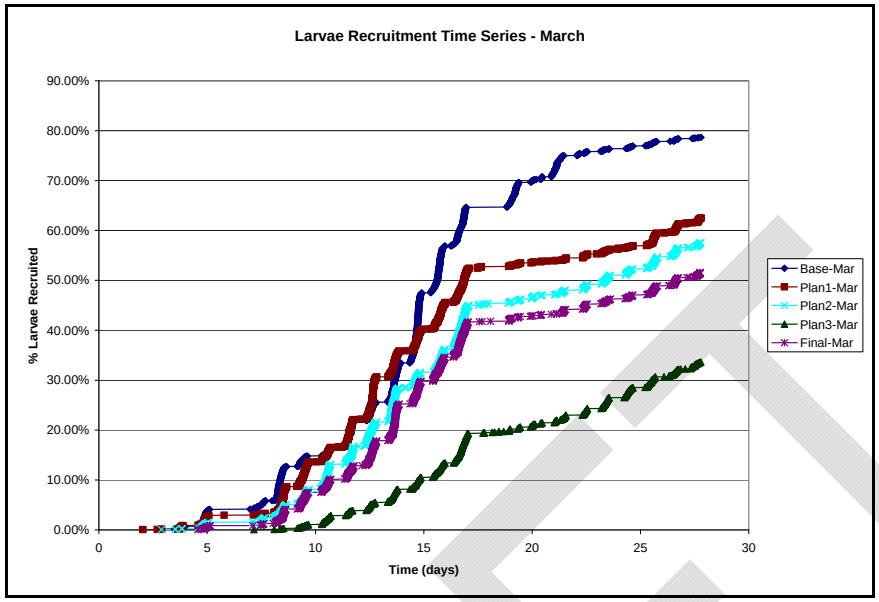

Figure 8-8 Comparison of Larvae Recruitment Time Series for the March 2008 Hydrodynamic, larval fish preferred path to the west. Particles anchored based on incoming tide to the west (2150 particles released).

Table 8-4 gives a summary of the total percentage of particles transported to the recruitment areas for both the September 2007 and March 2008 hydrodynamic periods. These results support the observations from the recruitment time series figures. Generally the base case has the greatest percentage of particles recruited. The percentages decrease as the plan number increases. The final plan values are very close to plan 2 values.

Table 8-3 Percentage of larvae recruited for each construction phase for simulations in which particles are anchored based on incoming tide to the west (2150 particles released).

Construction Phase	Percent Recruited – September 2007	Percent Recruited – March 2008
Base	67.91	78.5
Plan 1	58.60	62.51
Plan 2	49.86	57.58
Plan 3	24.42	33.63
Final Plan	42.05	51.58

DRAFT

The percentage of particles recruited at the Seabrook and Chef Menteur recruitment regions are presented in Figures 8-9 and 8-10 (% recruited = number of particles recruited per behavior/total number of particles of that behavior*100). For the September 2007 case the number of particles recruited for the base plan is largest for the bottom and tidal vertical movers. These two characteristic types both have anchoring added to their behavior, suggesting that anchoring greatly increases the chance that the particle will be recruited. It can also be seen that the greatest number of particles are recruited at Seabrook. Because the direction of the incoming tide within the GIWW is to the west towards Seabrook, this is the logical result. The recruitment percentages decrease slightly for the tidal vertical and bottom movers as the plan number increases from 1 to 3. However they decrease drastically for the tidal lateral and passive particles. As the particles represented by the passive behavior do not have anchoring, these results show the importance of that characteristic for recruitment. Although the tidal lateral particles do have anchoring, because that behavior is only applied when the particle reaches the side of the channel, there is a lag in the effect of this transport characteristic. Final plan results are extremely close to plan 2 results as expected. March 2008 results show similar trends, though because of the increased flow velocities a larger amount of passive particles are recruited.

DRAFT

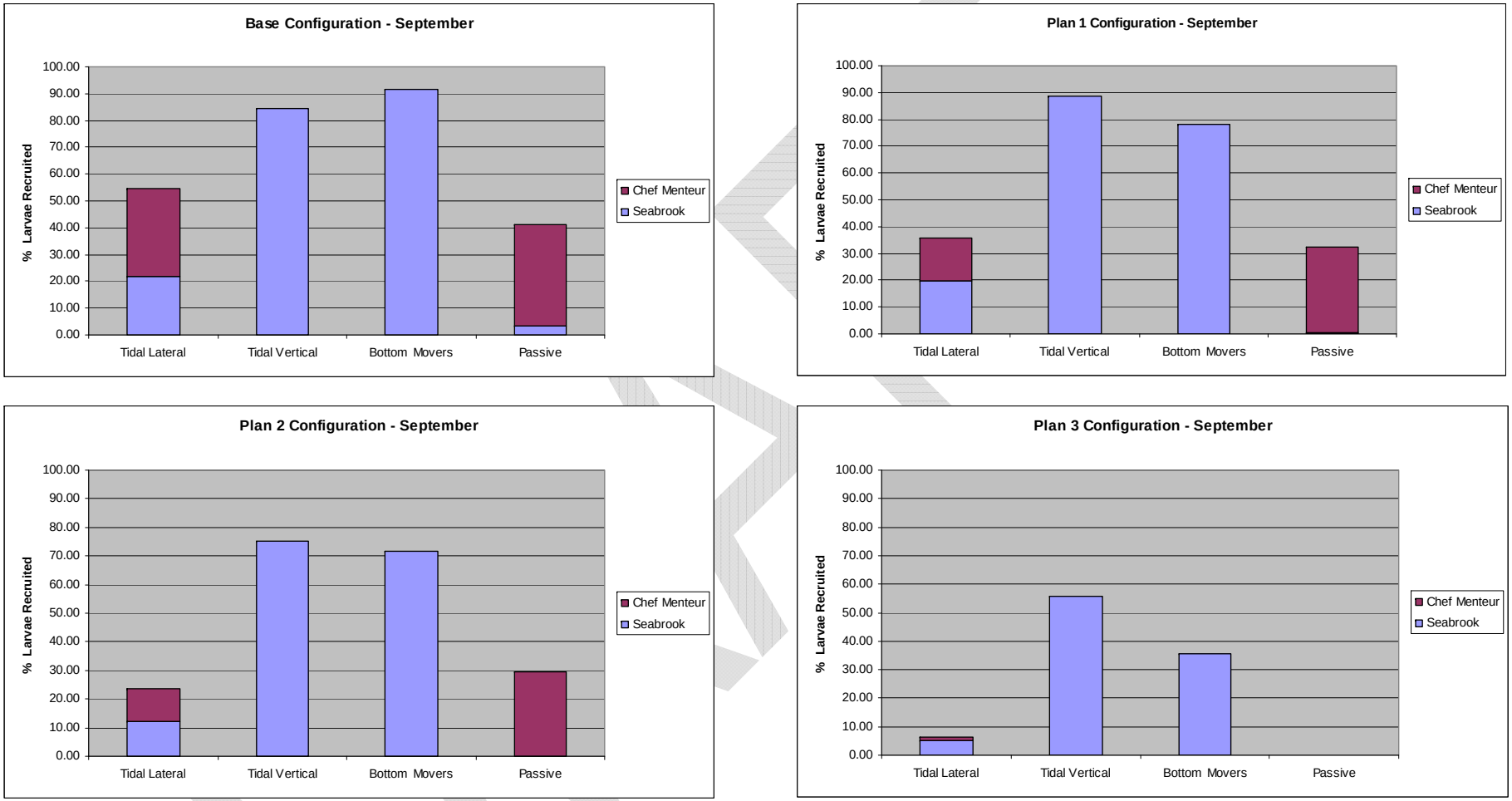

Figure 8-9 Percentage of larvae recruited at Seabrook (blue) and Chef Menteur (red) for base, plan1, plan2, and plan3 configurations using September 2007 hydrodynamics, larval fish preferred path to the west. (Maximum value possible 25%) Particles anchored based on incoming tide to the west.

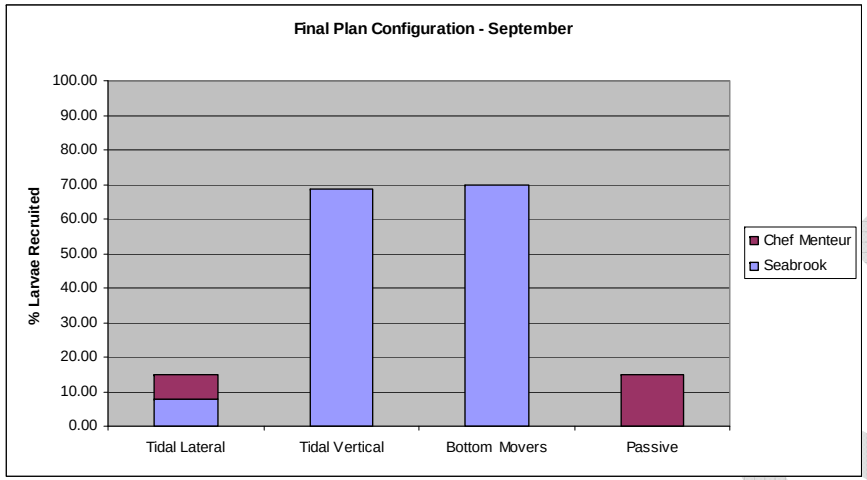

Figure 8-9 (continued) Percentage of larvae recruited at Seabrook (blue) and Chef Menteur (red) for Final Plan configuration using September 2007 hydrodynamics, larval fish preferred path to the west. (Maximum value possible 25%) Particles anchored based on incoming tide to the west.

DRAFT

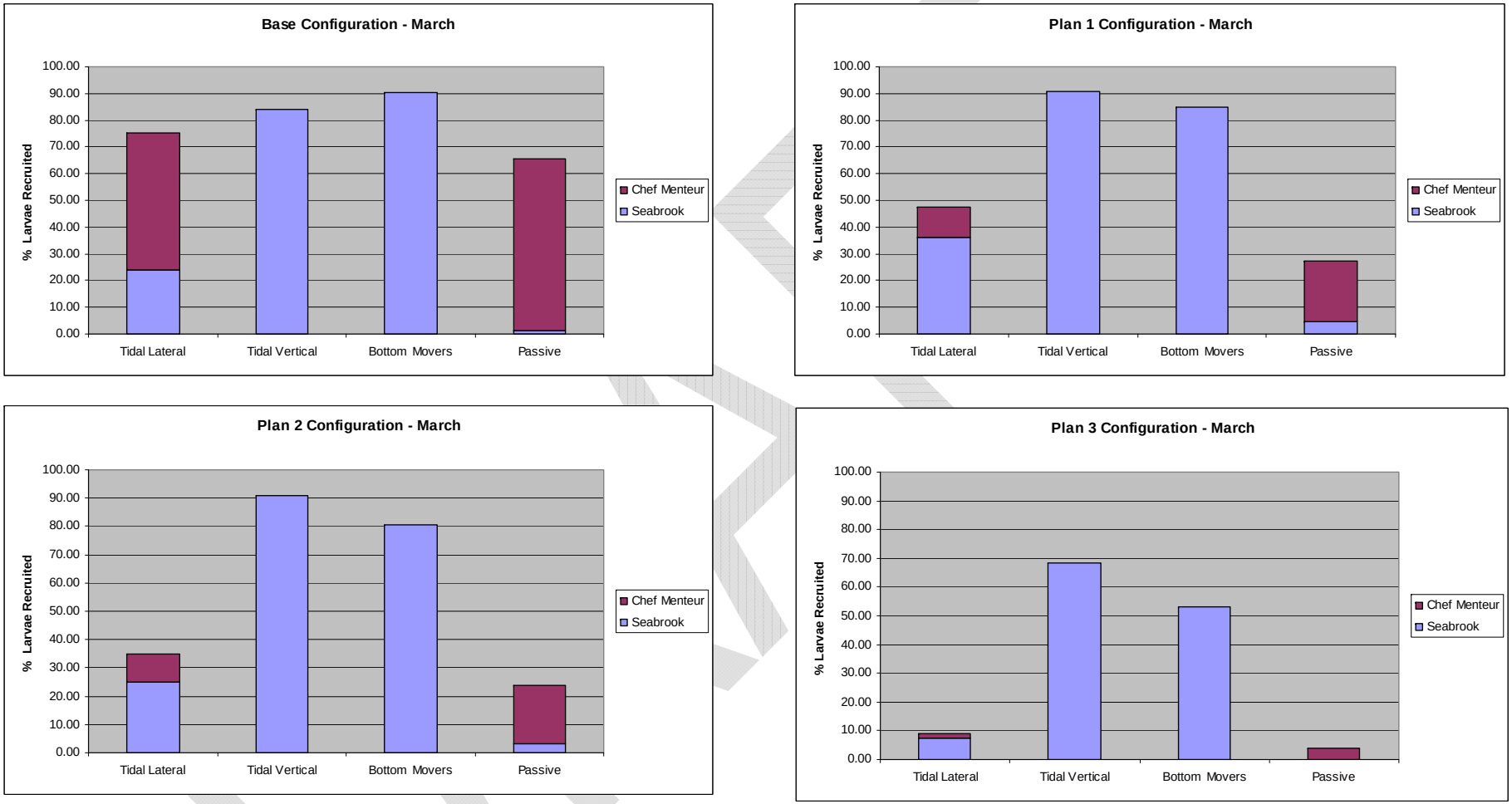

Figure 8-10 Percentage of larvae recruited at Seabrook (blue) and Chef Menteur (red) for base, plan1, plan2, and plan3 configurations using March 2008 hydrodynamics, larval fish preferred path to the west. (Maximum value possible 25%) Particles anchored based on incoming tide to the west.

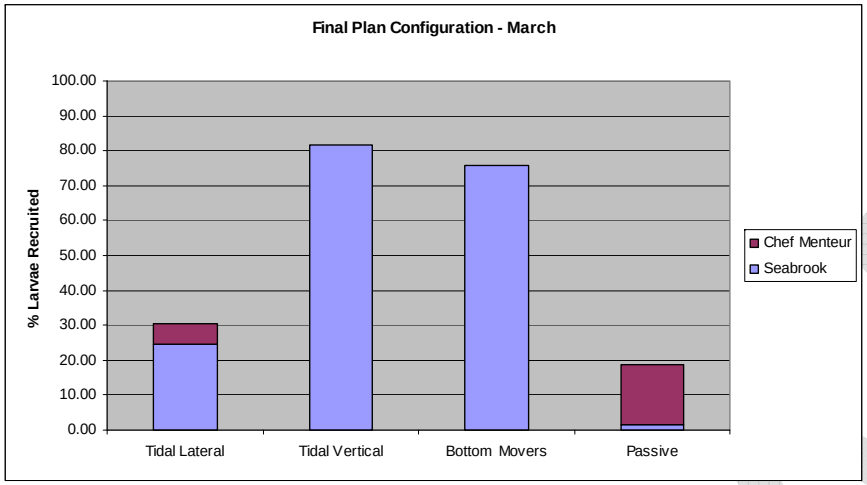

Figure 8-10 continued Percentage of larvae recruited at Seabrook (blue) and Chef Menteur (red) for the final plan configuration using March 2008 hydrodynamics, larval fish preferred path to the west. (Maximum value possible 25%) Particles anchored based on incoming tide to the west.

DRAFT

Incoming Tide- East

In this section, the incoming tide within the circled region of Figure 8-1 is specified as eastward. This means that the preferred pathway for particles introduced into the GIWW will be towards the east and the Chef Menteur recruitment region. Figures 8-11 through 8-14 show snapshots in time of the particle positions after 1day, 1week, and 4 weeks. Particles are color coded based on behavior. Cyan particles are tidal lateral, green particles are tidal vertical, yellow particles are bottom movers, and pink particles are passive. In these simulations, September 2007 and March 2008 hydrodynamics are used. Only base and final plan configurations are displayed. The base case (Figure 8-11) shows similar results to that seen in the previous section. Initially particles are clustered near the release point. After one week particles have been transported along the GIWW. Some particles have made it to the MGRO. After four weeks, the majority of the particles have been recruited with some remaining in the MRGO and Lake Borgne. Once again it can be seen that the majority of the particles residing in Lake Borgne are passive and lateral movers. The final plan results illustrate the effect of the slower velocity. Fewer particles appear to have reached the recruitment area. An additional effect is that more particles reach Lake Borgne. Now bottom movers and tidal vertical particles are also in Lake Borgne. This is due in part to the slower velocities near the GIWW entrance to Lake Borgne which allows for an easily accessible transport pathway into the lake. In addition there is perhaps a blocking mechanism to transport out of the lake due to phasing. These concepts are supported by the March 2008 particle transport results. Figure 8-13c and 8-14c depict the particle positions for the base and final plan configurations respectively. Many more particles exist in Lake Borgne for the final plan design phase.

DRAFT

a)

b)

c)

Figure 8-11 September, base condition larvae positions after a) 1 day, b) 1 week, c) 4 weeks. Particles anchored based on incoming tide to the east and color coded based on behavior.

a)

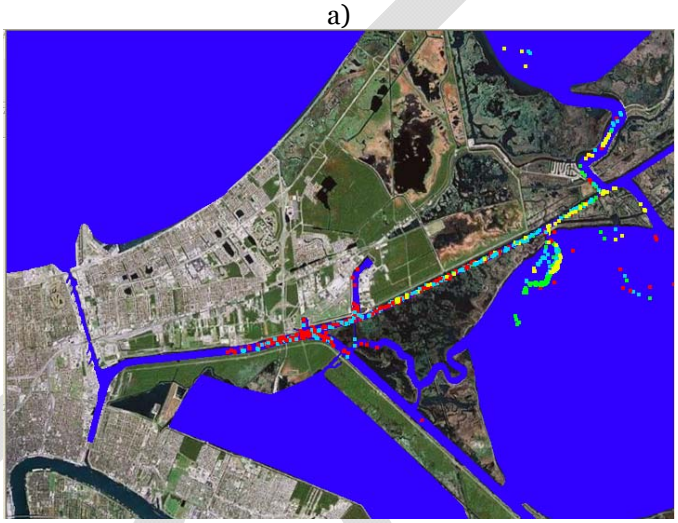

b)

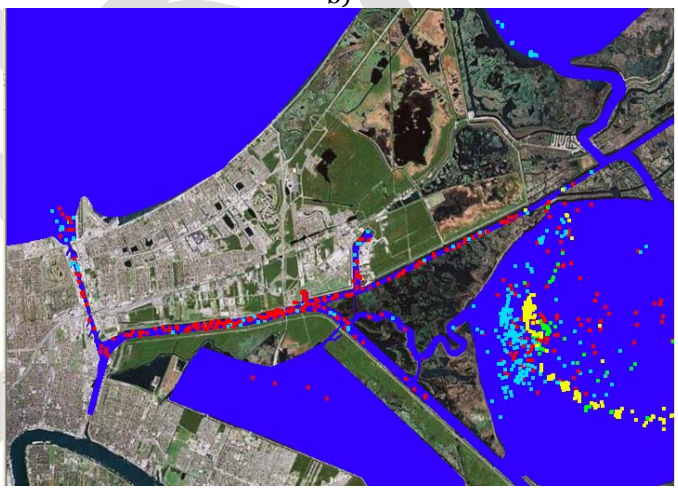

c)

Figure 8-12 September, final plan condition larvae positions after a) 1 day, b) 1 week, c) 4 weeks. Particles anchored based on incoming tide to the east and color coded based on behavior.

DRAFT

a)

b)

c)

Figure 8-13 March, base condition larvae positions after a) 1 day, b) 1 week, c) 4 weeks. Particles anchored based on incoming tide to the east and color coded based on behavior.

a)

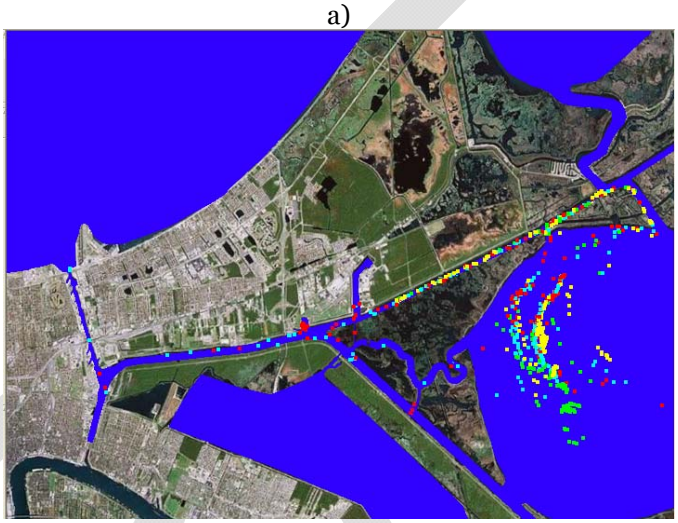

b)

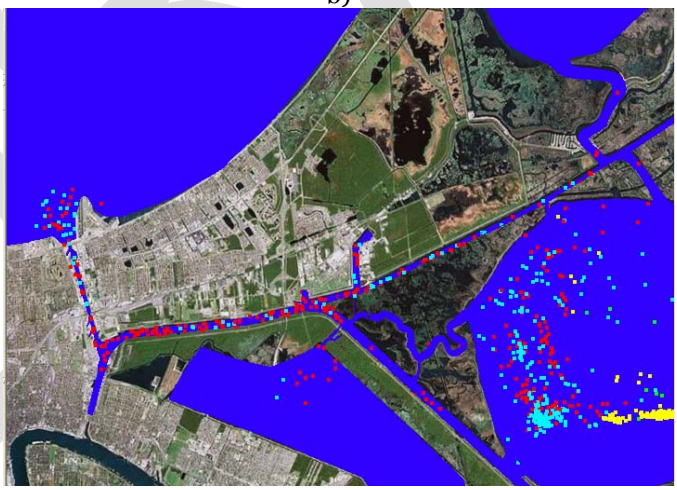

c)

Figure 8-14 March, final plan condition larvae positions after a) 1 day, b) 1 week, c) 4 weeks. Particles anchored based on incoming tide to the east and color coded based on behavior.

Recruitment time series (Figures 8-15 and 8-16) present a similar trend as seen in previous simulations. The base case has the greatest recruitment rates and the plan 3 case has the lowest. The final plan results show increased recruitment in comparison with plan 3. This is as expected due to the changes in the Seabrook design changes. There is a great increase in the overall number of particles recruited within the plan 1-3 design phases in comparison to the unanchored particle cases seen in Chapter 7. An unexpected result is that the plan 1 and plan 2 configurations show almost identical time series. The plan 2 case for the March 2008 hydrodynamics actually has a larger number of particles recruited than the plan 1 case. The March 2008 plan 3 case appears to have a greater reduction of particles in comparison to the base case than the September 2008 conditions. Figure 8-14 shows that a large portion of particles in this case enter Lake Borgne and remain there until the end of the simulation period.

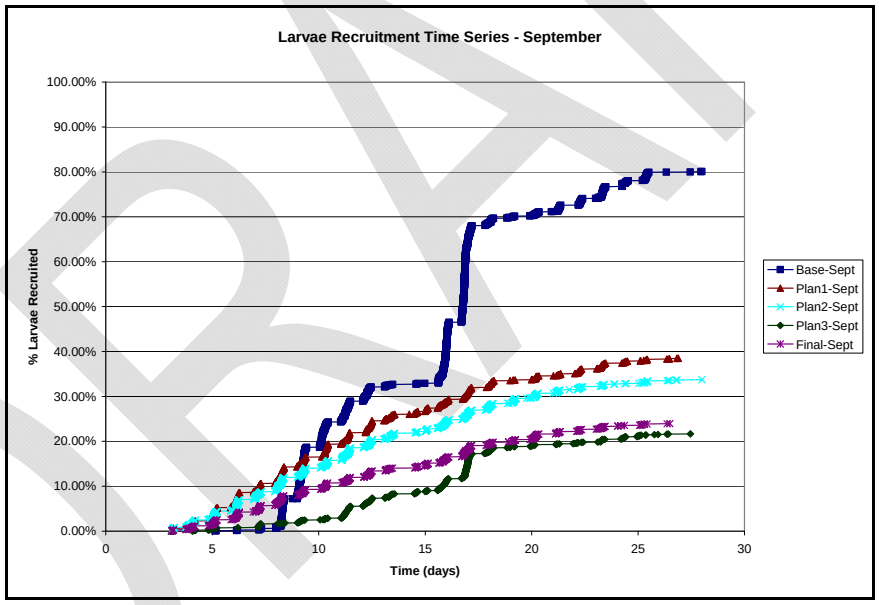

Figure 8-15 Comparison of Larvae Recruitment Time Series for the September 2007 Hydrodynamic, larval fish preferred path to the east. Particles anchored based on incoming tide to the east.

DRAFT

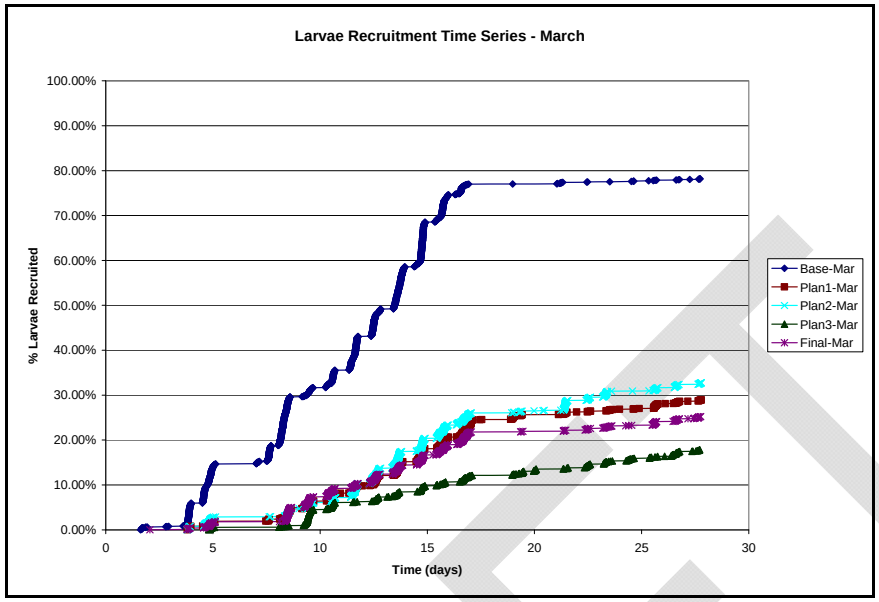

Figure 8-16 Comparison of Larvae Recruitment Time Series for the March 2008 Hydrodynamic, larval fish preferred path to the east. Particles anchored based on incoming tide to the east.

Table 8-4 gives a summary of the total percentage of particles transported to the recruitment areas for both the September 2007 and March 2008 hydrodynamic periods. The values for the plan 1-3 and final plan configures are lower than those seen in Table 8-3 in which the recruitment direction is towards the west.

Table 8-4 Percentage of larvae recruited for each construction phase for simulations in which particles are anchored based on incoming tide to the east (2150 particles released).

Construction Phase	Percent Recruited – September 2007	Percent Recruited – March 2008
Base	80.09	78.19
Plan 1	38.51	28.98
Plan 2	33.72	32.79
Plan 3	21.67	17.86
Final Plan	23.95	25.23

DRAFT

Figures 8-17 and 8-18 give comparisons of the percentages of particles recruited based on behaviors for the September 2007 and March 2008 hydrodynamic conditions. The figures show that most of the particles are recruited at Chef Menteur for these simulations. This is because the preferred pathway in the GIWW is eastwards towards the Chef Menteur recruitment region. The September base case shows high percentages for the tidal lateral, tidal vertical, and bottom movers. Only about half of the passive particles are recruited. Almost all of these values decrease for the plan 1 case. The values generally decrease slightly for plan 2 and then again for plan 3. The final plan values increase, existing somewhere between plans 2 and 3. An interesting effect is that particles which have the tidal lateral characteristic behavior appear to be the least effected by the design phase. This is perhaps because a large portion of particles are transported into Lake Borgne. However due to the lateral movement, these particles may avoid that pathway. The great reduction of particles that are transported within the plan1-3 and final case may also be an indication that the westward direction is the preferred pathway for particles. The previous results for the westward incoming tidal direction show the percentage of recruited particles as greater for the plan cases. The current results for the eastward incoming tidal direction may depict the results of particles working counter to the incoming tidal direction, thereby reducing the number of particles which are recruited. The March 2008 results follow similar trends to those seen in the September 2007 case.

DRAFT

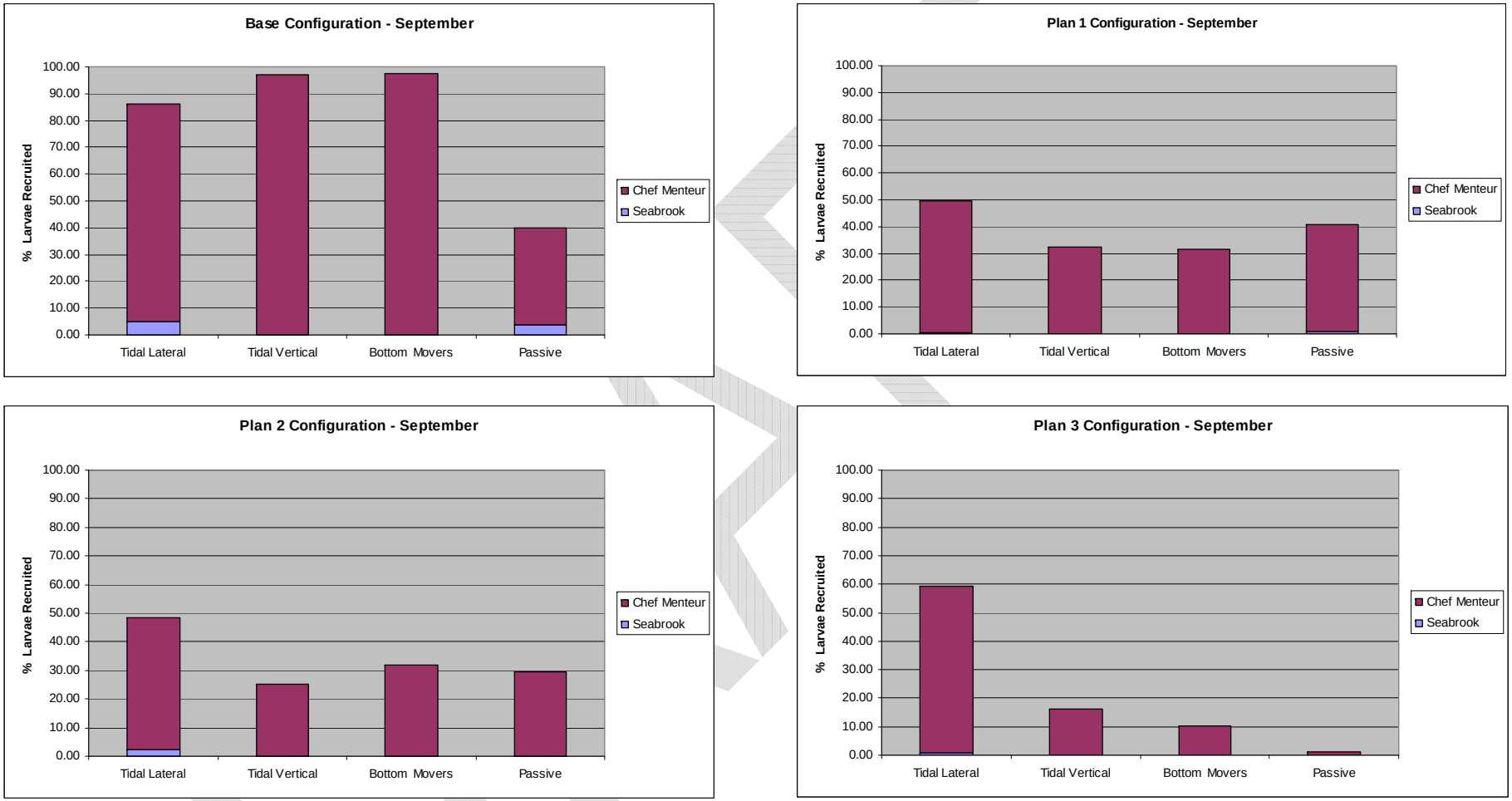

Figure 8-17 Percentage of larvae recruited at Seabrook (blue) and Chef Menteur (red) for base, plan1, plan2, and plan3 configurations using September 2007 hydrodynamics, larval fish preferred path to the east(Maximum value possible 25%) Particles anchored based on incoming tide to the east.

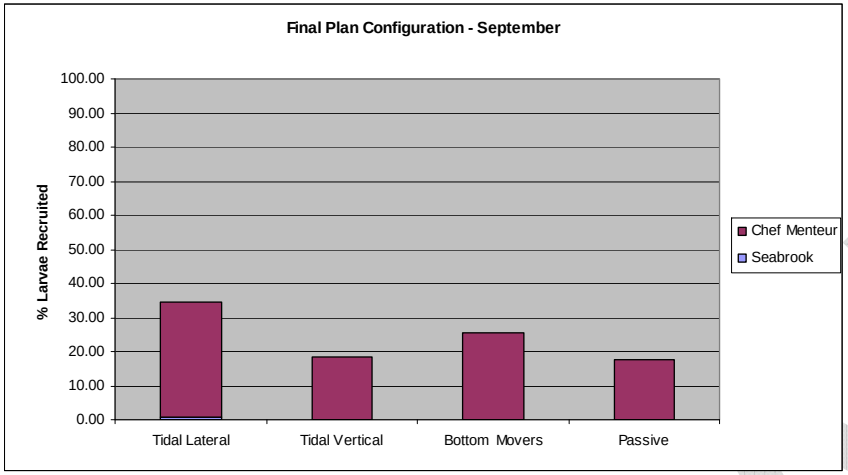

Figure 8-17 continued Percentage of larvae recruited at Seabrook (blue) and Chef Menteur (red) for final plan configuration using September 2007 hydrodynamics, larval fish preferred path to the east(Maximum value possible 25%) Particles anchored based on incoming tide to the east.

DRAFT

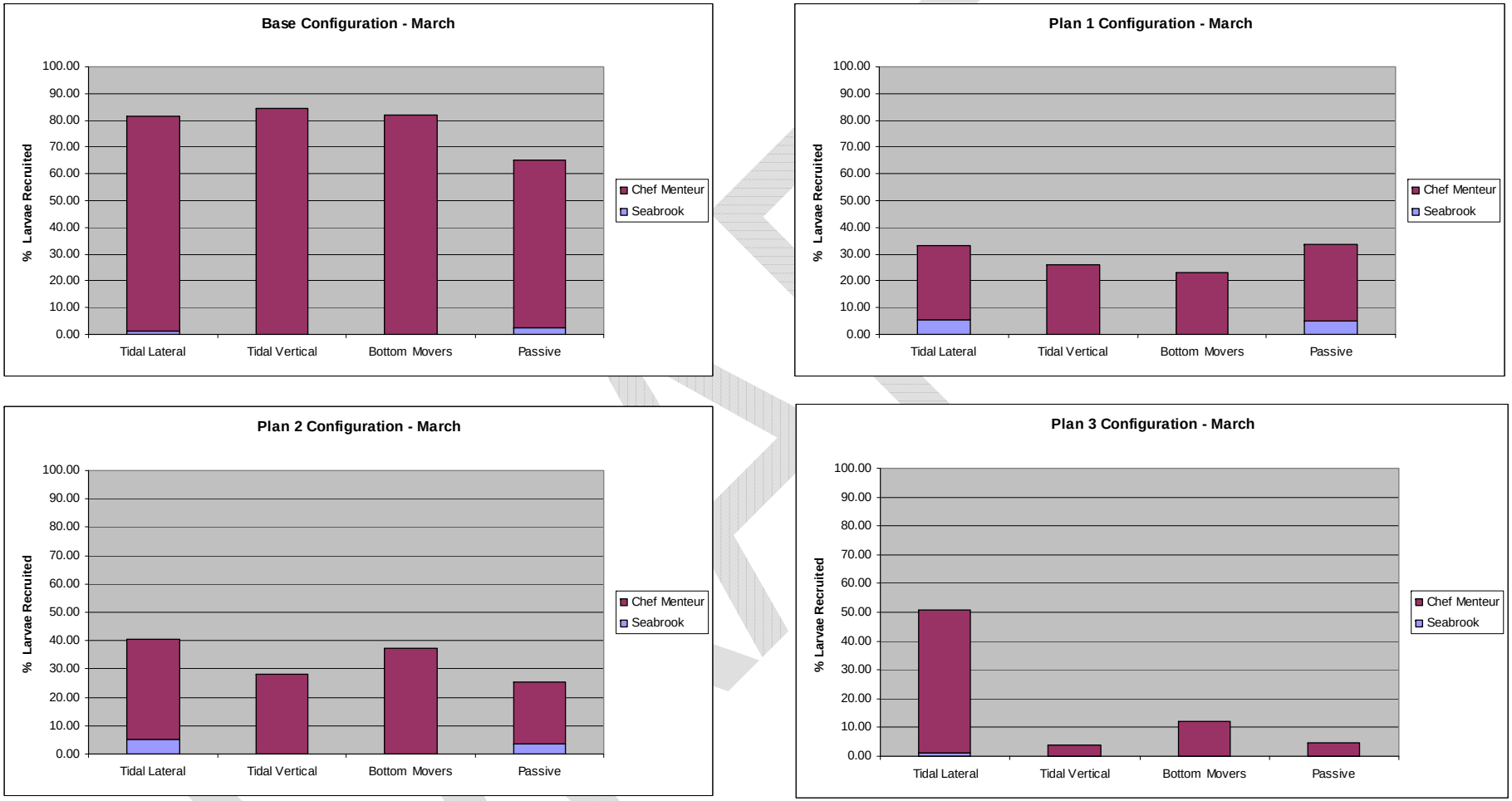

Figure 8-18 Percentage of larvae recruited at Seabrook (blue) and Chef Menteur (red) for base, plan1, plan2, and plan3 configurations using March 2008 hydrodynamics, larval fish preferred path to the east. (Maximum value possible 25%) Particles anchored based on incoming tide to the east.

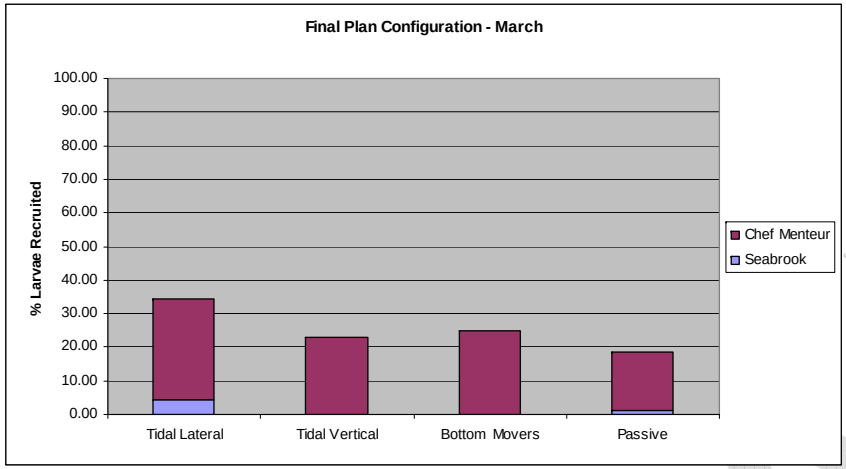

Figure 8-18 continued Percentage of larvae recruited at Seabrook (blue) and Chef Menteur (red) for final plan configuration using March 2008 hydrodynamics, larval fish preferred path to the east. (Maximum value possible 25%) Particles anchored based on incoming tide to the east

DRAFT

9 Conclusions

The modeling efforts discussed in this document were performed for analysis of flow and circulation changes in the IHNC, MRGO, and GIWW areas due to several planned hurricane protection structures. The hydrodynamic model was verified to current 2008 conditions and these results are provided. Two analysis periods were then simulated to determine how the flow patterns and velocity magnitudes change within the system due to these structures. The hydrodynamic solutions were then provided to drive the larval fish transport simulations. All of this information can together give insight into how the system changes as well as how certain species will be affected by these changes.

The results of the hydrodynamic simulations show that by cutting off the MRGO, as in Plan 1, the entire circulation pattern within the GIWW/MRGO system changes. The velocities in the GIWW and Bayou Bienvenue increase, but the velocity at Seabrook decreases due to the reduction of flow volume since the MRGO is cut off from the Gulf of Mexico. With Plan 2, the MRGO is blocked further north and structures are placed on Bayou Bienvenue and the GIWW. The flow at these structures increases, but again the flows at Seabrook are reduced due to restricted flow into the system. Plan 3 includes a structure at Seabrook. With this structure in place, the velocities at the GIWW and Bayou Bienvenue structures reduce, although the velocity at the Seabrook structure is increased. The increase when the structures are introduced is likely due to the reduced cross-sectional area. In the western section of the GIWW, the reduction of flow into this area is visible due to reduced velocity magnitudes with each plan configuration. As the GIWW/IHNC area becomes more constricted with structures at each end, the flow through this area is also reduced.

It is a concern of the navigation industry that velocity magnitudes not increase beyond the limit for safe navigation. A percent exceedence analysis was performed at several locations within the model domain to show how often the velocities reach certain values. Although there are some extreme velocity magnitudes in the structures, these values are not typical and only occur for a small fraction of the time, typically under storm circumstances when flows and winds are well above average.

DRAFT

Larval fish transport modeling within the IHNC, MRGO, and GIWW regions are shown for four cases which are differentiated by initial particle positions. In addition to source changes, the hydrodynamic period and plan configurations are also varied. Particles initiated in the MRGO at Loutre currently take 1.5 to 2 weeks to reach the Bayou Bienvenue closure area for the base case. This pathway is not available for plans 1-3 due to the closure of the MRGO at La Loutre.

Transport of particles within the system is dominated by the hydrodynamics of the system. The tidal intensity and regularity of the tidal signal are a major factor of transport. Particles released during stronger events, such as those seen in the March 2008 hydrodynamic period, may be recruited at a greater rate than a less intense flow condition such as the September 2007 hydrodynamic period. However recruitment rate is additionally affected by the larval fish characteristic transport behaviors.

Analysis of simulation results signify that the rate of particle recruitment is affected by the plan configuration for cases 2-4. The base configuration shows the highest recruitment values and plan 3 configuration shows the lowest recruitment values. The final plan configuration shows a decrease of particles reaching recruitment areas in comparison to the base design, plan 1, and plan 2. However recruitment values for the simulations using the final plan geometry increase with respect to plan 3. This is most likely due to the increase of cross sectional area shown in the final plan. Results indicate an approximate 10-15 percent recruitment decrease between plans 1 and the final plan. Case 3 results show that there is no real difference between the transport pathways from Lake Borgne to Chef Menteur with respect to the plans. The base case generally has a slightly higher value of recruited particles; however plans1-3 and the final plan differ within 5 percent.

Characteristic fish behavior affects the recruitment rate of particles. When the transport mechanism of anchoring is added to particle transport behavior, recruitment occurs at a much faster rate than without the mechanism. Generally passive particles have the lowest recruitment values, followed by tidal lateral behavior, bottom movers, and finally tidal vertical movers.

DRAFT

References

Lackey, T.C. and Smith, S. J (2008) "Application of the Particle Tracking Model To Predict the fate of Dredged Suspended Sediment at the Willamette River" *Proceedings Western Dredging Association Twenty-Eighth Annual Technical Conference,* St. Louis, MO.,USA.

Lackey, T.C. and MacDonald, N.J. (2007). "The Particle Tracking Model Description and Processes" Proceedings XVIII World Dredging Congress 2007, WEDA, Lake Buena Vista, Florida, USA.

McAnally, W.H., and Berger, R.C. (1997). "Salinity Changes in Pontchartrain Basin Estuary Resulting from Bonnet Carre` Freshwater Diversion," Technical Report CHL-97-2, U.S. Army Waterways Experiment Station, Vicksburg, MS.

MacDonald, N.J., Davies, M.H., Zundel, A.K., Howlett, J.D., Demirbilek, Z., Gailani, J.Z., Lackey, T.C., and Smith, S.J. (2006) "PTM: Particle Tracking Model; Report 1: Model Theory, Implementation, and Example Applications" Technical Report ERDC/CHL TR-06-02, U.S. Army Waterways Experiment Station, Vicksburg, MS.

Martin, Keith, Dennis Webb, Gaurav Savant, and Gary Lynch. (In review). "Lake Borgne Surge Barrier Navigation Study," Technical Report in review, U.S. Army Engineer Research and Development Center, Vicksburg, MS.

Tate, J.N., Carrillo, A.R., Berger, R.C., and Thibodeaux, B.J. (2002). "Salinity Changes in Pontchartrain Basin Estuary, Louisiana, Resulting from Mississippi River-Gulf Outlet Partial Closure Plans with Width Reduction," Technical Report CHL-TR-02-12, U.S. Army Engineer Research and Development Center, Vicksburg, MS.

"SMS version 8.0 Reference Manual for the Surface Water Modeling System," 2002, Brigham Young University, 1997, Engineering Graphics Laboratory, Provo, Utah [http://chl.wes.army.mil/software/tabs/docs.htp].

DRAFT

Wu, Jin. (1969). "Wind Stress and Surface Roughness at Air-Sea Interface," *Journal of Geophysical Research,* Vol. 74, No. 2, 444-455.

DRAFT

Acknowledgements

We would like to acknowledge the contributions of the interagency team for the Keith Lake Fish Passage study for providing the general description of larval fish transport characteristics. We would also like to acknowledge the Seabrook interagency team for the additional larval fish transport mechanism information concerning anchoring and their discussion of larval fish behavior. We thank Ionnis Y. Georgiou for his assistance with regard to conceptualizing modifications to tidal flag definitions within PTM and his additional discussion of hydrodynamic transport mechanisms. We appreciate the assistance of Gary Brown, Joseph Gailani, and Jarrell Smith with regard to conceptualizing modifications to larval fish transport including tidal flag definitions and decay algorithms. We thank Cassandra Ross and Francisco Velez for their general assistance with this work. We acknowledge the contributions of Keith Martin and Gaurav Savant on the Lake Borgne surge barrier work which preceded this study.

Research funding for the Particle Tracking Model comes from the Dredging Operations and Environmental Research program (DOER) as well as the Coastal Inlets Research Program (CIRP). Adaptive Hydraulics (ADH) research funding is providing under the System-Wide Water Resources Program (SWWRP).

DRAFT

Appendix A : Hydrodynamic Sensitivity Simulations

Plan 3 wide

Velocity Magnitudes

The three initial design alternatives as documented in the previous sections are given below. After the initial results were reviewed by HPO, an additional alternative was modeled for hydrodynamics. This alternative is similar to Plan 3 except the dimensions of the Seabrook structure are increased. These analyses were performed prior to the determination of Plan 3 Final, which is not included in the results provided in this appendix.

- Base - condition includes the fully open MRGO, GIWW, and IHNC
- Plan 1 – close the MRGO at La Loutre
- Plan 2 – close the MRGO at La Loutre, include the Borgne alignment (56 ft X 8 ft gate on Bayou Bienvenue, and two 150 ft X 16 ft gates on GIWW)
- Plan 3 – close the MRGO at La Loutre, include the Borgne alignment, include the 95 ft X 16 ft gate at Seabrook structure with southern scour hole filled
- Plan 3-wide – close the MRGO at La Loutre, include the Borgne alignment, include the 115 ft X 30 ft gate at Seabrook structure with southern scour hole filled

Velocity data were taken in the location of the structures for the Bayou Bienvenue structure, the GIWW sector gate, the GIWW barge gate, and the Seabrook structure. Figures A-1 and A-2 show these locations. For the base condition and plans 1 and 2, data are analyzed at a location north of the Seabrook structure location where the velocities are highest. The analysis for plan 3 (original and widened) is at the location in the Seabrook structure where the velocity magnitudes are the greatest. It is important to keep in mind that velocities will increase for a given flux when the cross-sectional area is reduced simply due to continuity. Therefore, once a

DRAFT

structure is in place at these locations, it is not unlikely that the velocity magnitudes will rise.

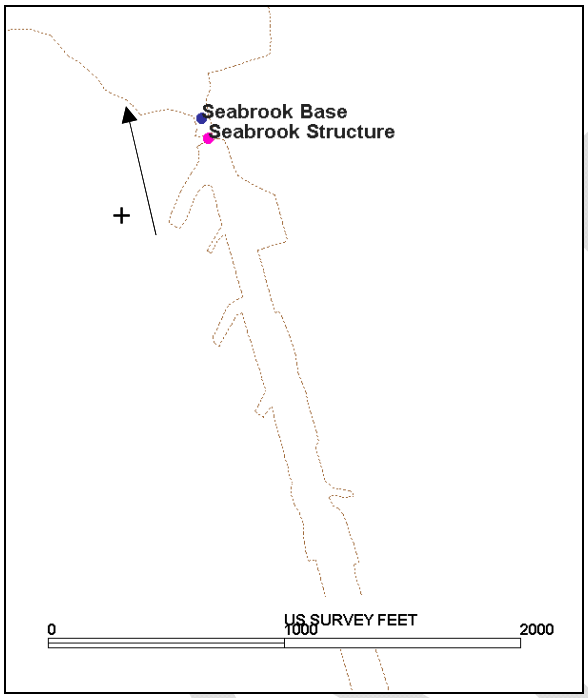

Figure A-1. Hydrodynamic analysis locations – Seabrook

DRAFT

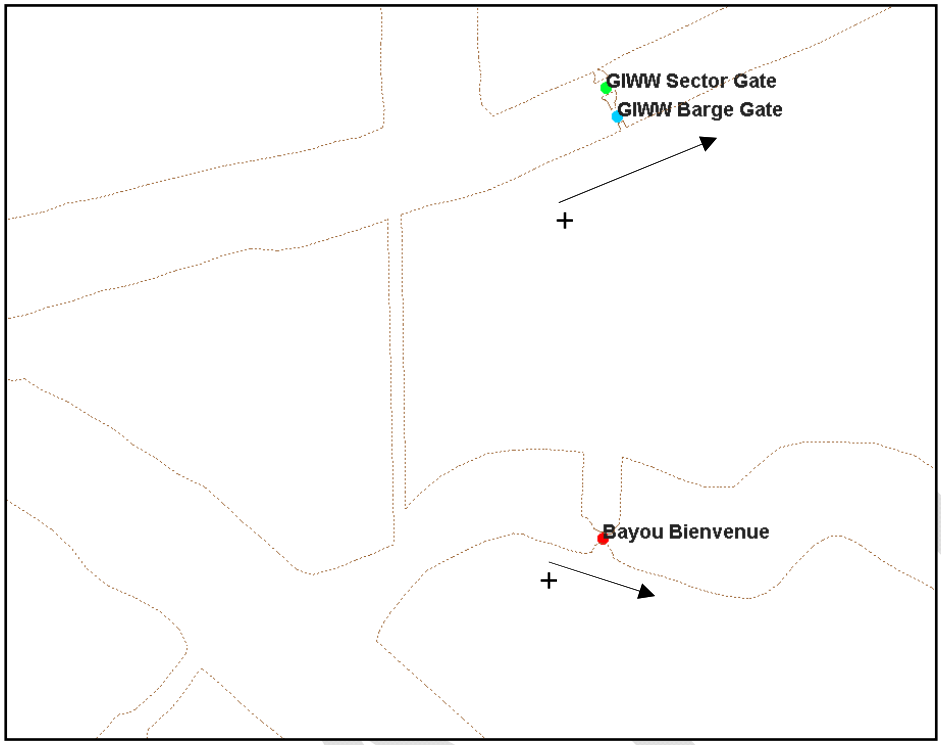

Figure A–2. Hydrodynamic analysis locations – Bayou Bienvenue Structure, GIWW Sector Gate, and GIWW Barge Gate

The average velocity for flood and ebb are determined at each location and time period for the base and three plans as are the maximum velocities for all conditions. Since there is a circulation within this system through the GIWW, the definition of flood and ebb can be misleading. For this reason a definition of positive and negative or flood and ebb is necessary. Positive values are defined as those directed predominantly toward the north or east and negative values are defined as those directed predominantly toward the south or west. The arrows in Figures A-1 and A-2 show the positive direction for each location. The results of this analysis are given in Figures A-3 through A-10. A direction arrow is included for each location to help define the flow direction.

It is easily seen that the increase in the opening at Seabrook creates a reduction of the velocity magnitudes at this location. This pattern is produced for both the average and extreme values for both September and March. The velocity magnitudes at this location are actually lower than the values for the Base condition for most times. However, the effect of increasing the size of this opening is propagated throughout the system and changes are visible at the GIWW structures and the Bayou Bienvenue

structure. The increased size of the Seabrook opening increases the velocity magnitudes at each of these locations as compared to the original, smaller structure opening. The velocities increase to just under the magnitudes generated with the Plan 2 implementation, which includes no changes to the Seabrook area.

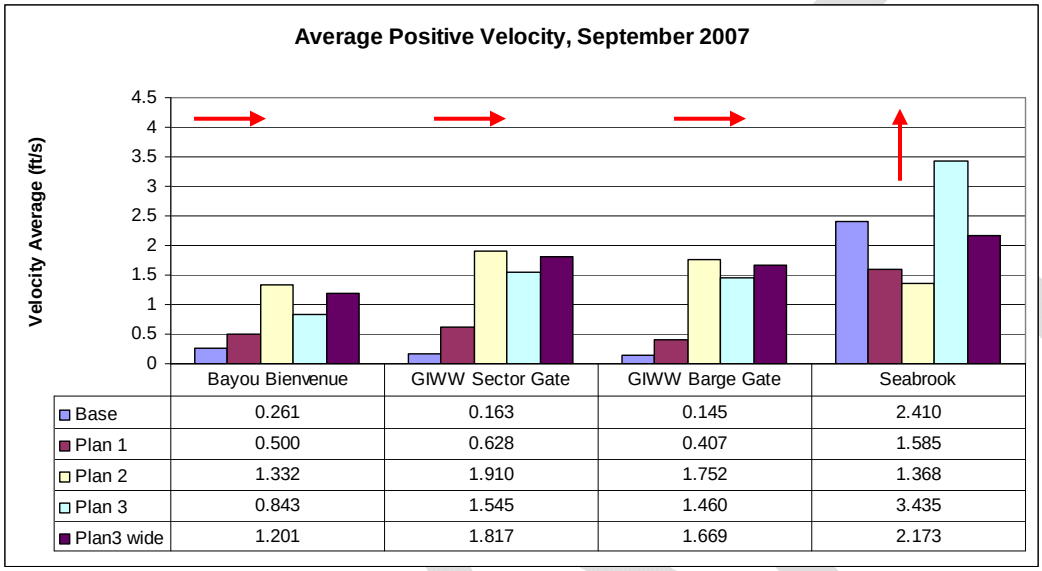

	Bayou Bienvenue	GIWW Sector Gate	GIWW Barge Gate	Seabrook
Base	0.261	0.163	0.145	2.410
Plan 1	0.500	0.628	0.407	1.585
Plan 2	1.332	1.910	1.752	1.368
Plan 3	0.843	1.545	1.460	3.435
Plan3 wide	1.201	1.817	1.669	2.173

Figure A-3. Velocity average for September (positive)

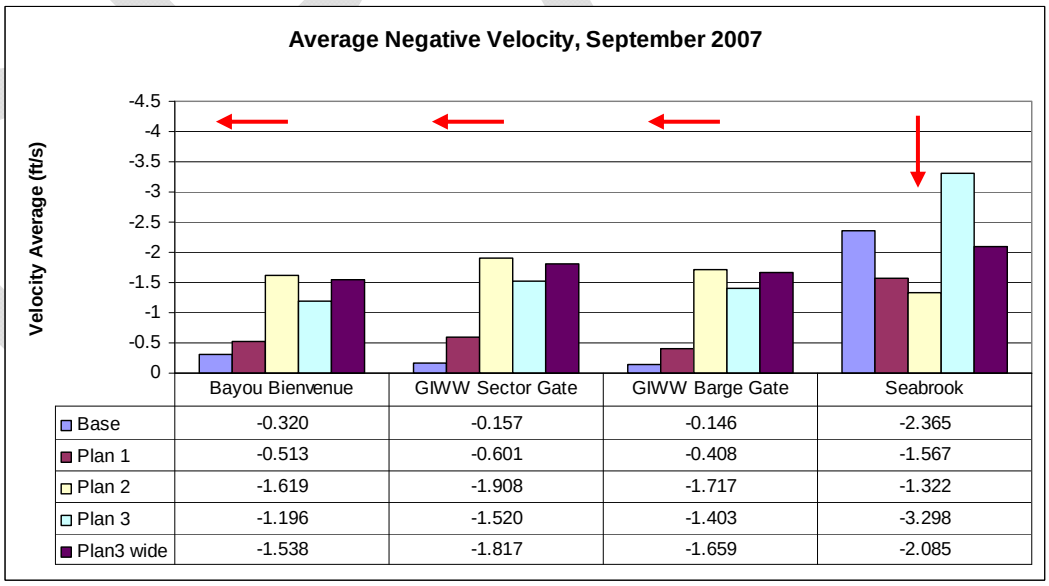

	Bayou Bienvenue	GIWW Sector Gate	GIWW Barge Gate	Seabrook
Base	-0.320	-0.157	-0.146	-2.365
Plan 1	-0.513	-0.601	-0.408	-1.567
Plan 2	-1.619	-1.908	-1.717	-1.322
Plan 3	-1.196	-1.520	-1.403	-3.298
Plan3 wide	-1.538	-1.817	-1.659	-2.085

Figure A-4. Velocity average for September (negative)

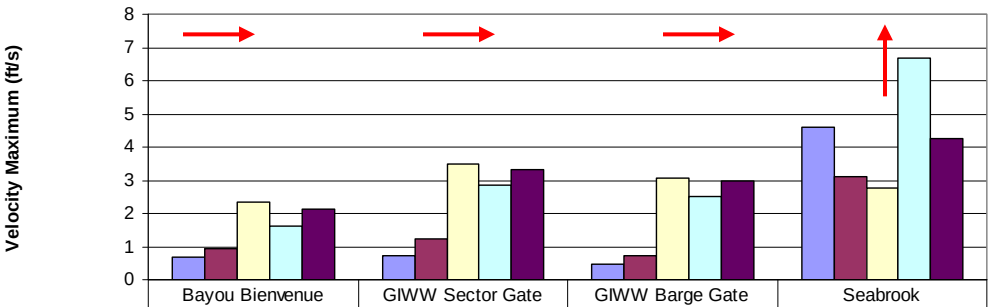

	Bayou Bienvenue	GIWW Sector Gate	GIWW Barge Gate	Seabrook
Base	0.679	0.714	0.473	4.580
Plan 1	0.954	1.215	0.729	3.122
Plan 2	2.327	3.503	3.083	2.765
Plan 3	1.601	2.836	2.524	6.663
Plan3 wide	2.125	3.313	2.969	4.261

Figure A-5. Velocity maximum for September (positive)

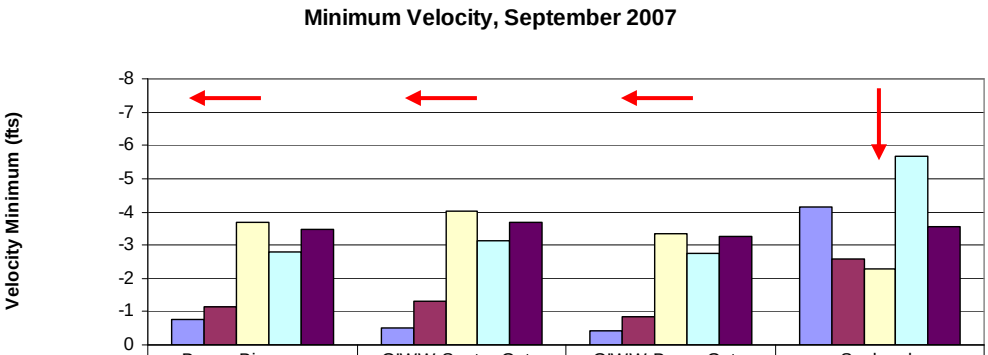

	Bayou Bienvenue	GIWW Sector Gate	GIWW Barge Gate	Seabrook
Base	-0.756	-0.491	-0.409	-4.134
Plan 1	-1.129	-1.311	-0.835	-2.583
Plan 2	-3.685	-4.001	-3.344	-2.279
Plan 3	-2.793	-3.140	-2.761	-5.652
Plan3 wide	-3.457	-3.694	-3.247	-3.560

Figure A-6. Velocity minimum for September (negative)

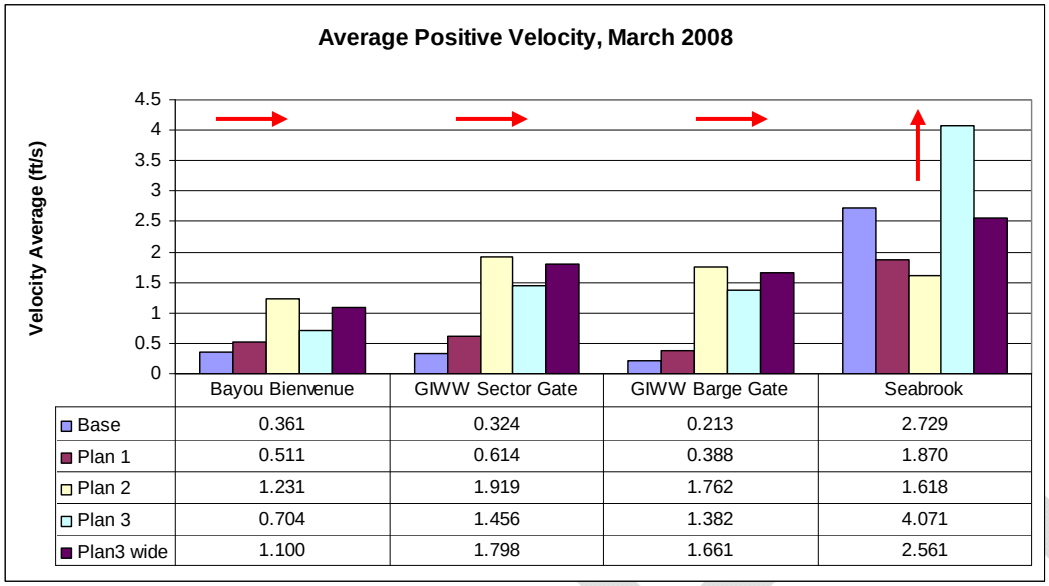

	Bayou Bienvenue	GIWW Sector Gate	GIWW Barge Gate	Seabrook
Base	0.361	0.324	0.213	2.729
Plan 1	0.511	0.614	0.388	1.870
Plan 2	1.231	1.919	1.762	1.618
Plan 3	0.704	1.456	1.382	4.071
Plan3 wide	1.100	1.798	1.661	2.561

Figure A-7. Velocity average for March (positive)

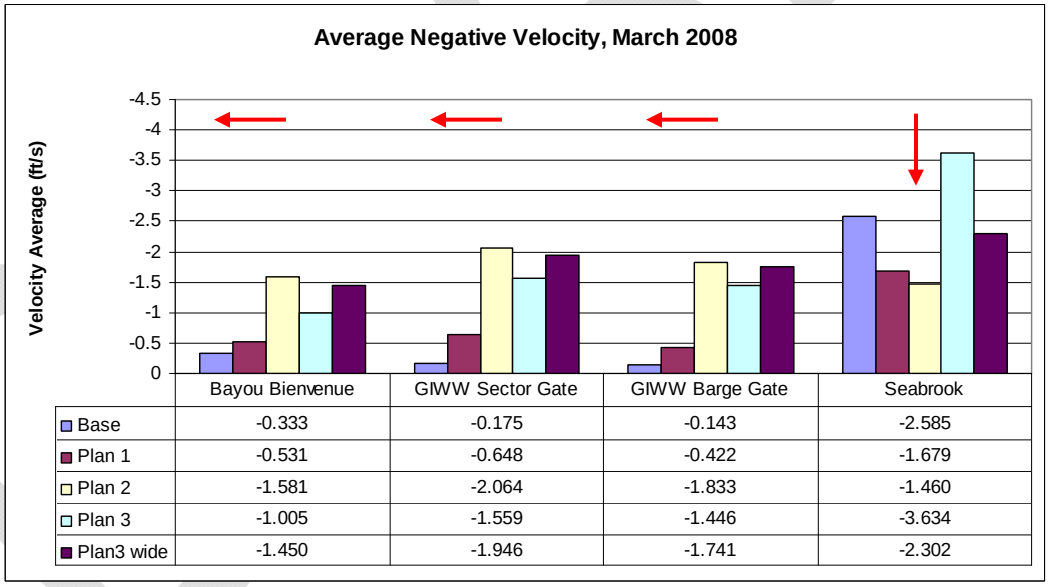

	Bayou Bienvenue	GIWW Sector Gate	GIWW Barge Gate	Seabrook
Base	-0.333	-0.175	-0.143	-2.585
Plan 1	-0.531	-0.648	-0.422	-1.679
Plan 2	-1.581	-2.064	-1.833	-1.460
Plan 3	-1.005	-1.559	-1.446	-3.634
Plan3 wide	-1.450	-1.946	-1.741	-2.302

Figure A-8. Velocity average for March (negative)

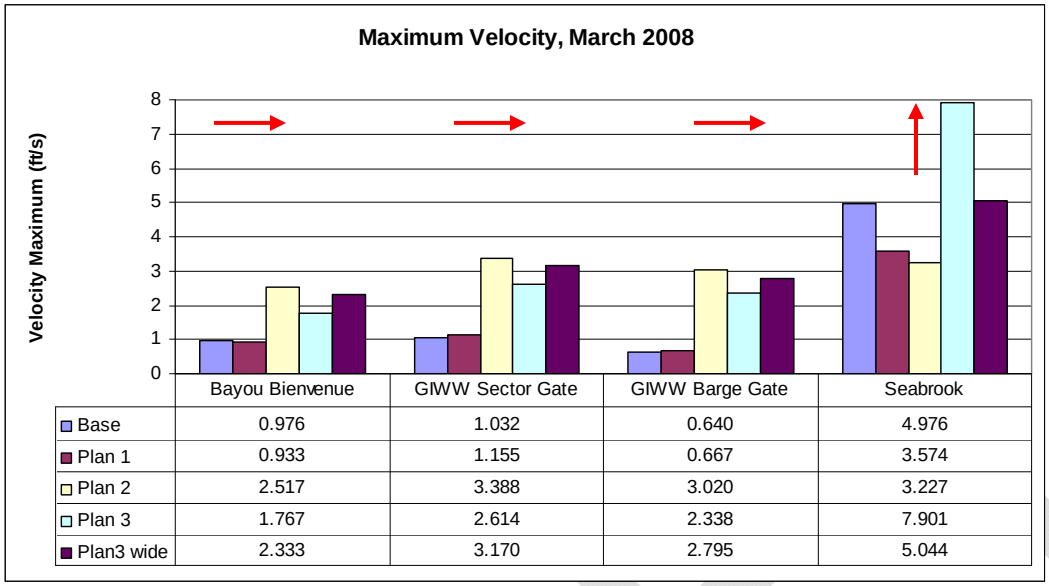

	Bayou Bienvenue	GIWW Sector Gate	GIWW Barge Gate	Seabrook
Base	0.976	1.032	0.640	4.976
Plan 1	0.933	1.155	0.667	3.574
Plan 2	2.517	3.388	3.020	3.227
Plan 3	1.767	2.614	2.338	7.901
Plan3 wide	2.333	3.170	2.795	5.044

Figure A-9. Velocity maximum for March (positive)

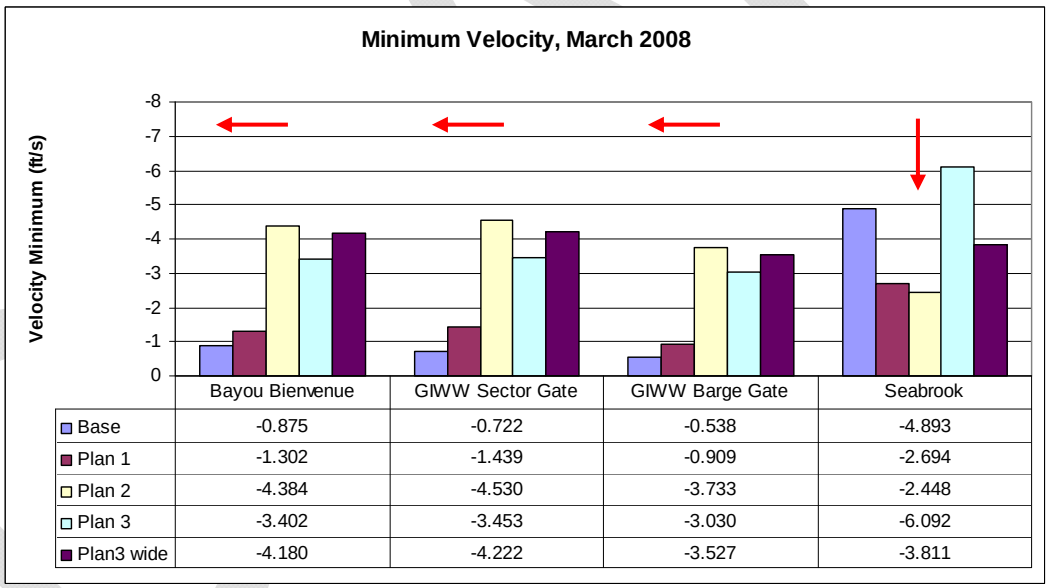

	Bayou Bienvenue	GIWW Sector Gate	GIWW Barge Gate	Seabrook
Base	-0.875	-0.722	-0.538	-4.893
Plan 1	-1.302	-1.439	-0.909	-2.694
Plan 2	-4.384	-4.530	-3.733	-2.448
Plan 3	-3.402	-3.453	-3.030	-6.092
Plan3 wide	-4.180	-4.222	-3.527	-3.811

Figure A-10. Velocity minimum for March (negative)

Velocity exceedance plots are provided for the locations at the GIWW sector gate and the Seabrook structure in Figures A-11 through A-16. These locations experience the largest velocities when the structures are in place.

These figures support the results that by increasing the opening at Seabrook, the velocities are reduced.

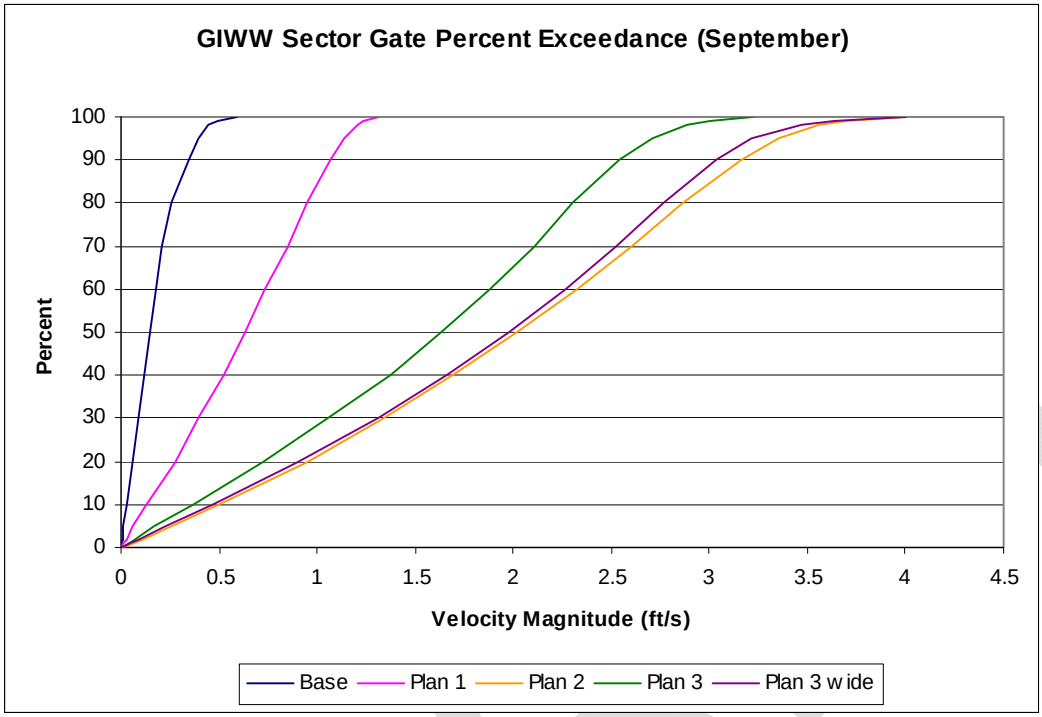

Figure A-11. Velocity exceedance at the GIWW sector gate for September

DRAFT

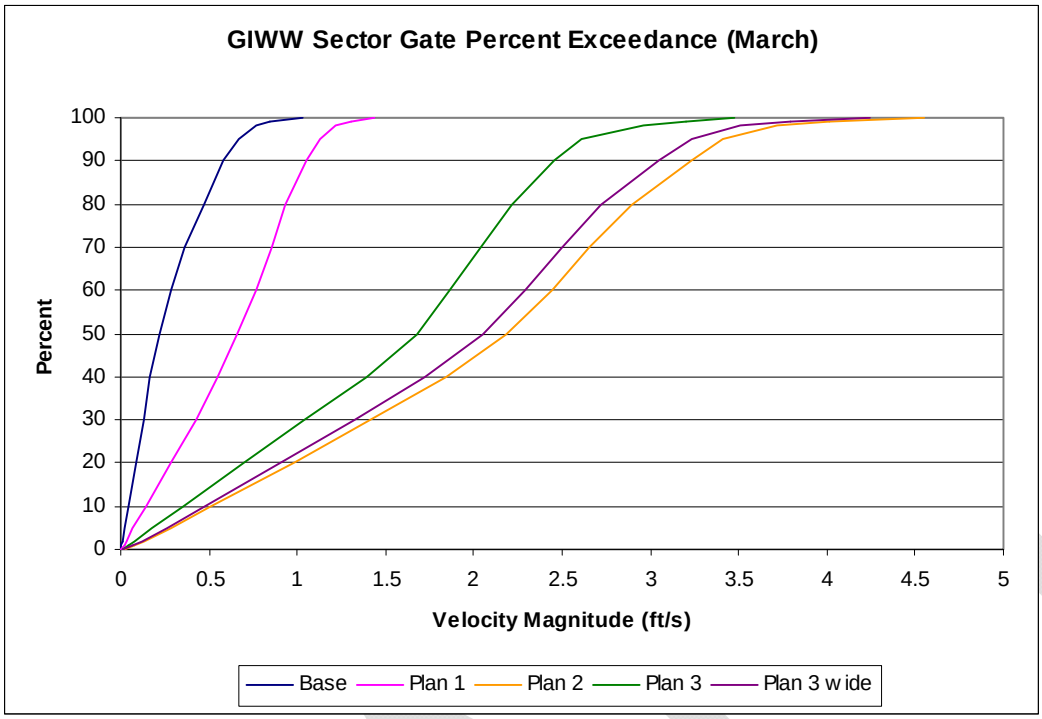

Figure A-12. Velocity exceedance at the GIWW sector gate for March

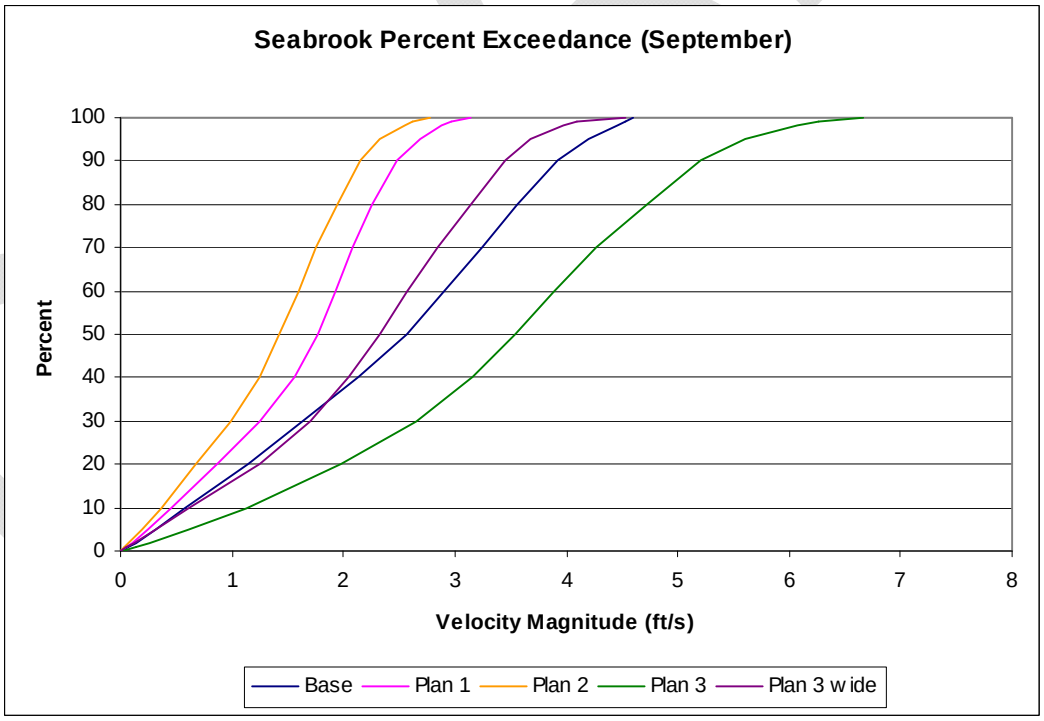

Figure A-13. Velocity exceedance at the Seabrook structure for September

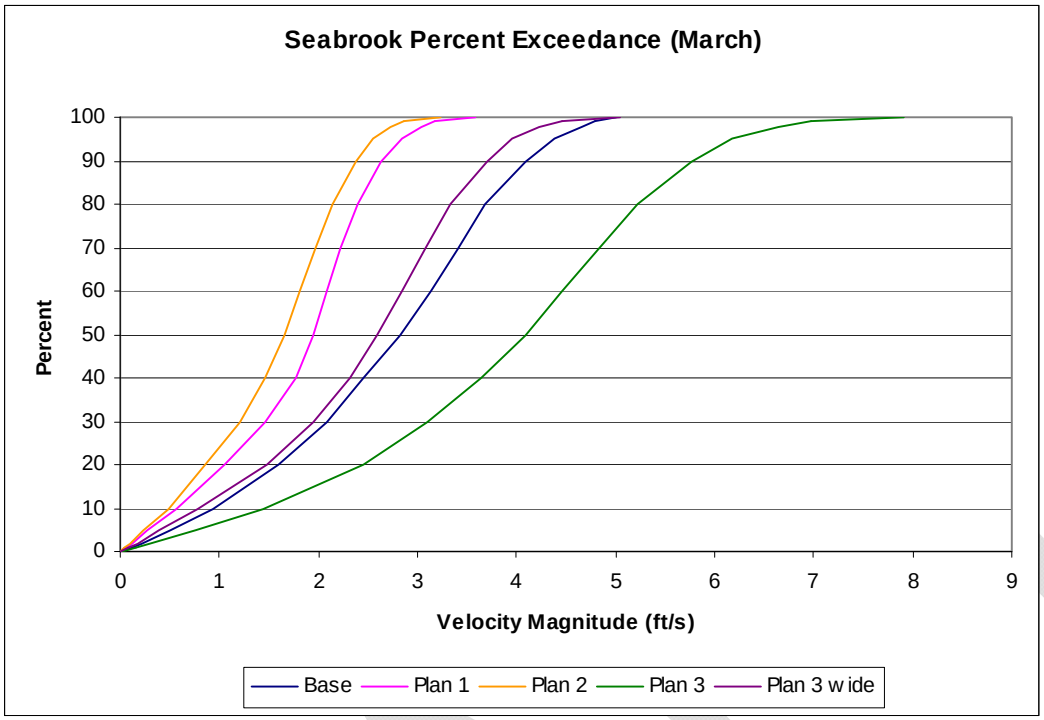

Figure A-14. Velocity exceedance at the Seabrook structure for March

Water Surface Analysis

An analysis of the water surface elevation as it reacts to the plan conditions is shown in the following figures. An arc was drawn from the east side of the GIWW sector gate, through this structure, along the GIWW, up the IHNC, through the Seabrook structure, and ending in southern Lake Pontchartrain. Figure A-15 shows this arc. The arc is divided into 1000 ft increments for reference such that the GIWW structures are at 1800 ft, the IHNC joins the GIWW at 40,000 ft, and the Seabrook structure is at 56,000 ft. Figures A-16 and A-17 show the water surface elevation along this arc for midnight August 27, 2007 and March 3, 2008. These times were chosen to show a high ebb event from August and a high flood event from March for the Seabrook region such that the water level differences between Lake Borgne and Lake Pontchartrain are large. Figures A-18 and A-19 focus on the GIWW sector gate and Figures A-20 and A-21 focus on the IHNC and Seabrook structure.

These figures show that there is a change in the water surface elevation as the flow passes through these structures. This concept of elevation changes or head differences on each side of a constriction is supported by basic hydraulic theory due to constriction of flow volume and high veloci-

ties through the narrow structure. Since water flows from high to low elevation, the flow will be directed from the higher toward the lower water surface elevation and will move fastest when this difference is greatest.

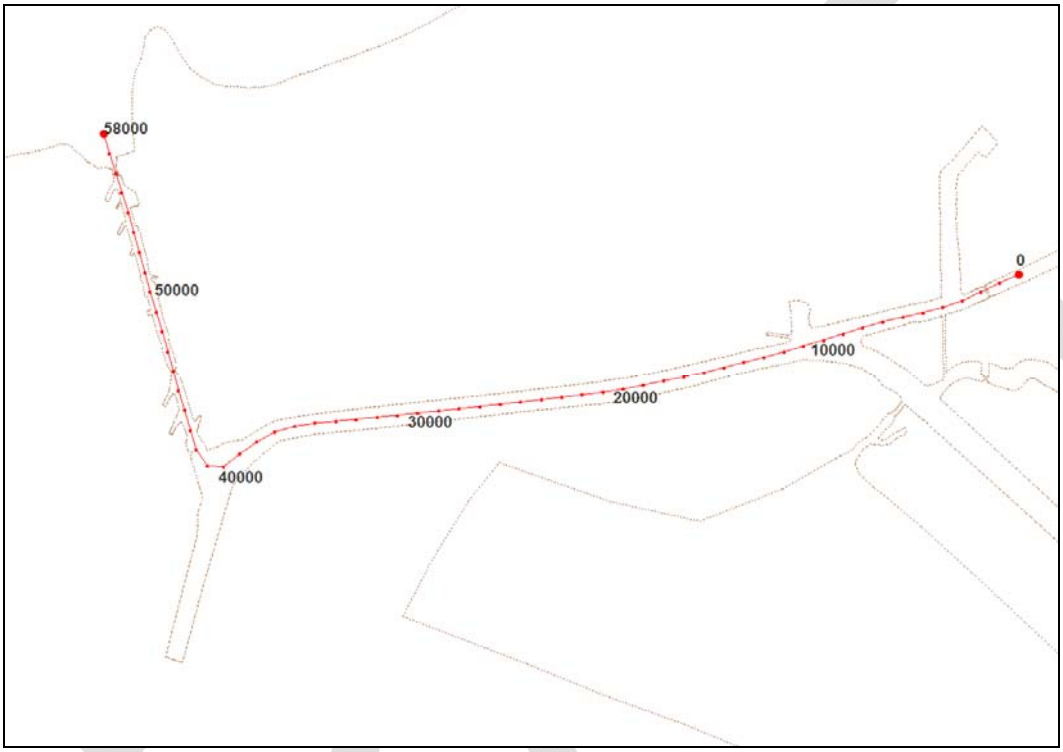

Figure A-15. Water surface analysis arc and location reference in 1000 ft increments

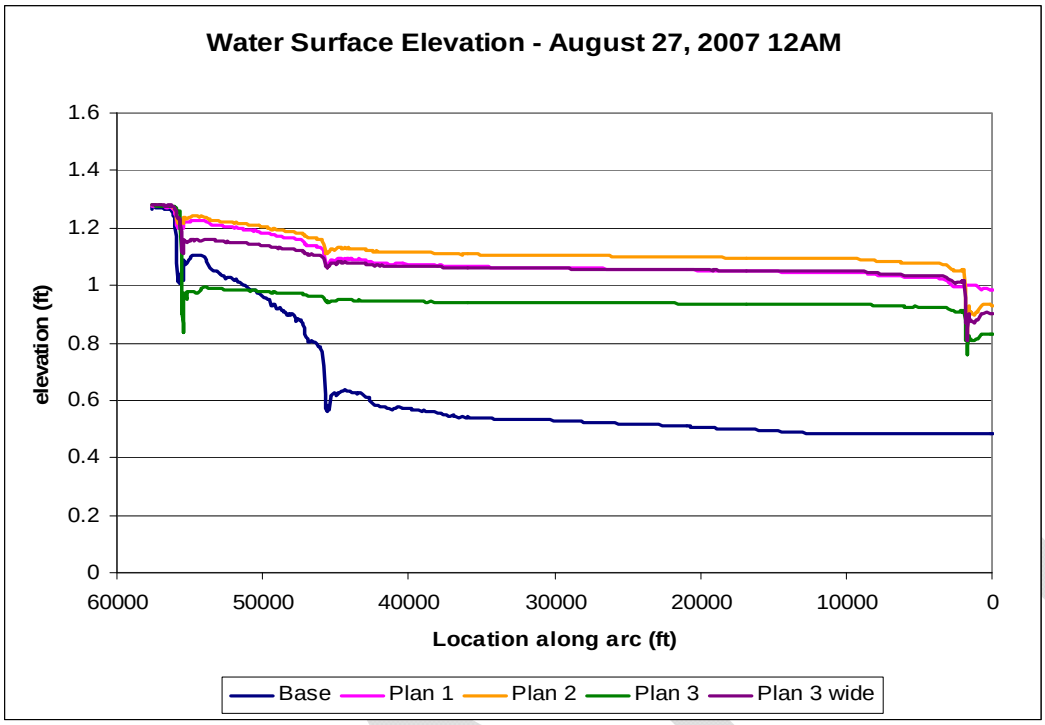

Figure A-16. Water surface elevation along arc for Base and all plans for August 27, 2007

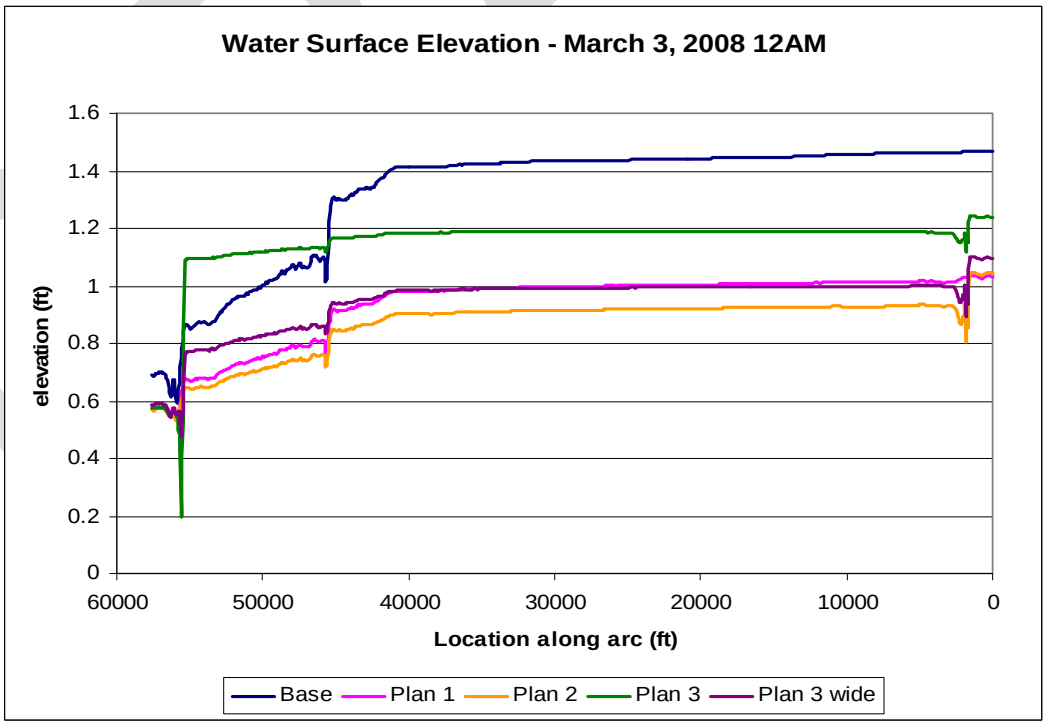

Figure A-17. Water surface elevation along arc for Base and all plans for March 3, 2008

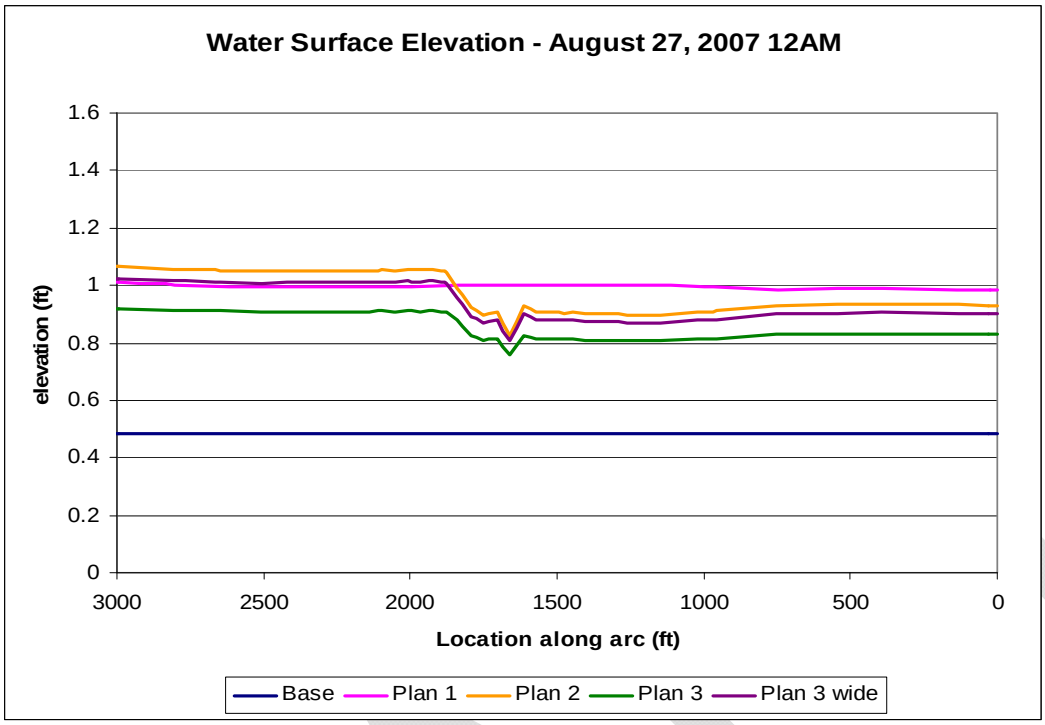

Figure A-18. Water surface elevation through GIWW sector gate (August)

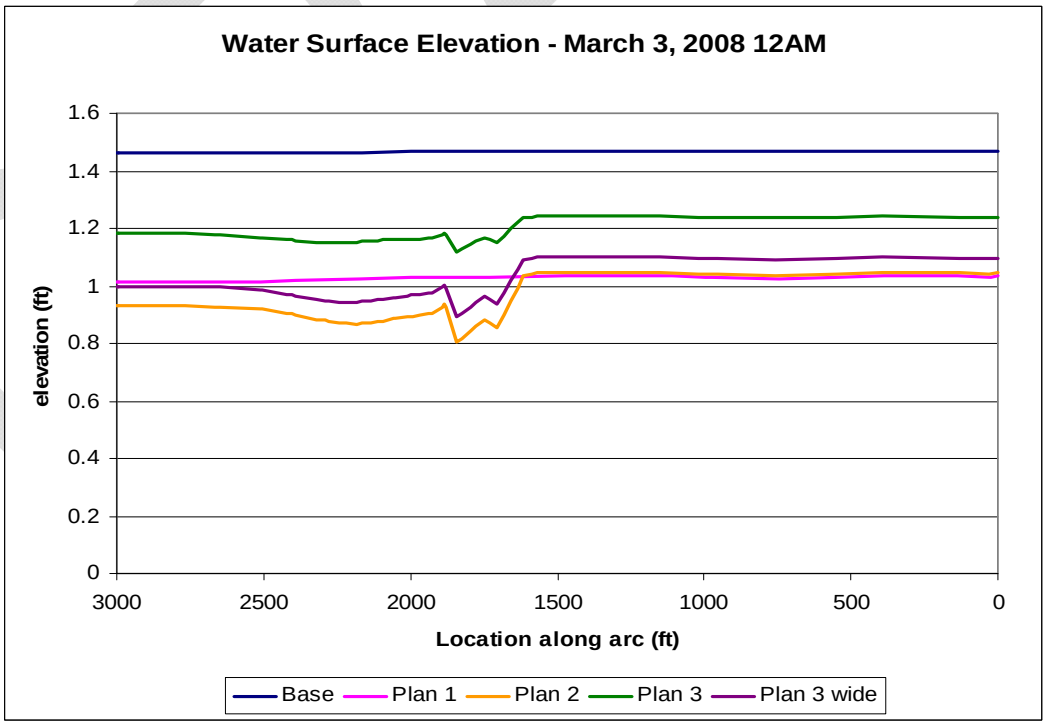

Figure A-19. Water surface elevation through GIWW sector gate (March)

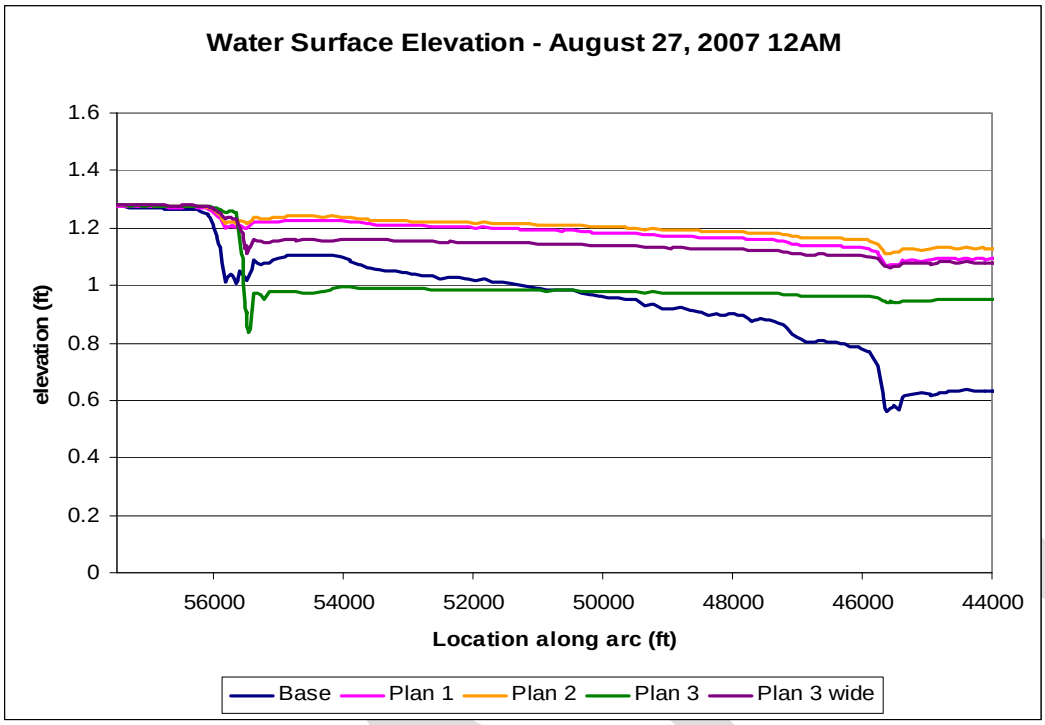

Figure A-20. Water surface elevation through IHNC and Seabrook structure (August)

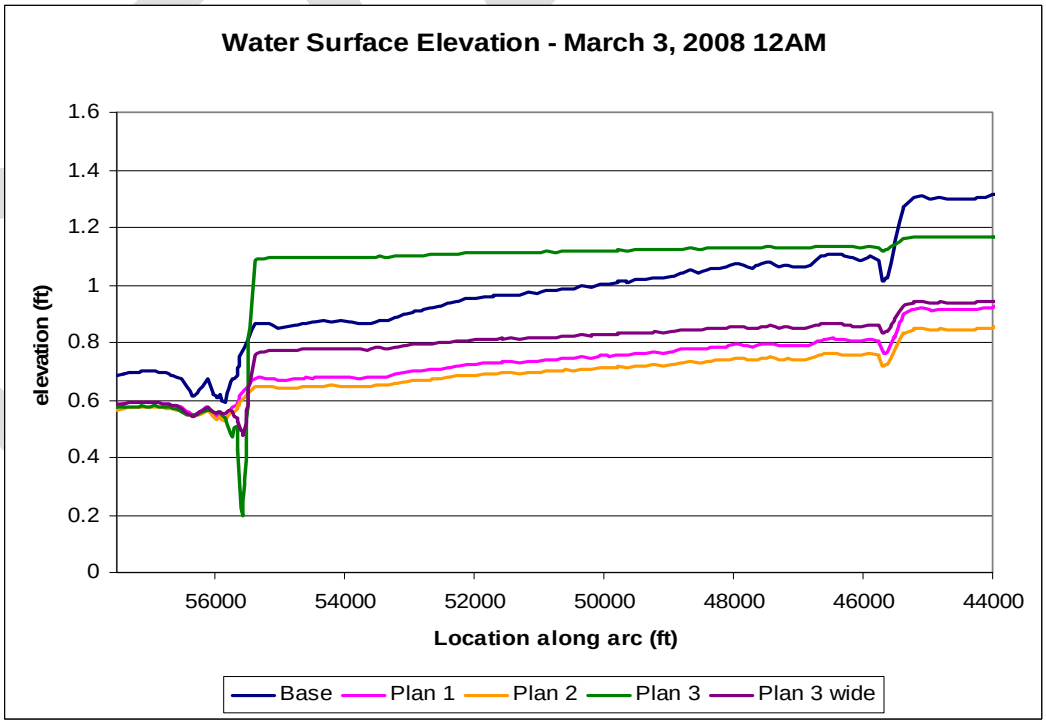

Figure A-21. Water surface elevation through IHNC and Seabrook structure (March)

Cofferdam Simulations

During the construction of the Seabrook gate, a cofferdam may be placed in the IHNC as a construction method option. However, flow around this cofferdam may be too large to accommodate any through traffic and possibly generate erosion problems. The following figures show the analysis effect of the 246 X 100 ft cofferdam, which can accommodate a 96 ft wide structure, at several locations within the system – at the Bayou Bienvenue structure, the GIWW barge gate, the GIWW sector gate, and at three locations at Seabrook (north of the structure, at the northwest corner, and at the northeast corner). These simulations include all additions through Plan 2 and the fill of the southern scour hole at Seabrook. Figure A-22 shows these additional Seabrook locations. Figures A-23 and A-30 show the average and maximum velocity magnitudes at these locations for both the positive and negative flow directions over the four week simulation periods.

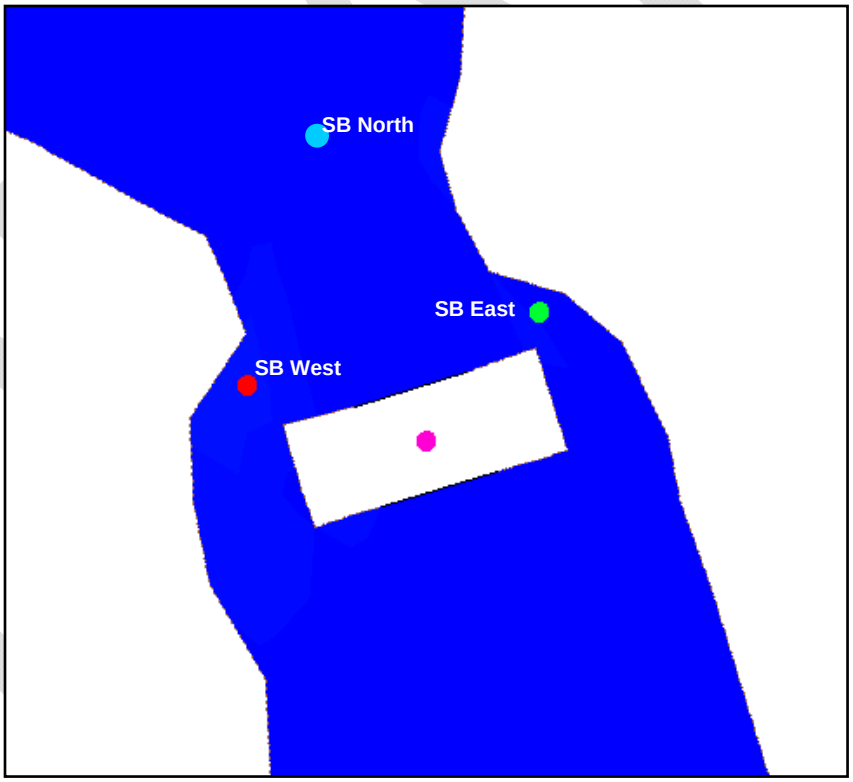

Figure A-22. Seabrook analysis locations for cofferdam simulation

DRAFT

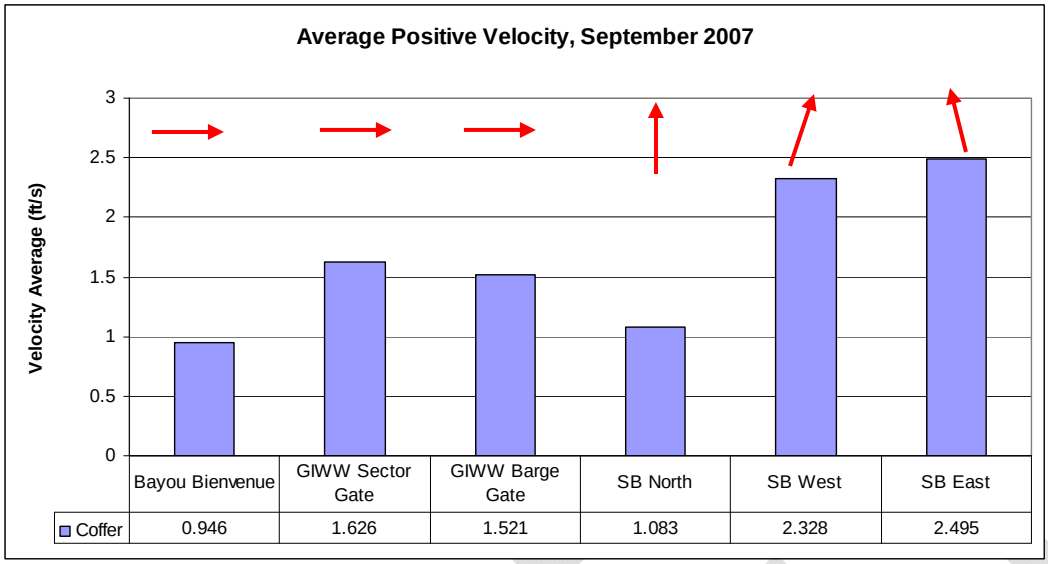

Figure A-23. Velocity average for September with cofferdam (positive)

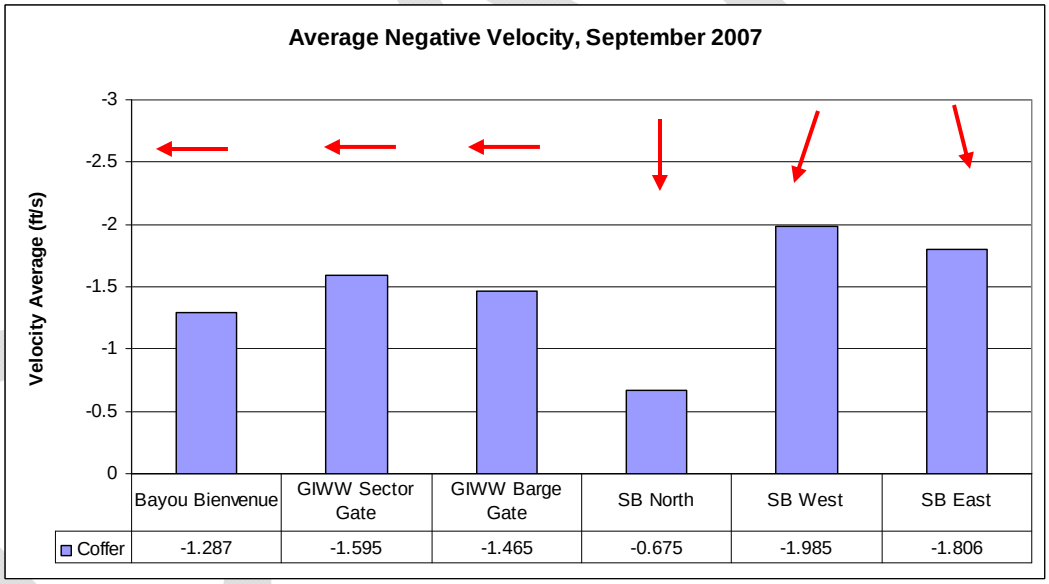

Figure A-24. Velocity average for September with cofferdam (negative)

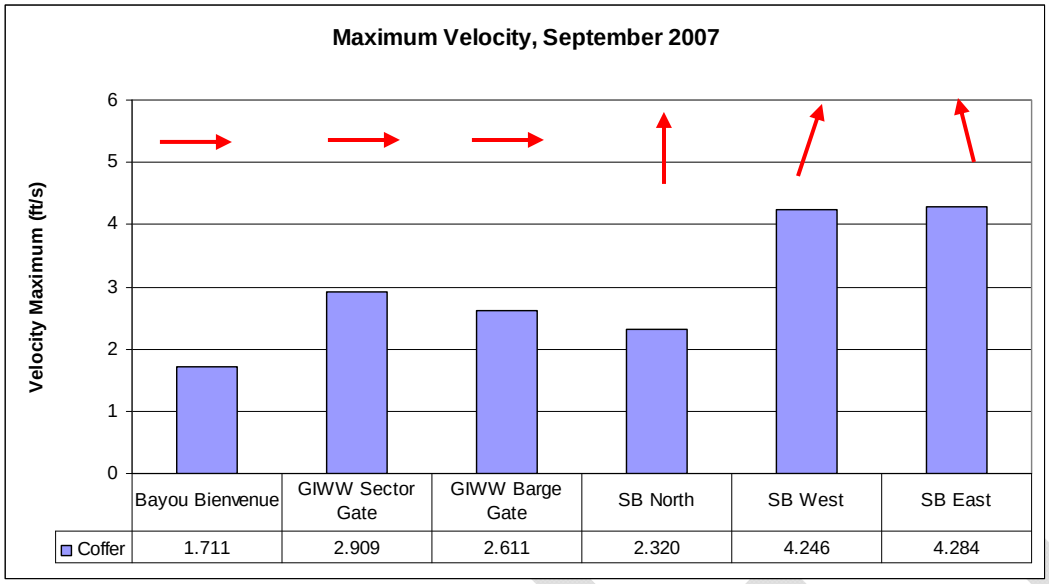

Figure A-25. Velocity maximum for September with cofferdam (positive)

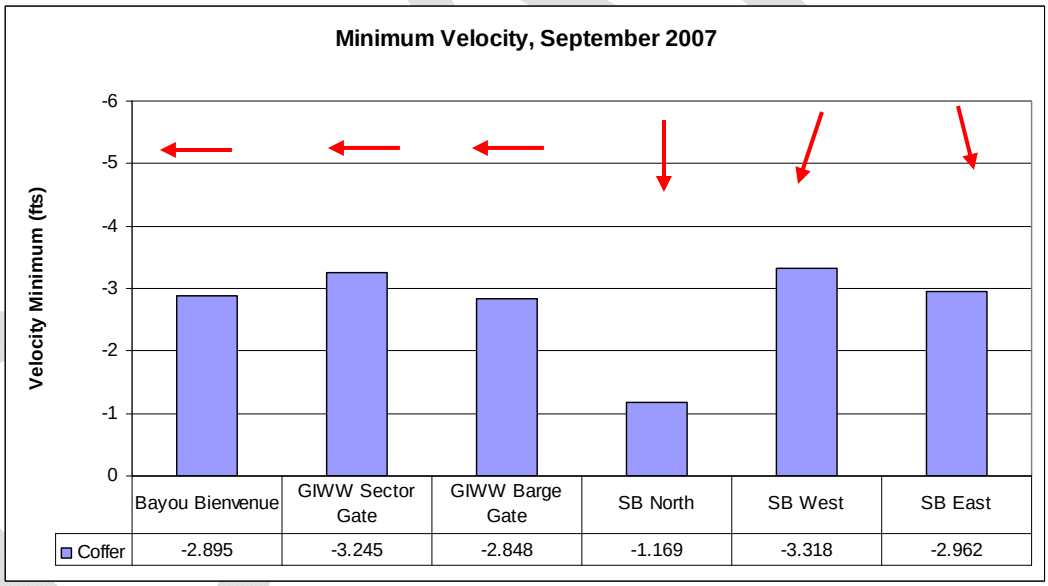

Figure A-26. Velocity minimum for September with cofferdam (negative)

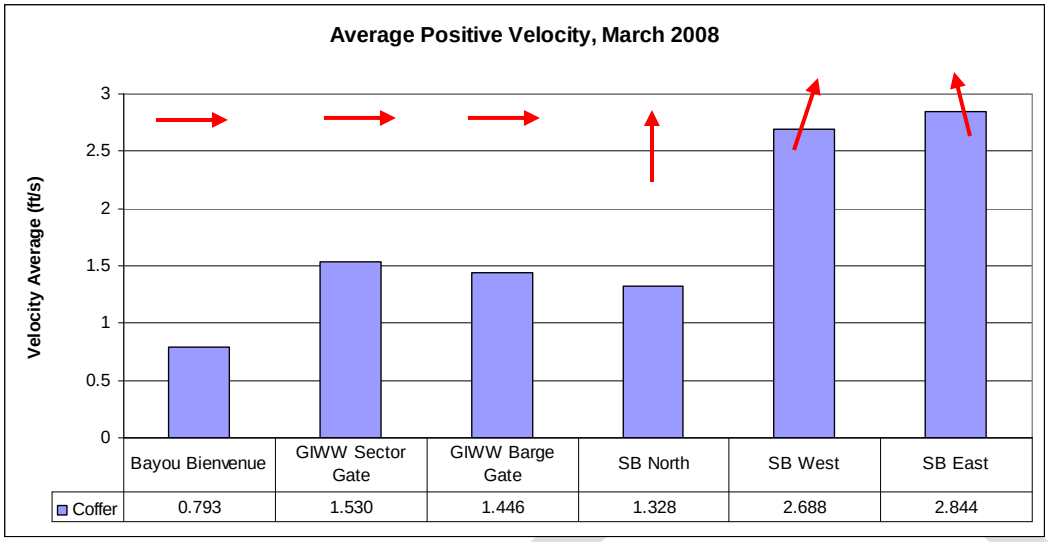

Figure A-27. Velocity average for March with cofferdam (positive)

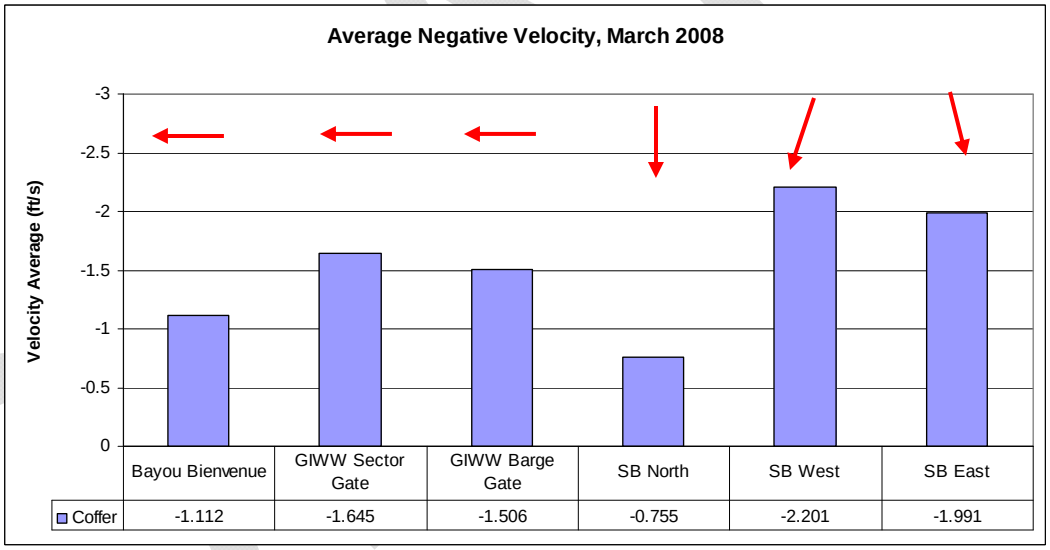

Figure A-28. Velocity average for March with cofferdam (negative)

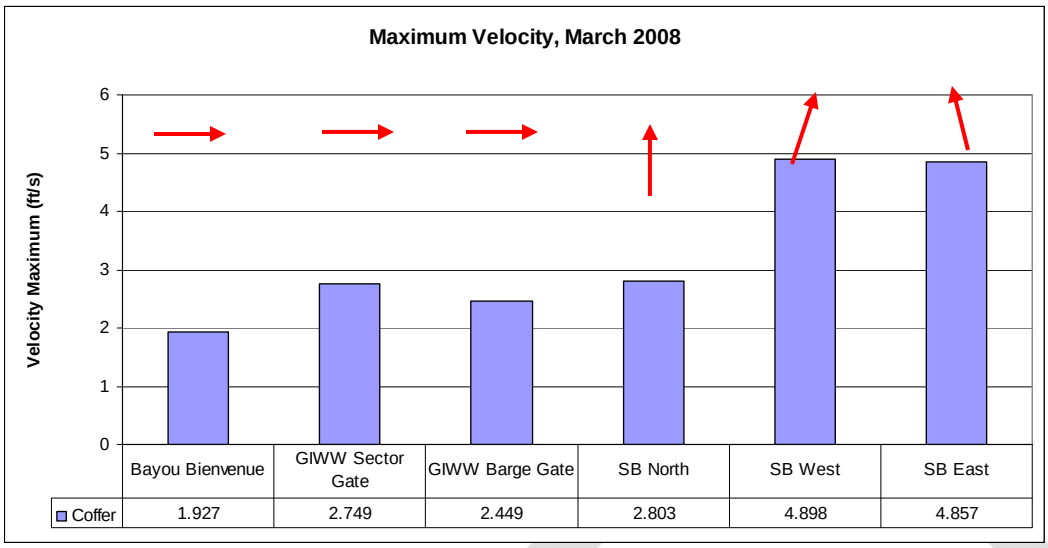

Figure A-29. Velocity maximum for March with cofferdam (positive)

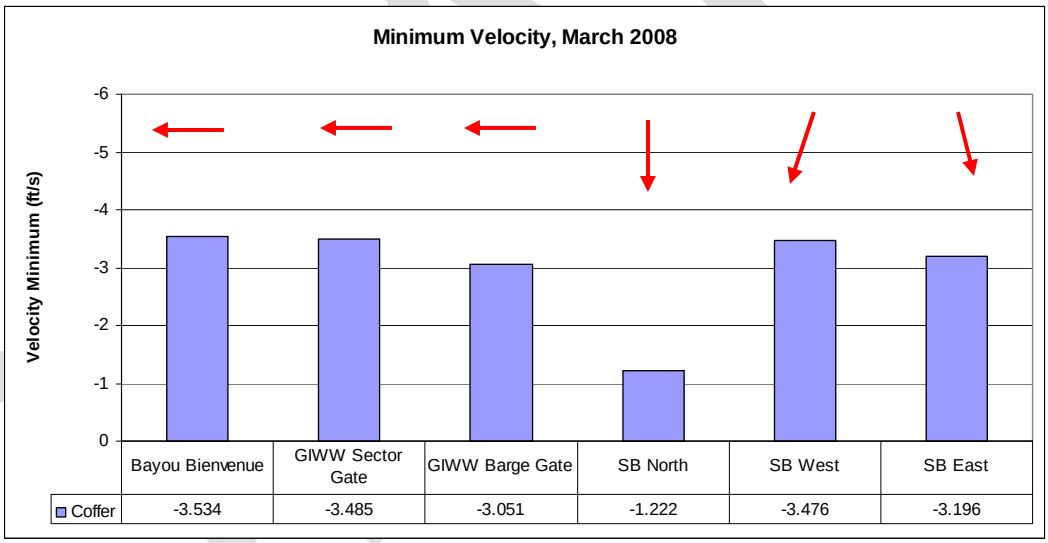

Figure A-30. Velocity minimum for March with cofferdam (negative)

Based on the above figures, the velocities with the cofferdam in place during construction of the Seabrook structure (Plan 3) are reduced from those with the structure in place. These values are lower because the total cross-sectional area on each side of the cofferdam (at the narrowest location) is 2570 ft^2 whereas the cross-sectional area for the Plan 3 structure is only 1520 ft^2. Although the discharge through this area will be affected some due to the change in shape and effects of the other structures in the sys-

tem, there is enough area on each side of the cofferdam to prevent the velocities from reaching the levels observed due to the implementation of Plan 3. Figures A-31 and A-32 show a snapshot of the velocity magnitude and direction at a time when the flows are large for both an incoming and retreating tide event. The location of highest velocity, as seen in the below images, is closer to the model boundary than the location of the East and West points in Figure A-22. This indicates that the extreme velocities will be slightly higher than the value given in the previous figures, although still not on the order of the values for Plan 3.

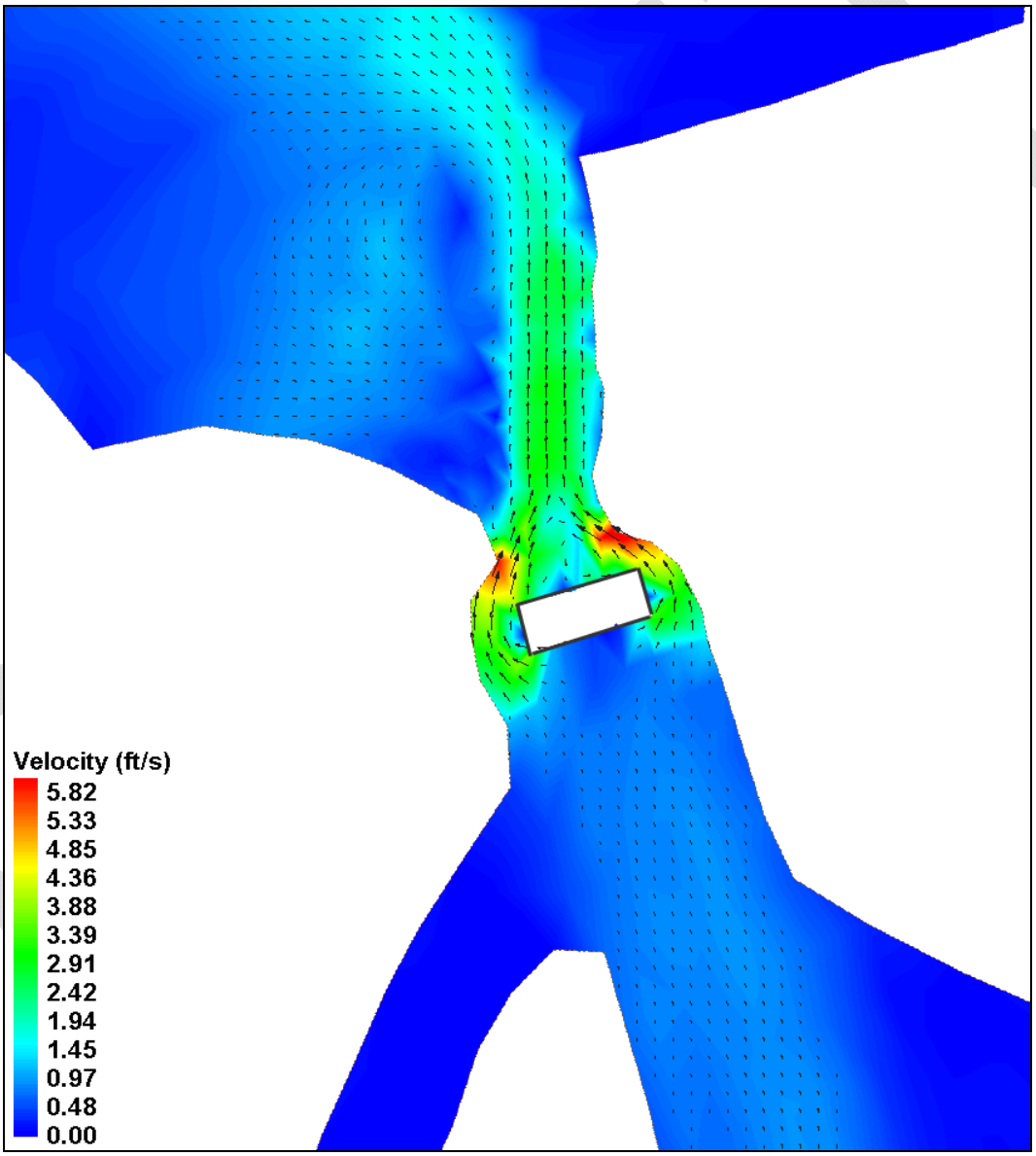

Figure A-31. Velocity magnitude and direction at the cofferdam for a high flood flow in March (a single snapshot in time)

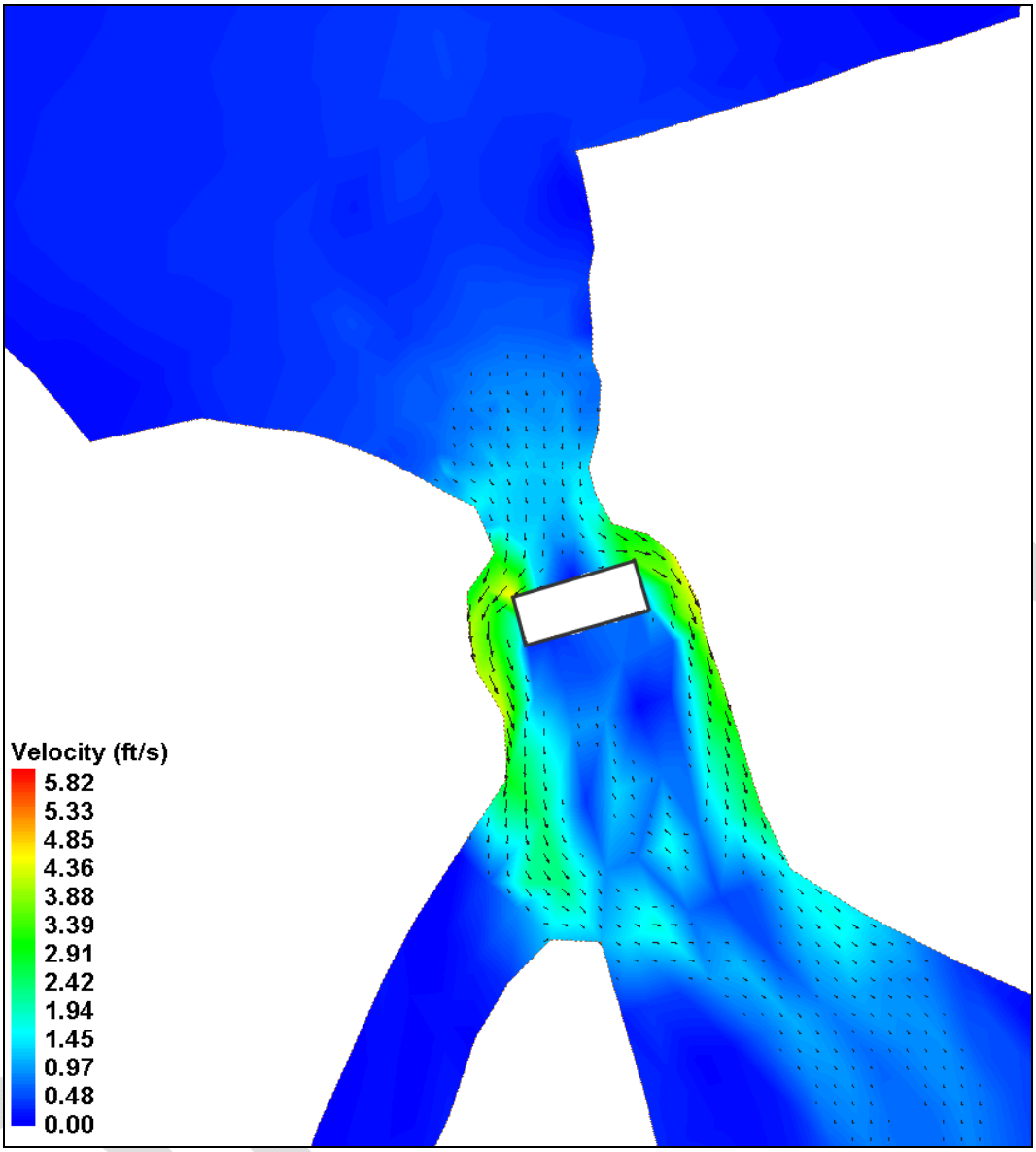

Figure A-32. Velocity magnitude and direction at the cofferdam for a high ebb flow in March (a single snapshot in time)

Bridge Pier Sensitivity

A railroad bridge is stationed just north of the proposed location of the Seabrook structure. All previous simulations did not include the bridge piers, so a sensitivity run was made in which the bridge piers are included in the Plan 3 simulations. In this configuration the Seabrook structure is 95 X -16 ft, the southern scour hole is filled to approximately -39 ft, and the bridge piers are included for the railroad bridge. Figure A-33 shows the geometry for the Seabrook section of the model domain with the bridge piers included. Figures A-43 through A-41 show the average and maximum velocity magnitudes at various locations within the model domain for the Base and three original plan conditions as well as the condition including the bridge piers. The data locations are the same as those presented Figures A-1 and A-2. Figures A-42 and A-43 show a snapshot of the velocity magnitude and direction at a time when the flows are large for both an incoming and retreating tide event.

From these figures, it is evident that the bridge piers have little effect on the velocity magnitudes in this area. At Seabrook, the bridge piers seem to generate a very small decrease in the velocity magnitudes while at the other locations the effect of the piers may be a little higher or lower than the Plan 3 condition, but still very small.

Since this sensitivity was made using the original dimensions for the Seabrook structure, caution must be used when extrapolating these results to other structure dimensions. However, since the changes to the velocity magnitudes are very small at Seabrook, they actually drop slightly, the effect of the bridge piers will probably be even less with the wider structure because the wider structure has lower velocities in the Seabrook area than the original.

DRAFT

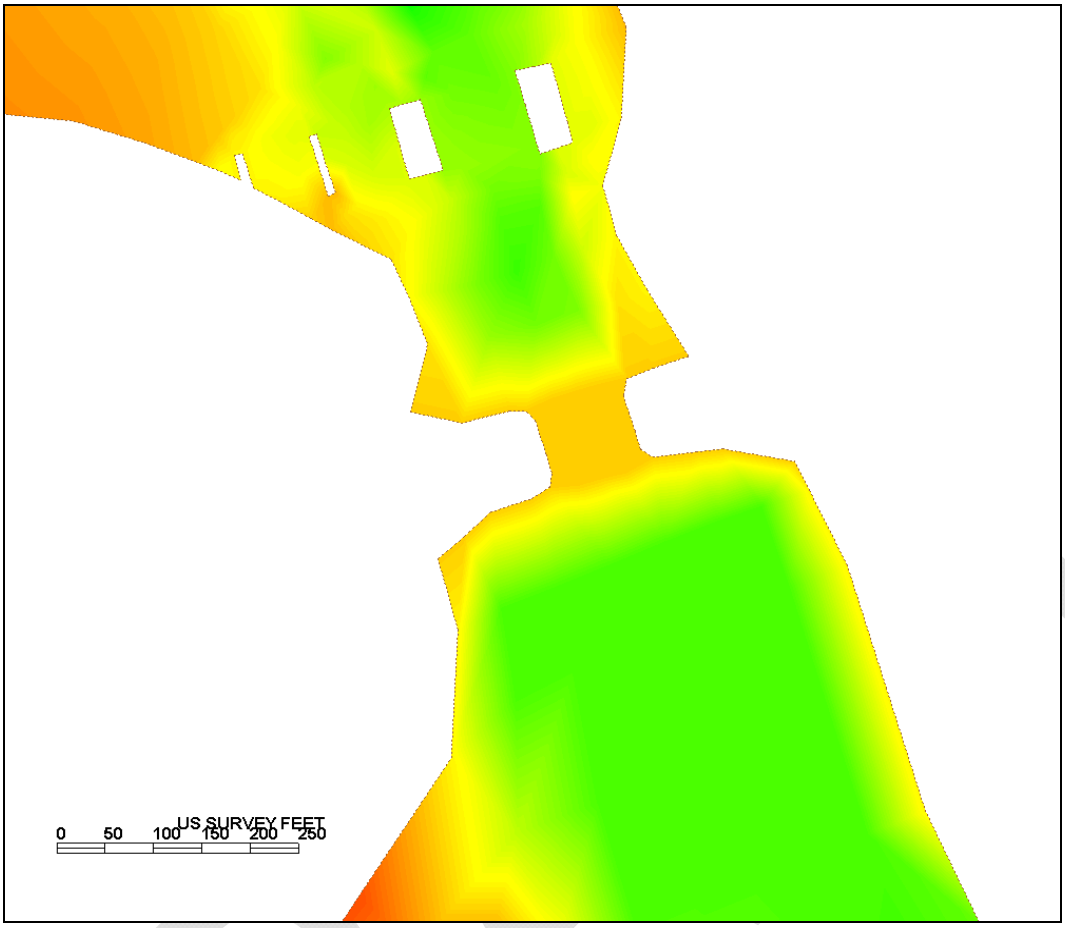

Figure A-33. Plan 3 geometry configuration (95 X 16 ft Seabrook structure) with bridge piers (includes MRGO cut at La Loutre and the Borgne alignment)

DRAFT

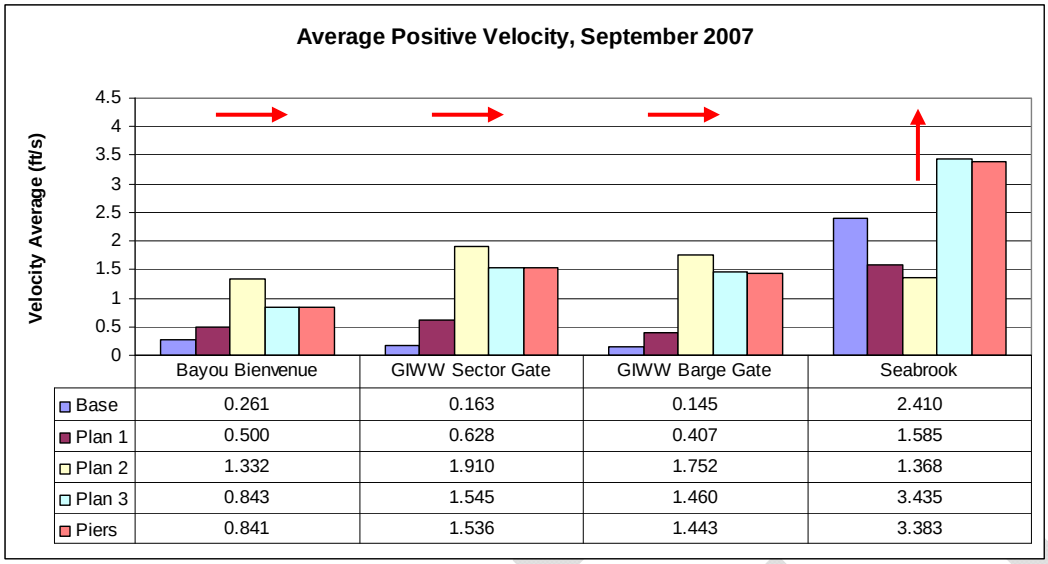

	Bayou Bienvenue	GIWW Sector Gate	GIWW Barge Gate	Seabrook
Base	0.261	0.163	0.145	2.410
Plan 1	0.500	0.628	0.407	1.585
Plan 2	1.332	1.910	1.752	1.368
Plan 3	0.843	1.545	1.460	3.435
Piers	0.841	1.536	1.443	3.383

Figure A-34. Velocity average for September with bridge piers (positive)

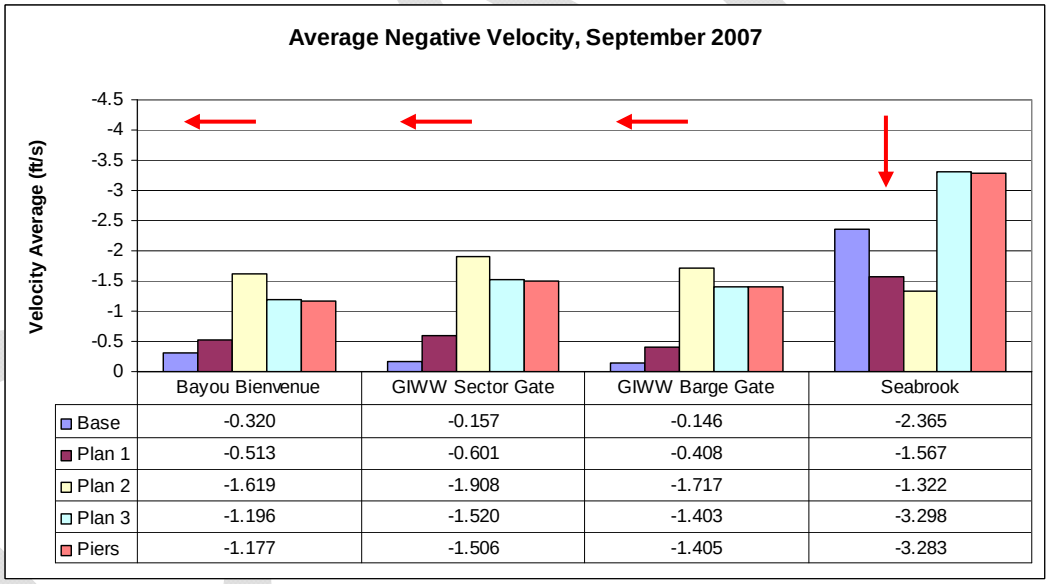

	Bayou Bienvenue	GIWW Sector Gate	GIWW Barge Gate	Seabrook
Base	-0.320	-0.157	-0.146	-2.365
Plan 1	-0.513	-0.601	-0.408	-1.567
Plan 2	-1.619	-1.908	-1.717	-1.322
Plan 3	-1.196	-1.520	-1.403	-3.298
Piers	-1.177	-1.506	-1.405	-3.283

Figure A-35. Velocity average for September with bridge piers (negative)

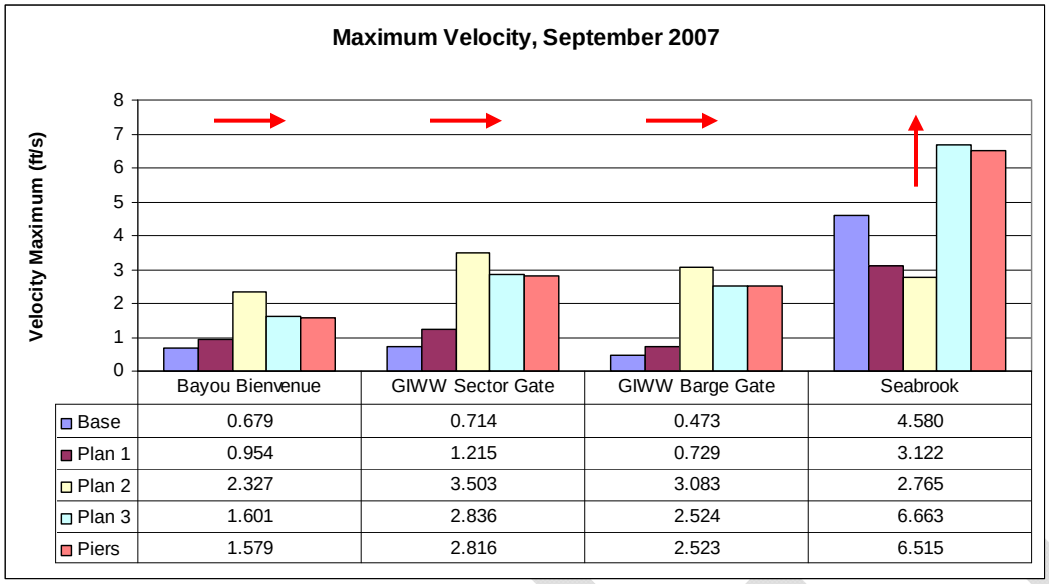

	Bayou Bienvenue	GIWW Sector Gate	GIWW Barge Gate	Seabrook
Base	0.679	0.714	0.473	4.580
Plan 1	0.954	1.215	0.729	3.122
Plan 2	2.327	3.503	3.083	2.765
Plan 3	1.601	2.836	2.524	6.663
Piers	1.579	2.816	2.523	6.515

Figure A-36. Velocity maximum for September with bridge piers (positive)

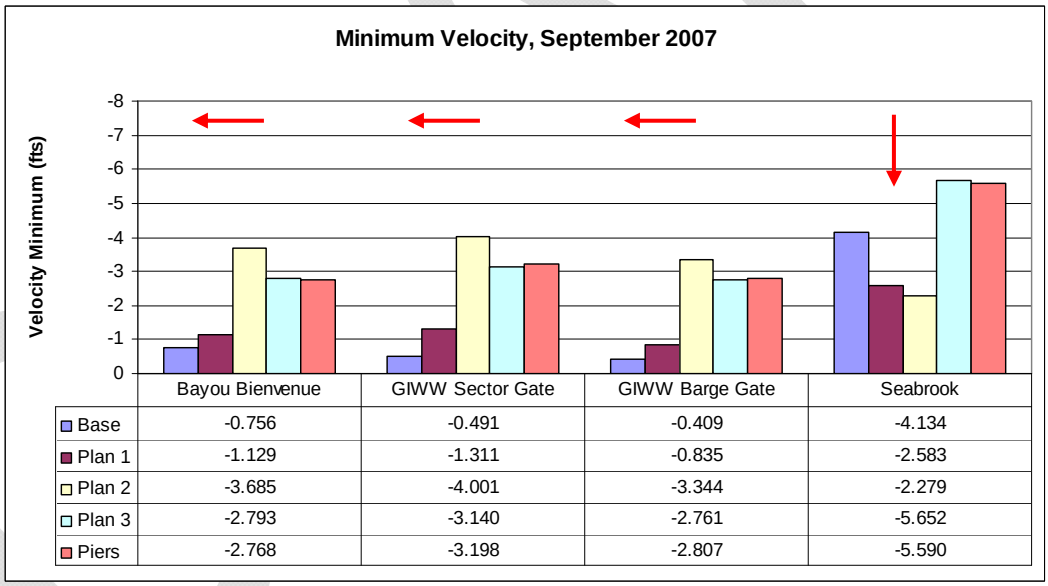

	Bayou Bienvenue	GIWW Sector Gate	GIWW Barge Gate	Seabrook
Base	-0.756	-0.491	-0.409	-4.134
Plan 1	-1.129	-1.311	-0.835	-2.583
Plan 2	-3.685	-4.001	-3.344	-2.279
Plan 3	-2.793	-3.140	-2.761	-5.652
Piers	-2.768	-3.198	-2.807	-5.590

Figure A-37. Velocity minimum for September with bridge piers (negative)

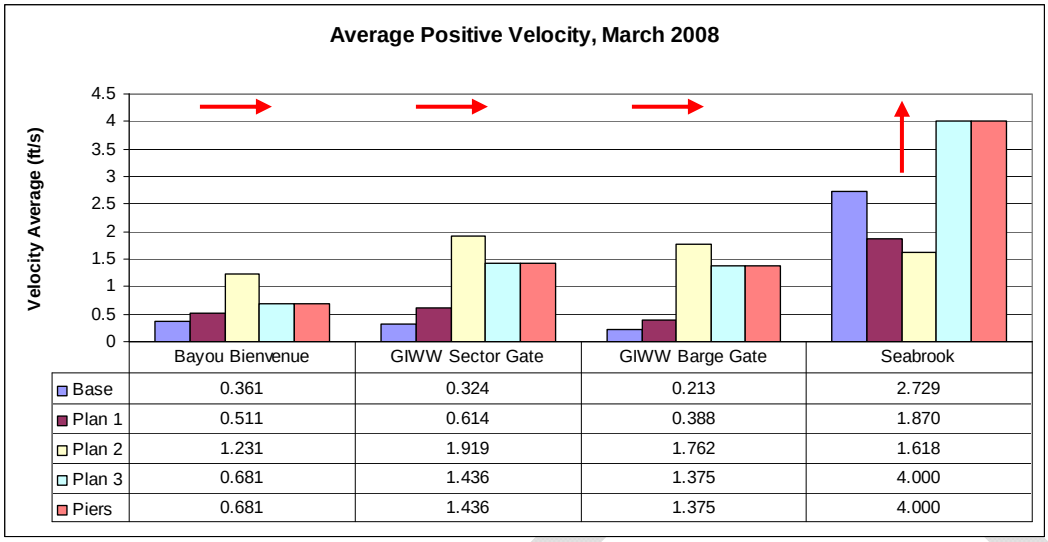

	Bayou Bienvenue	GIWW Sector Gate	GIWW Barge Gate	Seabrook
Base	0.361	0.324	0.213	2.729
Plan 1	0.511	0.614	0.388	1.870
Plan 2	1.231	1.919	1.762	1.618
Plan 3	0.681	1.436	1.375	4.000
Piers	0.681	1.436	1.375	4.000

Figure A-38. Velocity average for March with bridge piers (positive)

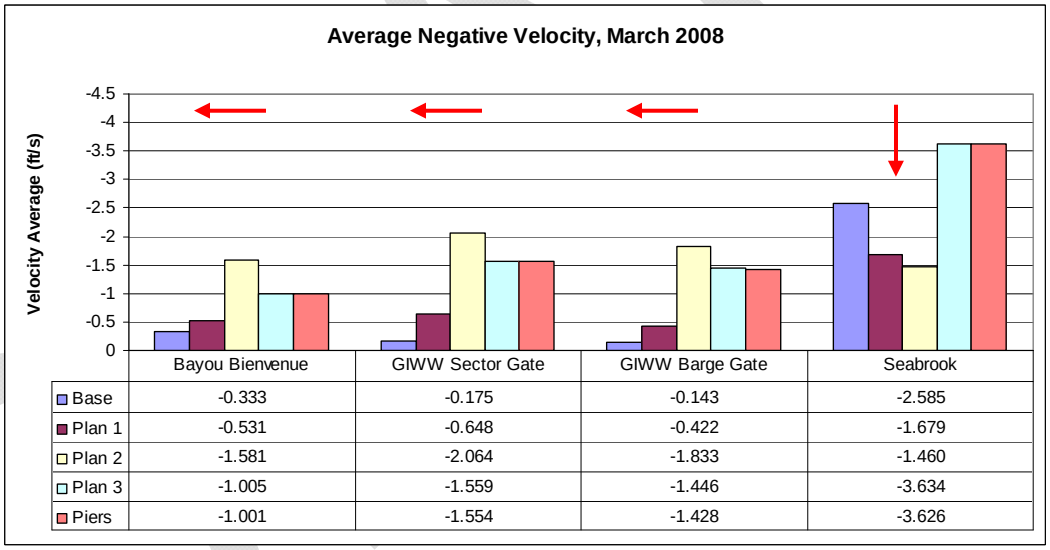

	Bayou Bienvenue	GIWW Sector Gate	GIWW Barge Gate	Seabrook
Base	-0.333	-0.175	-0.143	-2.585
Plan 1	-0.531	-0.648	-0.422	-1.679
Plan 2	-1.581	-2.064	-1.833	-1.460
Plan 3	-1.005	-1.559	-1.446	-3.634
Piers	-1.001	-1.554	-1.428	-3.626

Figure A-39. Velocity average for March with bridge piers (negative)

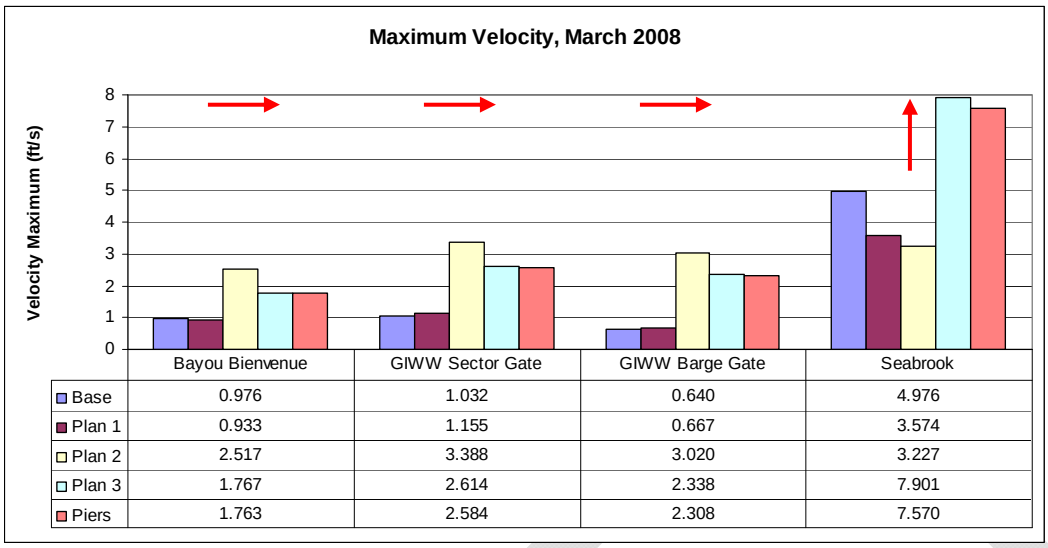

	Bayou Bienvenue	GIWW Sector Gate	GIWW Barge Gate	Seabrook
Base	0.976	1.032	0.640	4.976
Plan 1	0.933	1.155	0.667	3.574
Plan 2	2.517	3.388	3.020	3.227
Plan 3	1.767	2.614	2.338	7.901
Piers	1.763	2.584	2.308	7.570

Figure A-40. Velocity maximum for March with bridge piers (positive)

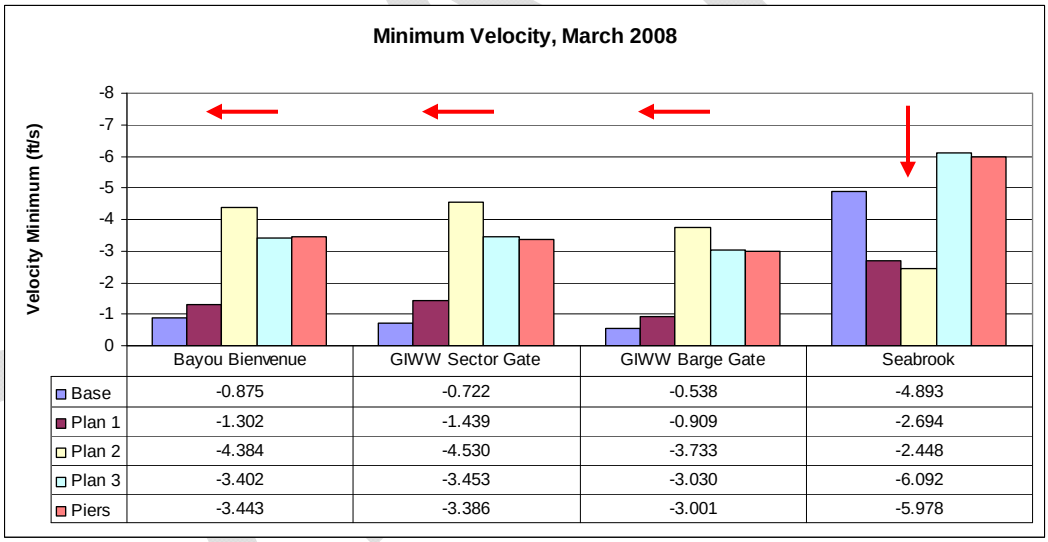

	Bayou Bienvenue	GIWW Sector Gate	GIWW Barge Gate	Seabrook
Base	-0.875	-0.722	-0.538	-4.893
Plan 1	-1.302	-1.439	-0.909	-2.694
Plan 2	-4.384	-4.530	-3.733	-2.448
Plan 3	-3.402	-3.453	-3.030	-6.092
Piers	-3.443	-3.386	-3.001	-5.978

Figure A-41. Velocity minimum for March with bridge piers (negative)

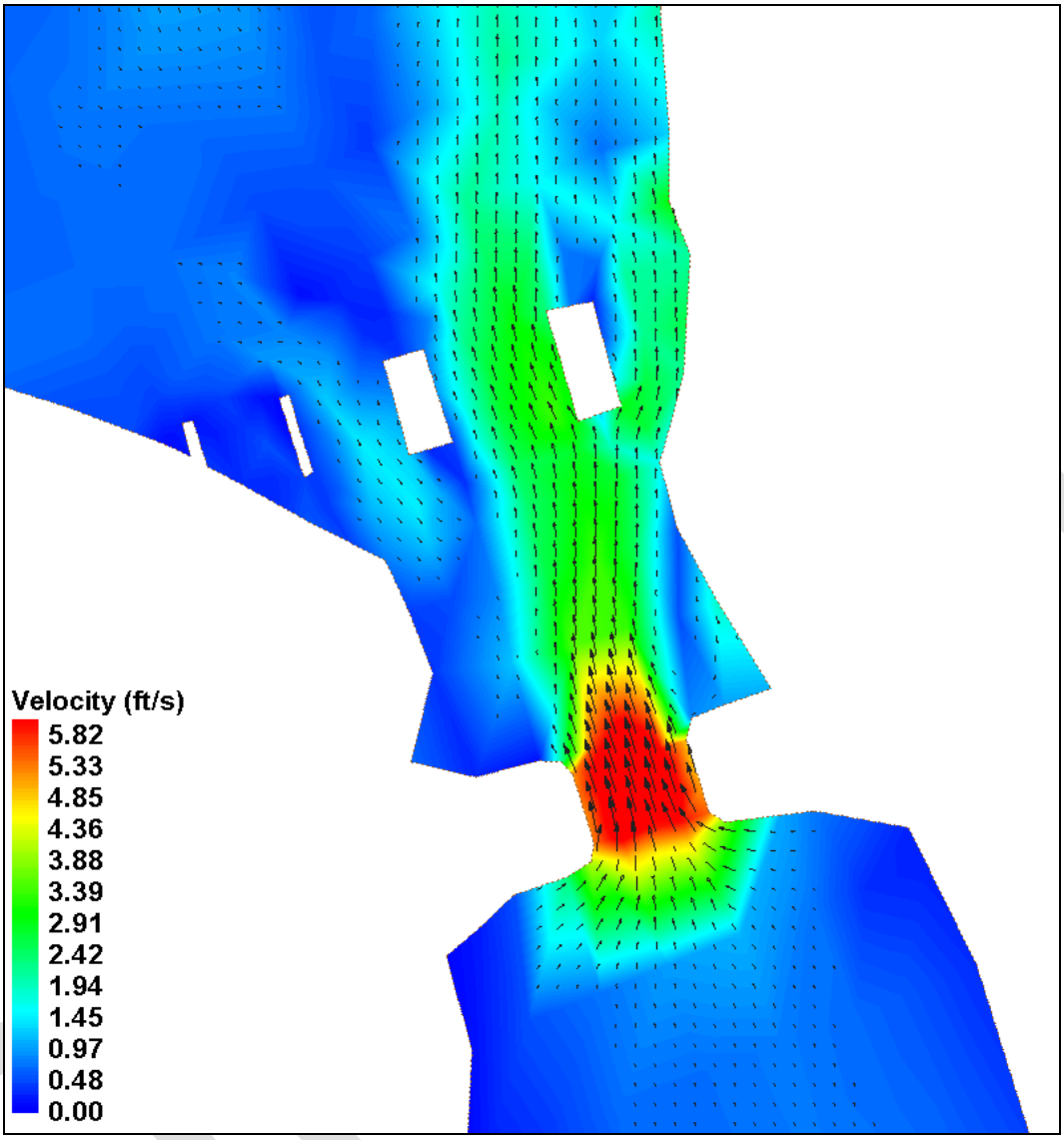

Figure A-42. Velocity magnitude and direction with bridge piers for a high flood flow in March (a single snapshot in time)

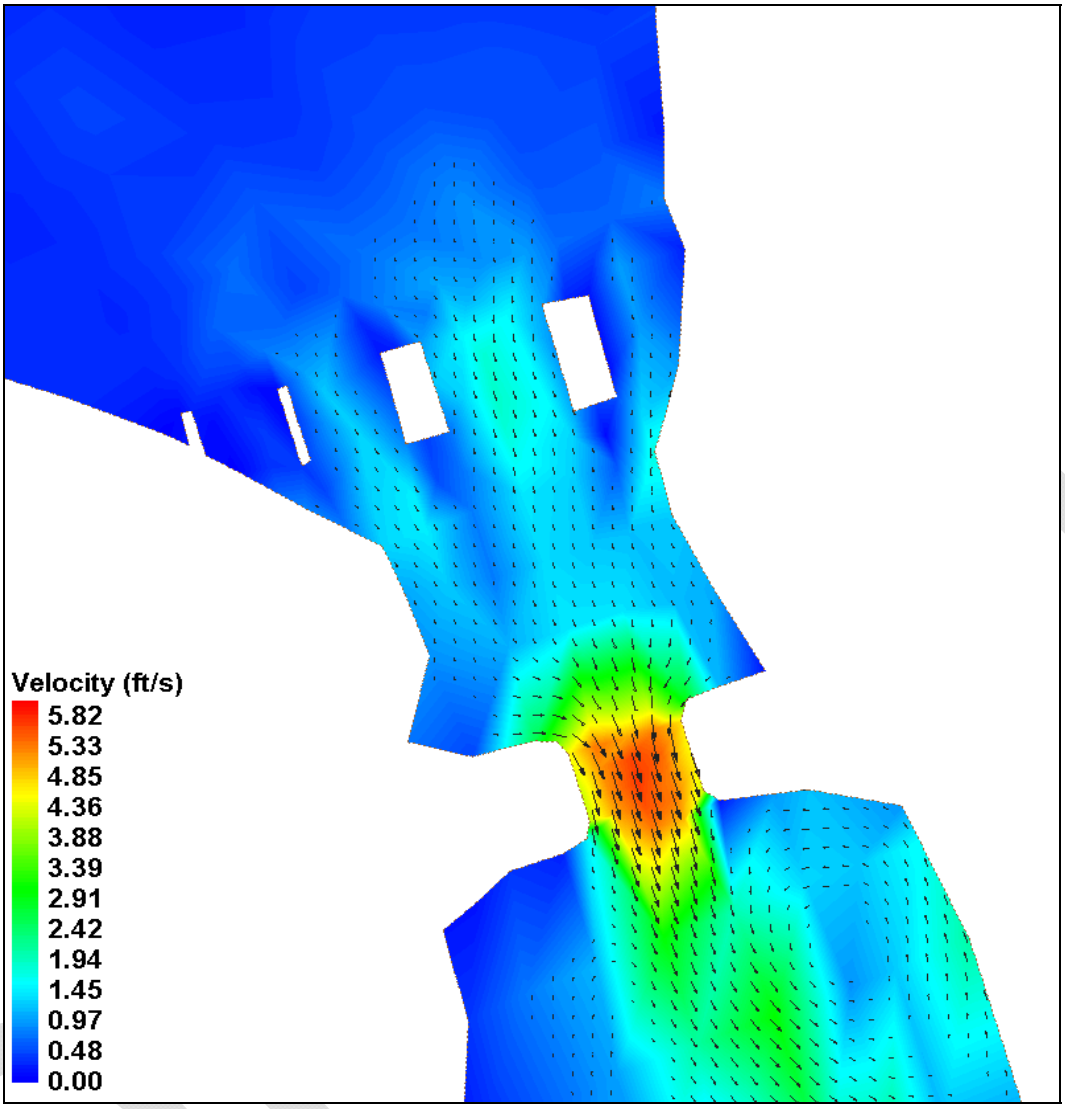

Figure A-43. Velocity magnitude and direction with bridge piers for a high ebb flow in March (a single snapshot in time)

Appendix B : Description of the Adaptive Hydraulics Model (ADH)

ADH is a state-of-the-art Adaptive Hydraulics Modeling system developed by the Coastal and Hydraulics Laboratory. It is capable of simulating both saturated and unsaturated groundwater, overland flow, three-dimensional Navier-Stokes flow, and two- or three-dimensional shallow water problems with the current study utilizing the two-dimensional shallow water module. The 2D shallow-water equations used for this application are a result of the vertical integration of the equations of mass and momentum conservation for incompressible flow under the hydrostatic pressure assumption. Written in conservative form, the 2D shallow water equations are:

$$\frac{\partial \mathbf{U}}{\partial t} + \frac{\partial \mathbf{F}}{\partial x} + \frac{\partial \mathbf{G}}{\partial y} + \mathbf{H} = 0 \tag{1}$$

where

$$\mathbf{U} = \begin{Bmatrix} h \\ uh \\ vh \end{Bmatrix} \tag{2}$$

$$\mathbf{F} = \begin{Bmatrix} uh \\ u^2 h + \frac{1}{2} g h^2 - h \dfrac{\sigma_{xx}}{\rho} \\ uvh - h \dfrac{\sigma_{yx}}{\rho} \end{Bmatrix} \tag{3}$$

DRAFT

$$\mathbf{G} = \begin{Bmatrix} vh \\ uvh - h\dfrac{\sigma_{xy}}{\rho} \\ v^2 h + \frac{1}{2} g h^2 - h\dfrac{\sigma_{yy}}{\rho} \end{Bmatrix} \tag{4}$$

and

$$\mathbf{H} = \begin{Bmatrix} 0 \\ gh\dfrac{\partial z_b}{\partial x} + n^2 gh\dfrac{u\sqrt{u^2+v^2}}{C_o h^{1/3}} \\ gh\dfrac{\partial z_b}{\partial y} + n^2 gh\dfrac{v\sqrt{u^2+v^2}}{C_o h^{1/3}} \end{Bmatrix} \tag{5}$$

where:

ρ = fluid density

g = gravitational acceleration

z_b = riverbed elevation

n = Manning's roughness coefficient

h = flow depth

u = x-component of velocity

v = y-component of velocity

DRAFT

C_o = dimensional conversion coefficient (1 for SI units, 1.486 for U.S. customary units)

σ's = the Reynolds stresses due to turbulence, where the first subscript indicates the direction, and the second indicates the face on which the stress acts.

The Reynolds stresses are determined using the Boussinesq approach to the gradient in the mean currents.

$$\sigma_{xx} = 2\rho v_t \frac{\partial u}{\partial x} \tag{6}$$

$$\sigma_{yy} = 2\rho v_t \frac{\partial v}{\partial y} \tag{7}$$

and

$$\sigma_{xy} = \sigma_{yx} = 2\rho v_t \left(\frac{\partial u}{\partial y} + \frac{\partial v}{\partial x} \right) \tag{8}$$

where v_t = kinematic eddy viscosity (which varies spatially).

The ADH shallow-water equations are placed in conservative form so that mass balance and the balance of momentum and pressure are identical across an interface. This is important in order to match the speed and height of a surge or hydraulic jump.

The equations are represented in a finite element approach. The quality of the numerical solution depends on the choice of the basis/trial function and the test function. The trial function determines how the variables are represented and the test function determines the manner in which the differential equation is enforced. In the Galerkin approach the test functions

DRAFT

are chosen to be identical with the trial functions. When the flow is advection-dominated, the Galerkin approach produces oscillatory behavior. The Galerkin form of the test function cannot detect the presence of a node-to-node oscillation and so allows this spurious solution. The approach used in ADH is to enrich the standard Galerkin test function with an additional term that can detect and control this spurious solution.

The Petrov-Galerkin method used here is based on elemental constants for coefficients. This reduces the stabilization to the nonconservative form. This is not a problem since the stabilization is only applied within the elements and uses the Galerkin test function to enforce "flux" balance across element edges. For illustration, consider the shallow-water equations in nonconservative form

$$\frac{\partial U}{\partial t} + A\frac{\partial U}{\partial x} + B\frac{\partial U}{\partial y} + H = 0 \tag{9}$$

where $A = \frac{\partial F}{\partial U}$ and $B = \frac{\partial G}{\partial U}$. The trial functions (or interpolation/basis functions) are the Lagrange polynomials. These are piecewise linear functions that are continuous across element boundaries. Spatial derivatives, however, are not continuous across these element edges. Each of the dependent and independent variables is interpolated via these trial functions. For example,

$$\tilde{u}(x) = \sum_{j=1}^{N} \phi_j(x) u_j , \tag{10}$$

means that the approximate solution is made up of the product of the trial function for node j and the nodal value at that location. The test function is chosen as:

$$\phi_i^* = \phi_i I + \alpha \left(\frac{\partial \phi_i}{\partial x} A + \frac{\partial \phi_i}{\partial y} B \right) \tag{11}$$

where,

$$\alpha = 0.5\,l\left[\bar{v}\bullet\bar{v} + gh + \left(\frac{l}{\Delta t}\right)^2\right]^{-1/2} \tag{12}$$

l	=	$(\Omega_e)^{1/2}$, the square of the element area
$\bar{v}$	=	$(\bar{u}, \bar{v})$, the element average velocity components
Δt	=	time step size

The finite element statement becomes:

$$\int_\Omega \left(\phi_i \frac{\partial U_l}{\partial t} - \frac{\partial \phi_i}{\partial x} F_l - \frac{\partial \phi_i}{\partial y} G_l + \phi_i H_l\right) d\Omega +$$

$$\int_{\partial\Omega} \phi_i \left\{F_l n_x + G_l n_y\right\} ds + \sum_e \int_{\Omega_e} \alpha \left(\frac{\partial \phi_i}{\partial x} A_l + \frac{\partial \phi_i}{\partial y} B_l\right)$$

$$\left(\frac{\partial U_l}{\partial t} + A_l \frac{\partial U_l}{\partial x} + B_l \frac{\partial U_l}{\partial y} + H_l\right) = 0 \tag{13}$$

Where, the subscript l indicates the finite element approximation. The Petrov-Galerkin contributions are integrated on the interior of the elements, but not across element edges. This contribution stabilizes the Galerkin approach. This contribution stabilizes the Galerkin approach. This scheme utilizes a single scaling factor α. This is different from the scheme reported in Berger and Stockstill (1995). That scheme involved scaling each eigenvalue, but that method does not converge using the iterative solver in ADH. Instead, a single value scaling (Equation 12) is used.

DRAFT

One of the major benefits of ADH is its ability to adapt the mesh in areas where additional resolution is needed to properly resolve the hydrodynamics. This process is done by normalizing the results so that an error quantity is determined for each element. If this error exceeds the tolerance set by the user, then the element is refined. ADH is also able to unrefined previously refined areas when the added resolution is no longer needed. ADH contains other essential features such as wetting and drying, completely coupled sediment transport, and wind effects. A series of modularized libraries make it possible for ADH to include vessel movement, friction descriptions, as well as a host of other crucial features. ADH can run in parallel or on a single processor and runs on both Windows systems and UNIX based systems.

DRAFT

Appendix C: Description of the Particle Tracking Model Processes and Algorithms

PTM employs three modes of operation: 2D, Quasi-3D, and 3D. The differences in these three modes are determined by the algorithms that are utilized for the calculations. The 2D representation of particle motion is the simplest. It provides a preliminary assessment of particle motions and pathways. A 3D approach is required for applications where interaction with the native bed is significant, or where the vertical movement and settling of sediment particles are concerned. The Quasi-3D mode involves a combination of empirical particle transport functions and a 3D advection, settling, and dispersion routine to mimic some of the key 3D transport processes. The 3D mode performs more comprehensive 3D particle entrainment, deposition, and re-suspension routines, but takes longer computational time due to the requirement of smaller time-steps.

The internal procedure for PTM follows four steps. First initial particle positions are determined for a time step. This is accomplished either by user source input or (after the first time-step) through output from the previous time-step. The code then goes through a series of mesh based Eulerian Calculations. Framework calculations establish background data such as water depth, flow velocities, frictional information, native (bed) sediment characteristics. Bed form calculations are performed to predict sub-grid scale bed forms over the domain. Shear and mobility calculations predict the influence of the flow field on the bed sediments over the domain. Transport calculations approximate the potential sediment transport fluxes over the domain and bed change calculations estimate the local instantaneous rates of erosion and deposition of bed materials (expressed as the time rate of bed change, dz/dt) using the potential transport fluxes. The frequency of updating shears, bedfoms, and mobility are determined by the user.

Next Lagrangian computations are performed for each particle. Because hydrodynamic data is most likely available less frequently than that required by Lagrangian calculations, values are interpolated in time. Flow algorithms are performed which interpolate the local flow and wave conditions spatially at the particle's location. Mobility calculations determine the mobility of the particle and, if deposited, the likelihood of its entrain-

DRAFT

ment in the flow using the flow and wave conditions at the particle's location. The trajectory integration determines the position of the particle at the end of the time-step using an advection-diffusion routine with consideration of settling, deposition, and erosion. Particle inertia is not considered. Particle positions are then checked for violation of boundary conditions. And finally sediment traps are checked to determine if a particle's destination falls within a sediment trap. These newly calculated positions are the input for the next iteration.

PTM contains algorithms that appropriately represent initiation of motion, transport, settling, deposition, mixing, and resuspension processes in nearshore wave/current conditions. In this section we discuss the algorithms for both the mesh based Eulerian calculations and the Lagrangian particle transport calculations. As mentioned in the previous section, PTM operates in three different modes (2D, Quasi-3D, and 3D). For simplicity we discuss here only those algorithms which pertain to fully 3D calculations. More detailed information about the other two modes can be found in MacDonald et al (2006).

Eulerian Transport Calculations

Shear Stress

Shear stress is a function of both the flow and sediment bed conditions. As it plays a major role in many of the subsequent calculations, we will begin by describing the methods used to calculate these quantities. First it should be mentioned that there are actually four types of shear stresses calculated in PTM. They are the shear stress due to skin friction and the shear stress due to form drag for both current-induced and wave-induced stresses. In this document we will denote these variables as follows:

1. Current-induced shear stress due to skin friction, τ_c' .
2. Current-induced shear stress due to form drag, τ_c'' .
3. Wave-induced shear stress due to skin friction, τ_w' .
4. Wave-induced shear stress due to form drag, τ_w'' .

PTM implements methods described in van Rijn (1993) to calculate shear stress. The bed shear stress (Pa) can be calculated from the depth-averaged velocity, $\overline{U}$, as:

DRAFT

$$T_c'' = \frac{\rho \overline{U}^2}{(C'')^2} \tag{1}$$

Here ρ is the water density, and C'' is the dimensionless Chézy coefficient, which for rough turbulent flow is approximated by:

$$C'' = 2.5 \ln\left[11 \frac{h}{k_s''}\right] \tag{2}$$

where h = flow depth (m). For the current-induced shear stress due to form drag, τ_c'', the form roughness height, k_s'', is estimated using a combination of the bed form length and steepness. The bed shear velocity, u_* (m/sec), is computed from:

$$u_* = \sqrt{\frac{T_c''}{\rho}} = \frac{\overline{U}}{C''} \tag{3}$$

For rough turbulent flows, the bed shear velocity, u_* is dependent upon the flow depth, h, the characteristic roughness of the flow, k_s'' and $\overline{U}$:

$$u_* = \frac{\overline{U}}{2.5 \ln\left(11 \frac{h}{k_s''}\right)} \tag{4}$$

For the current-induced shear stress due to skin friction, τ_c' a roughness height, k_s' representative of the skin, or grain-size, roughness of the bed is used. In PTM, skin roughness is taken as 3 times the D_{90} of the bed material for erodible beds, where D_{90} is the grain size that 90 percent of the sediment is finer (by weight). The model interface can override this value with a user-specified value. It should also be noted that the calculations becomes more complicated in the case of combined wave and current flows. Details of these calculations can be found in the technical report (MacDonald et al 2006).

DRAFT

Initiation of Motion

The initiation of motion for PTM particles located at the bed is dependent on the critical shear stress τ_{cr}. This value is utilized in the critical Shield's parameter. Defined by the Shield's curve, the dimensionless parameter θ (Sheild's parameter) gives the threshold of motion for particles at the bed (see Yalin (1977) for complete discussion).

$$\theta = \frac{\tau}{\rho g(s-1)D} \tag{5}$$

In this equation, D is the characteristic grain size, ρ is the density, g is the gravitational acceleration, and s is the relative density ratio of the particles. The value of θ at which the inception of sediment transport occurs is then called the critical Shield's parameter θ_{cr} and is given by:

$$\theta_{cr} = \frac{\tau_{cr}}{\rho g(s-1)D} \tag{6}$$

PTM uses a analytical representation of this equation based on later work performed by Soulsby and Whitehouse (1997) who developed a relationship based on the dimensionless grain size, D_{gr}.

$$D_{gr} = D_{50}\sqrt[3]{\frac{(s-1)g}{\nu^2}} \tag{7}$$

Here D_{50} is the grain size at which 50 percent of the sediment is finer (by weight) and ν is the kinematic viscosity of the fluid. The resulting new equation determined by Soulsby and Whites for θ_{cr} is:

$$\theta_{cr} = \frac{0.30}{1+1.2D_{gr}} + 0.55\left[1-e^{-0.020D_{gr}}\right] \tag{8}$$

Transport Mobility

The dimensionless mobility, M is the ratio of the skin shear stress acting on the bed, τ' to the critical shear stress, τ_{cr}, and is defined as:

$$M = \frac{T'}{T_{cr}} = \frac{\theta}{\theta_{cr}} \tag{9}$$

DRAFT

The critical shear, τ_{cr} (Pa), can be determined from:

$$\tau_{cr} = \theta_{cr}\rho(s-1)gD \tag{10}$$

The dimensionless transport parameter, T, is also commonly used to assess sediment mobility. It is defined as:

$$T = \frac{\tau' - \tau_{cr}}{\tau_{cr}} = M - 1 \tag{11}$$

From the known distributions of the native (bed surface) sediments and the flow conditions over the domain, the mobility of the bed sediments (and particles on the bed) may be determined.

Bedform Calculation

Estimating bed form geometry is necessary to calculate the shear stress due to form drag, τ'' and the overall flow resistance offered by the bed. The equilibrium dimensions of bed forms under waves and currents are computed using the technique of van Rijn (1984c) for currents and the technique of Mogridge et al. (1994) for combined current and wave conditions. Van Rijn's (1984c) bed form and roughness calculation methodology is as follows. The equilibrium bed form height, η_b is determined on the basis of mobility, flow depth, and grain size as follows:

$$\begin{aligned} n_b &= 0 && M \le 1 \\ n_b &= 0.11h\left(\frac{D_{50}}{h}\right)^{0.3}\left[1-e^{-0.5(M-1)}\right](24-M) && 1 < M \le 24 \\ n_b &= 0 && M > 24 \end{aligned} \tag{12}$$

These are steady-state equations, predicting no bed forms for conditions where the mobility, M, is less than unity (no transport) and for high flow conditions where bed forms would be washed out (M > 24). Bed forms do not develop for very fine materials (D_{50}< 0.05 mm). In PTM, it is assumed that if D_{50} < 0.05 mm, bed roughness is defined solely by skin friction and is:

$$k_s' = 3D_{90} \tag{13}$$

The above equations compute the equilibrium bed form height. In nature, bed forms continually adjust to changing flow conditions. The rate of

change of bed forms is related to the local bed load transport rate (van Rijn 1984a; Nielsen 1992). In PTM, a simple algorithm has been implemented to allow bed forms to gradually adjust from their present height to their new equilibrium height. The rate of change of bed form height is related to the overall transport rate. In this case, PTM uses the transport pickup rate, q_p (m/sec), to estimate the maximum temporal rate of change of the bed. At time t in a simulation, the bed form height, η, existing on the bed is compared to the equilibrium bed form height, η_b, from the predictive equations. If η is less than η_b, then the bed forms are growing; if η is greater than η_b, then the bed forms are decaying. The time rate of change of bed form height is then calculated as:

$$\begin{aligned} \frac{\partial \eta}{\partial t} &= -q_p \quad \eta > \eta_b \\ \frac{\partial \eta}{\partial t} &= q_p \quad \eta < \eta_b \end{aligned} \tag{14}$$

The bed form length is assumed to respond instantly to changes in flow conditions.

Potential Transport Rate

PTM requires potential transport rates over the model domain to compute gradients in transport to estimate the potential for erosion and deposition of the native bed materials. These rates are used to determine the likelihood of burial of a sediment particle once deposited. PTM offers a choice of two techniques, Soulsby-van Rijn (Soulsby 1997) and van Rijn (1993), for the potential total load transport rate under combined wave-current conditions.

Lagrangian Transport Calculations

Transport of particles in PTM is accomplished by three basic steps: 1) Particle location, 2) Particle interpolation, and 3) Particle integration. That is, first particle positions are located within the mesh. Then the Eulerian forcings are interpolated from the surrounding mesh to the particle position. Finally a new particle position is calculated by solving the basic equation

$$\frac{d\vec{X}}{dt} = \vec{V} \tag{15}$$

DRAFT

This simple differential equation states that the change in the position ($\vec{X}$) over time dt is equal to the velocity ($\vec{V}$). Therefore the most basic solution to these equations determine that

$$\vec{X}^{n+1} = \vec{X}^{n} + \vec{V}dt \tag{16}$$

By thus solving this equation, the new particle position $\vec{X}^{n+1}$ can be calculated at each time t. The main difficulties come in calculating the value of $\vec{V}$ which is a function of several quantities that will describe later.

Particle Position Integration

The basic Euler scheme shown in equation 16 is the simplest algorithm to the above differential equation. The scheme is first order accurate and often requires very small time steps as flows become very complex or when dealing with intricate sediment transport such as near bed particle behavior. Therefore a more accurate method must be used to allow for greater accuracy and larger time steps. Testing focused on determining effects of accuracy and efficiency for the PTM integration scheme is currently being performed.

As a first step in this direction, PTM v1.0 utilizes a two step predicator corrector scheme. This scheme is by nature second order accurate. In step 1 of the scheme, the particle position is integrated one half time steps. Then in step 2 this value and the initial particle position are used to calculate the new particle position, $\vec{X}^{n+1}$. In the following equations $\vec{X}'$ is the half time step particle position and $\vec{V}'$ is the velocity of the particle at this time.

$$\text{STEP 1: } \vec{X}' = \vec{X}_n + \frac{1}{2}(\vec{V}dt) \tag{17}$$

$$\text{STEP 2: } \vec{X}^{n+1} = \vec{X}_n + (\vec{V}'dt) \tag{18}$$

Velocity Calculations

As seen in the previous section, the velocity calculations play an important role in determining the particle position at each time step. The particle velocity term V in the previous equations is actually a mixture of various forcing elements. To understand this better, first we separate the particle velocity into the horizontal (U) and vertical (W) components. Within

DRAFT

these components we can further compartmentalize the velocity as follows:

In the horizontal directions:

$$U = U_A + U_D \tag{19}$$

where A indicates advective forcing and D indicates diffusion. In the vertical direction we get similar terms

$$W = W_A - W_S + W_D \tag{20}$$

The horizontal velocity of each particle is equal to the fluid velocity at the vertical elevation of the particle added to the velocity due to diffusion. The vertical velocity however is determined by the vertical velocity component of the fluid at the point z_p minus the settling velocity, W_s of the particle. The vertical velocity component due to advection from the flow W_A can be determined by an assumed velocity profile if the hydrodynamic input is two-dimensional or obtained exactly from three-dimensional hydrodynamic input. The particle fall velocity, W_S (m/sec), is defined as a function of the dimensionless grain size, D_{gr} and can be approximated by the following equations proposed by Soulsby (1997). They have been adapted for extremely fine grain sizes (D_{gr} < 0.0672) for PTM.

$$\frac{W_S D}{\nu} = \begin{cases} \sqrt{107.33 + 1.049 D_{gr}^3} - 10.36 & D_{gr} \geq 0.672 \\ 0.0077 D_{gr}^2 & D_{gr} < 0.672 \end{cases} \tag{21}$$

PTM uses a random walk diffusion model to calculate the velocity due to diffusion. The random walk representation of the horizontal dispersive velocity U_D is computed as:

$$U_D = 2(\Pi - 0.5)\sqrt{\frac{6E_t}{dt}} \tag{22}$$

where Π is a random number uniformly distributed between 0 and 1. Note that the horizontal dispersive velocities are isotropic. The vertical diffusion velocity is:

DRAFT

$$W_D = 2(\Pi - 0.5)\sqrt{\frac{6E_v}{dt}} \tag{23}$$

The turbulent diffusion coefficients in the previous equations are estimated as presented in Fischer et al. (1979) and as applied by Shen et al. (1993) amongst others. The turbulent diffusion coefficient, E_t is estimated to be:

$$E_t = K_{E_t} h u_*'' \tag{24}$$

The empirical coefficient K_{E_t} relates the turbulent diffusion to the local shear velocity and water depth. Typically, K_{E_t} ranges from 0.15 to 0.6. The variable u_*'' is the shear velocity associate with form drag only. Slight modifications have been made to this equation in PTM to account for enhanced mixing due to wave breaking. The vertical diffusion coefficient is modeled using a parabolic-shaped distribution,

$$E_v = M_b K_{E_t} U_x \left[\frac{z_p (h - z_p)^2}{h^3} \right] \tag{25}$$

where M_b is a wave breaking coefficient and h is the flow depth and z_p is the vertical particle location.

Particle-bed Interactions

This section describes the series of algorithms developed to simulate the behavior of particles near the bed. It includes a hiding and exposure function, frequency of entrainment calculations, as well as deposition and re-entrainment algorithms.

Hiding and Exposure Function

On a mixed bed with mean sediment size D_{50}, smaller particles hide behind larger particles and require a larger shear stress for the onset of mobility. Similarly, particles larger than D_{50} are more exposed and require a smaller shear stress for mobility. This is treated in PTM by means of a hiding and exposure function (Egiazaroff 1965; Kleinhans and van Rijn 2002). The function is a correction factor, and it is applied to the critical shear stress for inception of motion as:

$$\dot{\theta}_{cr} = \xi \theta_{cr} \tag{26}$$

where ξ is a dimensionless hiding and exposure correction factor. The hiding and exposure function is given by (Egiazaroff 1965):

$$\xi = \frac{5}{3}\left[\log\left(19\frac{D}{D_{50}}\right)\right]^{-2} \tag{27}$$

This function is valid for $0.3 < D/D_{50} < 10$, and limits the particle's mobility threshold to be no greater than 3 times and no less than one-third of the critical Shields parameter of that particle. The hiding and exposure function is only applied to particles that are deposited on the bed.

Frequency of Entrainment

In nature, the behavior of a particle at the bed can be extremely complex. Particles deposit at the bed and can be re-entrained right away or can perhaps mix with the active sediment transport layer and then become entrained some time later. To include this interaction within PTM, a probabilistic approach is used. The frequency of entrainment of a particle from the bed is computed as a function of the potential transport rate for the particle. This is combined with other factors that account for the likelihood of mixing of the particle within an active transport layer and the likelihood of burial of the particle by ambient transport processes.

In PTM, particle entrainment is based on the mean shear stress, critical shear stress for erosion as defined by the Shields curve, and by the following five supplemental considerations:

1. The turbulent fluctuations in the instantaneous shear stress.
2. Modifications to the critical shear stress to account for hiding and exposure effects of graded sediment beds.
3. The transport pickup rate from the bed.
4. The ambient transport conditions on the bed (erosion/deposition), leading to an estimate of the depth of burial of the particle.
5. Mixing of the particles within the active transport layer, which is based on the thickness of the active transport layer.

The details of these calculations are lengthy and can be found in MacDonald et al 2006. Once calculated, these processes have then been imple-

DRAFT

mented in a manner such that the frequency that a particle is picked up from the bed, f_e is determined as:

$$f_e = K_{burial} K_{mixing} f_p \tag{28}$$

In this equation, f_p is the frequency of pickup based on the estimated particle transport pickup rate for the particle. K_{mixing} is a reduction factor to account for the fact that the particle may lie anywhere within the thickness of the active sediment transport layer at the particle location. K_{burial} is a reduction factor to account for the possible burial of the particle by ambient sediments. The units of f_e are sec^{-1} or Hz.

Particle Deposition and Re-entrainment

Particles are deposited on the bed once they pass below one-quarter of the skin roughness height, k_s'.

$$\text{if} \quad z_p \begin{cases} < \dfrac{k_s'}{4} & deposits \\ \geq \dfrac{k_s'}{4} & active \end{cases} \tag{29}$$

If a particle becomes deposited, it will cease to move until it is re-entrained. The frequency of entrainment, f_e, is computed considering the particle pickup rate, the mixing depth of native sediment in the active transport layer, and the likelihood of burial by native sediments.

The entrainment elevation is computed using a Rouse-type random number generator. This generator will produce random numbers that are distributed according to a Rouse sediment concentration profile for the specific sediment and flow conditions. As a result, the random numbers will be biased towards 0 (taken as the bed) rather than 1 (taken as the surface). The new elevation of a re-entrained particle is taken as:

$$z_p = \Psi h \tag{30}$$

where Ψ is a random number between 0 and 1 distributed according to a Rouse sediment concentration profile.

DRAFT

Boundary Conditions

PTM uses the land and open boundaries given in the mesh file. Particles may pass through an open boundary. If a particle passes through an open boundary, it ceases to be included in the computation. However, a particle may not pass through a land boundary. The particle will be placed alongside the boundary in question. If a particle is driven onto a dry point, it becomes stranded. Wetting and drying are included, if the original hydrodynamic model was run with this capability.

DRAFT